ABSTRACT

YUAN, YUE. Enzyme Immobilization in Biobased Polymeric Fibrous Matrices for Biocatalytic Textiles: Material Innovation, Mechanistic Studies and Applications. (Under the direction of Dr. Sonja Salmon).

This dissertation summarizes our innovation and exploration of a new category of functional material called biocatalytic textiles. The catalytic efficiency of entrapped diffusion limited enzymes in a reaction containing solid, liquid and gas phases is facilitated when dissolved enzyme substrate is transported by liquid flowing through the textile structure. This research is motivated by the challenges existing in global management of CO_2 emissions and recent research on applying biocatalyst (carbonic anhydrase, CA), a class of enzymes that catalyze CO_2 hydration in an ultrafast manner, as an alternative to high energy and high cost traditional liquid solvents in CO_2 scrubbing processes. Therefore, the ultimate goal of this dissertation research is to develop a biocatalytic column packing material with improved enzyme longevity by restraining the enzyme and protecting it from exposure to harsh conditions, through enzyme immobilization and assay development.

Enzyme entrapment is one of the promising methods in enzyme immobilization due to its versatility, high enzyme loading, and mild interactions between the physical supports and enzymes. However, the mass transfer barrier introduced by the entrapment may hinder the overall catalytic efficiency after immobilization, especially when diffusion limited enzymes are entrapped. In order to develop an efficient column packing system with CA enzymes, another diffusion limited enzyme, catalase (CAT) was used as the model enzyme to screen the polymers, fiber formation methods and immobilization approaches in our material innovation. To address the above limitation in enzyme entrapment, with CAT, a robust biocatalytic textile with controllable liquid transport properties is created by coating thin layers of chitosan containing

catalase onto a cellulosic yarn. The resulting material integrates enzyme catalytic functionality with protective coating properties of chitosan and structural functionality of the textile, providing a novel and versatile enzyme immobilization strategy. When the material is tested with a flow-through configuration, it decomposes at least two times more peroxide in a twenty-times smaller reaction zone volume compared to a stirred tank configuration. A constrained wicking mechanism that benefits biocatalytic yarn performance was elucidated by in-situ neutron radiography and neutron computed tomography (CT), from which the liquid transport through the textile structure and liquid spatial distribution within the textile structure were characterized. This CAT immobilized material was then applied to water recycling studies for cotton textile bleaching and dyeing processes, where the immobilized CAT significantly improved the water reusability and decreased the enzyme consumption requirement. Then, the immobilization method was applied to fabricate a lab-scale CO_2 scrubbing packing material with CAs. Without any optimization, the biocatalytic textile has more than twelve times CO_2 absorption compared to a typical Raschig ring packing with lower total weight. To prepare for further characterization of entrapped enzymes in the chitosan layer, this dissertation research also includes a novel biosynthesis of deuterium-labeled chitosan from microorganisms using deuterated glucose in H_2O medium, without the need for conventional chemical deacetylation. After extraction and purification, the chemical composition and structure were determined by Fourier-transform infrared spectroscopy (FTIR), nuclear magnetic resonance (NMR), and small angle neutron scattering (SANS), providing information about the position of the deuterons in the glucose backbone and changes in the molecular assembly after the deuterium substitution. The deuteration work provides a valuable chemical with enzyme compatibility for future mechanistic study of the interaction between entrapped enzymes and the biopolymer.

Enzyme Immobilization in Biobased Polymeric Fibrous Matrices for Biocatalytic Textiles: Material Innovation, Mechanistic Studies and Applications

by
Yue Yuan

A dissertation submitted to the Graduate Faculty of
North Carolina State University
in partial fulfillment of the
requirements for the degree of
Doctor of Philosophy

Fiber and Polymer Science

Raleigh, North Carolina
2021

APPROVED BY:

_____	_____
Dr. Sonja Salmon Committee Chair	Dr. Flora Meilleur
_____	_____
Dr. Wei Gao	Dr. Robert Rose

DEDICATION

To my parents, Huangwei Yuan and Xiangyu Hu,

who inspire me, encourage me, support me, and never gave up on me.

BIOGRAPHY

Yue Yuan was born and raised in Gezhouba, Hubei, China, a community contributed to the construction of the Three Gorges Dam located at Yangtze River. Instead of becoming a civil engineer, she obtained Bachelor of Engineering in Apparel Engineering at Wuhan Textile University in 2013. At that time, she planned to do research in functional apparels, and dreamed to work on protective apparels for fire fighters, and space suits for astronauts.

Yue arrived Manhattan, Kansas, United States on Dec. 31st, 2014, where she started her master's study at Kansas State University. Due to the unexpected faculty relocation, she changed her research direction to fibrous materials and chemistry under the direction of Dr. Jooyoun Kim (now at Seoul National University) and co-advised by Dr. Seong-O Choi, at Nanotechnology Innovation Center of Kansas State. Yue loved the years at K-State where she took classes from Chemistry, Chemical Engineering, and Biology etc. She met many wonderful faculty members who helped her laying foundations in these fields and supported her in her research projects. She enjoyed driving on I70 from Manhattan to Lawrence for experiments at University of Kansas.

In August 2017, Yue moved to Raleigh, North Carolina to continue her research in Fiber and Polymer Science, under the direction of Dr. Sonja Salmon. She started working with enzymes and obtained a graduate minor in Biochemistry. Other than major research presented in this dissertation, Yue enjoyed bio lab work such as culturing microorganism and protein production. In summer 2019, Yue participated in an internship at Oak Ridge National Laboratory where she deuterated the chitosan from fungus under the direction of Dr. Hugh O'Neill.

Yue met her husband, Joshua D. Geeting, a graduate in Theatre Education, in Raleigh. They married in February, 2020 and their first child, Miles Edward, was born on March 17th, 2021. The kitchen is their shared "lab space" for invention and optimization.

ACKNOWLEDGMENTS

This work would not have been possible without the groups and individuals that I have met in the past few years. First of all, I would like to express my sincere appreciation to my committee chair, Dr. Sonja Salmon, her visions and guidance with experiences from both industry and academia enriched this research work. I am truly thankful to Dr. Flora Meilleur, advisor of my graduate minor in Biochemistry, who is also a scientist at Oak Ridge National Laboratory (ORNL). She brought me to the neutron world and the neutron techniques have been critical tools in studying the prototype developed in this research. I would also express my sincere thanks to committee members Dr. Wei Gao and Dr. Robert Rose, for the lab space and equipment they shared, training they offered and discussions we had for research and career development.

Interning at ORNL was an incredible experience to me. I would like to acknowledge my mentors Dr. Hugh O'Neill and Qiu Zhang. The achievement would not have been possible without all the scientists and postdocs who I worked with at ORNL, from Neutron Scattering Division to the Center for Nanophase Material Science, and to the Bioscience Division. I see the power of collaboration in science from these brilliant people and open minds. In addition, I appreciate The Ellen Rohde Leadership Initiative - Professional Development Support Grants, which made my research visit at ORNL possible in December 2018. I also appreciate the lab managers at Wilson College of Textiles (Ms. Judy Elson, Dr. Birgit Andersen) and AIF (Dr. Chuck Mooney, Dr. Chuanzhen Zhou) for the resources and training in this research. I appreciate Mike Elder and Alan House at Novozymes North America, Inc. for providing enzyme samples used in this dissertation research. I am thankful for the funding supports from the Wilson College of Textiles, including the North Carolina Textile Foundation Fellowship, American Association

of Textile Chemists and Colorists (AATCC) (Student Research Support Grant), and the Department of Energy's Bioenergy Technologies Office (DOE-BETO).

I would like to appreciate my husband, Joshua, who criticizes my work as my always general audience and who has been humorous enough to handle the stress of a Ph.D. student, especially during the pandemic. I appreciate the support from my family in China as well as families, friends and lab cohorts from Manhattan, KS to Raleigh, NC, to Salem, OR. I acknowledge Dr. Jooyoun Kim, who brought me into the fiber and polymer research six years ago, and Dr. Seong-O Choi, who also helped a lot during my time at K-State. Last but not the least, I would like to express gratitude toward my parents for their enduring love and endless support.

TABLE OF CONTENTS

LIST OF TABLES

LIST OF FIGURES

LIST OF ABBREVIATIONS

CA	carbonic anhydrase
bCA	bovine (erythrocyte) carbonic anhydrase
NCA	Novozymes (microbial) carbonic anhydrase
CAT	catalase
CO_2	carbon dioxide
HCO_3^-	bicarbonate
DF	dilution factor (DF = final volume/initial volume)
DMG	N,N-dimethylglycine
Tris	tris(hydroxymethyl)aminomethane
K_2CO_3	potassium carbonate
$KHCO_3$	potassium bicarbonate
RT	room temperature (~21°C)
CCS	Carbon Capture and Storage
KOH	potassium hydroxide

CHAPTER 1: INTRODUCTION

Enzymes, nature's biocatalysts, were discovered and still can only be synthesized in biological systems. Enzyme catalysis occurs with high selectivity of substrates for specific chemical reactions. Enzyme performance is limited by surrounding conditions such as temperature, pH, and ionic strength. The unique catalytic function and optimal catalytic condition of a specific enzyme is determined by the primary amino acid sequence, which is critical in the correct folding of molecular chains to form a three dimensional catalytic site.

Enzymes play crucial roles in cell metabolism and signaling pathways in living organisms. These biomolecules have been extensively studied to understand human disease as well as for drug discovery in medical or pharmaceutical fields. In the present-day market, enzyme and enzyme products have been produced and applied in various industries, such as biofuels (Chapman et al., 2018; Ebaid et al., 2019; Srivastava et al., 2018), food (Kirk et al., 2002; Minussi et al., 2002) and textiles (Buchholz et al., 2012; Buschle-Diller et al., 2001; Madhu & Chakraborty, 2017). Examples are, casein precipitation in cheese production by protease, residual peroxide decomposition in fabric bleaching using catalase, or stain removal at low temperature by formulating multiple enzymes into detergent products. To meet demands of enzyme products in both industrial applications and household consumption, biotechnology approaches including recombinant DNA insertion in microorganisms and fermentation processes have been used to develop and manufacture stable and efficient enzyme products at large scale. Beyond the intensive research in fields such as enzymology, molecular biochemistry and biophysics, where studies of enzyme protein structure, function, evolution, and genetic modification aim to find and develop robust enzymes, enzyme immobilization is another broad and widely investigated technical approach toward improving enzyme performance and utility. One consequence of genetic

modification could be to develop more robust enzymes that tolerate broader immobilization conditions (e.g. ionic strength, solvent, and temperature) for biocatalytic matrix innovation. Therefore, overall, enzyme immobilization is an interdisciplinary research topic involving material science, chemistry, biochemistry and engineering (Bilal et al., 2019).

After a long history of using "naked enzyme" (or free enzyme, dissolved enzyme), immobilized enzymes have been studied and developed for decades. Initially, enzyme immobilization aimed to reuse enzymes in industrial processes, where insoluble enzyme complexes or enzyme-support complexes can be separated from soluble catalytic substrate and products, rather than fabricating novel biocatalytic materials. As true catalysts, enzymes are not consumed in the reaction. However, many commercial enzyme catalyzed reactions are carried out in liquid environments, such as batch reactions, where the catalysts are lost when draining the liquid after the process is complete. Among the motivations for developing retrievable biocatalytic material with desired enzyme longevity is to reduce the costs of using enzyme products at industrial scale. One of the most successful examples of using immobilized enzymes in continuous fixed bed reactors is the production of high fructose corn syrup (HFCS) by immobilized glucose isomerase (Klibanov, 1983). Another example of reusing immobilized enzymes with batch tank reactors is using immobilized lipase (e.g. Novozym® 435) to obtain enantiomerically pure drug intermediates and active pharmaceutical ingredients (APIs). In addition to the reusability, these immobilized enzymes are stable over a broader pH or temperature compared to naked enzymes. Beyond the existing applications of immobilized enzyme in industrial production, modern studies in enzyme immobilization also focus on fabricating novel biocatalytic materials with good enzyme performance and recyclability. It must, therefore, be expected that a good enzyme immobilization method or enzyme immobilized material has to meet two key criteria: high retained activity after

immobilization and longevity of immobilized enzyme, and easy versatile immobilization method with low cost.

As summarized in most review articles (Grigoras, 2017; Krajewska, 2004), enzyme immobilization studies are made on a case-by-case basis, which means the retained activity of immobilized enzymes reported in prior studies is very specific to the enzyme, support matrix and the immobilization method used in that particular study. Also, selection of enzymes and materials for immobilization in prior studies are usually application driven or selected based on individual interests or access to enzyme resources, materials, and facilities. The diversities in enzymes and support materials together with the material-dependent evaluation methods make direct comparison of different enzyme immobilization work challenging. Thus, there are still many unknowns and uncertainties to be further explored in this interdisciplinary and still emerging research field.

From a materials perspective, the composition of the immobilization matrices can be varied from inorganic support such as silica or carbon based material, to soft matter such as polymers. Rational selection of the support materials in prior studies relies on choosing the chemical structures or other properties that benefit the immobilization process. Typically, materials chosen to serve as immobilization matrices are selected for their fabrication and in-use performance properties, with disposal after use being a secondary consideration. However, one of the key desirable and inherent features of enzymes is their biodegradability. This feature can be lost when immobilizing enzymes, depending on the properties of the immobilization matrix. For small volume applications, losing the biodegradability feature may not be critical, but for very large biocatalyst applications this aspect cannot be overlooked. Therefore, starting with biobased or biodegradable raw materials to fabricate enzyme immobilized matrices can not only provide better

compatibility between matrices and biocatalysts, but also make the integrated materials more versatile and sustainable.

The geometry of enzyme immobilization supports can vary from one dimensional particles to two dimensional tubes or fibers to three dimensional foams or gel networks. The size of supports can also range from nanoscale (around 10-100 nm) such as gold nanoparticles to mesoscale (0.1-1 mm) like calcium alginate beads. Though fibrous polymeric matrices have gained attention in the last decade, these still lack in depth investigation and need further development in both materials and methods. For example, nonwoven electrospun mats have been considered as promising carriers for enzyme immobilization, as recently reviewed (D. Li et al., 2019; Soares et al., 2018; Z.-G. Wang et al., 2009), whereas other textile materials, for which mature manufacturing techniques and facilities exist, have not been extensively explored as enzyme immobilization matrices.

Immobilization methods can be classified into two main categories: attachment and incorporation. Immobilization is often achieved by adsorbing or crosslinking enzymes to a pre-formed matrix in "attachment", while immobilization by incorporation usually happens simultaneously with the material formation, such as encapsulating enzyme in liposome or entrapping enzymes when casting films. In considering enzyme immobilization with textile-based materials, both immobilization methods are applicable: post immobilizing of enzyme can be done after fiber or fabric production, or enzymes can be entrapped into the matrix during fiber formation.

The two immobilization methods have different risks of enzyme inactivation as a result of immobilization. Chemical crosslinking used during covalent attachment immobilization may cause inhibitory chemical reaction with functional groups on the enzyme that block the active site or can induce conformational alteration of enzyme structure by allosteric effects (Cao, 2006). The

entrapment method is restricted to using materials that can be dissolved in mild conditions for processing, where enzyme can be mixed in without falling apart. Also, the entrapment method risks that enzyme will become "hidden" or obstructed by the molecules of the immobilization matrix, preventing substrates from reaching the enzyme active site.

Material selection for the two methods overlaps. For example, presence of chemical functional groups in the support material is a key parameter for both methods. In chemical attachment the presence of functional groups determines the upper limit of enzyme molecules that could be immobilized, while in entrapment, the interactions between enzyme and functional groups of a support material contribute to the overall properties of the integrated catalytic matrix and can participate in preventing the enzyme from leaching out. In generic, non-specific entrapment approaches, no special functional groups on the enzyme are required, giving entrapment the potential of being a more universal method to immobilize enzymes among all immobilization methods. Notably, in biological systems, highly specialized enzyme entrapment immobilization occurs, for example, in membrane-bound enzyme systems, where the hydrophobicity/hydrophilicity in different regions of the protein structure govern the enzyme's position in the membrane. In these systems, it is not one or even a few chemical groups that are responsible for the immobilization, but entire regions of the protein structure. These concepts can help inspire future enzyme immobilization development.

Retained activity and enzyme longevity are critical characteristics in describing the overall performance of immobilized enzyme systems for technical applications. To measure the retained activity, developing an appropriate assay is crucial. This is because in immobilized enzymes the molecules are no longer catalyzing the chemical reaction in their free form (i.e. dissolved in a reaction liquid), where the mass transfer between enzyme and substrate is high. Using a traditional

assay for enzyme immobilized material, where the enzyme molecules will in some way be confined by their surroundings, may change the assay response time, limit the use of certain substrates, or cause practical obstacles in conducting the assay in the presence of a solid material. In addition to evaluation of the catalytic function, techniques (e.g. microscopy, spectroscopy) are needed to characterize the physical properties of the enzyme immobilization supports and how different immobilization methods may influence these. Morphology of the materials, chemical compositions, chemical bonding, and other properties usually are characterized together with the percentage of retained enzyme activity after a period of time (e.g. days, compared to the free enzyme). However, only limited research has presented direct evidence of enzyme distributions in/on immobilization matrices, and research that elucidates what actually causes the observed reduction or enhancement in enzyme activities that occurs as a result of immobilization is even more limited. The catalytic function of enzymes is affected by their three dimensional conformation and this is influenced by the surroundings. Better understanding of the folding, partial unfolding, unfolding or even refolding of enzyme molecules as a result of the immobilization process would help evaluate not only the appropriateness of the support material but also the immobilization procedure. Depending on the application, physical properties of the immobilization matrix are also important, such as mechanical strength and surface properties such as ionic charges or hydrophilicity/hydrophobicity. Thus, appropriate characterizations of both the catalytic performance and the overall properties are needed, in order to develop better immobilized enzymes as high performance, sustainable catalytic materials. To achieve this, novel and/or systematic characterization methods may be needed to better understand the immobilization technique and enzyme performance after immobilization, together with synthesizing novel chemicals. For certain applications, using fibrous materials, especially flexible textile materials

with biobased polymeric building blocks, offers unique opportunities in fabricating novel flexible catalytic materials with good potential for scaling up using existing manufacturing processes. To successfully fabricate, evaluate and improve these new materials, it is necessary to develop proper methods to characterize these novel catalytic materials and connect the material, method, and product together.

Beyond all these above, as mentioned earlier, one drawback of enzyme immobilization, especially using physical support to immobilize ultrafast enzymes through incorporation methods, is the additional mass transfer barrier introduced by immobilization. In this dissertation work, a systematic study of enzyme entrapment in biobased fiber- and film-forming polymeric materials was conducted using two diffusion-limited enzymes, catalase (E.C. 1.11.1.6) and carbonic anhydrase (E.C. 4.2.1.1). Catalase (CAT) catalyzes the decomposition of hydrogen peroxide (H_2O_2) to molecular oxygen (O_2) and water (H_2O) at moderate temperature with a turnover frequency of 4 x 10^7 s^{-1} (Heck et al., 2010). Carbonic anhydrase (CA) catalyzes the reversible reaction of carbon dioxide (CO_2) with water (H_2O) to form bicarbonate (HCO_3^-) with a turnover frequency of about 10^6 s^{-1} (Lindskog & Coleman, 1973). Therefore, both enzymes catalyze reactions that are influenced by gas-liquid mass transfer phenomena because their substrates and/or products are gas molecules. When these two ultrafast enzymes are immobilized into/onto a support matrix, the catalyzed reactions involve gas, liquid and solid (catalytic matrix) as three phases. Using the model enzyme CAT, prototype flexible biobased catalytic textiles were made in different ways. The goal was to create rationally designed biocatalytic materials with improved retained enzyme activity and enzyme longevities leading to more efficient catalytic performance in key continuous flow process applications. The developed prototype materials were then expanded to

CA immobilization with a focus on developing novel low energy and low cost CO_2 gas separation packing materials with the biocatalysts.

Because entrapment is a versatile enzyme immobilization method with the advantages indicated, and supported by our preliminary results, it has been selected as the key immobilization method for this study. Due to material flexibility and mature manufacturing industry for scaling up, we chose fibrous materials (e.g. electrospun nanofibers, wet spun fibers, fabrics) as the support materials for developing prototypes with polymers in preliminary experiments. Initial experiments, involving entrapping enzymes in chitosan (a solution-processable biobased polysaccharide) matrix at a mild conditions then applying a thin chitosan-enzyme coating on cellulosic fibers, showed good retained enzyme activity, significantly reduced enzyme leaching, extended enzyme longevity in both actual application and storage, improved catalytic efficiency and promising potentials for material up-scaling. Along with the material fabrication, characterizations of enzyme, polymer and integrated biocatalytic materials is critical in providing guidelines for optimizing the immobilizing parameters and conditions. After establishing suitable conditions (temperature, solvent, pH etc.) for immobilization, prototype materials were fabricated and the integrated materials were thoroughly characterized to bridge the structural and chemical features of the biocatalytic textile to the improved catalytic function and enzyme longevity.

As indicated, assays developed for free enzymes dissolved in solutions may not be appropriate for solid immobilized enzymes. Depending on the characteristics of the integrated biocatalytic material and its potential application, modified assays or novel test methods were developed. Also, the measured activity of the biocatalytic textiles was affected by both the enzyme stability and properties of the integrated material. Along with the retained activity and longevity of immobilized enzyme materials developed during the research, the properties of the matrices

(e.g. liquid transport inside material) was also investigated using advanced techniques. In addition, characterizing the structural stability of entrapped enzyme in chitosan requires new techniques and new chemicals, such as neutron scattering and biodeuteration. Therefore, the production and characterization of a novel deuterium labeled chitosan were conducted at Oak Ridge National Laboratory (ORNL) and presented this dissertation research.

With interests and initial motivations in creating biocatalytic materials for low energy and low cost industrial post-combustion CO_2 gas scrubbing, the enzyme CA-chitosan-cellulose composite developed in this dissertation research was then expanded to material fabrication with different coating techniques (e.g. dip-coating vs. padding) and conditions (e.g. enzyme-chitosan weight ratio, pH). The results of this work supported a collaboration with the National Renewable Energy Laboratory (NREL) and the University of Kentucky Center for Applied Energy Research (UK-CAER). Cellulosic substrates coated with chitosan entrapped CAs were fabricated into various column packing materials and tested with compatible solvents in a lab scale CO_2 scrubber. Selected candidate will be delivered to UK-CAER for further testing to fulfill the goals of the Department of Energy-Bioenergy Technologies Office (DOE-BETO) funded project in 2021-2022.

As a foundation for the experimental details selected for enzyme immobilization with biobased materials to produce fibrous biocatalytic textile matrices, prior research in enzyme immobilization is reviewed in Chapter 2, with a specific focus in each section. Chapter 2.1 reviews the historical trends in enzyme immobilization and answers general questions like, why are immobilized enzymes used and how have enzymes already been immobilized. The general materials and methods used in enzyme immobilizations are reviewed with analysis of their pros and cons. Chapter 2.2 is a general review of methods that have been used in enzyme

immobilizations. These methods can be classified into two categories: attachment immobilization where enzymes were immobilized after the support formation and incorporation immobilization where enzymes were immobilized during the material formation. Chapter 2.3 reviews the materials that have been used as physical supports, along with the parameters of the physical supports such as the chemistry and, geometrical shape, which have significant impacts on the immobilization outcomes. Due to their abundance and processability, the polymeric supports used in enzyme immobilization are reviewed in Chapter 2.4. The advantages of introducing fibrous structure in polymeric support materials in enzyme immobilization and the parameters that may affect enzyme immobilizations in/onto fibrous materials are reviewed in Chapter 2.5. Because the characterization and evaluation of enzyme immobilized materials are essential for obtaining guidance for material and process optimization, Chapter 2.6 reviews characterization methods used in prior research for both catalytic functions and other properties of the integrated materials. Unmet needs, beneficial features, limitations and knowledge gaps emerging from the reviewed literature provide the basis for why certain types of polymers, enzymes, immobilization methods and characterization methods were chosen in the presented dissertation research, as well as what knowledge gaps will be filled in enzyme immobilization research by this work.

Chapter 3 includes the development of a prototype biocatalytic textiles with CAT. The study demonstrates that when a fibrous matrix with a hierarchical structure and modified surface chemistry was used as a continuous flow reactor, the mass transfer barrier for the entrapped biocatalyst was significantly reduced. The developed prototype was also tested for its benefits in water reutilization for textile bleaching and dying processes. Chapter 4 presents a novel biodeuteration work in which a deuterium labeled chitosan was produced from filamentous fungus using a novel approach. The resulting deuterated chitosan has the potential for future neutron

scattering characterization. Chapter 5 contains the work on immobilization of CA based on the biocatalytic textile prototype developed using CAT. The envisioned application for this new material is low energy and low cost CO_2 scrubbing process. The work conducted with immobilized CA, included assay development, material fabrication and evaluation of the catalytic performance.

CHAPTER 2: LITERATURE REVIEW

2.1 Enzyme Immobilization

Immobilized enzymes are enzymes attached to an insoluble support or formed as an insoluble complex. Present-day enzyme immobilization research has expanded from improving enzyme stability or obtaining insoluble enzyme products, such as CLEA®s, for controllable catalyzed up- and downstream processing (Buchholz et al., 2012; Cao, 2006; Cao et al., 2003; Pialis & Saville, 1998; Roger A. Sheldon, 2007; Velasco-Lozano et al., 2016). to modern applied fields. These fields include sensors (Asakura et al., 1992; Baliyan et al., 2016; Gupta & Chaudhury, 2007; Yingshuai Liu & Yu, 2016), biomedical devices or accessories (David T Arazawa et al., 2012; Babadi et al., 2016; Kimmel et al., 2013), filtration or separation materials with high selectivity (David T Arazawa et al., 2012; J. B. Costa et al., 2019; H. Yang et al., 2008) and many others. Through enzyme immobilization, diagnostic or catalytic materials that contain enzymatic functionality can be fabricated. Enzyme immobilization has also been used to make model systems for exploring the protein-material interaction (Ait Braham et al., 2018; Bagheri et al., 2007), in order to optimize immobilization techniques and design catalytic materials with better performance (Ait Braham et al., 2018) or to understand the biological environments by mimicking the cellular environment (Kuznetsova et al., 2014).

Two core benefits of immobilizing enzymes on support materials include stabilizing the biocatalyst by providing a restricted environment for maintaining correct peptide chain folding, which is essential to the catalytic function of the enzyme; and enabling enzyme reuse by converting enzymes to an insoluble form that can be separated from the (typically liquid) reaction medium, which enhances the enzyme longevity and catalytic efficiency in applications (especially in applications requiring continuous process flow). In addition to these central improvements for

biocatalysts, immobilization may enable creation of novel integrated materials with both catalytic functionality from enzymes and desired physical properties from the immobilization supports.

Though enzyme immobilization techniques have developed for decades, and commercialized immobilized enzyme products have been widely used in various industries (Buchholz et al., 2012; Cao, 2006; Roger A. Sheldon, 2007; Velasco-Lozano et al., 2016), the correlations between enzyme, support material and immobilization method have not been understood thoroughly. For example, it was found that a lack of sufficient enzyme immobilization knowledge could affect further optimizing enzyme-enabled functional materials such as biofuel cells or sensors (Babadi et al., 2016; Gupta & Chaudhury, 2007). Therefore, careful evaluations of the materials and methods in enzyme immobilization are critical for developing stable biocatalyst products and novel functional materials.

Unfortunately, diversities that exist in enzyme families, support materials and immobilization methods bring difficulties in direct comparison of different immobilization studies. As mentioned in previous reviews (Buchholz et al., 2012; Cao, 2006; Grigoras, 2017; Krajewska, 2004; Zdarta et al., 2018), limitations in understanding enzyme immobilization stems from the fact that optimized immobilization procedures with maximum retained enzyme activity are discovered and characterized on a case-by-case basis. Thus review articles and chapters for enzyme immobilization tend to focus either on specific enzymes (González & Fisher, 2014; Grigoras, 2017) or specific materials (Adeel et al., 2018; Krajewska, 2004). The catalytic function of an enzyme is determined by its structure and dynamics, thus the optimal catalytic conditions (**Figure 2.1**) for each enzyme, even among its isozymes, could be varied. The interaction between enzyme and immobilization support material can be complicated, and interactions or the presences of other molecules can either enhance the correct enzyme folding or can cause the opposite effect

(Kuznetsova et al., 2014; Mohamad et al., 2015; Zdarta et al., 2018). Each method and support material has its own unique advantages in prototyping a certain type of material with specific applications, while a positive immobilization outcome can be highly dependent on the particularities of the enzyme-support pairing as well as the immobilization method.

In this section, through reviewing the motivations and purposes of enzyme immobilization, we define the core principles in enzyme immobilization and of enzyme immobilized materials as: achieve high relative enzyme performance (retained activity) and achieve high enzyme longevity. Accordingly, immobilization methods and support materials are reviewed with emphasis on contributions of these methods and materials in relative enzyme performance and enzyme longevity.

2.1.1 Motivation and purpose of enzyme immobilization

Enzymes are biocatalyst derived from biological systems having catalytic functions that are highly associated with the molecular structure and conformation. They generally have performance curves as show in **Figure 2.1** (solid line), where optimal conditions exist at which the enzyme exhibits highest catalytic activity. The peak of the curve can be narrow or broad, depending on the specific enzyme and conditions being evaluated. The optimal activity conditions may or may not correspond to the conditions at which the enzyme structure is most stable. For example, a partially denatured (unfolded) enzyme might exhibit higher than usual catalytic activity (provided that the active site is still intact) because the active site may be more exposed to its substrate and (especially if higher temperature is a factor in the partial unfolding) the reaction kinetics will be faster**.** Both the relative enzyme catalytic activity and the overall three dimensional structural stability can be affected by the reaction conditions, such as temperature, pH, ionic strength, or others. Changes in these conditions can lead to a conformational change of the enzyme

molecule or a disturbed dynamic of the enzyme catalytic active site. If the enzyme molecule folds correctly, as the consequence of the combination of enzyme function and surrounding conditions, it will normally exhibit its maximum catalytic rate. Outside of the optimal enzyme activity zone, the molecule, or some molecules as a population, may still catalyze the reaction but at slower rates, showing a reduced overall enzyme activity. When some parameters approach extreme conditions, such as high temperature or excessively acidic or alkaline environments, enzymes can be denatured over time, resulting in unfolded structures and loss of catalytic activity.

To maximize enzyme catalytic function in real applications, one option is to create protein engineered enzymes that can tolerate harsher conditions than wild-type (those found in nature) enzymes through recombinant DNA techniques. An alternative approach is to protect the enzyme biocatalysts by keeping them at relatively mild conditions. One way to achieve this is by immobilization. Enzyme immobilization produces more stable biocatalyst products for industrial applications. Prior studies show that immobilized enzymes often demonstrate higher tolerance to more extreme process conditions (dash line in **Figure 2.1**) (Buchholz et al., 2012; Cao, 2006; Madhu & Chakraborty, 2017; Migneault et al., 2004; Roger A Sheldon, 2007). Immobilization also converts soluble enzyme to an insoluble form. Thus, immobilized enzyme can be separated from the process liquids during or after the catalytic cycle. In some cases, this separation prevents biocatalyst from being exposed to subsequent (harsher) process steps, thereby eliminating the risks of denaturation in following steps that might contain extreme conditions. It also allows recycling of biocatalysts, using the biocatalysts in continuous process flow reactions (such as packed bed reactors), and enhancing the performance longevity resulting in lower enzyme consumption (and higher “catalytic efficiency”).

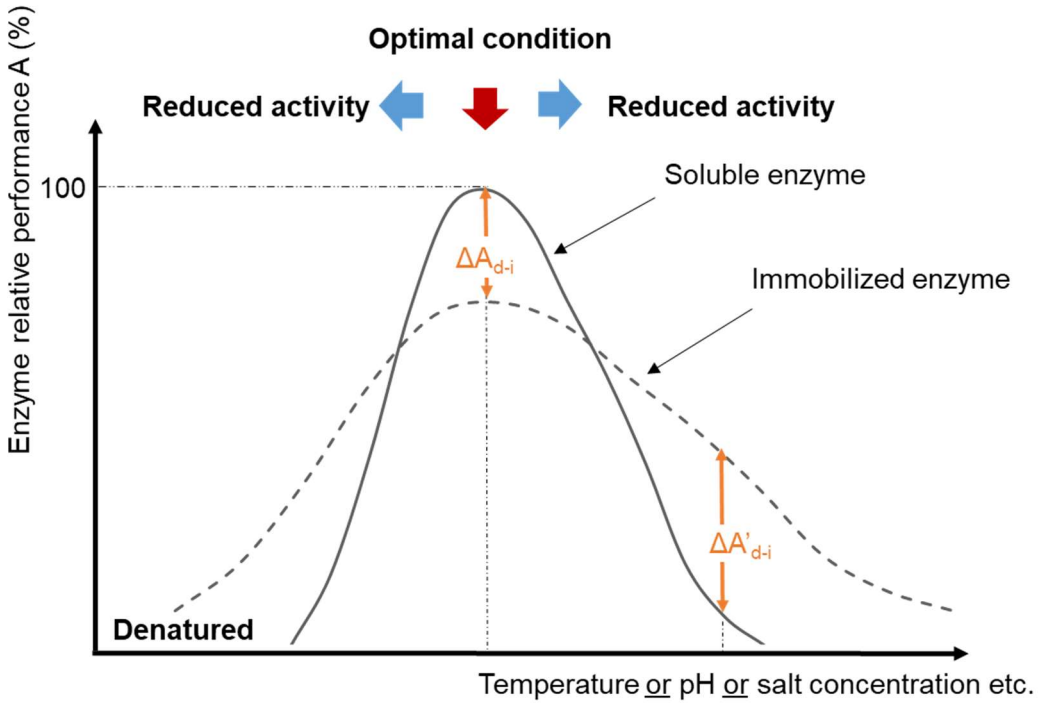

Figure 2.1 Schematic diagram of normalized enzyme activity and/or structural stability and process conditions for catalytic reactions.

For commercial processes, it is often essential that immobilized enzyme should have improved catalytic efficiency (total moles of substrate converted per mole of enzyme protein) after immobilization to both accommodate the extra cost and complexity of producing the materials and generate cost savings that can motivate adopting the technology. There are some exceptions to this, such as production of high value products that cannot be made by other methods or use of enzyme protein for certain kinds of sensor design (Huang et al., 2002), in which the redox potential of the metal bound at the enzyme active site is more important than the chemical catalytic function of the correctly folded enzyme molecule. Nevertheless, in most cases extended enzyme catalytic longevity is fundamental for justifying immobilized enzyme use, and retention of enzyme structural stability is a prerequisite for enzyme activity. **Figure 2.2** illustrates a comparison of enzyme longevity for dissolved "free" enzymes and immobilized enzymes as the normalized catalytic performance of soluble enzyme (in its free dissolved form in liquid) or immobilized

enzyme versus time. Enzyme longevity refers to the retained activity of fixed amounts of enzymes over specified time periods, and is a key criteria for evaluating the catalytic efficiency of biocatalytic materials.

The vertical axis in **Figure 2.2** is presented as normalized (or relative) enzyme performance because when enzymes are immobilized, the measured activity is not only a consequence of specific enzyme activity and reaction conditions but also includes other factors such as mass fraction of immobilized enzymes in the support, chemical or physical properties of the support materials and accessibility of enzymes in the immobilization matrix **(Figure 2.3**).

According to prior research, some immobilized enzymes, especially ones in retrievable solid matrices such as films, membranes, or fibers, demonstrated lower activities at optimal conditions compared to that of the soluble enzyme ($A_{i0}/A_{d0} < 1$ in **Figure 2.2**). This lower activity is attributed to the increased mass transfer barrier between substrates/products and enzyme in the presence of the immobilization matrix (Altinkaynak et al., 2016; Bagheri et al., 2007). Although the difference in instantaneous enzyme performance between soluble and immobilized enzyme ($\Delta A_{d\text{-}i} < 0$, **Figure 2.1**) is observed when actual measurements are made at optimal reaction conditions for the soluble enzyme, the true benefit of using an immobilized enzyme emerges when the real application may expose soluble enzymes to conditions that are no longer tolerated, whereas immobilized enzyme can be protected from those conditions ($\Delta A'_{d\text{-}i} > 0$, **Figure 2.1**). Dissolved (or "free") enzymes can experience significant activity or performance drop over short time periods in real applications (solid blue line in **Figure 2.2**), if no supplemental enzymes are added (Qi et al., 2018). Different enzymes may exhibit different stability to stressful reaction conditions, yet all kinds may lose all activity in a relatively short period of time (days to weeks). This rapid activity loss of soluble enzyme can be attributed either to enzyme denaturation or to the difficulties

of recovering and reusing dissolved enzymes. Denaturation can happen if soluble enzyme travels together with liquid flow and passes through reaction zones having extreme conditions. The dissolved enzyme can also be lost if the liquid needs to be replenished during separation of substrates and products from the catalyzed reaction.

As another benefit, many immobilized enzymes demonstrate better catalytic performance at broader pH or temperature ranges in comparison with dissolved enzymes, suggesting a positive $\Delta A_{d\text{-}i}$ at conditions outside the optimal conditions for the soluble enzyme (**Figure 2.1**) (Abdelrahim et al., 2017; Akgöl et al., 2001; Arola et al., 2012; Asakura et al., 1992; Bankeeree et al., 2016; Hwang et al., 2004). The exact reasons for improved thermal and pH stability through immobilization are not always clear, but the most common and acceptable explanation is that the presence of the support provides confined environments to restrict the unfolding of enzymes when conditions become unfavorable. Studies also found that the presence of macromolecules crowding around the protein can tighten the protein structure and assist the protein folding. (Kuznetsova et al., 2014)

Over time, immobilized enzyme may also exhibit decreases ($A_{it} < A_{i0}$) in relative performance compared with its ideal scenario (lower straight dash line, red, **Figure 2.2**) in which the apparent enzyme activity would remain the same forever. Eventually, immobilized enzymes will lose activity. Commonly, a first abrupt performance decrease is observed over a relatively short time period (e.g. hours to days), which is usually attributed to enzyme leaching from the support matrices and can be detected by measuring for enzyme protein or enzyme activity in the reaction liquid. A slower biocatalyst inactivation, or slower decrease in relative enzyme performance is then observed over a much longer period (e.g. weeks to years). A number of factors can contribute to this slower inactivation of immobilized enzyme, including gradual enzyme

leaching, erosion or degradation of the support matrix, and accumulation of contaminants in/around the immobilized system. The magnitude of retained catalytic performance at specific times for immobilized enzyme (A_{it}/A_{i0}) is determined by various parameters such as inherent enzyme stability, support material properties, methods of immobilization and reaction conditions. Enzyme immobilization development efforts typically focus on selecting or investigating these parameters in order to maximize A_{it}/A_{i0} for enzyme-immobilized material.

Note that in the illustration, the horizontal axis, which is the time period used in evaluating the relative enzyme performance, is important. In the illustration, which is based on performance observations for real systems, the soluble enzyme has no relative enzyme performance within days while the immobilized enzyme has retained catalytic function for years, though it decreases over time. A real application in which this kind of behavior occurs is for glucose isomerase used in the form of immobilized granules in large packed bed columns for the continuous production of high fructose corn syrup.

This retained activity over a very long period compared to that of the soluble enzyme is a hallmark of the improved enzyme longevity that can be obtained via immobilization (shaded area in **Figure 2.2**). Therefore, immobilization not only provides more robust enzyme products against harsh catalytic condition (as an alternative approach to protein engineered enzymes), but also provides high enzyme catalytic efficiency that can enable commercial processes within the cost window allowed by the application.

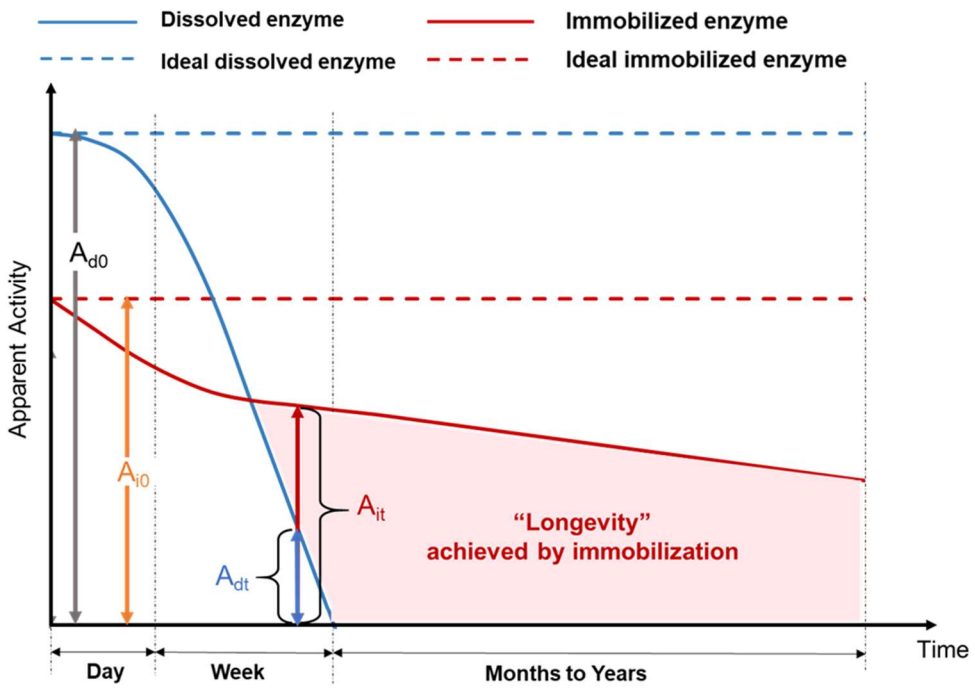

A_{d0} = Initial catalytic performance of dissolved enzyme

A_{dt} = Catalytic performance of dissolved enzyme at time, t

A_{i0} = Initial catalytic performance of immobilized enzyme

A_{it} = Catalytic performance of immobilized enzyme at time, t

Retained catalytic performance after immobilization = $A_{i0} / A_{d0} \times 100\%$

Retained catalytic performance at specified time for dissolved enzyme = $A_{dt} / A_{d0} \times 100\%$

Retained catalytic performance at specified time for immobilized enzyme = $A_{it} / A_{i0} \times 100\%$

Figure 2.2 Relative enzyme performance versus process time for free and immobilized enzymes as justification for immobilizing enzymes to fabricate biocatalytic materials.

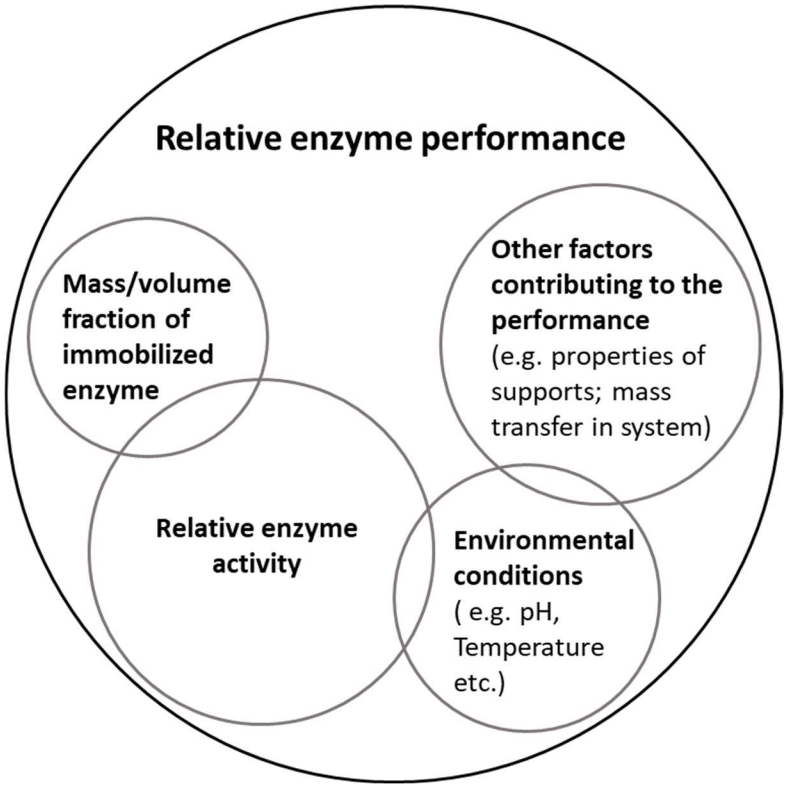

Figure 2.3 Illustration of relative enzyme performance and components contributing to the performance.

2.1.2 Model enzymes in immobilization studies

As mentioned earlier, for a soluble enzyme, the longevity is determined by its structural stability and is influenced by the reaction environment. Therefore, some enzymes can last longer in soluble forms in application while some enzymes lose activity within short time periods. Whenever possible, researchers choose enzymes for their immobilization studies that already have high intrinsic stability, because this implies the immobilized biocatalyst will also have better longevity. However, there can be a trade-off between enzyme stability (extended activity even under stressed conditions) and enzyme catalytic activity (the rate at which substrates are converted to products), and this must be taken into consideration in comparisons of overall catalytic efficiency.

Table 2.1. Enzyme classes of the NC-IUBMB enzyme list. (McDonald & Tipton, 2014)

Class	Name	Reaction catalyzed
1	Oxidoreductases	$AH_2 + B = A + BH_2$ or $AH_2 + B^+ = A + BH + H^+$
2	Transferases	AX + B = A + BX
3	Hydrolases	$A\text{-}B + H_2O = AH + BOH$
4	Lyases	A =* B + X-Y = X-A-B-Y
5	Isomerases	A=B
6	Ligases	A + B +NTP = A-B + NDP + P or A + B +NTP = A-B + NMP + PP

* refers to double bond between A and B.

Of course, the main reason for using an enzyme in the first place is related to the (typically) highly selective reactions that different classes of enzymes can catalyze (**Table 2.1**). For instance, laccase, which belongs to the polyphenol oxidase class of enzymes, has been immobilized and used for (dye) decolorization reactions (Abadulla et al., 2000; Koloti et al., 2016). Due to its catalytic role in oxygen reduction, laccase has also been immobilized on cathodes for biofuel cell production whereas glucose oxidase or glucose dehydrogenase has been immobilized on the anode (Babadi et al., 2016). Glucose can be converted to electrochemical energy *in vivo* with the presence of these two enzymes on electrodes (Babadi et al., 2016). For any particular catalytic function, different enzymes within the same class ("isozymes") have been immobilized, depending on the specific applications. For example, bovine carbonic anhydrase (which has high catalytic activity, but does not have especially high thermal stability) has been immobilized for biomedical implants (D. T. Arazawa et al., 2015) while highly thermostable carbonic anhydrases from bacteria have been evaluated for high temperature gas separation process (Migliardini et al., 2014). Well-characterized, versatile, robust "workhorse" enzymes, such as lipase (S.-F. Li et al., 2007; Shuai et al., 2017) or horseradish peroxidase (HRP) (Bilal et al., 2017) have been used frequently when

exploring immobilization conditions across broad temperature or pH ranges, from which new immobilization methods and novel enzyme immobilized materials were developed.

Having selected the relevant catalytic functionality for a particular immobilization application, the structural and chemical characteristics of enzyme molecules provide many possibilities for immobilizing these molecules on support materials through various interactions. The dipole moment in the backbone peptide bond as well as titratable side chains on some amino acids, such as lysine, aspartic acid, etc., contribute to either the binding or association between enzyme and support material through covalent bonds, hydrogen bonds, ionic pairing, or van der Waals forces (Buchholz et al., 2012; Cao, 2005, 2006). These reactive groups and the location of these groups in the enzyme structure can either promote or inhibit the interactions needed for enzyme immobilization, and might have impacts on the orientation of the enzymes after immobilization (Yingshuai Liu & Yu, 2016). Folding of enzyme molecules can also be affected by these interactions either directly or indirectly, contributing to the level of enzyme activity retained after immobilization. The orientation of the enzyme molecules after immobilization can influence the accessibility of substrates to the enzyme catalytic sites, which is a critical factor in the overall catalytic performance of the material (**Figure 2.3**). In enzyme-immobilized sensors, the orientation of enzyme molecules has huge impacts on the sensitivity of the device, as well as on the detection range of the sensor (Yingshuai Liu & Yu, 2016; Y. Yang et al., 2014). However, the irregularity of amino acids in an enzyme structure and the allosteric effects of enzymes prevent immobilization from being a simple process. Enzyme structure and chemistry, especially the surface chemistry of enzyme molecules, allows for the diversity encountered in immobilization methods and supports while creating intricacies in optimizing the immobilization recipes. In a

related, though even more complex case, mixtures of intracellular enzymes can be immobilized through whole cell immobilization (Buchholz et al., 2012).

2.1.3 Challenges in enzyme immobilizations

Compared to a soluble enzyme in a liquid, it is more complicated to describe the relative activity of an immobilized enzyme. **Figure 2.3** illustrates the factors that contribute to the relative enzyme performance after immobilization. The core component is the relative enzyme activity after immobilization, which is directly determined by the structural stability of the enzyme after the immobilization process and during utilization. Conditional parameters such as pH, temperature, solvents, etc. that are used during the immobilization procedure contribute to the molecular conformation in the final product. These conditional parameters also have impacts on enzyme catalytic efficiency during use, by affecting the retained enzyme activity, enzyme longevity and support durability (**Figure 2.3**), though the same conditional parameters, such as pH, may have distinctly different impacts on soluble enzymes versus the corresponding immobilized enzymes.

The mass/mass (or mass/volume) fraction of enzyme in an enzyme-immobilized system is the effective enzyme loading in immobilization. In prior studies, depending on the applications and methods used, the weight ratio of enzyme to support material vary from less than 0.1% to over 300%. In theory, a higher mass fraction of enzyme yields higher catalytic performance, due to increased biocatalysts presence in the solid material. However, it was found that overloading of enzymes might have the reverse effect on relative enzyme performance (Akgöl et al., 2001; Buchholz et al., 2012). Also, the amount of enzyme molecules that can be stably bound to a support matrix can be limited by the number of specific binding sites on the support or can depend on the

selected immobilization method. As a result, unbound enzymes might leach out over short time periods during the first few utilization cycles.

In addition to the mass fraction of immobilized enzyme, the distribution and localization of enzyme molecules has significant impact on the diffusion of reaction substrates and products to the enzyme active site and surroundings, respectively. Beyond the enzyme distribution and localization, the rate of mass transfer in catalytic reactions, can also be influenced by intrinsic properties of the enzyme-immobilized support, such as pore size, hydrophobicity/hydrophilicity, etc. Other physical, chemical, or mechanical properties of support materials might contribute to the overall catalytic performance in many ways, depending on the applications, enzymes, and immobilization methods. For instance, a hydrophobic surface has been preferred for adsorbing carbonic anhydrase to a membrane surface in a gas scrubbing application (Xu et al., 2019); whereas the hydrophobic medium in a chemically modified silica gel can cause significant reduction in activity of entrapped enzyme. (Roger A. Sheldon, 2007) Based on prior studies, several general parameters need to be taken into consideration to obtain an enzyme-immobilized material with high relative enzyme performance and enzyme longevity:

- Enzyme loading
- Enzyme-support material interaction
- Localization or distribution of enzymes in the immobilized material
- Conditional parameters in enzyme immobilization (solvent, temperature, pH, time, etc.)
- Conformation and orientation of enzyme after immobilization
- Structural flexibility of enzyme in a confined environment (enzyme dynamic)

- Conditional parameters of using enzyme-immobilized materials (solvent, temperature, pH, time, etc.)
- Physical, chemical, and geometrical properties of support material

The above factors that relate to relative enzyme performance and longevity can be manipulated through three basic components in enzyme immobilization studies: enzyme, support material and immobilization methods. **Figure 2.4** illustrates their correlations and their contributions to generating ideal enzyme-immobilized materials, which have properties including well-functioning enzyme molecules, good affinity between enzyme and the support that enables enzyme longevity and a reduced or eliminated mass transfer barrier for catalytic performance of the integrated material. With these considerations in mind, common immobilization methods and support materials presented in the literature are reviewed in the following sections with their pros and cons in achieving high relative enzyme performance and enzyme longevity.

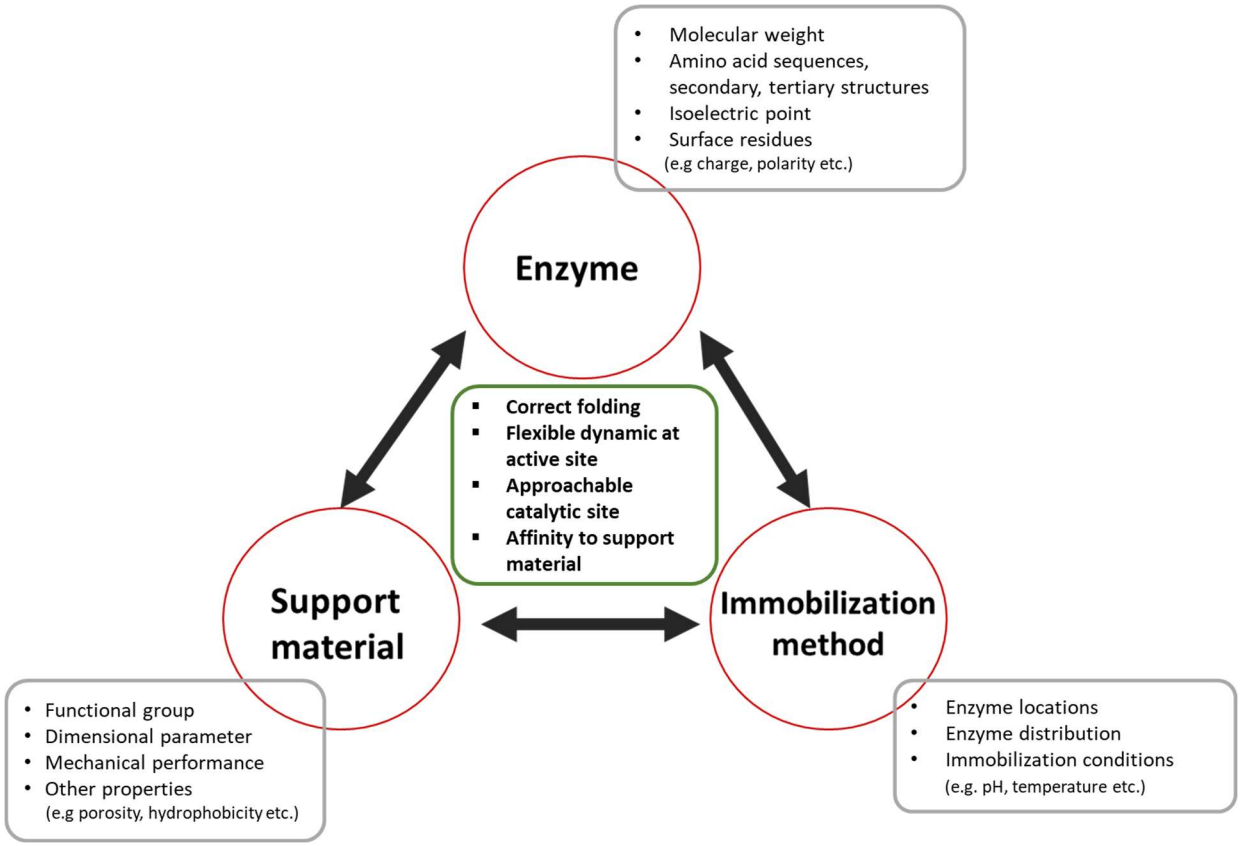

Figure 2.4 Interrelationships between enzymes, support materials and immobilization methods.

2.2 Methods of Enzyme Immobilization

As illustrated in **Figure 2.4**, the selection of immobilization method and the outcome of the immobilization can be affected by both the enzyme and the support material, but each specific immobilization method has its own pros and cons in terms of achieving high retained enzyme performance after immobilization and enzyme longevity.

In general, there are two major categories of methods used for immobilizing enzymes: attachment immobilization and incorporation immobilization (**Figure 2.5**). In attachment immobilizations, enzymes are immobilized onto/into support material after the material formation (e.g. solidification from melts), whereas enzymes are immobilized into the support along with the material formation (e.g. solvent evaporation, liposome assembly) by the incorporation method.

Attachment immobilization has been a dominating method among previous studies because enzymes can be immobilized at a mild condition in this method, without being exposed to harsh material fabrication conditions. The common procedure of attachment immobilization is to submerge or suspend neutral support materials in a buffer solution (pH 7) comprising enzymes. By this method, material that is fabricated from harsh conditions, such as extreme temperature or pH, organic solvent, UV radiation etc., can be used as the immobilization support (Akgöl et al., 2001; Gong et al., 2017; Yingshuai Liu & Yu, 2016). With this advantage, the attachment immobilization method allows support selections across a broad range of physiochemical properties (e.g. conductivity, shape).

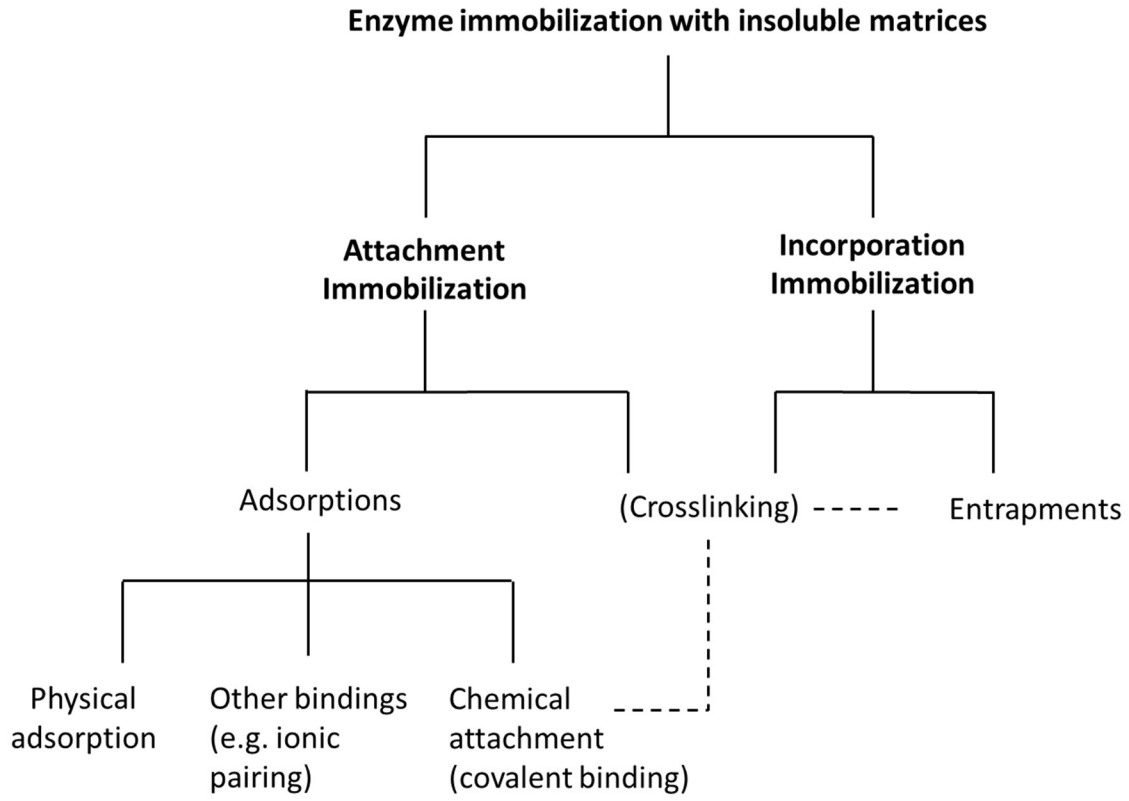

Figure 2.5 Categories of enzyme immobilization methods.

Among all the attachment immobilization methods, adsorbing enzyme to support surfaces through weak interactions, such as van der Waal (VDW) forces, electrostatic attractions, hydrogen bonds etc., is a straightforward one. Characteristics of enzyme molecules such as hydrophobicity of the side chains, charges on titratable side chains, and the distribution of these amino acids in the globular structure, enabling or facilitating these physical adsorption processes (Buchholz et al., 2012). These mild interactions between enzymes and support materials in physical adsorption are known for their advantages in preserving enzyme activity through maintaining the structural stability and flexibility of immobilized enzymes (Buchholz et al., 2012; Grigoras, 2017; Shuai et al., 2017; Z.-G. Wang et al., 2009). However, studies reported a large range (e.g. 48-78%) of retained activity ($\Delta A_{i\text{-}d}$) among physically adsorbed enzymes (Akgöl et al., 2001; Solas et al., 1994). In addition, when the surface is in contact with a liquid medium, desorption of immobilized enzyme molecules from the surface can easily happen through partitioning, diffusion, or conformational change (Buchholz et al., 2012; Cao, 2006). This accelerates enzyme leaching from the solid support, thus lowering the longevity of the immobilized enzyme. With regard to enzyme immobilization efficiency, physical adsorption can be slow with low yields (Ait Braham et al., 2018; Akgöl et al., 2001; Solas et al., 1994). Importantly, it was found that the over adsorption of enzyme on support surfaces had a reversed impact on relative enzyme performance, due to enzyme stacking or aggregation (Buchholz et al., 2012; Cao, 2006). Therefore, while the physical adsorption method is a versatile and gentle attachment immobilization method, the efficiency of immobilization and longevity of the immobilized enzymes are major concerns when developing long-term biocatalytic materials to catalyze reactions in a liquid medium. However, possible desorption of immobilized enzyme may not be an issue for applications such as gas phase sensors (Debeche et al., 2005) or paper-based disposal sensors (Böhm et al., 2018). Reversible

immobilization also has advantages in designing therapeutic enzyme delivery system, from which the enzyme molecules can be released into the medium in a controlled manner (e.g. pH or salt concentration). Notably, pH is a criteria in most attachment immobilization cases, in order to achieve an ideal enzyme loading (Akgöl et al., 2001), adsorption rate (Ait Braham et al., 2018) and/or the orientation of enzyme molecules on surface after immobilization (da Natividade Schöffer et al., 2017; Yingshuai Liu & Yu, 2016). For example, enzyme activity can be varied by immobilization pH by 2 to 4 folds in a previous study (Ait Braham et al., 2018). Also, the pH of an enzyme solution affects the protonation/deprotonation of amino acid side chains as well as the overall charge of the enzyme molecule, which are responsible for the interaction between the enzyme and support (Akgöl et al., 2001) .

Another attachment immobilization method is chemical adsorption, or chemical attachment, which has been considered a "standard" method for immobilizing enzymes. In this method, functional groups in enzyme molecules, usually the reactive end groups on amino acid side chains, interact with the functional groups or moieties on a support to form covalent bonds. For support materials with inherent reactive functional groups, enzyme can be attached to the support with the presence of catalysts and suitable conditions, while for materials without reactive groups, pre-functionalization is required to introduce necessary end groups or moieties by chemical reaction, plasma treatment, or radiation treatment etc. (Edwards et al., 2011; Shikha et al., 2017; Sulaiman et al., 2017; Vinoba et al., 2011). Chemical attachment provides robust linkages between enzymes and support, resulting in improved longevity by preventing enzyme leaching from the support. However, earlier research has found that the direct covalent interactions between enzymes and the support can cause conformational change of enzymes, which leads to unexpected unfolding or partial unfolding of enzymes (Buchholz et al., 2012; Cao, 2005). Later

on, it has been elucidated that the distance between the covalently immobilized enzyme molecule and the support surface is critical for structural stability of immobilized enzymes (Buchholz et al., 2012; Yuhong Wang & Hsieh, 2004). Therefore, much previous research effort has focused on in controlling spatial distance between enzyme and support surfaces using crosslinking agents, in order to obtain positive immobilization outcomes.

Crosslinking (**Figure 2.5**) has been used as an independent immobilization method for carrier-free immobilized enzyme (Cao et al., 2003; Migneault et al., 2004; Velasco-Lozano et al., 2016) or as assisted method to enhance stability of immobilized enzyme and to prevent enzyme leaching (Çetinus & Öztop, 2003; Tang et al., 2014). With at least two reactive functional groups in the structure, crosslinking agents can joint soluble enzyme molecules together to form insoluble enzyme complexes, allowing the recovery of biocatalysts from liquid media.

In addition to the drawbacks of enzyme leaching in physical adsorption and enzyme inactivation in chemical adsorption, a shared limitation within attachment immobilizations methods is that the total enzyme that can be effectively immobilized on the support is restricted to the available surface area and accessible functional groups. Therefore, nanomaterials with extremely large surface area have gained research interests as immobilization supports in recent years (Altinkaynak et al., 2016; Canbolat et al., 2017; J. B. Costa et al., 2019; Doğaç et al., 2017; Fu et al., 2015; J. H. Kim et al., 2017; X. Liu et al., 2018; Shuai et al., 2017; Sulaiman et al., 2015, 2017; Vinoba et al., 2012; Yuanming Wang et al., 2015; Weiser et al., 2016; Y. Yang et al., 2014). As an alternative, incorporation immobilization, or the entrapment method, offers the opportunity to achieve high mass fraction of enzyme from simple procedures, provided that the conditions employed are compatible.

During incorporation immobilization, enzyme immobilization happens simultaneously with material formation. Therefore, either a mild material fabrication procedure or a robust enzyme is required when using this method. This extensively restricts the selection of support materials. Silica or silica-based particles have been studied as enzyme incorporation matrices through sol-gel methods (Cui et al., 2018; Gupta & Chaudhury, 2007). Water-soluble polymers are preferred when entrapping enzymes into the polymeric support (Bankeeree et al., 2016; Bilal et al., 2017; Doğaç et al., 2017; Grigoras, 2017; Kobayashi et al., 1987; Yadav et al., 2012). However, a limitation with water-soluble polymers is the undesired poor enzyme longevity due to enzyme leaching over time when using these materials in a liquid medium. To overcome this problem, crosslinking agents have been used to reduce the pore size of gel networks with enzyme entrapped (Bankeeree et al., 2016; Y.-T. Zhang et al., 2009, 2010). Entrapped enzymes show higher pH and thermal stability according to the literature (Bankeeree et al., 2016), and the presences of macromolecules can protect the enzyme from conditional fluctuation (Kuznetsova et al., 2014). Lower relative enzyme performance as compared with free enzymes and surface immobilized enzymes was observed for immobilizations by entrapment, due to mass transfer barriers that depend on the localization of the entrapped enzymes. To reduce the influences of mass transfer, efforts have been made to increase the internal surface area of the matrix (e.g. porous support) (Akermin, 2013; Y. Wang & Hsieh, 2008) and to control the localization of entrapped enzymes (e.g. core-shell support) (Ulu et al., 2018; Yu Zhang et al., 2019). With regard to the potential for scaling up the biocatalytic materials, enzyme entrapment is an advantageous approach, which can simplify procedures for immobilization (Salmon & Yuan, 2020) and reduce utilization of chemicals. As another benefit, entrapped enzymes have been used as flexible coatings in fabrication of novel biocatalytic materials (Asakura et al., 1992; Drevon et al., 2003). Flexible

sensors were fabricated by entrapping glucose oxidase in structural protein networks, before coating them onto flexible nonwoven materials, from which the immobilized enzymes exhibited higher stability in pH fluctuation by more than 1 unit further toward acidic or alkaline pH (Asakura et al., 1992).

Each different immobilization method has advantages and disadvantages for fabricating efficient biocatalytic materials with high catalytic performance and enzyme longevity. Attachment immobilization is the most frequently used method for enzyme immobilization, due to its allowance for using various matrix materials to immobilize enzymes. However, immobilization recipes (e.g. chemical reactions, conditions) developed and reported by using this method are very specific to the model enzyme and selected support. On the contrary, the enzyme incorporation method has the potential of bringing the immobilization from case-by-case studies to a more versatile technique, although its limitations are centered on the composition and processing of the support material and in reaction mass transfer efficiency of the immobilized material in the application. Therefore, the important research questions for the entrapment immobilization method are how to prevent enzyme leaching from the matrix as well as how to reduce the mass transfer barrier. Crosslinking agents have been used to alter the pore size in support materials to prevent enzyme leaching, and has also been widely used in attachment immobilization methods to reduce enzyme inactivation. Therefore, cross-linking could be an approach to improve entrapment performance, if needed. Moreover, to maintain the enzyme catalytic function after immobilization, published biocatalytic materials, especially the post chemical attachment, require sophisticated fabrication steps with numerous chemical reaction steps, some of which are toxic and all of which introduce higher costs. Therefore, gaps do exist between laboratory prototypes and what is needed to produce commercialized products for industrial applications. Importantly, the selection of

immobilization method is closely related to the properties and processing of the support materials (**Figure 2.4**). Therefore, support materials that have been used in enzyme immobilization are reviewed in the next section.

2.3 Materials in Enzyme Immobilizations

Previous review articles summarized the evolution of enzyme immobilization from its underdeveloped period in earlier 1960s to the past decade (Buchholz et al., 2012; Cao, 2006). Interesting support materials have been broadly evaluated from inorganic substrates such as glass and carbon to advanced nanoscale composites and flexible soft matter. A recent review by Zdarta et al. (Zdarta et al., 2018) indicated main features of these support materials, including stability, insolubility, high affinity to enzymes, biocompatibility, presence of reactive functional groups, availability and reusability. Recent discoveries in material research also inspired tests for adopting these novel materials for enzyme immobilization. Previous work reports distinct immobilization recipes and the geometrical parameters (e.g. shape, size) of the supports across broad ranges, however, the fundamental basis for these immobilization studies shared similarities in the chemical functional groups and moieties involved in the immobilizations.

"Carrier-free" enzyme immobilization has been used to produce insoluble enzyme complexes through crosslinking (Cao et al., 2003; R A Sheldon, 2007; Velasco-Lozano et al., 2016). In this immobilization method, enzyme molecules are joined together through interactions between reactive side chains in amino acids (e.g. amine group in glutamine or asparagine) and reactive functional groups in crosslinking reagents (e.g. glutaraldehyde) (Migneault et al., 2004) . As mentioned above, attachment immobilizations have broad selections in support materials, and the immobilization outcomes depended on the chemical nature of the support and enzymes.

Functional groups on these supports are essential for getting a good immobilization outcome through potential enzyme-matrix interactions (Bankeeree et al., 2016; Gupta & Chaudhury, 2007; Kobayashi et al., 1987; Yadav et al., 2012). Therefore, functional groups involved in enzyme immobilizations are reviewed. Considering the impact of support materials on overall catalytic performance, an illustration of common supports with different geometrical forms that have been used in recent immobilization studies, along with their contributions to the retained catalytic performance after immobilization and enzyme longevity is presented. Due to the abundance of functional groups in polymer structures, polymers used in enzyme immobilization as well as polymeric fibrous supports for immobilization are reviewed.

2.3.1 Functional groups

Reactive functional groups (e.g. $–NH_2$, –OH, –SH, C=O, –COOH) are essential for some immobilizations and are critical in achieving good enzyme performance and enzyme longevity. Considering enzyme molecules, amine groups in lysine and arginine, carboxyl group in aspartic acid and glutamic acids, imidazole group in histidine, and reactive thiol group in cysteine are potential sites for immobilization events.

The amine group (e.g. $-NH_2$) is one of the most commonly seen functional groups in enzyme immobilization, especially for post chemical attachments. Primary and secondary amine groups and amide groups are also abundant in protein structures (e.g. N-terminal amine, side chain amine, amide in peptide bond). In these structures, electron rich nitrogen atoms can act as nucleophiles to make new covalent bonds for immobilization. At low pH, free amine groups in protein structures can be positively charged, allowing for ionic pairing with negatively charged functional groups on the support. Materials with intrinsic amine groups on the surface have been used for enzyme immobilization support (Grigoras, 2017; Krajewska, 2004), while studies

introducing amine groups to support material surfaces by chemical reactions, as pre-steps for enzyme immobilization have also been reported (Arola et al., 2012; Bulmuş et al., 1997; S. H. Lee et al., 2018; Magne et al., 2002; Shikha et al., 2017; Song et al., 2017). Bagheri *et al.* utilized spherical dendrimers with multiple amine end groups to covalently attach enzymes to a film surface, elucidating the critical roles of this functional group in achieving a robust immobilization and mechanism of covalent immobilization through the amine functional group (Bagheri et al., 2007). The study also found that the number of available amine groups on the support does not have a linear relationship with the specific activity of the immobilized enzymes, suggesting that excessive functional groups on the support material may have reverse influence on immobilization outcomes (Bagheri et al., 2007). In addition, reduced enzyme activity was observed within some immobilizations, which is attributed to the unexpected conformational change of multisite attached enzymes (Bagheri et al., 2007).

Oxygen containing functional groups, such as hydroxide group (-OH) and carbonyl group (R-CO-R') (David T Arazawa et al., 2012; Chiou & Wu, 2004) have been considered as potential sites for enzyme immobilization. Some studies introduced amine groups through the hydroxyl groups on the surface to create support materials for enzyme immobilization (Arola et al., 2012; Baliyan et al., 2016; Böhm et al., 2018; Bulmuş et al., 1997). Methods such as oxidation (Baliyan et al., 2016; Bulmuş et al., 1997), other chemical activation (David T Arazawa et al., 2012; Kimmel et al., 2013) or plasma activation (S. H. Lee et al., 2018) have been used to active hydroxide groups before conducting immobilizations or introducing other functional groups. When using gel networks to entrap enzymes, hydroxyl groups have been used as the active sites in crosslinking the matrix, in order to prevent enzyme leaching by decreasing the pore size of the matrix (Bankeeree et al., 2016).

Thiol functional groups (-SH) have also been used for enzyme attachment immobilization. The interaction between the thiol group in cysteine and gold nanoparticles enables the formation of enzyme-gold conjugates for sensors (F. Liu et al., 2015). Because the abundance of cysteine is much lower than amine groups in typical enzyme structures, the presence of thiol groups allows for site-directed immobilization where the orientation of immobilized enzymes is under control. Gold particles with adsorbed human CA enzymes were subsequently attached to amine/thiol-functionalized porous silica beads (Vinoba et al., 2011) resulting in higher enzyme loading within supports that have hierarchical structures.

According to the literature, crosslinking agents have been used to introduce useful functional groups on support surfaces to achieve immobilization, or to avoid enzyme inactivation by adjusting the spatial distance between the immobilized enzyme and the surface. Some studies found that the length of "spacer" molecule impacts the enzyme performance as a result of immobilization. (Bulmuş et al., 1997; Cao, 2006)

Glutaraldehyde (GA) is the most common crosslinking agent for both carrier free enzyme immobilization and enzyme covalent attachments (Bulmuş et al., 1997; Dessouki et al., 2001; J. Kim et al., 2001; Migneault et al., 2004; Silva et al., 2007). However, it has been reported that the presence of GA can cause enzyme inactivation throughout the immobilization (Bagheri et al., 2007; Tong et al., 2008). Therefore, the ratio of GA to enzyme must be controlled, and kept at a low level (e.g. less than 0.5%) to avoid excessive enzyme inactivation. Recently, Braham *et al*. (Ait Braham et al., 2018) elucidated the mechanism of using GA to promote an energetically unfavored immobilization system, in which a slow intrinsic immobilization rate was observed (Ait Braham et al., 2018). In addition to GA, other crosslinking agents with desired functional groups,

such as silanes and cyanogen bromide, have been applied for enzyme immobilization based on the chemistry of the supports (David T Arazawa et al., 2012; Baliyan et al., 2016).

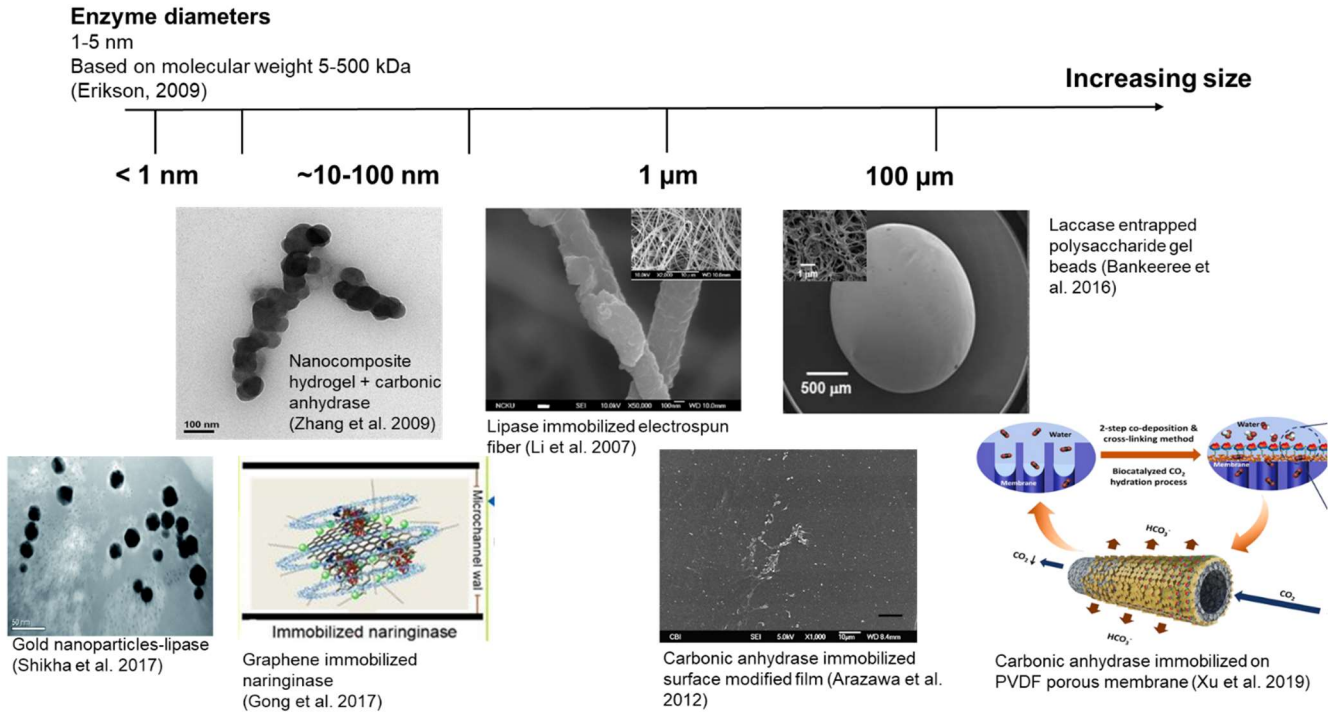

Figures 2.6 Support materials for enzyme immobilization with a size scale. (Images are respectively from Shikha *et al.* (Shikha et al., 2017), Zhang *et al.* (Y.-T. Zhang et al., 2009), Gong *et al.* (Gong et al., 2017), Li *et al.* (S.-F. Li et al., 2007), Arazawa *et al.* (David T Arazawa et al., 2012), Bankeeree *et al.* (Bankeeree et al., 2016), Xu *et al.* (Xu et al., 2019).

2.3.2 Geometrical shapes of support material in enzyme immobilization

Beyond shared characteristics in chemistry in the immobilization support, the size, shape, and other geometrical parameters of support materials also contribute to the efficiency as well as the outcomes of enzyme immobilization (**Figure 2.6**).

Solid materials in granular form have been widely used as immobilization supports. High potential surface area and ease of handling for certain type of packed bed and batch reactors are key reasons of using these granular supports. Two approaches give more advantages of using these

materials, by either introducing extremely small particle sizes, like nanoparticles (Fu et al., 2015; F. Liu et al., 2015; Shikha et al., 2017; Vinoba et al., 2012), or by having porous structure inside particles with larger size (Ispas et al., 2009; Vinoba et al., 2011). Depending on the physical/chemical properties and fabrication process of the material, either one of these two features or both have been employed in order to facilitate the immobilization outcomes.

Silica-based particles have been used as immobilization supports in either attachment immobilization or enzyme entrapment through sol-gel methods (Crosley & Yip, 2017; Cui et al., 2018; Hwang et al., 2004; Ispas et al., 2009; Lundqvist et al., 2004; Yong et al., 2015). To increase the enzyme loading, Vinoba and co-workers proposed a hierarchical composite support, where enzyme-adsorbed gold nanoparticles were covalently bound to mesoporous silica particles (Vinoba et al., 2011). Metallic nanoparticles are another commonly used granular immobilization support for research in which immobilized enzymes showed improved thermal (from 5 to 20 °C differences) and pH (with more than 1 unit toward more acidic or alkaline condition) stability (Fu et al., 2015; F. Liu et al., 2015; Shikha et al., 2017; Vinoba et al., 2012). In consideration of the harsh conditions (e.g. solvents, pH) used for preparing nanoparticles, post attachment immobilization is preferable to immobilize enzymes on these inorganic particles.

Studies also advocate the use of polymeric microbeads (Bulmuş et al., 1997; Giovagnoli et al., 2004) and macroscale beads (Bankeeree et al., 2016) for enzyme immobilization because they can be made with intrinsic functional groups and some of these materials are readily available. Again, conditions needed for polymerization or solidification of these polymeric supports, such as pH, catalysts, solvents, or UV, could cause enzyme inactivation. Thus attachment immobilization methods are advantageous when using these support materials (Çetinus & Öztop, 2003; Masri et al., 1978). Polysaccharide beads that are precipitated from aqueous solution through mineralization

have been used as enzyme entrapment matrices, by which entrapped enzyme demonstrated improved thermal stability and retained over 65% activity after six catalytic cycles (Yadav et al., 2012). However, for these fragile and soft granular supports, additional mechanical support such as metal mesh or ceramic plate might be required for applications.

Therefore, granular, bead or microparticle shaped immobilization supports have a number of advantages and are good choices for certain applications where the reactor system is well-adapted to the particle shape and physical properties (e.g. hardness). However, in some applications, having a particulate immobilization format would not be the best choice for needed reactor system. In particular, particles may not be the best choice for an application requiring efficient gas-liquid contact. Also, the recovery of immobilized biocatalysts with a granular shape requires extra liquid-solid separation procedures, which increases the costs for industrial applications.

Two dimensional (2D) carbon based nanomaterial have been highlighted in recent reviews as enzyme immobilization supports (Altinkaynak et al., 2016; Shuai et al., 2017; Zdarta et al., 2018) in fabrications of bioactive electrochemical devices such as biofuel cells and sensors (Babadi et al., 2016; Yingshuai Liu & Yu, 2016). Some carbon-based materials require chemical modifications prior to the immobilization steps, in order to introduce surface functionalities for efficient immobilizations, while others can be directly used for immobilization, with their intrinsic reactive groups or moieties (Adeel et al., 2018; Gong et al., 2017). Graphene and its derivatives have been studied as enzyme immobilization supports (Adeel et al., 2018; Yan Zhang et al., 2013). These honeycomb-like, planar carbon sheets structures provide larger than 2300 m^2/g surface area (S. Zhang et al., 2020) for enzyme immobilization, and π - π bond stacks or functional groups on the sheet surface facilitate the interactions between enzyme and the support (Adeel et al., 2018).

Owing to the abundant nucleophilic groups on surface, such as epoxy, hydroxyl and carboxylic group, oxygenated graphene (GO) has been considered as an ideal support in attachment immobilizations of enzymes (Adeel et al., 2018; Gong et al., 2017; Yan Zhang et al., 2013). Covalently immobilized lipase on GO sheets exhibited up to 65% activity at 70 °C, demonstrating 10-fold higher thermal stability compared to dissolved enzyme (Hermanová et al., 2015), and GO particle immobilized ketose 3-epimerase showed improved rate of substrates conversion in sugar production (Dedania et al., 2017). The production of these 2D materials often requires concentrated acids or thermal reduction, which would cause inactivation of most enzymes. Thus, attachment immobilizations are preferred methods for these supports, where enzymes are immobilized to the supports from mild buffers.

High enzyme loading and improved enzyme stability have been addressed within the above carbon-based supports (Dedania et al., 2017; Hermanová et al., 2015) or hybrid support with nanostructures (Altinkaynak et al., 2016). However, similar to the granular immobilization supports, enzymes that are immobilized on these supports cannot be fixed at desired positions in liquid flows to avoid potential inactivation, and recycling of immobilized enzyme requires additional efforts. More recent work tried integrating enzyme immobilized nanoscale materials to a retrievable support, without obstructing their good properties as immobilization supports (J. B. Costa et al., 2019; Hou, Dong, et al., 2015).

Films (Bagheri et al., 2007; Çetinus & Öztop, 2000; Crosley & Yip, 2017; S. Lu et al., 2009; Tong et al., 2008), membranes (Akgöl et al., 2001; D. T. Arazawa et al., 2015; J. B. Costa et al., 2019; Fazel et al., 2016; Kimmel et al., 2013; S.-F. Li et al., 2007; X. Liu et al., 2018; Sulaiman et al., 2017; Y. Wang & Hsieh, 2008; Xu et al., 2019) and gel networks (Asakura et al., 1992; Gill & Ballesteros, 2000a, 2000b; Gupta & Chaudhury, 2007; Y.-T. Zhang et al., 2009,

2010) have been investigated as retrievable enzyme immobilization supports. For these three-dimensional (3D) supports, the accessibility of functional groups inside the support material could be a challenge when attachment immobilization is used. To resolve this problem, fibrous membranes with ultrafine fiber structures have extensively been investigated as enzyme immobilization supports (Chiou & Wu, 2004; S. He et al., 2017; S.-F. Li et al., 2007; Z.-G. Wang et al., 2006; J. Zhu & Sun, 2012). Later sections will review fibrous supports used as enzyme immobilization supports, along with their fabrication methods.

In addition to increasing the surface area for immobilization by introducing fine structures, an alternate solution is to entrap enzymes inside membranes. Water-soluble polymers (or polymers that can be dissolved in a mild pH, temperature, salt concentration etc.), or enzymes with solvent tolerance, have been used to form such membranes with entrapped enzymes (Dai et al., 2011; D. Li et al., 2019; Z.-G. Wang et al., 2009; Weiser et al., 2016). Among the existing membrane supports with enzyme entrapped, enhanced thermal (e.g. up to 373K) and pH stability (1 to 2 units) of enzymes are reported (Abdelrahim et al., 2017; Bagheri et al., 2007; G. J. Chen et al., 2012; Cui et al., 2018; Debeche et al., 2005; C. Lee et al., 2018; Nemestóthy et al., 2018; Turner et al., 2005). Swellable polymeric networks (e.g. hydrogel) with appropriate pore size have been used as enzyme entrapment supports, exhibiting desired enzyme stability along the enzyme longevity (Gill & Ballesteros, 2000a, 2000b). Of course, risk of creating mass transfer barriers is the challenge of using entrapped enzymes. The presence of entrapment matrices can inhibit the diffusion of catalytic substrates and products between medium and entrapped enzyme. In a limited study to address this problem, a thin layer of silk fibroin gel comprising enzyme was coated onto natural and synthesized polymeric textile supports (viscose rayon, poly-ethyleneterephthalate, nylon-6, and polypropylene) to reduce the mass transfer barriers (Asakura et al., 1992). The resulting

enzyme immobilized support gave a higher output signal as a glucose sensor, in comparison with thick gel membrane entrapment, due to the increased surface area of the fibrous support and improved diffusivity of the substrate in the thin layer. (Asakura et al., 1992) This result supports the idea of creating high surface area thin coatings as a way to overcome mass transfer barriers.

Each category of immobilization support materials has pros and cons with respects to the enzyme performance and enzyme longevity as a consequence of their chemistry and the geometry. Combinations of multiple support materials (e.g. at different geometric scales) could be the trend of fabricating future biocatalytic materials. With these combinations, advantages of one type of support can be integrated with another, resulting in hybrid materials that have characteristics of high surface area, functionality on the surface, capability of stabilizing enzymes, and ease in recycling immobilized biocatalysts. Also, flexibility could be a very important property for these integrated biocatalytic materials, especially when using them in reactors with certain geometries. However, the flexibility aspect has only been addressed in a very limited way in previous immobilization studies. According to above demands, indeed polymers are promising materials for enzyme immobilization with their abundancy and processability. Polymeric materials with fibrous structure and mechanical strength (e.g. textiles) could be a good candidate for developing efficient enzyme immobilization supports. Therefore, recent enzyme immobilization developments in polymeric and polymeric fibrous materials are reviewed in the following sections.

2.4 Polymers in Enzyme Immobilization Studies

2.4.1 Synthetic polymer used as immobilization support

Synthetic polymers have been used to fabricate enzyme immobilization supports in forms of particles, films, membrane and fibers (An et al., 2015; Daneshfar et al., 2015; Han et al., 2011; Jia et al., 2002; D. Li et al., 2019; Z.-G. Wang et al., 2009; Xu et al., 2019; J. Zhu & Sun, 2012),

and synthetic oligomers have been used as crosslinkers to facilitate the attachment immobilization procedure (Bagheri et al., 2007; Canbolat et al., 2017; Yuhong Wang & Hsieh, 2004). One of the advantages of using synthetic polymers is the abundant and diverse functional groups possible in their structures and their processability (Buchholz et al., 2012; Virgen-Ortíz et al., 2017; Zdarta et al., 2018). The intrinsic properties (e.g. solubility, polarity, hydrophobicity) of the synthetic polymers are governed by the arrangement of the monomers, which indirectly influences the immobilization procedure as well as the immobilization outcome (Giovagnoli et al., 2004). An advantage of synthetic polymers is that the monomers can be polymerized in a designated manner, meaning, the interaction between enzymes and the support are controllable as a result of the polymer synthesis and immobilization. Other properties (e.g. permeability and degradability) also have impacts on the overall performance of enzyme immobilized materials when using them in applications, including the enzyme performance and enzyme longevity. For instance, hydrophobic synthetic polymers have been preferred in fabricating bioactive separation membranes for carbon dioxide scrubbing, due to facilitated gas permeation by the hydrophobic nature of the polymer (G. Chen et al., 2018; Hou, Dong, et al., 2015; Xu et al., 2019). Considering material availability, some synthetic polymers are widely available and relatively inexpensive, however polymers with specialized chemical functionality or physical properties can become costly to produce and the after-use disposal of these materials can cause negative influences in the environment.

As an alternative, biodegradable synthetic polymers have been used as enzyme immobilization supports for certain specialized (pharmaceutical) applications. These degradable polymeric materials comprising enzymes have been used to deliver reversibly immobilized protein molecules at targeted locations by desorption, or to release encapsulated enzymes to the medium throughout the degradation of the matrix (S A Costa et al., 2005). Giovagnoli *et al.* encapsulated

superoxide dismutase (SOD) and catalase (CAT) in microspheres made of poly (D,L-lactide-co-glycolide) (PLGA) and poly(D,L-lactide) (PLA), in order delivery these antioxidants *in vivo* (Giovagnoli et al., 2004). Owing to the hydrophilicity of PLGA segments, and by manipulating the ratio of PLA and PLGA segments, high enzyme loading was achieved for long-term treatment of inflammatory manifestations (Giovagnoli et al., 2004).

Most petroleum based synthetic polymers need to be either melt processed or processed in organic solvent to form materials with desired geometries. Thus, attachment immobilization is preferable when using these polymers. For instance, urease has been immobilized onto polyacrylonitrile (PAN) membranes from phosphate buffer, forming bioactive urea hydrolysis material with reusability (Daneshfar et al., 2015). With advantage of dissolving in mild condition, water-soluble synthetic polymers (e.g. polyvinyl alcohol, polyethylene oxide) are more often being used for enzyme entrapment, followed by additional crosslinking steps to tune the solubility of matrices comprising enzymes (Y. Wang & Hsieh, 2008; Weiser et al., 2016). Another study investigated the immobilization of laccase into poly(ε-caprolactone) (PCL) nanofibers from organic solvents with and without cyclodextrin (Canbolat et al., 2017). When enzymes were entrapped together with γ-cyclodextrin or the pre-made enzyme-cyclodextrin inclusion compounds were used for enzyme entrapment, the specific activity of immobilized laccase had 3 to 9 fold increases compared with that of directly entrapped bare laccase from the organic solvents in PCL fiber formation, however, the cause of these immobilization outcomes remains unclear.

2.4.2 Natural polymer used as immobilization support

Polymers from renewable sources have attracted research interests as sustainable alternatives to petroleum-based chemicals in many emerging research areas including enzyme immobilization (Arola et al., 2012; Asakura et al., 1992; J. H. Kim et al., 2017; X. Liu et al., 2018;

Yue Liu & Chen, 2016). In addition to their biodegradability, natural polymers have high affinity, or compatibility, with enzyme molecules. Having good biocompatibility is required to fabricate bioactive materials for biomedical purposes, and it was found that the biocompatibility of support materials could also stabilize the enzymes throughout the immobilization. Membranes made of structural protein have been used to immobilize glycerol dehydrogenase and diaphorase in sensor assemblies, by which the triglycerides in serum can be detected at relatively low concentration ranges in a short time (Winartasaputra et al., 1982). A recent study used polypeptide chains as additives to stabilize covalently immobilized enzyme on polymeric fibers, by which higher relative enzyme performance was observed at lower enzyme loadings (X. Liu et al., 2018). Silk fibroin has also been used to stabilize entrapped enzymes in developing novel materials and devices (Asakura et al., 1992; S. Lu et al., 2009).

Besides proteins that are used as enzyme immobilization supports or cofactors, polysaccharides, such as cellulosic materials, chitosan and chitin, alginate, and agarose, have been applied as biobased supports for immobilizing enzymes. Polysaccharide matrices have irregular porous morphologies, which enhance the internal surface area for higher enzyme loading (Buchholz et al., 2012). Owing to the abundant hydrophilic groups in the structure of polysaccharides, such as hydroxyl, amine and carboxyl groups, enzymes can be incorporated into the matrices with rather less inactivation. For instance, agarose obtained from seaweeds has been used to produce highly porous and mechanically resistant matrices for enzyme immobilization, and the pore size of matrices are adjusted by agarose concentration and crosslinking agents (Zdarta et al., 2018; Zucca et al., 2016). Using polysaccharides to immobilize enzymes offers opportunities for reusing industrial biomass. For example, xylan, a plant-based polysaccharide from pulp wastes, was used to entrap laccase for a dye decolorization process (Bankeeree et al., 2016).

Cellulosic material (**Figure 2.7**, a) has been a good candidate for immobilizing enzymes, including cellulose nanocrystals (Arola et al., 2012), bacterial cellulose (J. H. Kim et al., 2017; Sampaio et al., 2016), regenerated cellulosic materials (Yuhong Wang & Hsieh, 2004; C. Zhu et al., 2016), cellulosic paper (Böhm et al., 2018) and cellulosic fabrics (Magne et al., 2002). Attachment immobilization methods are preferred for this category of support materials, where enzymes are attached to the support surface through modified hydroxyl groups. Acetyl groups in cellulose acetate membrane were hydrolyzed to hydroxyl groups, to react with polyethylene glycol diacylchloride (ClOC-PEG-COCl) for immobilizing lipase (Yuhong Wang & Hsieh, 2004). Arola and co-workers utilized epoxy, amine and carboxylic functionalized nanocellulosic materials to attach alkaline phosphatase through covalent bonds, from which enhanced enzyme stability was observed (Arola et al., 2012). Recently, Böhm et al. reported a prototype chromatic paper-based microfluidic sensor with post immobilized glucose oxidase and peroxidase, which exhibits efficient glucose detection through an enzymatic cascade reaction (Böhm et al., 2018).

Due to the strong acidic or alkaline conditions used for solution processing of cellulosic materials, using cellulosic materials to entrap enzymes could be challenging. Emerging research in ionic liquids (Ils), including its applications in polysaccharides processing (L. Li et al., 2012; Pinkert et al., 2009; Shamshina et al., 2018) and its potentials for enzyme immobilization (Bagheri et al., 2007; C. Lee et al., 2018; Nemestóthy et al., 2018), provides insights for using new approaches to entrap enzymes into cellulosic materials. In a recent study by Lee *et al.*, entrapped lipase in cellulosic beads with the presence of ILs showed enhanced enzyme thermal stability at 65 ℃ (compared to 50 ℃ optimized condition of dissolved enzyme) and longevity (>700 hours) in a gas-phase catalytic bed for esterification (C. Lee et al., 2018). In addition to the ILs, fusion

proteins provide opportunities to enhance enzyme entrapment in cellulosic materials (e.g. carbohydrate binding domains) (Shoseyov et al., 2006).

Chitosan (**Figure 2.7**, b) is an extensively studied and remarkably versatile polysaccharide, having antimicrobial (Z. Hu & Gänzle, 2019), wound healing (Hamedi et al., 2018; Patrulea et al., 2015) and chelation (Pestov & Bratskaya, 2016) properties with broad applications in the food industry (Mujtaba et al., 2019; Singh, 2016), agriculture (Xing et al., 2015), biomedicine (Khan & Mujahid, 2019; Miguel et al., 2019) and environmental quality (Nangia et al., 2018; Pakdel & Peighambardoust, 2018). With renewable and abundant resources, this biopolymer is being considered as a sustainable polymer for enzyme immobilization (Krajewska, 2004). This aminopolysaccharide is produced at industrial scale by chemical hydrolysis of the *N*-acetylated parent polymer, chitin, which is abundantly found as a structural component in the mineralized exoskeletons of crustaceans, such as shrimp and crabs, and in the cell walls of fungi (Badawy & Rabea, 2011). Both chitin and chitosan are β-(1-4)-linked co-polymers of *N*-acetyl-D-glucosamine and D-glucosamine because some *N*-deacetylation occurs through natural biological processes and because chemical *N*-acetylation can be incomplete in biological systems. The distinction between these two polymers is empirically based on their solubility characteristics (Kasaai, 2009). Chitosan has a higher than 50% degree of deacetylation (DD), and is soluble in dilute acids through protonation of free amine groups located at the C2 position of sugar residues along the polymer chain, unlike chitin which is insoluble in most solvents due to extensive hydrogen bonding (Deringer et al., 2016). Additionally, the presence of free amine groups makes selective chemical modifications possible (Hoven et al., 2007), providing remarkable advantages in using chitosan as an enzyme immobilization support (Biró et al., 2008; Krajewska, 2004; Taqieddin & Amiji,

2004), a polycationic drug carrier (Criado-Gonzalez et al., 2019; Inphonlek et al., 2020; Ortiz et al., 2018), for formation of functional surfaces (Hoven et al., 2007) and for many other purposes (Badawy & Rabea, 2011; Dodane & Vilivalam, 1998) where the specific interaction between chitosan and other molecules are of special interest.

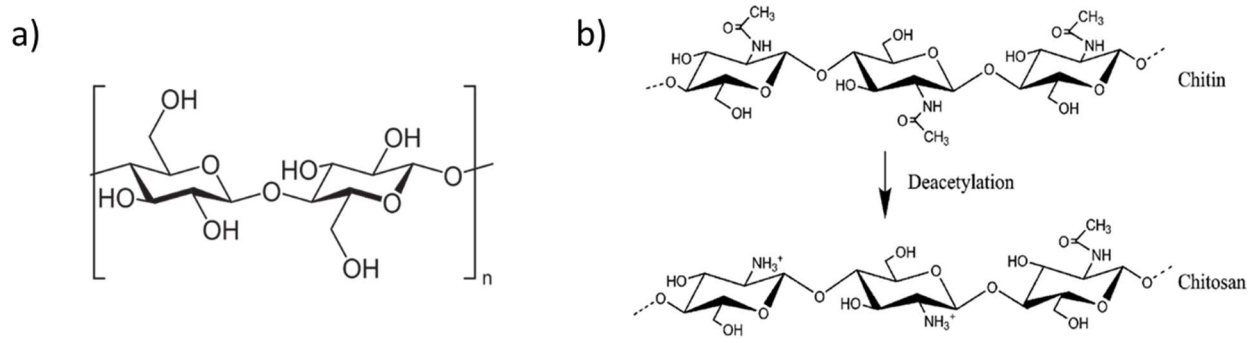

Figure 2.7 Chemical structures of a) cellulose and b) chitin/chitosan.

Chitosan is a polycationic molecule with a p*K*a around 6-6.5 (Chiappisi & Gradzielski, 2015). When the amine groups are uncharged, such as occurs upon exposure to an alkaline coagulation bath, the polymer becomes water-insoluble. Therefore, chitosan can be readily solution-processed using mild conditions, allowing it to be fabricated into many different forms, such as films, fibers, beads, coatings and gels (Anjum et al., 2016; Elsabee et al., 2012; Hamedi et al., 2018; Rani et al., 2010; Rathke & Hudson, 1994). However, the acidic conditions required to dissolve chitosan limits the selection of immobilization approaches due to the possibility of enzyme inactivation at low pH. On the other hand, the positively charged amine groups in chitosan at low pH conditions minimize leaching of physically adsorbed protein molecules through formation of ionic bonds with enzymes, and provides reactive sites for chemical attachment.(J. Liu et al., 2013; Mohamed et al., 2008) Therefore, attachment

immobilization has been the most commonly used immobilization method for chitosan support materials. (Çetinus & Öztop, 2000, 2003; Krajewska, 2004) In some limited studies, small amounts of chitosan were used as a "glue" to attach enzyme on other polymer or inorganic material surface (Huang et al., 2002), while in most cases, chitin and chitosan were used as physically independent supports for enzyme immobilization (Bilal et al., 2017; Krajewska, 2004; Pandey et al., 2017).

To fabricate chitosan supports for attachment immobilization, chitosan is solidified from acidic solution by coagulating in a strong alkaline bath, and the pH of chitosan supports are adjusted to neutral before immobilizing enzymes. (Grigoras, 2017; Pandey et al., 2017) In a recent work by Bilal *et al.*, peroxidase extracted from Horseradish root as a biocatalytic mixture survived the alkaline coagulation solution and was successfully entrapped into chitosan beads, showing higher stability in assisting a dye decolorization process (Bilal et al., 2017). Chitosan composite films comprising lysosome were fabricated for antibacterial surfaces against *E.coli*, where the immobilized enzymes are continuously released from the matrices (Park et al., 2004). Large amounts of glycerol were used to mediate the mixture of enzyme and chitosan acidic solution to entrap lysosome, although laccase is a less vulnerable enzyme at low pH. (Park et al., 2004) Therefore, retaining the activity of pH vulnerable enzymes after entrapping inside the chitosan has presented challenges.

To improve the immobilization outcomes, chitosan has been used in combinations with other polysaccharides with its cationic nature at lower pH. Positively charged chitosan was coated onto enzyme entrapped alginate beads through opposite charge attractions of these two polyelectrolytes (Simsek-Ege et al., 2002). Although chitosan is considered as an analogue of cellulose according to their chemical structure (**Figure 2.7**), and chitosan coated cellulosic

materials have been used as antimicrobial functional materials (Ali et al., 2017; X. D. Liu et al., 2001), the compatibility between these two polysaccharides has not yet been sufficiently explored or utilized for enzyme immobilization.

2.5 Polymeric Fibrous Support in Enzyme Immobilization

Fibrous materials by themselves have been utilized as functional materials in fields such as water purification, air filtration, wound dressings, or therapeutic implants; therefore, the additional biocatalytic function introduced by enzyme immobilization can broaden or facilitate the utilization of the fibrous material. As indicated earlier, advantages of using fibrous materials as the support are the increased surface area and material flexibility.

There are many ways to fabricate fibrous materials, and many of them can be scaled up with conventional or advanced textile and nonwoven industrial equipment. This could enable large-scale production of biocatalytic textile materials for industrial applications. Numerous fiber-forming precursors offer wide diversity in fibrous support materials for enzyme immobilizations. Inorganic fibers, synthetic polymeric fibers, fibers from natural resources, fiber spun from polymer blends with/without nanocomposites, etc. have been applied as immobilization support materials for lipase, glucose oxidase, peroxidase, laccase, urease, catalase, carbonic anhydrase, etc. (de Ruijter et al., 2006; Debeche et al., 2005; Doğaç et al., 2017; Fu et al., 2015; Han et al., 2011; S. He et al., 2017; D. Li et al., 2019; Pereira et al., 2016; Sulaiman et al., 2015; Weiser et al., 2016). Importantly, processing parameters in fiber formation govern the structural features of fibrous materials, such as the fiber diameter, porosity, and crystallinity, offering huge space to improve the relative enzyme performance and enzyme longevity. In the past decades, because interesting properties have been discovered with fibers that have nano- to submicron scale diameters,

electrospinning techniques which are capable of fabricating these fibers, and electrospun mats that are made of various polymers or inorganic compounds have been applied to many emerging research areas, including enzyme immobilization (Daneshfar et al., 2015; Doğaç et al., 2017; Fazel et al., 2016; D. Li et al., 2019; X. Liu et al., 2018; Oktay et al., 2015; Soares et al., 2018).

2.5.1 Attachment immobilization of enzymes to fibrous support

To utilize the large surface area and abundant functional groups on fibers, attachment immobilization has been prioritized in immobilizing enzyme to fibrous supports. The attachment immobilization method also allows broader selections in composition, dimension, morphology, and functionality of the support materials. With the attachment immobilization methods, fibers obtained from high temperature (e.g. melt extrusion) are able to immobilize thermally unstable enzymes, and enzymes with low tolerance to solvents can be post immobilized to fibers made from organic solvents.

Lipase has been physically adsorbed onto commercial inorganic glass fibers and carbon fibers, to catalyze gas phase esterification of ethyl acetate (Debeche et al., 2005). Compared to the classical catalysts bed, fibrous material exhibited superior performance in enhancing the gas flow rate and improving the mass transfer efficiency. To catalyze hydrolysis reactions in a liquid phase using immobilized enzymes, lipase has been covalently attached to polymeric electrospun webs. (Dai et al., 2011) Recently, Liu et al. utilized feather polypeptides as cofactors in preparing fibrous supports for lipase post covalent immobilizations, from which enhanced enzyme thermal stability was reported. (X. Liu et al., 2018) Moreover, by using electrospun collagen fibers that contain magnetic particles to post immobilize lipase, immobilized enzymes had one unit higher optimal pH compared to the dissolved enzymes (S. He et al., 2017). This study also demonstrated a rapid recycling process of the immobilized enzyme by applying a magnetic field (S. He et al., 2017).

This separation procedure provides new insights in developing novel, cost efficient methods to improve enzyme longevity for applications. In addition to the inorganic fibers, synthetic fibers and protein fibers, lipase has also been post-attached to modified cellulose fibers with assistance of oligomeric crosslinkers (Yuhong Wang & Hsieh, 2004).

Besides lipase, which is a model enzyme that has been used frequently to demonstrate novel immobilization methods, other enzymes such as glucose oxidase, laccase, carbonic anhydrase, peroxidase, have been post immobilized onto fibrous matrices to obtain functional materials such as hemostatic wound dressing materials (S A Costa et al., 2005; Edwards et al., 2011), antimicrobial surfaces (Kimmel et al., 2013; Sampaio et al., 2016), adhesion-reduced implants (D. T. Arazawa et al., 2015; Kimmel et al., 2013), gas scrubbing membranes (Hou, Dong, et al., 2015; Hou, Ji, et al., 2015; Yong et al., 2016).

Other than electrospun nanofibers, as-spun polymeric nonwoven textiles have been used as supports for immobilizing glucose oxidase, in fabrication of flexible glucose sensors. (Asakura et al., 1992) Amine functionalized woven PLA was applied for attachment immobilization of trypsin with the assistance of glutaraldehyde. The immobilized enzymes retained over 60% activity at 45 °C where dissolved enzymes had less than 35% activity. The pH stability of trypsin was also at a broader range (pH 4-6 and pH 12-13), where the dissolved enzymes were nearly all inactivated. In addition, reusability of the enzyme was reported as 30% retained activity after 15 catalytic cycles (Song et al., 2017). However, compared with electrospun fibers, studies in using woven and nonwoven fibrous supports to immobilize enzymes are limited. Traditional textiles, such as yarn and fabrics, have barely been studied as enzyme immobilization supports. Wool fabrics (protein-based) have been used to immobilize lysozyme. The purposes were to fabricate antibacterial fabric (Q. Wang et al., 2009) as well as to study the compatibility between enzyme and supports (J. Liu

et al., 2013). The retained catalytic performance after immobilization and improved enzyme longevity through immobilization was not reported.

According to the literature, most immobilizations of biomolecules on textiles are for biomedical applications (e.g. wound dressing), These applications can benefit from the advantages of large surface area, manipulatable chemical/physical properties, and flexibility of textile materials as the immobilization supports, however, the conditions of exposure in these applications are very different and mild (near neutral pH and near ambient temperature) compared to typical industrial processes. A recent study (Ali et al., 2017) reported remarkable potentials of using textiles (fabrics) in fabricating recyclable metallic catalysts, therefore, it is possible to use traditional textile supports for biocatalysts immobilization.

2.5.2 Incorporation immobilization of enzymes in fibrous supports

High temperature used in melt spinning limits the incorporation of most enzymes into melt-spun fibers; however, fibers spun from solutions (e.g. electrospinning, wet spinning, gel spinning) have the potentials for continuous enzyme entrapment during fiber formation.

Although electrospinning is a versatile method for ultrafine fiber formation, studies using this approach for enzyme entrapment are rare. This is because some polymers and fiber precursors require organic solvents or extreme pH to dissolve, which can cause enzyme inactivation. In recent work by Shamshina *et al.* (Shamshina et al., 2018), chitin-PLA fibers were made from ILs with desired mechanical properties. This offers opportunity of incorporating enzymes during the ultrafine fiber formation by using ILs (Abdelrahim et al., 2017; C. Lee et al., 2018). In addition to the uncertain solvent tolerance of enzymes, another unknown in using electrospinning to entrap enzyme is whether the electrostatic force, which is required for fiber formation, will inactive the enzyme.

Wet spinning has been extensively applied in industrial fiber productions and has potential for enzyme entrapment, however, only limited studies (Kobayashi et al., 1987) used this method for enzyme immobilization in alginate fiber. The entrapment yields of glucoamylase and pectinase in fiber are higher than those with polymer beads, and polymer chain alignment in the fiber structure prevents enzyme leaching (Kobayashi et al., 1987). In solution-based spinning techniques, the dissolved/suspended fiber precursors are solidified through non-solvent coagulation. The physical properties of the wet spun fiber, such as diameter, porosity, crystallinity, are governed by the strength of coagulant, coagulation time, lateral drawing forces and other factors. The challenges in entrapping enzymes in wet spun fibers are the compatibilities between enzyme and solvents/coagulants. Enzymes were entrapped in alginate wet spun fibers from aqueous solution followed by salt coagulation (Kobayashi, et al., 1987), which are relatively mild conditions for fiber formation as compared with other solvents or coagulants (e.g. organic solvents, strong acid, strong alkaline).

In summary, although enzymes have been used in textile industry for decades (Abadulla et al., 2000; Buchholz et al., 2012; Buschle-Diller et al., 2001), as sustainable solutions to reduce the chemical consumptions in apparel and textile manufacturing and to treat textile process effluents with the exception of limited studies (Ali et al., 2017; Wehrschütz-Sigl et al., 2010), using textile materials as enzyme immobilization matrices, and applying novel textile technologies to enzyme immobilization procedures is a new research field. In addition to material flexibility and good potentials for scaling up, the existing knowledge and research in functional textile materials can be utilized to improve the overall enzyme performance, and to inspire innovations in biocatalytic material fabrication. For instance, as further described in this dissertation, a textile (e.g. fabric, yarn) can act as a biocatalytic reactor to carry the catalytic substrate/products to a designated

immobilized enzyme through the wicking of the liquids comprising the substrate/products. Because the wicking profile of a textile is governed by its composition and structures, a biocatalytic reactor with controllable reaction rate can be designed based on knowledge thereof.

2.6 Characterization of Immobilized enzymes and Enzyme Immobilized Materials

Characterization of biocatalytic materials includes multiple aspects. Firstly, the biocatalytic function or performance of the material needs to be evaluated. Detectable enzyme activity in a material is straightforward evidence of the presence of the active enzymes, which can be measured by developing suitable assays for immobilized enzymes or the integrated biocatalytic material. Although enzyme structural stability is critical for enzyme activity, limited studies (Kienle et al., 2018; Mei et al., 2003) directly characterized this aspect of immobilized enzymes, due to the challenges in instruments and methods. However, results from general material characterizations (e.g. microscopy, spectroscopy) can be used as indirect evidence of the immobilization events. The overall properties of the integrated material are often reported, such as size, porosity, crystallinity, mechanical performance, as well as properties that are related to the applications, such as surface area and wettability. To optimize the immobilization approach for enzyme longevity in the application, studies also report the loading efficiency of enzyme, the stability of immobilized enzyme, the longevity of the immobilized enzyme, and changes in properties of the support material after immobilizing enzymes (Crosley & Yip, 2017).

2.6.1 Evaluations of the retained catalytic performance and enzyme longevity

High relative enzyme performance and enzyme longevity are two core goals in enzyme immobilization work. Other than comparing the analytical activity between the immobilized enzyme and soluble enzyme at optimal conditions, studies often compare the relative enzyme performance of immobilized enzyme with that of soluble enzyme at higher temperature (or

lower/higher pH, higher salt concentration). This is often reported as the improvement of enzyme thermal or pH stability introduced by immobilization (Dedania et al., 2017; Doğaç et al., 2017; Hermanová et al., 2015; J. Kim et al., 2001; Nemestóthy et al., 2018; Sampaio et al., 2016; Shikha et al., 2017; Tavares et al., 2015). Enzyme activity measurements can also be based on real applications responses. Therefore, bench-scale apparatus are designed to mimic the scenario in full-scale applications (David T Arazawa et al., 2012; Y. Zhu et al., 2016).

An important aspect of enzyme activity after immobilization that contributes to the retained catalytic performance of the biocatalytic material after enzyme immobilization is the mass fraction of enzyme in the material (**Figure 2.4**). To estimate the enzyme mass fraction on/in the support, total protein assays, such as BCA assay and Braford method, have been used to quantify the unbound enzymes in solutions after immobilization, and/or to measure the leached out enzymes in post washes. However, for some immobilization procedures (e.g. electrospinning entrapment), it is hard to accurately estimate the protein loss during the immobilization.

To measure the relative enzyme performance of biocatalytic materials in a liquid, the most common way described in literature is to simply dip or immerse the matrices into the solution comprising substrate and measure the concentration of product in the medium at predetermined time intervals (Dedania et al., 2017; Hermanová et al., 2015; J. Kim et al., 2001; Migliardini et al., 2014; Nemestóthy et al., 2018; Sampaio et al., 2016; Shikha et al., 2017; Tavares et al., 2015; Y. Zhu et al., 2016). To overcome the interference of mass transfer barrier when measuring the activity of immobilized enzyme, especially for entrapped enzymes, previous work applied vigorous mechanical mixings (e.g. rapid stirring) to facilitate the diffusion of products to the medium, without characterizing the biocatalytic materials afterwards (David T Arazawa et al., 2012). However, these mechanical forces may not always be possible in applications, or additional

costs are needed to achieve desired catalytic efficiency when used with the biocatalytic materials. In addition, continuous application of mechanical force might reduce the durability and longevity of the immobilized enzymes.

2.6.2 Generic instrumental characterizations for enzyme immobilized materials

Instrumental characterizations have been used to provide evidence of enzyme immobilization, as supplementary information to the detectable enzyme activities. Results from these instrumental analyses also provide information on the properties of the support materials.

Scanning Electron Microscopy (SEM) has been an extensively used characterization method for material surface morphologies analysis. Most SEM results in prior work showed the morphology of the overall matrices rather than showing immobilized enzymes, except for those with enzyme aggregations on the surface (Baliyan et al., 2016; Dai et al., 2011; S.-F. Li et al., 2007; Prabhu et al., 2009). This is because the enzyme sizes are at 1-5 nm (**Figure 2.8**) while the resolution of SEM is about 10 nm. Unfortunately, none of these works had additional information to prove the particles observed are enzyme aggregates rather than other compounds, such as could be present from materials used in sample preparation (e.g. salt crystals). In this case, the results from elemental analysis using Energy Dispersion Spectroscopy (EDS) as part of sample inspection by SEM could provide supportive data in proving the observed particles are enzymes. However, the technique may not work if the support has similar chemical components with enzyme (e.g. enzyme immobilized on proteins). In addition, SEM is a surface characterization tool with limited penetration from the sample surface, thus it may not be suitable for entrapped enzymes that are inside the matrices. Atomic Force Microscopy (AFM) has been used as a novel technique to visualize the post-immobilized enzymes on some supports (Arola et al., 2012; Bolibok et al., 2017;

Libertino et al., 2008). Arola *et al.* reported the 5-6 nm diameter of globular aggregated alkaline phosphatase on the nanocrystal surface with AFM characterization (Arola et al., 2012).

Additional spectroscopic methods have been used to give evidence of immobilization events with different probes, such as Fourier-Transfer Infrared Spectroscopy (FTIR) (Lv et al., 2015; Prabhu et al., 2009), X-ray photoelectron spectroscopy (XPS) (Libertino et al., 2008), and Raman spectroscopy (Ruan et al., 2006), by identifying the changes in bonding or chemical composition after immobilizations. However, the sensitivity or accuracy of these techniques could be limited to the immobilization method (e.g. enzymes localization) as well as the support materials (e.g. chemical compositions).

Only limited work has characterized the structural features of immobilized enzymes in matrices or on surfaces after immobilization, although structural stability (e.g. folding) of the enzyme has direct impacts on the enzyme activity. For dissolved enzymes in solutions, circular dichroism (CD) can be used to identify the secondary structure (Luo et al., 2009; Sreerama & Woody, 1993), providing structural information on protein folding status. Unfortunately, for enzymes that are immobilized on/in relatively large materials, rather than occurring as nanoparticles, this solution-based method is no longer suitable for characterizing their secondary structures. Scattering techniques have been used to provide structural information on the nanometer to micron length scale (Jung et al., 2009; Luo et al., 2009; Neylon, 2008). The large-scale structural data obtained from small angle scattering has been used to elucidate the molecular assembly and conformation of disordered proteins (or aggregates) with mathematical models. (Jung et al., 2009; Kikhney & Svergun, 2015; Neylon, 2008) Small angle neutron scattering (SANS) shows advantages in characterizing the structure of biological samples that are rich in hydrogen atoms, along with isotope labelling techniques. For instance, the end-to-end dimer

structure of gel-entrapped perdeuterated green fluorescent proteins (GFP) was elucidated by using SANS, in which 60% D_2O was used to match out the scattering signal from the silica gel. (Luo et al., 2009)

Overall, using combinations of various instrumental characterizations are necessary to understand the enzyme immobilization and enzyme immobilized materials thoroughly. The lack of systematic characterizations could be one of the reasons of why enzyme immobilizations studies are largely presented on a case-by-case basis. Compared with attachment immobilization at material surfaces, characterizing the enzymes that are incorporated inside the support is even more challenging. Fortunately, there are increasing developments of novel characterization methods in recent studies, such as neutron scattering with the phase-contrast variation technique, which could help better characterize these biocatalytic materials.

2.6.3 Characterization of material properties based on the applications

As indicated, enzyme immobilization research is driven by applications, therefore, both the catalytic performance and the overall properties of the biocatalytic materials are important. For bioactive biomedical devices, the biocompatibility and material durability in biological conditions need to be considered. For example, studies investigated the cell compatibility for tissue engineering and hemocompatibility for biocatalytic implants with enzyme immobilized. (D. T. Arazawa et al., 2015; David T Arazawa et al., 2012) Similar to the requirement for implantable biomedical devices, anti-fouling properties have huge impacts on the noise-to-signal ratio of enzyme immobilized sensors. (Gupta & Chaudhury, 2007) Also, when enzymes are entrapped in the polymeric matrix, they can act as impurities that disturb the crystallization of the polymeric material, thus reducing the mechanical performance of the integrated materials. (Asakura et al., 1992) For materials that have the same enzyme immobilized but with difference in applications,

the desired properties of the integrated material could be in opposite manners. For example, the immobilized CA has been used to develop both gas separation membrane and biomedical device, however, these two applications might require different surface properties. In CA assisted CO_2 separation membranes, hydrophobic polymeric support were preferred to facilitate the gas adsorption steps (Xu et al., 2019). On the contrary, Arazawa *et al.* found that hydrophilic hydroxyl group contributed to both the effective immobilization of carbonic anhydrase and the reduction of cell adhesion when using the bioactive membrane in blood dialysis (David T Arazawa et al., 2012).

2.7 Scopes and Objectives of This Doctoral Research

The ultimate goals of this doctoral research are to fabricate and investigate a novel, sustainable, efficient, durable, and scalable biocatalytic textile for industrial carbon dioxide (CO_2) gas scrubbing. To achieve these goals, methodologies in material fabrication and characterization will be developed based on knowledge from research fields of textiles, chemistry, and structural biochemistry. This project will generate new knowledge and improved understanding of the interrelated fundamentals of this interdisciplinary research area that covers fibrous materials, polymer science and biochemistry. By developing and studying such a versatile system with biocatalytic functionality, methodologies and procedures developed in this study can be adopted for broader applications of biocatalytic materials. Moreover, outcomes of this work will demonstrate the potential for fabricating traditional textile materials into novel functional materials that can expand opportunities for textiles utilization.

In initial work, suitable immobilization methods, materials, and characterizations for biocatalytic textiles were identified, and a functional preliminary candidate immobilization system using CAT as a model for demonstrating entrapped enzyme was established. Therefore, the first

objective of the continuing research was to evaluate and characterize the prototype system which included the mechanistic studies of the improved catalytic efficiency by introducing fibrous structure and using biocatalytic textile as a flow-through reactor. Because both the enzyme structural stability and mass transfer efficiency in the integrated biocatalytic textiles were expected to contribute to the retained activity after immobilization (apparent activity) we measured, part of the research was to produce a labeled matrix material, deuterated chitosan, for further structural studies. The final objective of this dissertation research was to fabricate and test CO_2 scrubbing textiles using this candidate immobilization system. Specifically, CA was immobilized on to cellulose fibrous support materials in which chitosan was used as a matrix for enzyme entrapment and the catalytic performance capability of this novel material was verified. Secondly, we further developed the prototype CO_2 scrubbing textiles by optimizing the immobilization composition, evaluating catalytic performance, and creating a suitable format for the reactor packing. In order to evaluate relative CA performance and CA longevity of the immobilized CA, appropriate assays were established for the catalyzed reaction that includes gas-liquid-solid in three phases. A custom designed lab-scale gas scrubbing reactor in Dr. Salmon's Lab was used to conduct application-based evaluations of the CA immobilized CO_2 scrubbing textiles. Well performing CO_2 scrubbing textiles from the lab-scale tests were further developed and tested and may be scaled up by using textile engineering techniques to provide sufficient materials for larger scale CO_2 scrubbing tests.

CHAPTER 3: PROTOTYPE BIOCATALYTIC YARN DEVELOPEMNT WITH CATALASE, MECHANISTIC STUDY OF IMMPROVED CATALYTIC FUNCTION AND APPLICATION

Part of this chapter was published in:

Yuan, Y.; Zhang, Y.; Bilheux, H.; Salmon, S. Biocatalytic Yarn for Peroxide Decomposition with Controlled Liquid Transport. *Adv. Mater. Interfaces* **2021**, *2002104*. (Yuan, Zhang, et al., 2021)

Salmon, S.; Yuan, Y. Chitosan Materials with Entrapped Enzyme and Biocatalytic Textiles and Other Biocatalytic Materials Comprising Same. US 20200276057, **2020**.

3.1 Catalase and catalase immobilization

Catalase (CAT) is a readily available, ultra-fast enzyme (turnover frequency of 1 to 4 $x10^7$ s^{-1} (Heck et al., 2010)) that catalyzes the decomposition of hydrogen peroxide, which is a toxic compound for living cells, to form water and oxygen ($2\ H_2O_2 \leftrightarrow H_2O + O_2\uparrow$) at moderate temperatures (Aebi, 1984; Grigoras, 2017; Miłek et al., 2014). Different CAT isozymes are found in nature, for example, bovine liver CAT is a tetramer made of 2024 amino acids and contains a heme group at each of the four catalytic sites (**Figure 3.1**). Soluble and immobilized catalase have been used in textile and food industries to remove residual peroxide in processing (e.g. cotton bleaching). A recent review (Grigoras, 2017) summarized the immobilization methods and support materials for CAT. The thermal or pH stability of CAT can be improved through immobilization (Cengiz et al., 2012; Çetinus & Öztop, 2000; Silgia A Costa et al., 2001; Grigoras, 2017; Pandey et al., 2017), however, when adsorbing CAT onto membrane surfaces, V_{max} , the reaction rate when enzyme is fully saturated by substrate, of the peroxide decomposition exhibits 2 to 24 folds decreases (Akgöl et al., 2001; Solas et al., 1994). This elucidates the fact that immobilization can reduce the relative enzyme performance at the

optimal condition compared with soluble enzyme due to creating mass transfer barriers. Therefore, reducing the mass transfer barrier for diffusion limited enzymes ($K_{cat} >> K_m$), such as CAT, in immobilization work is necessary. Also, CAT is a useful model for developing and exploring the performance of controlled liquid flow biocatalytic yarn systems in which mass transfer occurs among three reaction phases: immobilized enzyme (solid), dissolved hydrogen peroxide substrate (liquid), and evolved oxygen product (gas). The dimensions of catalase was reported around 6 × 10 nm (Mozaffar et al., 1986).

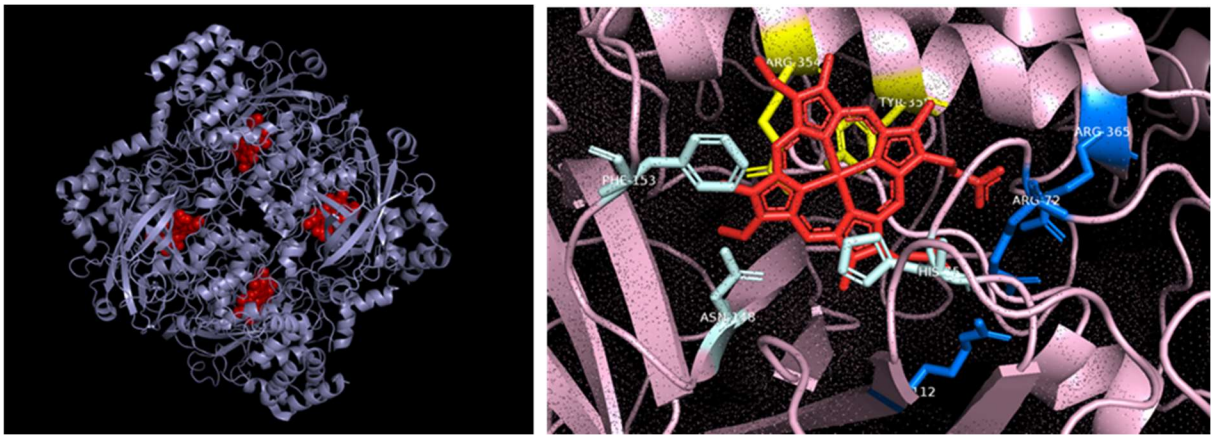

Figure 3.1 Structure and active site of bovine catalase (PDB:1TGU) drawn in PyMOL software (Schrödinger, NY)

3.2 Biocatalytic Yarn with Immobilized Catalase for Peroxide Decomposition

The present work introduces a straightforward approach for catalase immobilization by coating chitosan entrapped catalase onto cellulosic yarn resulting in a sustainable biocatalytic textile that is capable of simultaneous liquid transport and catalytic reaction.

Cotton yarn was chosen as the supporting structural component because it is an inexpensive, readily available material with high water absorption and wicking capacity (Hsieh, 1995; Kumar & Das, 2014) and because chitosan adheres well to cellulose (Myllytie et al.,

2009). Chitosan and cellulose can form composites with desirable chemical and physical properties used to fabricate antibacterial cotton textiles (Cheng et al., 2014; C.-E. Zhou & Kan, 2014), facilitate dye uptake by cotton textiles (Haji, 2017; Wijesena et al., 2015) and increase the strength and moisture barrier properties of paper products (Gatto et al., 2019; Kopacic et al., 2018). Recently, Ali *et al*. reported a method of using chitosan-coated cotton cloth to immobilize nanoscale inorganic catalysts by a sequence of adsorption and reduction to simplify catalyst recover (Ali et al., 2017). However, using chitosan coatings to immobilize enzymes on textiles is new. Because acidic conditions are normally used for dissolving chitosan and because enzymes may not tolerate low pH, the usual approach is to immobilize enzymes on the surface of chitosan materials after the chitosan has been fabricated into different forms by dissolution and resolidification (Çetinus & Öztop, 2000; Grigoras, 2017; Krajewska, 2004; Masri et al., 1978; Pandey et al., 2017). Therefore, as described herein, careful preparation of the chitosan solution makes it possible to dissolve chitosan at mild pH conditions that are compatible with enzymes. Furthermore, compared to submerged batch reactions presented in prior works, combining the liquid transporting functionality of a textile together with the catalytic functionality of an enzyme is also new. The biocatalytic yarn is easy to handle and withstands both extended dry storage and repeated washing. Neutron radiography and neutron computed tomography (M Parada et al., 2017) experiments revealed the path by which liquid transports though the biocatalytic yarn, providing a mechanistic basis for the favorable catalytic performance exhibited by this novel multifunctional material.

This study presents a novel demonstration of a biocatalytic textile as a self-contained continuous flow reactor. As indicated by the results, biocatalytic textiles can be used as unconfined materials in some applications, can be combined with supporting structures and

materials, or can be positioned inside reactor housings or wrappers, depending on the process objectives.

3.2.1 Materials

Shrimp shell chitosan powder with an average molecular weight of 10^7 g/mol was obtained from Primex (Iceland), and further deacetylated using hot sodium hydroxide (Salmon & Hudson, 1995) to a degree of deacetylation (DD) of 89%, measured by titration. Terminox® Ultra 50L catalase (TU-CAT), a liquid product containing fungal *Scytalidium thermophilum* catalase (Lončar & Fraaije, 2015; Miłek et al., 2014) was received from Novozymes A/S (Bagsvaerd, Denmark) and used as supplied. Glacial acetic acid, sodium acetate and 35% hydrogen peroxide solution were purchased from Fisher Scientific (Hampton, NH, USA). EMD Millipore™ MQuant™ Peroxide Test Strips (Fisher Scientific, Hampton, NH, USA) with a detection range of 0.5 to 25 mg/L H_2O_2, were used according to the package instructions. Triton™ X-100, a non-ionic liquid surfactant, was purchased from Sigma-Aldrich (St Louis, MO, USA). Pierce™ Rapid Gold BCA Protein Assay Kit (ThermoFisher Scientific, Waltham, MA, USA) was used to determine the enzyme concentration in liquids, where TU-CAT dilutions were used for the calibration curve rather than using the bovine serum albumin provided in the kit. SDS-PAGE gel electrophoresis was run using a Mini-PROTEAN Tetra Vertical Electrophoresis Cell (Bio-RAD, Hercules, CA) with Mini-PROTEAN TGX Stain-Free Protein Gels (Bio-RAD, Hercules, CA). All Blue Standards (Bio-RAD, Hercules, CA) were used to determine the molecular weight of catalase after Brilliant Blue (Fisher BioReagents, Hampton, NH, USA) staining. A 4-ply worsted Lily®Cotton cotton yarn (Spinrite LP, Listowel, ON), with a linear density of 0.665 (g/m), was purchased from a retail supplier and used as received.

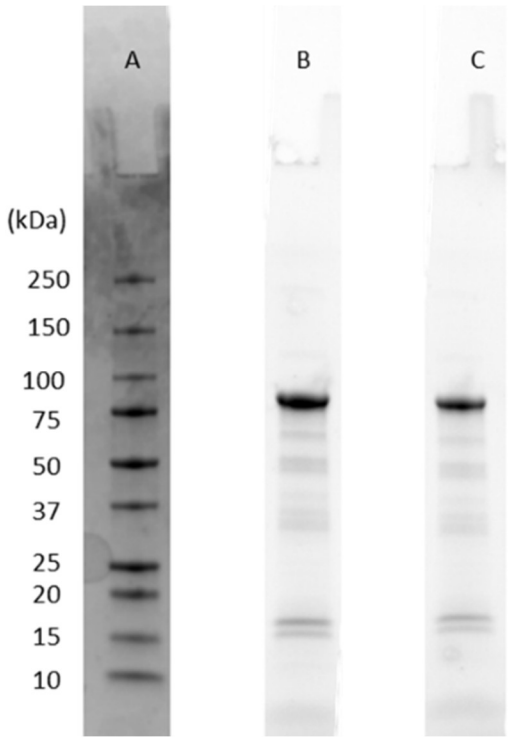

Figure 3.2 SDS-Page gel results of TU-CAT product. Column A is the stain free gel with molecular weight markers after staining with Brilliant Blue. Colum B and C are 4x and 8x dilutions of Terminox® Ultra 50L catalase, respectively, imaged directly from the stain free gel.

3.2.2 Preparation of Biocatalytic Yarns

Solutions containing enzyme and/or chitosan were applied to 4-ply cotton yarns by dip coating. Prior to dip coating, cotton yarns were cut into 40 cm lengths and pre-soaked in deionized (dI) water for two hours to wet the yarn, after which excess water was removed by squeezing along the length of the yarn. For the dip-coating procedure, pre-wetted yarns were submerged in different dip coating solutions for 4 hours before being air dried at ambient conditions for 12 hours. Table 1 lists sample descriptions and codes for the different dip coating treatments.

Chitosan solutions for dip coating were prepared at both acidic (pH 2.6) and acetate buffer (pH 5.0) conditions to evaluate the impact of immobilization process pH on physical and

biocatalytic performance. Chitosan powder was dissolved in 2% (v/v) acetic acid solution (pH 2.6) to form a 4% wt. viscous chitosan solution (Solution 1). A portion of chitosan Solution 1 was placed in a Teflon® tray in a ventilated fume hood to evaporate excess acetic acid, thus obtaining a chitosan-acetate film. Chitosan Solution 2 was prepared by redissolving the chitosan-acetate film at a concentration of 4% wt. in 100 mM sodium acetate solution (pH 5.0). Solution 1 was used for dip coating to prepare the Chi no-enzyme control sample, with a chitosan-to-cotton weight ratio of 3:7 (Equation 1) in the coating bath. Samples Chi-CAT(Ac) and Chi-CAT(NaAc), with catalase entrapped in the chitosan coatings, were prepared by pre-mixing catalase with either chitosan Solution 1 or chitosan Solution 2, respectively, at the weight ratio of enzyme-to-chitosan (E:Chi) reported in **Table 3.1** and calculated according to Equation 2. The solids content of TU-CAT solution, 0.76 % (w/w), was measured using a moisture analyzer (HC103, Mettler Toledo, Columbus, OH), and all solids were assumed to be catalase in the weight ratio calculations. In case of impurities, this assumption would lead to an over estimation of the amount of enzyme present in the tests. According to SDS-PAGE gel electrophorese (**Figure 3.2**), the liquid product contains relatively pure catalase protein, and the results concur with a molecular weight of around 320 kDa with four identical 80 kDa subunits (Sutay Kocabas et al., 2008). Prior to dip coating, dI water was added to each coating bath to reduce the chitosan solution viscosity from 6160 mPa·s to 520 mPa·s, measured by a rotational viscometer (DV-E, Brookfield, Middleboro, MA) at 22 °C. The weight ratio of the viscosity-adjusted coating solution-to-cotton yarn was kept at 12 g solution per gram dry yarn for all samples.

CAT (Ac), CAT (NaAc) and CAT (dI) samples were prepared as no-chitosan controls by dip coating cotton yarns with catalase diluted in 2% v/v acetic acid solution, 100 mM sodium acetate solution and dI water, respectively. The weight ratio of the enzyme-to-cotton (E:C) in the

coating bath for each sample was calculated using Equation 3 and is listed in Table 1. Pristine cotton yarn without any coating (Sample C), was included in the tests as a negative control.

Equation. 1

$$Chi{:}\,C\ ratio = \frac{Chitosan\ concentration\ in\ coating\ bath\ (\%) \times\ weight\ of\ coating\ bath}{Dry\ weights\ of\ cotton\ yarns\ in\ coating\ bath}$$

Equation. 2.

$$E{:}\,Chi\ ratio = \frac{Solid\ content\ of\ TU-CAT\ solution\ (\%) \times\ weight\ of\ TU-CAT\ solution}{Concentration\ of\ chitosan\ solution\ (\%) \times weight\ of\ chitosan\ solution}$$

Equation. 3.

$$E{:}\,C\ ratio = \frac{Solid\ content\ of\ TU-CAT\ solution\ (\%) \times\ weight\ of\ TU-CAT\ solution}{Dry\ weights\ of\ cotton\ yarns\ in\ coating\ bath}$$

Table 3.1 Sample codes and weight ratio of components in coating bath.

Sample code	Sample description	E:C*	E:Chi*
C	Pristine cotton yarn without coating	N/A	
Chi	Cotton yarn coated with chitosan Solution 1	N/A	
Chi-CAT (Ac)	Cotton yarn coated with chitosan Solution 1 containing TU-CAT	3:100	1:12.5
Chi-CAT (NaAc)	Cotton yarn coated with chitosan Solution 2 containing TU-CAT	3:100	1:12.5
CAT (Ac)	Cotton yarn coated with TU-CAT diluted in pH 2.6 acetic acidic solution	3:100	N/A
CAT (NaAc)	Cotton yarn coated with TU-CAT diluted in pH 5.0 sodium acetate solution	3:100	N/A
CAT (dI)	Cotton yarn coated with TU-CAT diluted in dI water	3:100	N/A

*E: C and E: Chi represent the enzyme: cotton yarn and enzyme: chitosan weight ratio, respectively.

3.3 General Description of the Samples and Material Characterizations

The dip coating approach used in these studies is a straightforward method in which dissolved coating compounds (chitosan, enzyme, or both) adsorb to the immobilization carrier (cotton yarn) and adhere to the carrier when solvent is removed, by drying. Coating durability depends on the affinity between the coating compounds and the carrier material, and on physical properties of the coating compounds themselves. Dry weight and moisture contents of samples were measured using a moisture analyzer. Samples and controls were placed at the same ambient conditions for at least 24 hours to reach equilibrium moisture content prior to measurement. For each yarn sample, approximately 1 gram of yarn, accurately weighed, was placed on a tared aluminum pan and heated at 110 °C until the change in weight was less than 0.01% per second. Moisture content was calculated as the percent difference between the initial and dry weight

relative to the initial weight, and was used to determine the corrected dry weight of yarn samples used in the flow and reaction studies. The dip coating method resulted in negligible change in the mass of the carrier material. The average weight of 40 cm pristine cotton yarn was about 266 mg ($\pm$5), and the weight gain after enzyme adsorption or chitosan-enzyme coating was not measurable due to the low enzyme to cotton weight ratio and because not all the chitosan in the dip coating bath adhered to the yarn during the soaking process. Therefore, other techniques than gravimetric methods were needed to confirm the presence of coating compounds on the cotton yarns. After drying, one direct observation was that the yarns coated with chitosan were stiffer than uncoated yarns, or than yarns only exposed to enzyme.

3.3.1 The presence of thin chitosan coating on the samples

A dye (Acid Orange 7, **Figure 3.3**) uptake experiment was conducted to show visual evidence of the presence of chitosan coating on the yarn, and to evaluate the durability of the chitosan coating. At mildly acidic and up to around neutral pH, solid chitosan will absorb acid dyes, such as Acid Orange 7, due to ionic attraction between protonated amines of chitosan and the anionic sulfonate group of the dye (Maghami & Roberts, 1988), however cotton will not. When amine groups of chitosan are thoroughly deprotonated by exposure to alkaline conditions, the affinity of anionic dyes for chitosan drops dramatically. To prove this, neutralized chitosan coated ("Chi yarn") samples were prepared for the Acid Orange 7 dye sorption test in order to support the statement that a thin chitosan coating with protonated amine groups on cotton yarn contributes to increased acid dye sorption. To neutralize the protonated amine groups in Chi sample, the yarn was immersed in 50 mL sodium bicarbonate solution (pH 9.5) for 10 minutes and air dried before the dye sorption test. Uncoated cotton yarn ("C yarn") was also treated at the same conditions for comparison. **Figure 3.4**, a-1 shows that Acid Orange 7 has low sorption on

cotton yarn alone. **Figure 3.4** a-2 shows that Acid Orange 7 has much lower affinity for $NaHCO_3$ treated Chi yarn compared to air dried Chi yarn. Therefore, the sorption of Acid Orange 7 can indicate the presence of chitosan on the cotton yarn when there are protonated amines in the chitosan.

Therefore, because yarns were air dried and not neutralized after dip coating, protonated amine dye sites were present in the chitosan coating and a higher dye uptake relative to the control indicates presence of chitosan on the yarn. In the experiment, a 10 cm yarn specimen (0.07 g) was placed in 10 mL 0.1 g/L Acid Orange 7 dye solution (pH 7.0) and the vial was incubated at 30 °C in a shaker with a speed of 100 rpm for 24 hours. The residual dye concentration in the vial after incubation was quantified by comparing with a calibration curve of absorbance *versus* dye concentration. The absorbance was measured using a spectrophotometer (Spark Microplate Reader, TECAN, USA) in a 96-well plate at a wavelength of 484 nm.

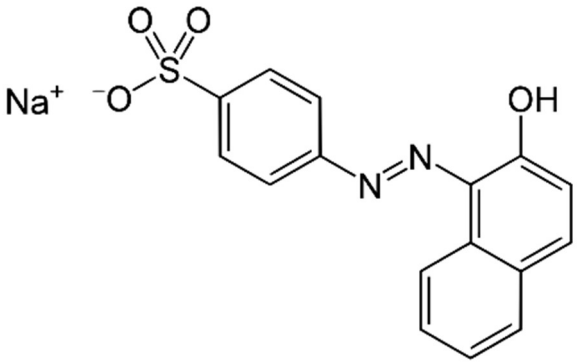

Figure 3.3 Chemical structure of Acid Orange 7, also called Acid Orange II (C.I. 15510).

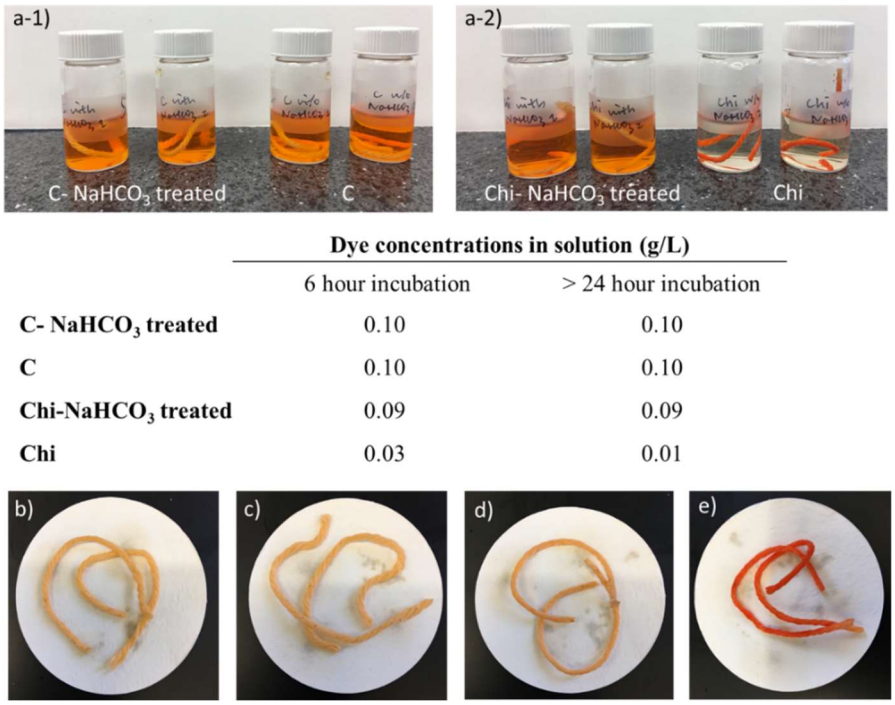

	Dye concentrations in solution (g/L)	
	6 hour incubation	> 24 hour incubation
C- $NaHCO_3$ treated	0.10	0.10
C	0.10	0.10
Chi-$NaHCO_3$ treated	0.09	0.09
Chi	0.03	0.01

Figure 3.4 Acid dye sorption experiments with neutralized Chi samples: a-1) dye solution with C yarn samples after 24 hours, a-2) dye solution with Chi yarn samples after 24 hours and yarn samples b) $NaHCO_3$ treated C yarn, c) C yarn, d) $NaHCO_3$ treated Chi yarn and e) Chi yarn after 24 hour dye sorption tests.

The presence of chitosan on the Chi, Chi-CAT(Ac) and Chi-CAT(NaAc) yarns was evident by the results of the Acid Orange 7 sorption test (**Figure 3.5**). After incubation, chitosan coated yarns adsorbed most of the dye in solution, thus yielding colorless solutions, while the dye concentrations in vials containing yarn without chitosan coating (pristine cotton yarn or yarns with physically adsorbed enzyme) remained unchanged (**Figure 3.5**). The strong dye adsorption on chitosan coated yarns implies that amine groups in chitosan are protonated, providing cationic sites that attract the anionic dye. Since chitosan was applied to cotton at a pH (~pH 5) less than the pKa of chitosan (~pH 6), amine groups along the chitosan polymer chains were protonated. This cationic property of chitosan contributes to electrostatic affinity for the

cellulose in cotton, which has a mild anionic character when immersed in water(Maurer, 2009; Myllytie et al., 2009; Sadeghi-Kiakhani & Safapour, 2015) due to multiple hydroxyl groups.

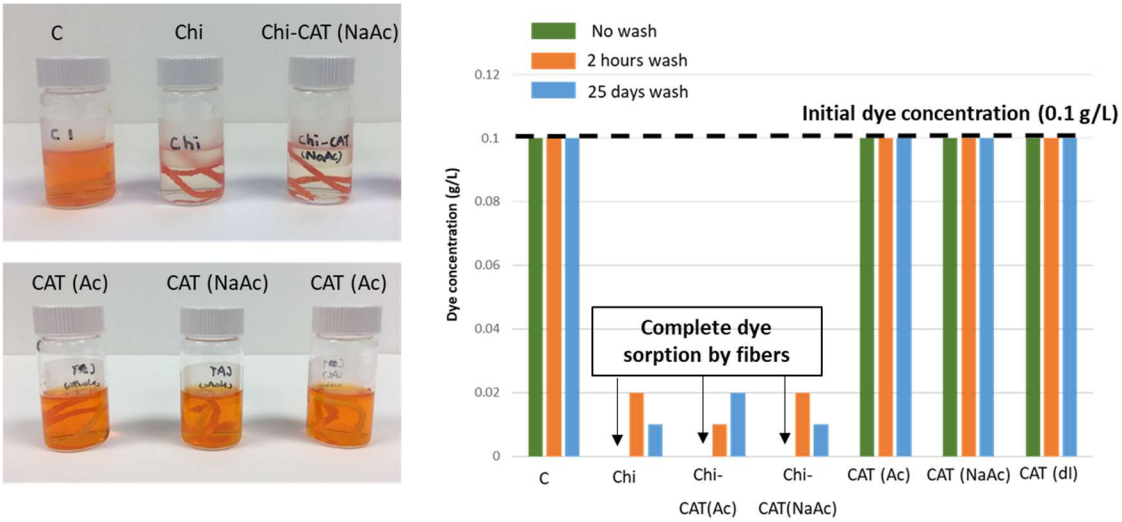

Figure 3.5 Acid Orange 7 dye sorption test for detecting chitosan coating on yarns: left) after incubating 10 cm yarn samples for 24 hours in 10 mL 0.1g/L dye solution; right) dye concentration in solution from comparing absorbance at 484 nm to a calibration curve.

Morphological features of samples and controls were imaged using scanning electron microscopy (SEM) (Verios, FEI, USA). Yarn samples were cut in liquid nitrogen and the yarn cross section was subjected to microscopic imaging. Images were analyzed using Image J software (NIH, USA) (Abràmoff et al., 2004; Schneider et al., 2012). Fiber morphologies of yarn samples before and after chitosan dip coating or enzyme adsorption are shown in **Figure 3.6**. Rather than forming a thick film on the yarn surface, chitosan adhered to cellulosic fibers as thin layers, retaining the hierarchical fibrous structure inside the yarn (**Figure 3.6**, b and c). The chitosan coating thickness, measured using Image J software from the cross section in **Figure 3.6**, b, was about 0.45 (± 0.18) µm. Yarn samples with physically adsorbed catalase have the

same morphology as pristine cotton yarn (C), without observable protein aggregation on the fiber surface (**Figure 3.6**, d).

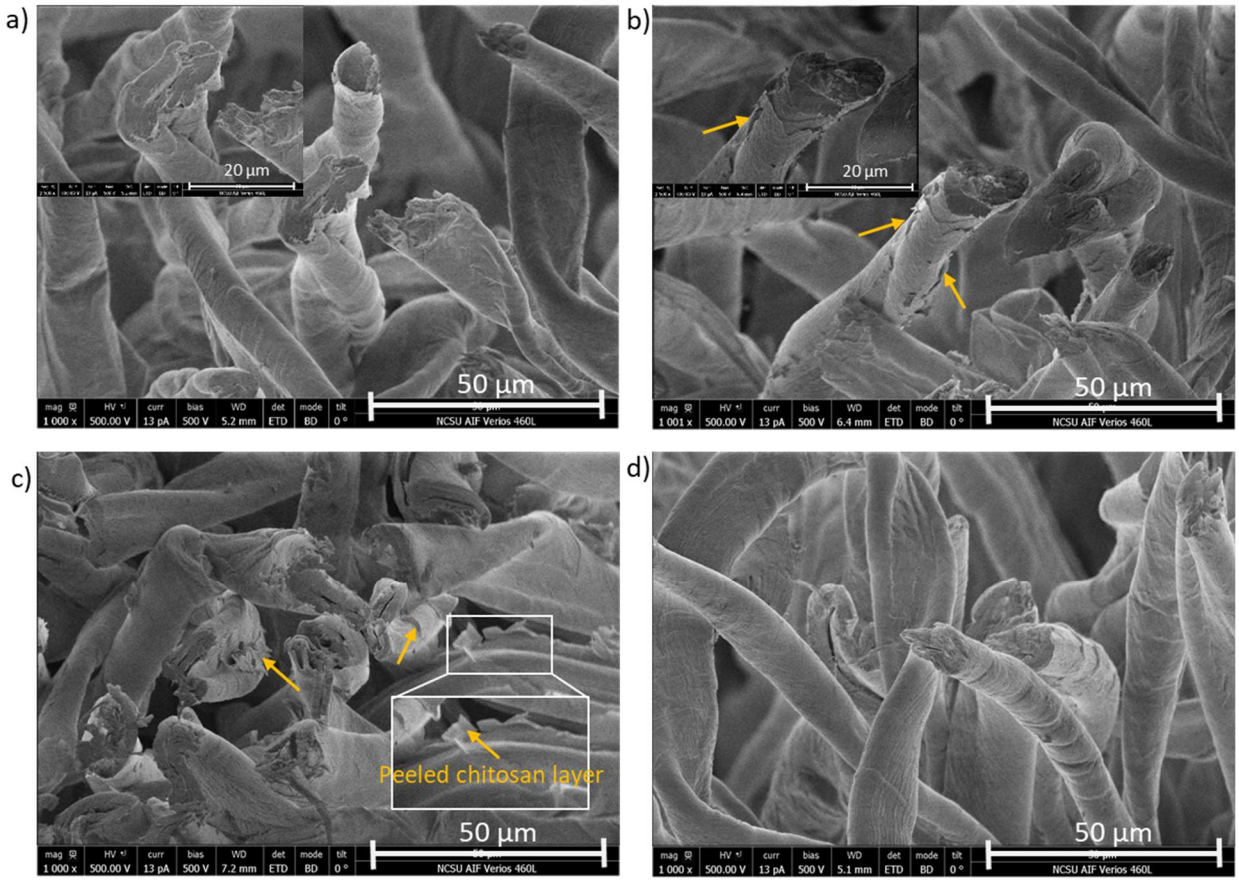

Figure 3.6 Scanning electron microscopic (SEM) images of: a) pristine cotton yarn; b) Chi yarn; c) Chi-CAT (NaAc) yarn and d) CAT(NaAc) yarn. Arrows emphasize the presence of chitosan coating.

Yarn surface chemistry was characterized by Fourier Transform Infrared Spectrometry (Nicolet Nexus 470, ThermoFisher Scientific, USA), with a Nicolet OMNI Germanium Crystal Attenuated Total Reflection (ATR) sampling head. All specimens were stored in a desiccator overnight before measurement to minimize moisture in the samples. A spectrum of each sample was collected from 64 scans with a resolution of 4 cm^{-1} and backgrounds were collected every 30

minutes during the measurements. The presence of chitosan on the Chi, Chi-CAT(Ac) and Chi-CAT(NaAc) yarn samples was confirmed by FTIR results. The overall spectra of chitosan coated yarn and pristine cotton yarn (**Figure 3.7 and Figure 3.8**) were very similar, due to the low weight ratio of chitosan or enzyme to cotton (**Table 3.1**), and because the chemical structure of chitosan only differs from cellulose by the presence of amine groups at the C2 position. Peaks around 3340 cm^{-1} and 2890 cm^{-1} in the spectrum are attributed to O-H and C-H bond stretching, which are typical characteristics of cellulose.(M. Fan et al., 2012) Peaks around 1162 cm^{-1}, 1315 cm^{-1} and 1429 cm^{-1} are assigned, respectively, to the C-O-C asymmetrical stretching, CH_2 vibration at C6 and OCH in-plane bending in the cellulose structure.(M. Fan et al., 2012) In Figure , the FTIR spectrum of chitosan coated cotton yarn (Chi) shows a peak at 1560-1600 cm^{-1}, which is attributed to the primary amine in the chitosan structure.(Lawrie et al., 2007; J. Yang et al., 2018) This difference was also observed between the catalase immobilized yarns with chitosan and the one without chitosan (**Figure 3.8**). In the inset of **Figure 3.8**, the broad peak at 1560-1600 cm^{-1} was observed in both Chi and Chi-CAT(NaAc) samples while it was not observed in the CAT(NaAc) sample, which justifies attributing this peak to amine groups in chitosan.

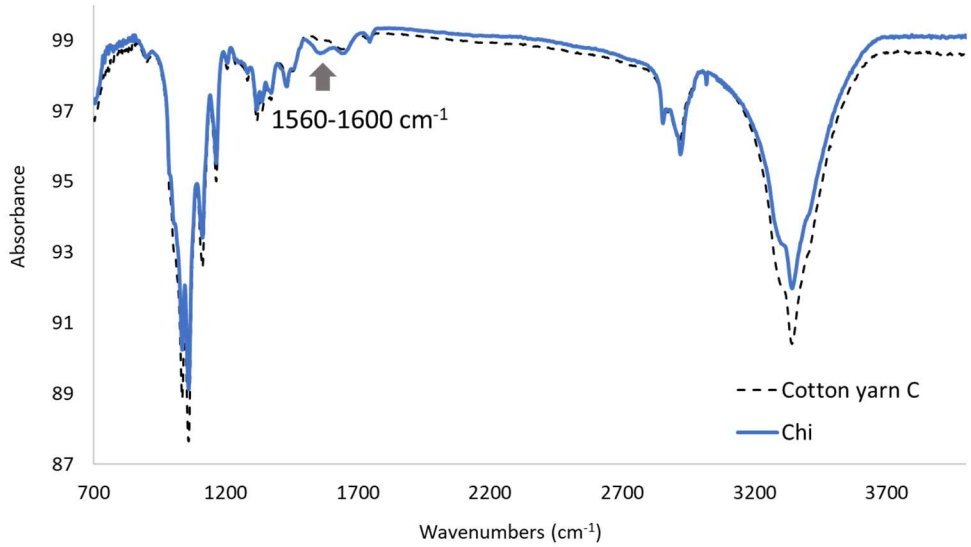

Figure 3.7 FTIR spectra of pristine cotton yarn and chitosan coated cotton yarn.

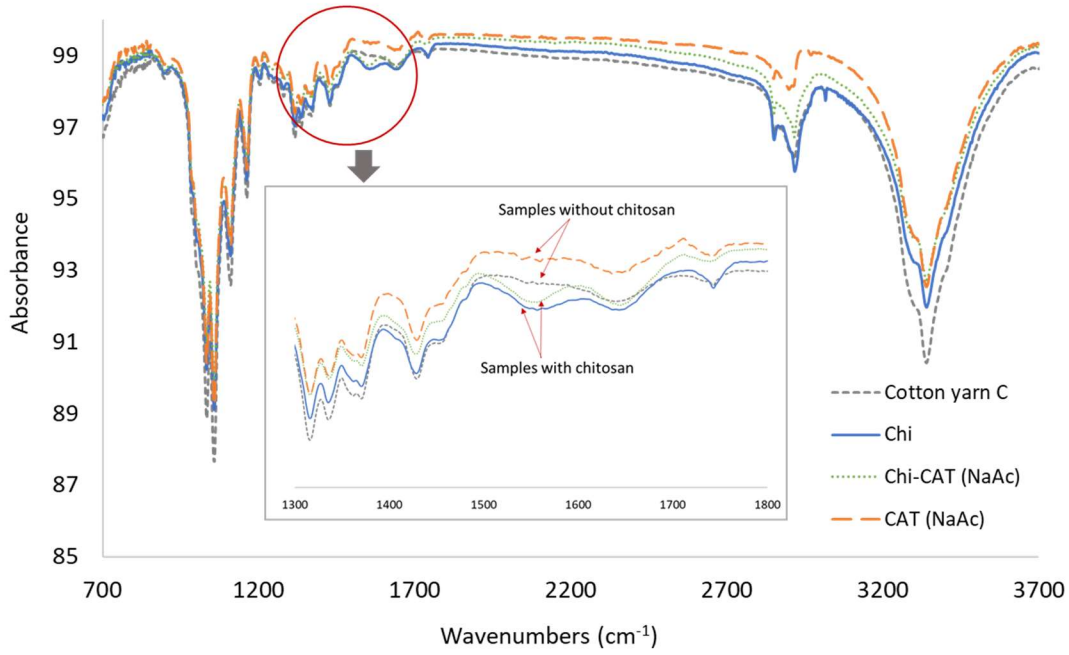

Figure 3.8 FTIR spectra of pristine cotton yarns, chitosan coated cotton yarn, and catalase adsorbed yarn.

3.3.2 The presence of immobilized catalase on the samples

The presence of active catalase on the yarns was detected by oxygen bubble formation when immersing yarns into a 1360 mg/L peroxide solution. No bubble formation was observed for C and Chi samples in the peroxide solution, showing that catalase is the only component contributing to peroxide decomposition in these tests. Notably, when submerging Chi-CAT(Ac) and Chi-CAT(NaAc) yarn samples into the peroxide solution, oxygen bubbles were only observed at the surface of the yarn, while in the assay with CAT(Ac), CAT(NaAc) or CAT(dI), bubble formation was distributed throughout the liquid, indicating that physically adsorbed enzymes leached from the yarn and were released into the liquid, even without vigorous mixing.

3.4 Catalytic Activity of the Biocatalytic Yarn

Catalytic performance of the dip coated yarn samples was evaluated after storing the samples in sealed plastic bags at ambient conditions for at least two months. The yarns were subjected to different tests in which catalase enzyme activity was detected either by observation of bubble formation due to the decomposition of hydrogen peroxide or by a decrease in the detectable hydrogen peroxide concentration in a liquid.

3.4.1. Catalytic activity of decomposing peroxide

Catalase catalyzes the degradation of hydrogen peroxide (H_2O_2) at room temperature producing oxygen (O_2) and water. The reaction happens rapidly, causing the formation of oxygen gas bubbles that originate from the vicinity of catalase enzyme molecules. When catalase enzymes are dissolved in an aqueous liquid to which H_2O_2 is added, rapid bubble formation can be observed throughout the liquid, indicating that catalase is present throughout the liquid. When catalase enzymes are immobilized in or on a solid material that is immersed in an aqueous liquid containing H_2O_2, evolution of gas bubbles from the solid material is a positive test for the

presence of active catalase in or on that material. The test is validated by conducting the same test on a piece of the solid material, absent catalase. If no gas bubbles form, the material itself does not cause gas bubble formation, and the gas bubble formation observed in the presence of catalase is attributed to catalase catalytic activity only.

Peroxide Test Strips and an aqueous peroxide test solution (1360 mg/L) were used to quantify the extent of peroxide decomposition achieved in the presence of yarn with immobilized catalase. Upon immersing the test strip into the test liquid, a dark blue color of the test strip corresponds to a high concentration of hydrogen peroxide (> 25 mg/L), while a white color of the test strip (no color change) corresponds to no detectable peroxide in the liquid. Varying shades of pale blue color correspond to a hydrogen peroxide concentration in the range between 0.5 to 25 mg/L (**Figure 3.9**, a).

3.4.2. Wicking test

A gravity-assisted wicking test (**Figure 3.9**, b and c) was used to demonstrate and evaluate the functional participation of the yarn in the biocatalytic decomposition of a hydrogen peroxide solution passing through the structure of a yarn containing immobilized catalase. In the experiments, a liquid containing 1360 mg/L H_2O_2 flowed through biocatalytic yarn samples or through control samples. A schematic drawing of the wicking test is shown in **Figure 3.9**, b, where the liquid flow through the yarn starts in the upper container by hydrophilic moisture absorption and capillary action that work against gravity. Then, the liquid flows downward from the top to the bottom container, assisted by gravity. One end of the yarn was immersed in 15 mL peroxide solution in upper container 1 and another end of the yarn was placed inside the top of an empty container 4 (**Figure 3.9**, b). The distance between the bottom of the upper container and the bottom of the lower container was about 25 cm. The efficiency of peroxide

decomposition during the wicking test was determined by periodically immersing Peroxide Test Strips in the upper and lower containers to measure residual peroxide concentrations of the liquids. The wicking test apparatus is illustrated in **Figure 3.9**, c.

To demonstrate the improved catalytic efficiency of the biocatalytic yarn, peroxide decomposition in a flow-through process configuration was compared side-by-side with a stirred tank configuration. In the flow-through configuration, peroxide solution was forced to flow through a certain length of Chi-CAT(NaAc) yarn at a selected flow rate. In the corresponding stirred tank reaction, a Chi-CAT(NaAc) yarn of the same length was immersed in peroxide solution and the solution was stirred at 300 rpm. Two concentrations of aqueous H_2O_2 (1360 mg/L and 340 mg/L) were used as substrates for comparison. Chi-CAT(NaAc) yarns with lengths of 5, 15 and 40 cm were tested.

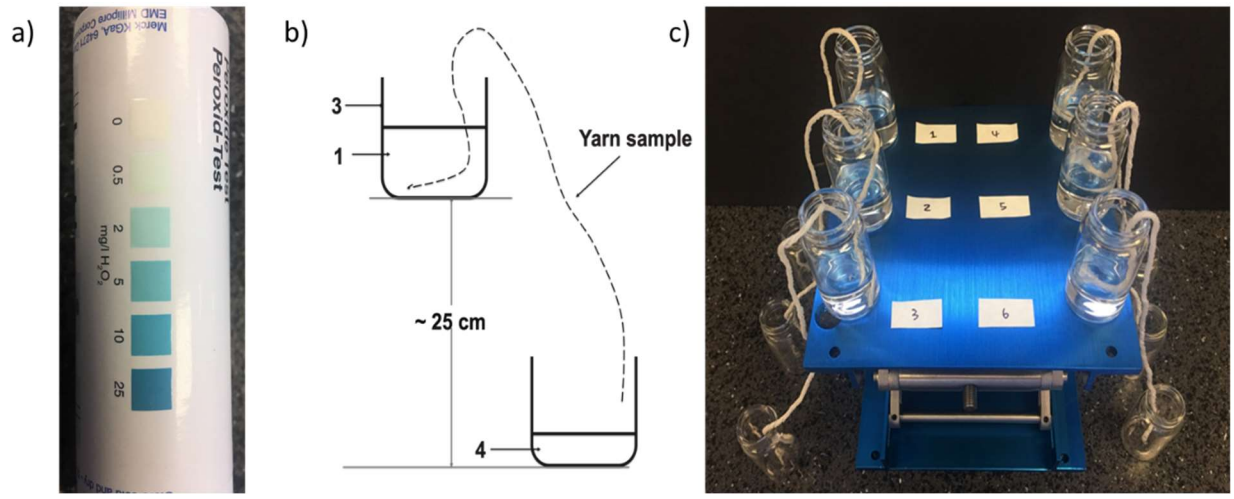

Figure 3.9 Gravity-assisted wicking test a) using Millipore™ MQuant™ Peroxide Test Strips to monitor peroxide concentration, b) illustrated by a schematic diagram and c) showing a lab-scale wicking apparatus.

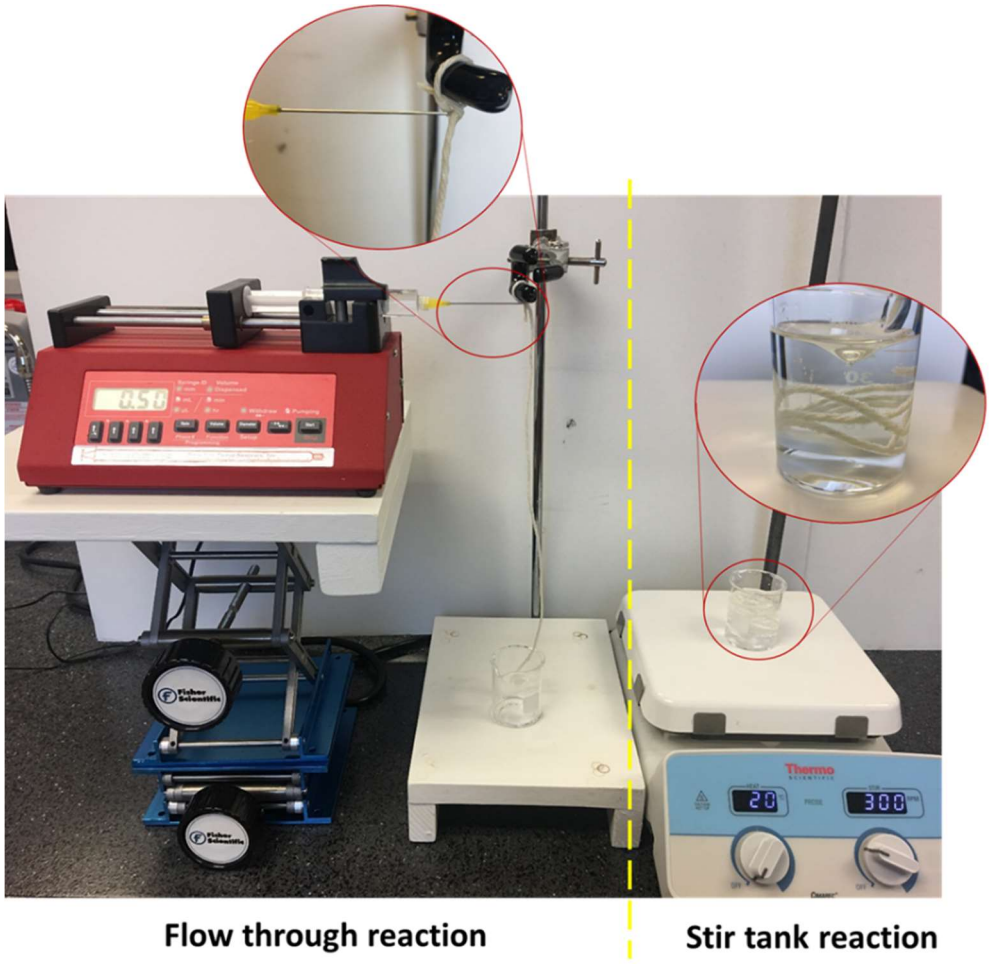

Figure 3.10 Apparatus for (left) flow-through reaction and (right) stir tank reaction for peroxide decomposition test with Chi-NaAc yarn. Yarn length was different for different tests. The picture shows a test set using 40 cm long yarn.

Yarn catalytic performance was evaluated by either immersing the yarns into a 1360 mg/L peroxide solution or allowing the peroxide solution to wick through the yarn assisted by gravity (**Figure 3.9**). According to the results in **Table 3.2** and **Table 3.3**, cotton yarn and cotton with chitosan coating only are not able to decompose peroxide. Therefore, removal of peroxide in the liquid is caused by the presence of active enzymes. In the immersion test, yarn samples with adsorbed enzymes had the best catalytic performance (**Table 3.2**). This is expected because weak interactions between cellulose and physically adsorbed enzymes allow enzymes to diffuse into the liquid, accelerating peroxide decomposition in solution and giving a high apparent

catalytic performance. However, this enzyme leaching behavior is a drawback of using physically adsorbed enzymes in aqueous environments when biocatalytic longevity is important.(Jesionowski et al., 2014) Enzyme entrapped by the chitosan matrix in Chi-CAT(Ac) and Chi-CAT(NaAc) samples were able to degrade peroxide in the immersion test, though at a slower rate due to substrate accessibility barriers. Because substrate diffusion limitations are commonly observed when enzymes are immobilized (Grubecki, 2017), methods that can overcome this limitation are desirable. Results presented here show that chemical transport by liquid wicking helps overcome mass transfer barriers. In the wicking tests for peroxide decomposition (**Table 3.3**), peroxide solution traveled through the yarn, making the contact between the substrate (peroxide) and the immobilized enzymes more efficient than immersing the yarn. Chi-CAT(Ac) and Chi-CAT(NaAc) had the same catalytic performance compared to the yarns with physically adsorbed catalase.

In addition to efficient catalytic performance by the gravity-assisted wicking test, the flow-through process configuration (**Figure 3.10**) was more efficient than the stirred tank configuration at decomposing hydrogen peroxide. The potential impact of water evaporation from the yarn exposed to ambient air on the flow through reaction was investigated. This was done by placing a non-dripping wet yarn, prepared in the same way as for a flow-through test, on an analytical balance and recording the weight loss during 50 minutes (**Figure 3.11**). The results showed that in 50 minutes, the rate of water evaporation from the yarn was 0.003 g/min (equal to 0.003 mL/min), which is ≤0.6 % of the flow rates used in the flow-through reactor (0.5- 1.5 mL/min). Therefore, this level of evaporation in the flow-through experiment was sufficiently small to not impact the conclusions. For experiments involving immersion mode, the liquid level remained the same after the 40 minute stirred tank reaction test and water evaporation was also considered to be

negligible. In almost all flow through tests (**Table 3.4-1 and Table 3.4-2**), the concentration of peroxide at the end of the tests was below the detection limit of the test strip (reported as 0 mg/L), whereas residual peroxide was detected in all the corresponding stirred tank tests. To estimate the efficiency improvement, tests with a similar level of detectable peroxide remaining at the end of the test were compared. For example, in the 15 cm yarn test, close to 0.5 mg/L peroxide remained in the flow-through test after processing a 45 mL volume of 1360 mg/L H_2O_2 and a similar amount remained at the end of the stirred tank test performed with 20 mL of H_2O_2. Therefore, the flow-through configuration was able to decompose at least two times more peroxide than the stirred tank configuration in the same amount of time. Whereas oxygen bubble formation occurred at the surface of immersed biocatalytic yarns, causing delay in release of gaseous products and a potential barrier to fresh substrate reaching enzyme active sites, the flow-through configuration did not exhibit macroscopic bubble formation, indicating rapid escape of evolved oxygen to the surrounding air, which could assist reaction efficiency.

Furthermore, the volume of the reaction zone for the flow-through configuration is substantially smaller than the volume for the corresponding stirred tank. With a nominal diameter of 3 mm, the 15 cm yarn can be approximated as having the shape of a pipe with a cylindrical volume of 1 cm^3 (an upper limit in this estimation), while the corresponding stirred tank has a reaction volume of 20 cm^3. Therefore, by using the flow-through configuration, at least two times more peroxide was processed in a twenty-times smaller reaction zone volume compared to the stirred tank configuration. Essentially, in flow-through mode, the biocatalytic yarn functions as both a catalyst and a compact reactor that conveys liquid through the process. As shown in **Figure 3.10** (left), the yarn in the flow-through configuration did not have to be perfectly vertical or straight to successfully transport the liquid without dripping. This

emphasizes the benefit of using a chitosan coated hydrophilic yarn to constrain and convey the aqueous solution. Multiple yarns can be assembled together in different sizes, configurations, and interlacing assemblies to achieve highly efficient and modularly-scalable chemical conversions.

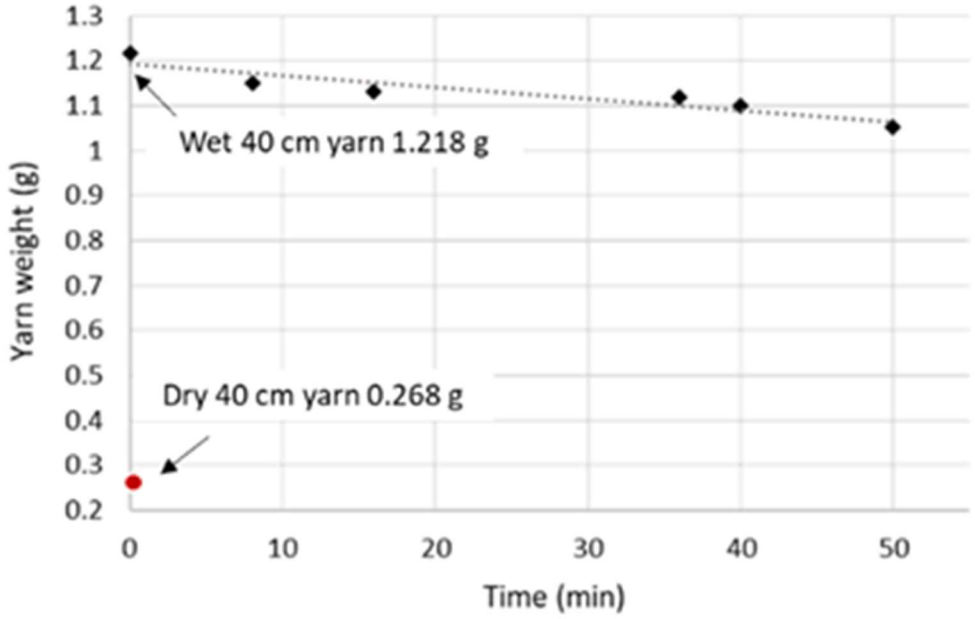

Figure 3.11 Results of measuring water evaporation from a wet biocatalytic yarn.

Table 3.2 Peroxide concentration of immersion test*.

Sample	Yarn samples before wash	Yarn samples after 25 day wash
C	>25	>25
Chi	>25	>25
Chi-CAT	0.5-2	0.5-2
Chi-CAT (NaAc)	0.5-2	0.5-2
CAT(Ac)	0	5
CAT (NaAc)	0	5
CAT (dI)	0	5

*Test was performed after 20 minutes without stirring.

Table 3.3. Peroxide concentration of gravity-assisted wicking test*.

Sample	Yarn samples before wash	Yarn samples after 25 day wash
C	>25	>25
Chi	>25	>25
Chi-CAT	0	0
Chi-CAT (NaAc)	0	0
CAT(Ac)	0	0-0.5
CAT (NaAc)	0	0-0.5
CAT (dI)	0	0-0.5

*Test was performed after all 15 mL peroxide transported to lower beakers for all samples.

Table 3.4-1 Comparison of flow-through reaction and stir tank reaction for Chi-CAT(NaAc) yarn peroxide decomposition with 1360 mg/L H_2O_2 solution.

Length of Chi-NaAc yarn (cm)	Flow rate (mL/min)	Time (min)	Peroxide volume (mL)	Peroxide concentration in flow through reaction (mg/L)	Peroxide concentration in stir tank reaction (mg/L)
40	0.5	40	20	0	0-0.5 close to 0
	1	40	40	0	0.5-2
	1.5	30	45	0	5
15	0.5	40	20	0	0.5 -2 close to 0.5
	1	40	40	0	2-5
	1.5	30	45	0-0.5 close to 0.5	5-10 close to 10

Table 3.4-2 Comparison of flow-through reaction and stir tank reaction for Chi-CAT(NaAc) yarn peroxide decomposition with 340 mg/L H_2O_2 solution.

Length of Chi-CAT(NaAc) yarn (cm)	Flow rate (mL/min)	Time (min)	Peroxide volume (mL)	Peroxide concentration in flow through reaction (mg/L)	Peroxide concentration in stir tank reaction (mg/L)
40	0.5	40	20	0	0-0.5 close to 0
	1	40	40	0	0.5-2 close to 0.5
	1.5	30	45	0	0.5-2 close to 2
15	0.5	40	20	0	0-0.5
	1	40	40	0	2-5
	1.5	30	45	0	2-5 close to 5
5	0.5	40	20	0.5-2	>25
	1	40	40	5	>25
	1.5	30	45	5-10 close to 10	>25

3.5 Neutron Imaging and Computed Tomography Characterization for Liquid Transport inside Biocatalytic Yarn

The water wicking in the yarn against gravity was investigated by neutron imaging at CG-1D beam line at High Flux Isotope Reactor (HFIR), Oak Ridge National Laboratory. Neutron imaging provides an in-situ nondestructive technique for measuring the wicking process.(Marcelo Parada et al., 2017) The in-situ neutron radiography experimental setup consists of a sample holder to support the yarn vertically and an aluminum pan was placed at the bottom of the yarn as a liquid reservoir, as shown in **Figure 3.12**. Moderated and collimated neutron irradiation with a wavelength range from 0.8 to ∼6 Å and a peak wavelength around 2.6 Å was used for imaging.(Crow et al., 2011; Santodonato et al., 2015) A scientific complementary metal-oxide semiconductor (sCMOS) detector was used to monitor the water transportation in yarns. A speed of 2 frames per second (f/s) was used to capture the initial fast movement, immediately followed by a speed of 0.1 f/s to continuously image the slow movement. The images obtained from experiments were analyzed in Image J (NIH, USA) software.

Neutron computed tomography (nCT) was also applied to study the water distribution in pristine cotton yarn samples (C) and in Chi-CAT (NaAc) yarn samples coated with chitosan-catalase. 3D-CT imaging was performed on yarn samples collected after gravity-assisted wicking (**Figure 3.9**, b) and was carried out using the same beam-line as the gravity-resisted wicking experiments, using a charge-coupled device (CCD) detector. Yarn samples from gravity-assisted wicking were covered in aluminum foil to prevent water evaporation during nCT measurement and were mounted vertically on an aluminum stage for the CT scan. Projections were acquired over a 360° with a rotation step size of 0.62°. The exposure time of each

projection was 55 s. The effective pixel size of the radiographic images was about 36 x 36 µm2 and the spatial resolution was about 75-100 µm in the tomogram. The tomogram was visualized and analyzed using Amira-Avizo, which is developed by Thermo-Fisher Scientific in collaboration with the Zuse Institute Berlin (ZIB),(Stalling et al., 2005) to spatially resolve water distribution inside each yarn structure after the gravity-assisted wicking experiments.

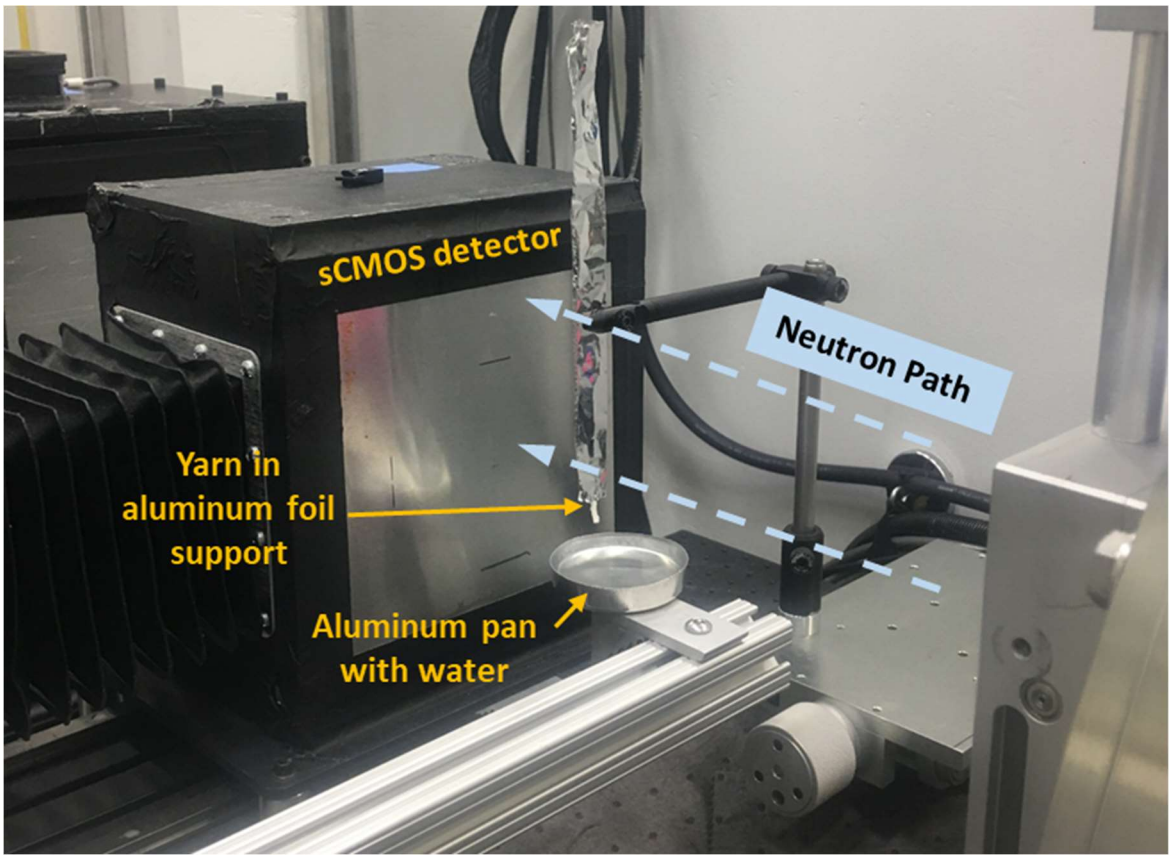

Figure 3.12 Experimental setup for neutron radiography measurement at CD-1G IMAGING beam line, HFIR, Oak Ridge National Laboratory.

Neutron imaging results elucidated changes in the interaction between water and cellulosic yarn or yarn with chitosan coating applied. In **Figure 3.13**, both the C and Chi-CAT(NaAc) yarn samples are shown as light grey structures because the thin chitosan coating does not significantly impact the overall neutron transmission of the sample. The dark horizontal

line at the bottom of each image represents the top surface of the water reservoir. Water wicking happened instantaneously along the yarn structure in the pristine cotton yarn sample (**Figure 3.13**, a). Liquid filled the space in between the different yarn plies through wicking. However, with a chitosan coating, the yarn wicking behavior changed dramatically (**Figure 3.13**, b), where the speed of water wicking upwards against gravity decreased significantly. This is attributed to the more hydrophobic yarn property after coating with chitosan. Eventually, wicking occurred, however water was confined to and followed the individual plies of the yarn structure, and the presence of water in between the yarn plies was greatly reduced. This wicking behavior was consistent with yarn moisture content results. The moisture content of pristine cotton yarn (7.3 %) and yarns with physically adsorbed enzymes (7.1 to 7.5 %) were similar, while significant decreases in moisture content were observed in yarns containing chitosan (1.29 to 1.34 %).

Neutron tomography corroborated the neutron radiography observations. C and Chi-CAT(NaAc) yarn samples were subjected to neutron tomography characterization after 10 mL of water was allowed to transport through each sample by gravity-assisted wicking (**Figure 3.9**, b). Samples were wrapped in foil to prevent water evaporation and were exposed to the neutron beam. The sample reconstruction volume is shown in **Figure 3.14**, where pseudo-color was used to represent the linear attenuation coefficient (cm^{-1}) of each voxel for easier visualization. Since both yarn samples showed similar attenuation power (gray appearance in **Figure 3.13**), the color variation observed in Figure was mainly contributed by the local water content. Therefore, the internal water distribution can be observed after virtually slicing the tomogram as shown in **Figure 3.14**. According to the vertical sliced tomogram (**Figure** , b), it is very clear that with the chitosan layer coated on fibers, the water that traveled through the yarn was confined inside each individual single-yarn ply of the overall 4-ply yarn structure, as indicated by the green, blue and

yellow (low water content) boundaries in the structure. On the contrary, cross sections of cotton yarn (C) have mostly orange and red (high water content) regions throughout the entire sample (**Figure 3.14**, a), indicating that the water is distributed both inside and in between all plies of the 4-ply yarn structure during wicking.

The tomography data of the yarn samples were virtually sliced horizontally and three random positions are shown in **Figure 3.14**. Again, the pristine cotton sample exhibited high water content throughout the entire yarn structure (**Figure 3.14**, c), including between the four yarn plies, making it difficult to distinguish between the different yarn plies. In contrast, water was largely confined within each single-ply yarn substructure of the chitosan coated 4-ply biocatalytic yarn due to the more hydrophobic chitosan coating (**Figure 3.14**, d). In the presence of water, the surface features of each individual ply of the 4-ply yarn are clearly visible when the chitosan coating is present and the yarn exhibits a higher apparent surface area compared to the yarn without chitosan coating. Higher surface area increases the gas-liquid interface between liquid contained in individual yarn plies and the air surrounding the plies. Furthermore, by applying the thin chitosan coating on cellulosic yarn, the water transportation behavior inside the yarn changed in a way that the movement of the liquid slowed down and was confined within each single-ply yarn structure, which could enhance diffusive interaction between dissolved substrate and immobilized enzyme.

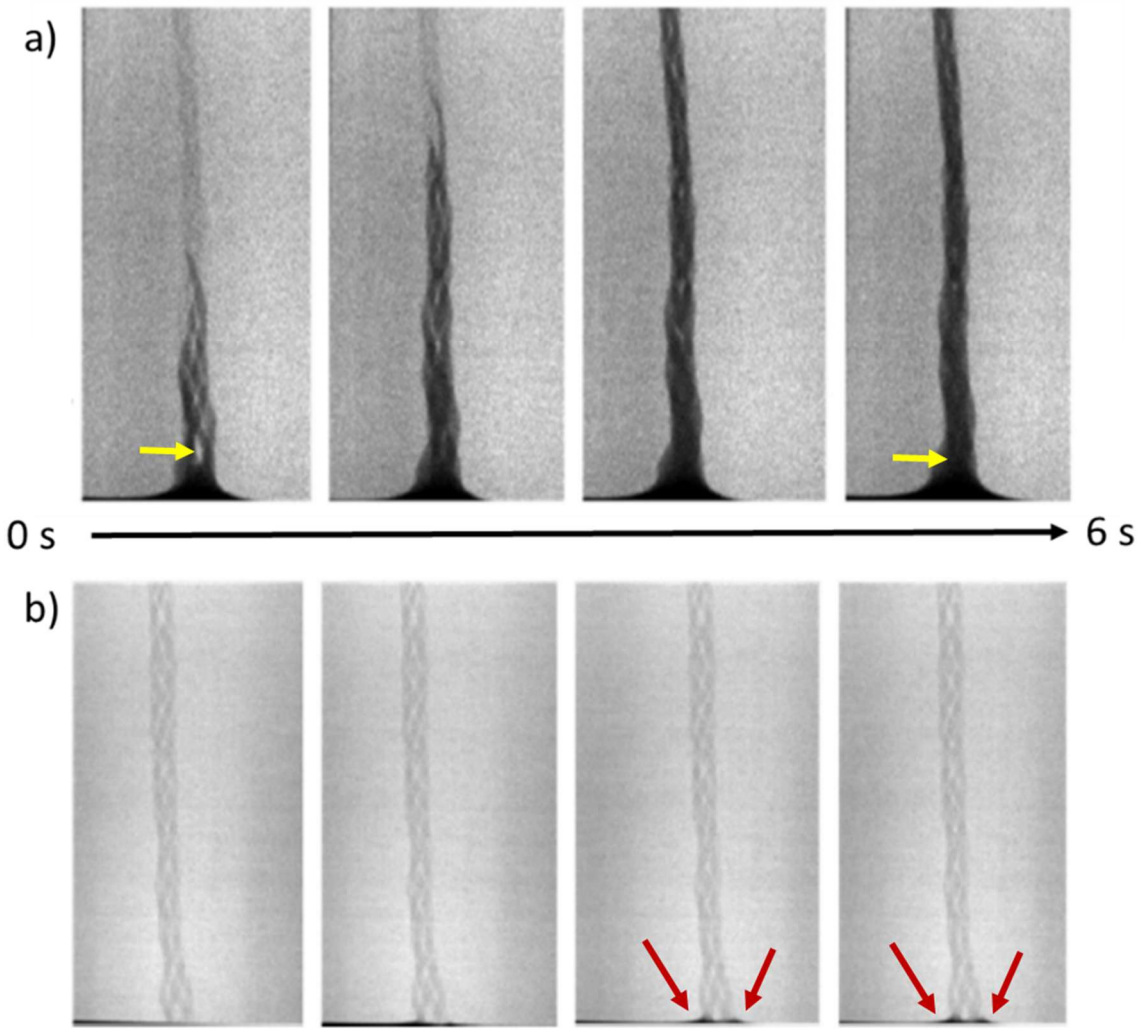

Figure 3.13 Illustration of water transportation in the yarn samples in the gravity-resisted wicking test with neutron radiography: a) wicking of water in cotton yarn, where yellow arrows indicate the space between different strands of yarn in the 4-ply yarn structure, and b) wicking of water in chitosan coated yarn, where red arrows indicate the delayed onset of wicking.

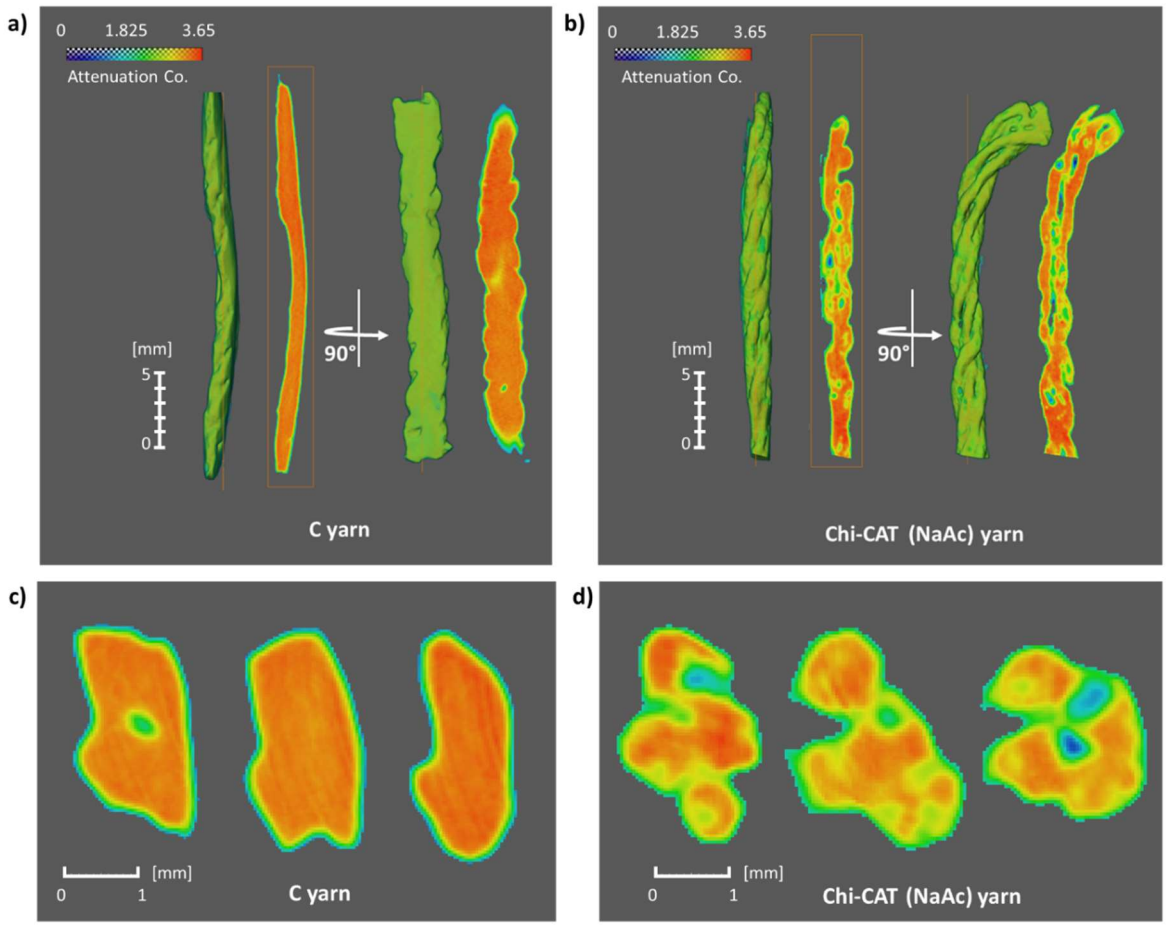

Figure 3.14 Neutron computed tomography of the C yarn and Chi-CAT(NaAc) yarn after gravity-assisted wicking experiments with water. Overall yarn tomography and vertical cross-sections of a) C yarn and b) Chi-CAT(NaAc) yarn. Horizontal cross-sections of the c) C yarn and d) Chi-CAT(NaAc) yarn. Red indicates a high concentration of water while blue indicates less water.

3.6 The Improved Catalase Longevity through Immobilization

To study biocatalyst longevity, washing tests of the biocatalytic yarns were conducted and catalytic performance was measured after washing. In the washing test, yarn samples were submerged in 40 mL dI water in conical tubes and the tubes were placed in a rotisserie with an end-over-end rotation speed of 25 rpm at 30 °C. Yarns were taken out at predetermined time intervals (2 hours, 24 hours and 25 days) and were air dried in a ventilated fume hood. Washing liquids were collected for catalase activity and protein concentration assays. Biocatalyst

longevity was evaluated on two aspects: protein leaching and residual biocatalytic activity of the yarn. The amount of protein and level of enzyme activity that leached out from yarns during the washing test were quantified. Residual biocatalytic activity of yarns was quantified by comparing the catalytic performance of the yarn before and after washing.

Collected washing liquid was filtered (Polytetrafluoroethylene syringe filters, 0.45 μm pore size) to remove loose fibers from the liquid. Filtered liquid was subjected to protein concentration assay using a Rapid Gold BCA Protein Kit (Pierce™, ThermoFisher Scientific, USA). The amount of protein leached out from the yarn at each sampling interval was quantified relative to a calibration curve based on fresh TU-CAT solutions. The activity of enzymes in the washing liquid was measured using a visual approach developed by Iwase et al.(Iwase et al., 2013) This is a quick, convenient method allowing the presence of active catalase in liquids to be measured immediately after application testing. In this method, 100 μL 1% v/v Triton X-100 solution was mixed with 5 mL liquid collected from the washing test, followed by adding 5 mL 1360 mg/L H_2O_2 solution. The O_2 gas from peroxide decomposition by enzyme was trapped as a foam due to the presence of surfactant, and the height of the white dense foam was measured as an indicator of the enzyme activity present in the washing liquid. Residual catalytic performance of the yarn after washing was measured as described previously.

Yarn samples were subjected to a washing test to evaluate the durability of the yarn structure and longevity of biocatalytic yarn performance. **Figure 3.15** illustrates the durability of yarn samples. Without a chitosan coating, loosened fibers and structural damage to the yarn were observed on CAT(Ac), CAT(NaAc) and CAT(dI) after the washing tests. Improved cotton yarn durability to washing in the presence of a chitosan coating is consistent with a mechanism where

chitosan has inherent affinity for cellulose across a broad pH range and can bind to cellulose to form a physically stabilizing protective layer.(Myllytie et al., 2009)

The liquid after washing was collected to determine the protein concentration and enzyme activity. **Figure 3.16** shows concentrations of protein that were leached from yarn samples after washing the samples for 2 hours and 25 days. C and Chi samples were washed as controls for CAT samples and Chi-CAT samples, respectively. The amount of leached protein was calculated by subtracting the absorbance of corresponding control samples. Chi-CAT(Ac) or Chi-CAT(NaAc) had 2.5 to 5 times lower protein leaching compared to physically adsorbed enzymes, indicating that the chitosan coating improves protein attachment to the cellulosic yarn. The Chi-CAT(NaAc) yarn had less protein leaching compared to Chi-CAT(Ac). Possible explanations are that in the Chi-CAT(Ac) preparation, both chitosan and protein were positively charged at the low pH (~2.6) condition, leading to repulsive interactions between proteins and chitosan (Forciniti et al., 1991; Zhao et al., 2003) or that the chitosan coating remained in a more soluble salt form when applied at low pH(Myllytie et al., 2009) leading to protein release.

Enzyme activity in the washing liquid was measured by a visual assay using hydrogen peroxide solution and surfactant.(Iwase et al., 2013) As shown in **Figure 3.17**, 5 mL of 1360 mg/L peroxide solution was added to each test tube containing surfactant and washing liquid samples. Five uniform gentle up-down shakes were applied to all the tubes. Tubes with active catalase began forming foam at the surface right away. Five minutes after mixing, the height of the foam in each tube was recorded. The experiment was conducted with three sample replicates and the averaged foam heights are listed in **Figure 3.17**. If vigorous mixing was applied, the foam height in tubes from CAT samples increased to above 2.5 cm while the appearance of tubes from Chi or Chi-CAT remained the same.

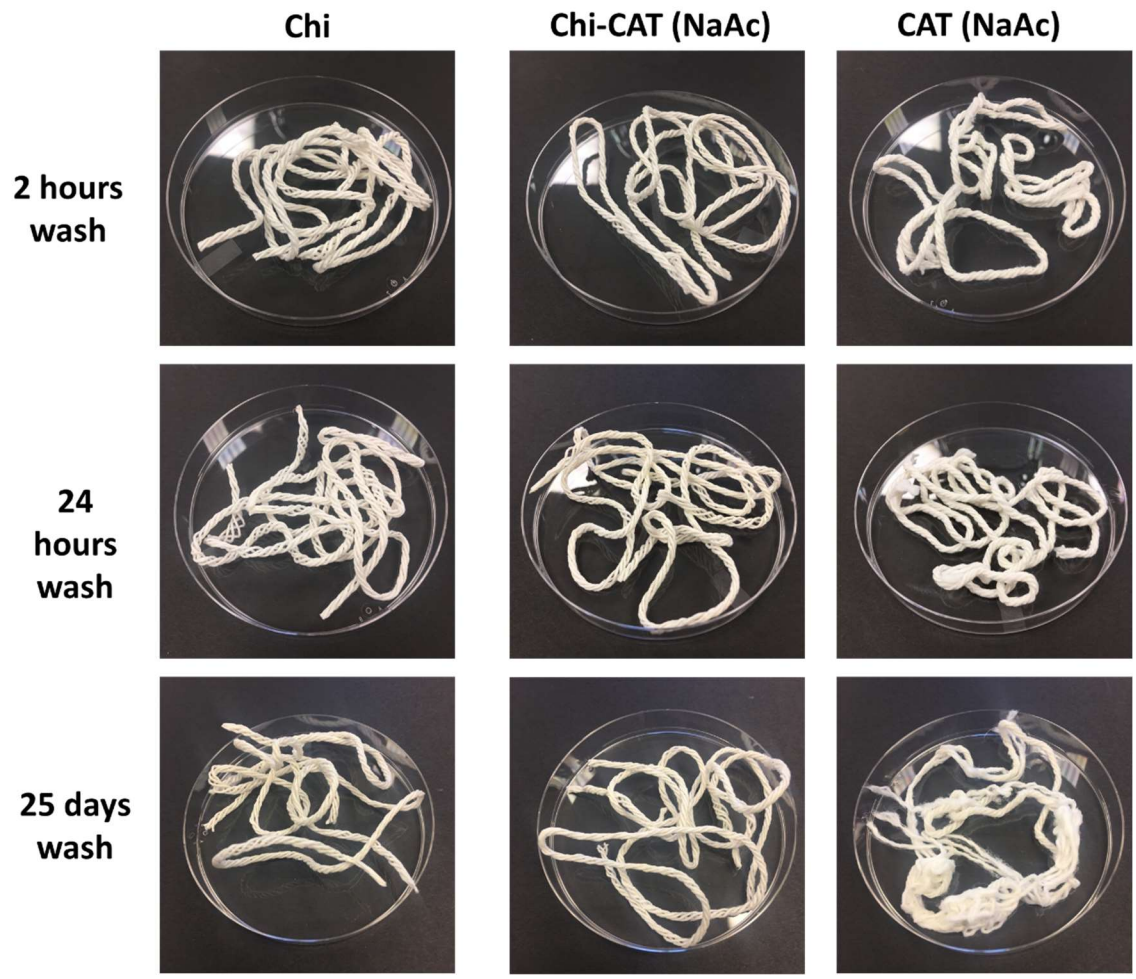

Figure 3.15 Photographs of Chi, Chi-CAT(NaAc) and CAT(NaAc) samples after 2 hour, 24 hour and 25 day washing in dI water in a rotisserie at 30 °C. Chi-CAT(Ac) samples, not shown, were similar to Chi and Chi-CAT(NaAc) while CAT(Ac) and CAT(dI), not shown, were similar to CAT(NaAc) samples.

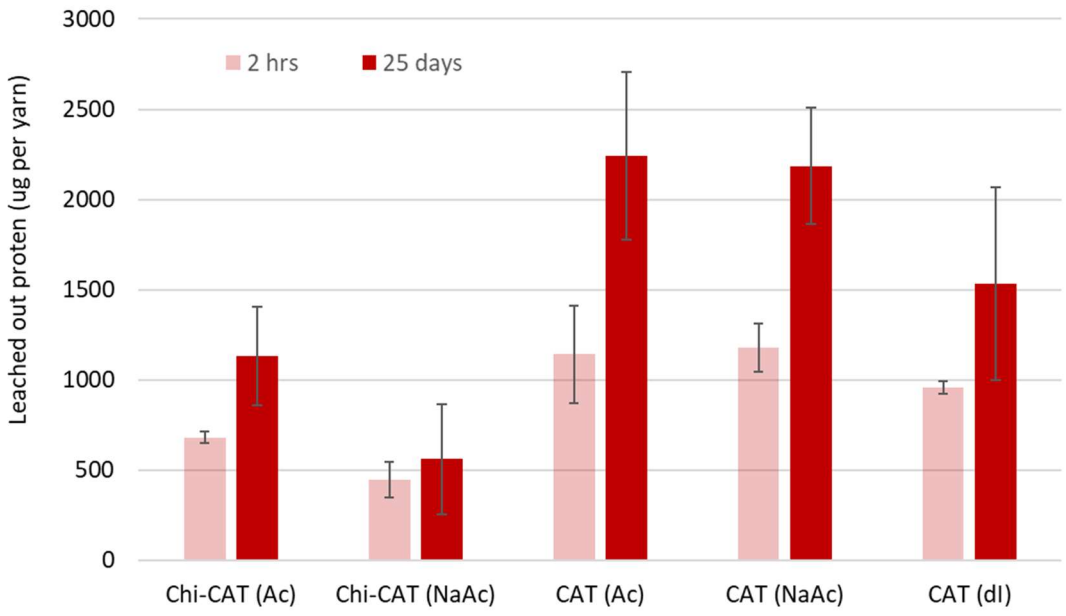

Figure 3.16 Cumulative protein leaching from yarns after 2 hour and 25 day washing in rotisserie.

No foam formed at all in the 2 hour and 25 day washing liquids from Chi yarn samples, indicating that no soluble components from Chi yarn cause peroxide decomposition. Immediately after adding peroxide, oxygen bubbles formed in tubes 4 to 6 (**Figure 3.17**, a-1) containing washing liquid from CAT(Ac), CAT(NaAc) and CAT(dI), due to the presence of active catalase enzymes that were leached from the yarns during the washing tests. Five minutes after mixing (**Figure 3.17**, a-2), about 1.5 cm height of trapped dense white foam was observed in the tubes containing washing liquid from yarn samples with physically adsorbed enzymes, confirming the presence of active catalase enzymes in these wash liquids. Rapid dense foam formation was not observed in tubes 2 and 3, which contained washing liquid from yarn samples with chitosan-entrapped enzymes, indicating the absence of active catalase in these wash liquids. After measuring foam height, peroxide concentration in each tube was measured using peroxide test strips. The light blue color on the peroxide test strip of tube 4 in **Figure 3.17**, a-2 showed

that washing liquid from CAT(Ac) has lower catalase activity compared to CAT(NaAc) and CAT(dI), although the amount of protein leached from CAT(Ac) was similar to CAT(NaAc) and CAT(dI) (**Figure 3.16**). This suggests the low pH (~2.6) dip coating can inactivate catalase during the immobilization process or limits the initial amount of catalase adsorption to the yarn. After 2 hour washing, peroxide test strips were dark blue (>25 mg/L) for tubes containing washing liquid from Chi-CAT(Ac) and Chi-CAT(NaAc) samples, which was the same color as for the control sample, Chi (**Figure 3.17**, a-2). Therefore, although protein was detected in the Chi-CAT(Ac) and Chi-CAT(NaAc) liquids after 2 hour washing (**Figure 3.16**), any catalytic activity associated with this protein was not detected by the foaming or peroxide strip tests for these samples. After the 25 day washing test, similar trends were observed: Chi (control) and Chi-CAT(Ac) had essentially no foam formation, while a small amount of foam formed with Chi-CAT(NaAc) (**Figure 3.17**, b), and CAT(Ac) generated a lower foam height than CAT(NaAc) or CAT(dI). Although the amount of protein leached from Chi-CAT(Ac) was higher than Chi-CAT(NaAc) according to **Figure 3.16**, the activity of leached proteins from Chi-CAT(Ac) was lower, which is consistent with the observations among CAT samples. Since Terminox® Ultra has an optimal pH between 6-8, the low pH (pH 2.6) during the Chi-CAT(Ac) and CAT(Ac) dip coating could lead to enzyme deactivation, explaining the lower catalytic activity of the (Ac) samples. Therefore, when utilizing chitosan solutions for enzyme entrapment, immobilization effectiveness is improved by adjusting a dissolved chitosan solution to a milder pH (around pH 5) before combining with enzyme. The foaming test and protein leaching test were run as independent tests, therefore, further experiments would be required to correlate the amount of leached protein content with the detectable residual enzyme activity in the foaming test.

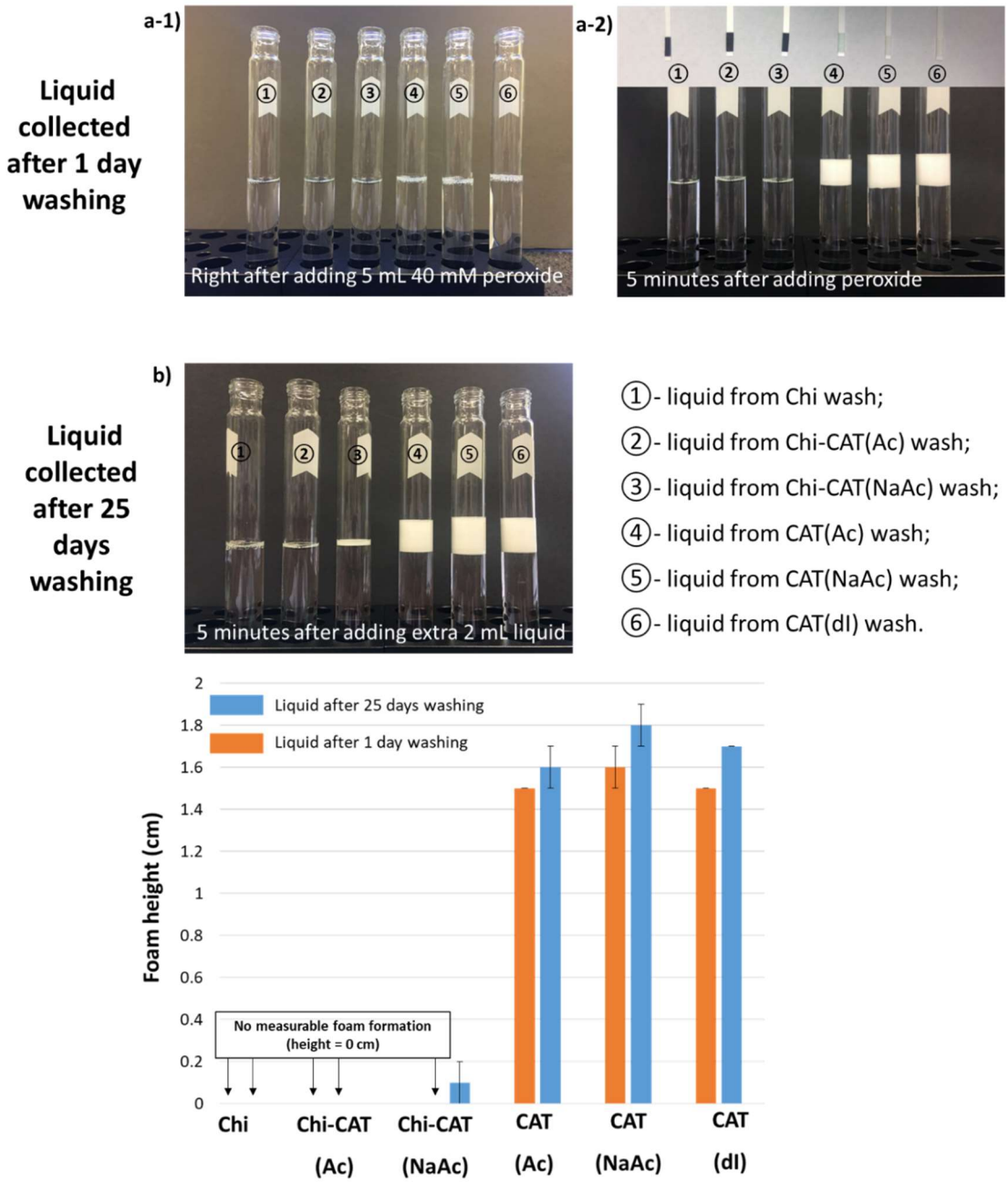

Figure 3.17 Illustration of the foaming tests for visualizing catalase activity in liquids after washing yarn samples. White foam was generated by oxygen gas trapped by surfactant.

Peroxide decomposition tests were repeated with 25 day washed yarns, using both the immersion test and wicking tests, to compare biocatalytic longevity of yarns prepared by enzyme entrapment and enzyme adsorption. When washed yarns were immersed in peroxide solution, CAT(Ac), CAT(NaAc) and CAT(dI) had much lower bubble formation at the yarn surface compared to corresponding unwashed samples, indicating that most adsorbed enzymes had washed off the yarn. However, dense bubbles continued forming at the surface of washed Chi-CAT(Ac) and Chi-CAT(NaAc) samples (**Figure 3.18**), confirming the presence and persistent biocatalytic activity of the thin chitosan coating on the cellulosic yarn. Small oxygen bubbles at the surface of the Chi-CAT(NaAc) yarn give it a blurry appearance (**Figure 3.18**), whereas the blurry appearance of the CAT(NaAc) yarn is due to loss of physical integrity of the yarn structure after washing. Strong interaction between the chitosan coating and cellulosic yarn was also supported by the results of dye sorption tests on washed yarn samples (**Figure 3.5**), where the dye sorption of Chi-CAT(Ac) and Chi-CAT(NaAc) was essentially unaffected after washing the yarns for 25 days. Also, the dye sorption results of 25 day washed Chi-CAT yarn samples are similar to the samples without washing (**Figure 3.5**), indicating high affinity between the thin chitosan coating and cellulosic textile support. Therefore, this immobilization method minimizes leaching of entrapped enzyme by utilizing the affinity between two polysaccharides. Low leaching is desirable for continuous process applications requiring extended biocatalytic longevity.

A comparison of immersion (**Table 3.2**) and wicking test (**Table 3.3**) results before and after 25 day washing shows the performance of Chi-CAT(Ac) and Chi-CAT(NaAc) yarns was relatively unchanged and these samples exhibit superior biocatalytic longevity compared to the CAT(Ac), CAT(NaAc) and CAT(dI) yarns. Therefore, chitosan dip coating was an effective

method for applying enzymes to the surface of cotton yarns, and for maintaining enzyme activity after exposure to extended washing. Especially important are the wicking test results, showing persistent high peroxide degradation performance for chitosan coated biocatalytic yarns even after 25 days washing, and even after the yarn samples were stored at ambient conditions for at least two months prior to the testing. These results emphasize how the containment and control of liquid transport inside a yarn structure, where immobilized enzymes are present in the structure, creates a flexible bioreactor that can be constructed and configured in essentially infinite ways to deliver and remove substrates to and from the active sites of enzymes, in a directed manner, without requiring excess liquid.

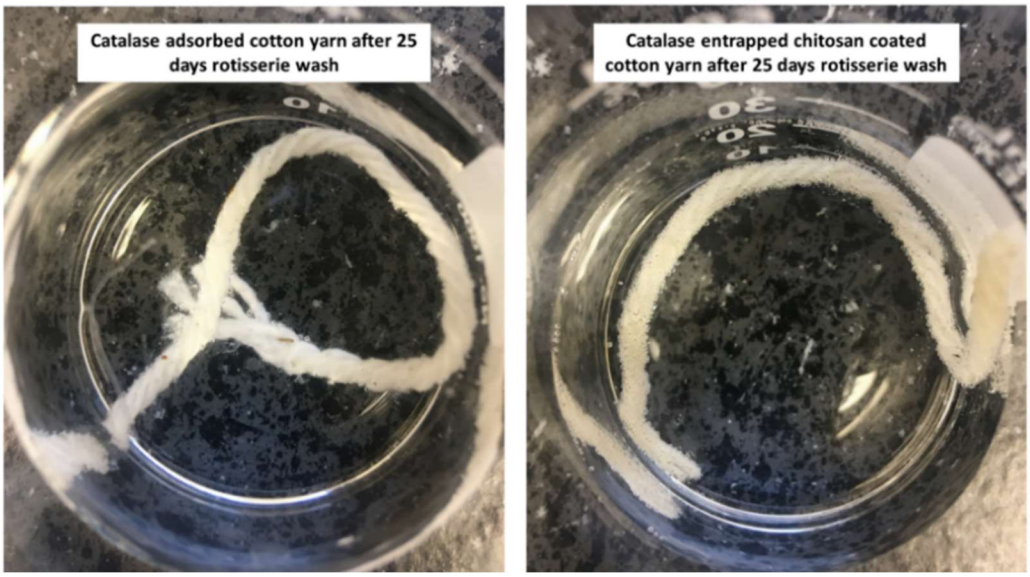

Figure 3.18 Photographs of immersing 25 day washed yarns in 1360 mg/L peroxide solution: left: CAT(NaAc), right: Chi-CAT(NaAc).

To investigate the extent of residual catalytic activity after extended storage of biocatalytic yarns, we prepared a fresh Chi-CAT(NaAc) yarn sample and compared its activity with a yarn that was stored at room temperature in a sealed container for 2 years. Cut lengths (40 cm) of Chi-CAT(NaAc) yarn after 2 years storage and freshly prepared Chi-CAT(NaAc) yarn were immersed

in 50 mL of 40 mM H_2O_2 solution at room temperature with stirring. Each liquid's absorbance at 240 nm was measured at predetermined times (**Figure 3.19**). Prior to use in the comparison, the freshly prepared Chi-CAT (NaAc) sample was washed 4 times in deionized water to remove unattached enzyme. The liquid after the fourth washing did not cause visible gas (O_2) formation in 5 minutes when mixed with 40 mM H_2O_2 solution at 1:1 volume ratio. The absence of bubble formation in the final wash liquid indicates that little to no catalase leached into the liquid. Therefore, peroxide decomposition activity in the subsequent assay was fully ascribed to immobilized catalase on the yarn. Furthermore, the absence of bubble formation during the test is important for accuracy of this absorbance-based assay. The peroxide degradation rate of freshly prepared Chi-CAT(NaAc) yarn in a stirred tank reaction was 0.78 O.D./hour while that of the yarn after 2 years storage was 0.49 O.D./hour, corresponding to 63% activity retention.

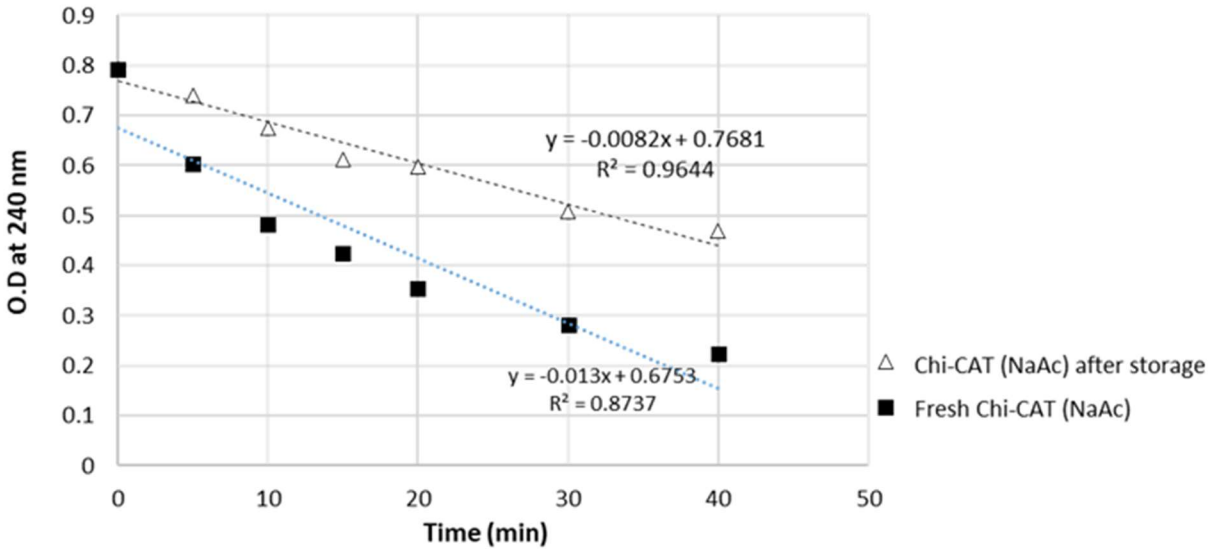

Figure 3.19 Results of peroxide decomposition rate using 40 cm freshly prepared Chi-CAT(NaAc) biocatalytic yarn and Chi-CAT(NaAc) biocatalytic yarn after two years storage.

3.7 Application of Immobilized Catalase for Water Reutilization in Cotton Bleaching and Dying Process

Hydrogen peroxide (H_2O_2) has been use as a major industrial bleaching agent for cotton textiles. To prevent the damage of dye by peroxide in the following dyeing procedure, catalase (CAT) enzymes have been applied to remove the residual peroxide in the bleach bath (Nielsen et al., 2009). The removal of residual peroxide in the bath also reduces the overall water consumption in cotton textile wet processing. However, the dissolved catalase cannot be separated from the liquid, which might impair the reusability of the liquid in preparing new bleach solution, or require inactivation of enzymes before using the liquid for a new bleach solution. Therefore, in this study, we investigated the potentials of applying immobilized CAT prepared in previous session instead of a dissolved catalase for peroxide removal in a bleach bath, in order to reuse the recycled and treated post bleach liquids for both dyeing and bleaching processes. To this end, we proved that the residual peroxide in post bleach liquids has negative influences on the dyeing outcomes when dying the fabrics with reactive dye. The post bleach liquids were treated with either dissolved CAT or textile immobilized CAT before subjecting to prepare the second dye bath and the second fresh bleach bath. The experiments were designed to test the hypotheses which include: 1) Post bleach liquid treated by immobilized catalase can be used directly for both dye bath preparation and new bleach bath preparation without any additional procedures; 2) Liquid treated with immobilized catalase can be used for dyeing process without damaging the dye.

3.7.1 Materials

The catalase immobilized 4-ply cotton yarn, Chi-CAT (NaAc), was prepared as described in section *3.3.2* and used after two years storage at ambient condition in this study. CI Reactive

Red 120 (**Figure 3.20**) was purchased from Sigma-Aldrich (St. Louis, MO, USA). Sodium carbonate (Na_2CO_3) and sodium sulfate (Na_2SO_4) and 35% hydrogen peroxide solution were purchased from Fisher Scientific (Waltham, MA, USA). Cotton fabrics with two different textile structures were purchased from Testfabrics Inc. (West Pittston, PA, USA). Fabric sample codes and descriptions are listed in **Table 3.5**. Unbleached cotton fabrics (400U and 460U) were used to test the outcomes of the bleach procedure with peroxide solution compared to commercially bleached fabrics (400 and 460), which have the same textile structures. Fabrics were cut into 4 inches by 4 inches swatches for all the experiments and tests.

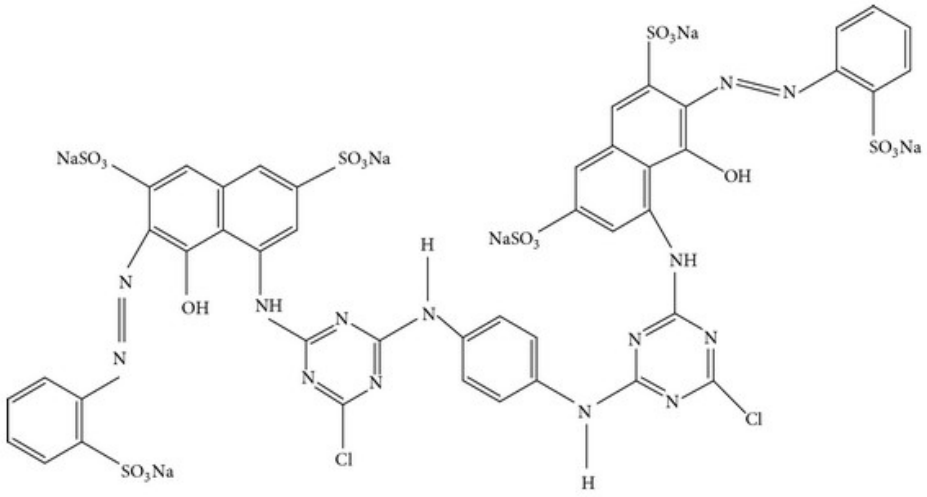

Figure 3.20 Chemical structure of CI Reactive Red 120.

Table 3.5 Sample codes and descriptions of the cotton fabrics used in the experiments.

Sample code	Product code	Descriptions	Weight (g/m^2)
U-woven	400 U	Desized, Unbleached Cotton Print Cloth	108
Woven	400	Bleached Desized Cotton Print Cloth	98
U-knit	460 U	Unbleached Cotton Interlock Knit 30" Tubular	198
Knit	460	Bleached Cotton Interlock Knit 30" Tubular	194

Each process including fabric bleaching and dying was repeated with two separate batches, and four replicates of each sample from two separate preparations were used to collect colorimetric data using an X-Rite Color i7 spectrophotometer (25 mm aperture, D65 light source and specular included mode) and analyzed in X-Rite Color I Match software. For each fabric sample, the data was obtained by averaging readings from two random areas.

3.7.2 Cotton bleaching with peroxide and treatment of post-bleach solutions with catalase

In the experiments, unbleached woven (U-woven) and knitted (U-knit) cotton fabrics were firstly bleached with 100 mM (3.4 g/L) peroxide solution (pH 9.5) at 60 °C for 12 hours with a liquor ratio of 1: 20. Partial post bleach liquids were used to test the impact of residual peroxide from bleaching on dyeing process with Reactive Red 120. The remainder of the post bleach liquids were subjected to the peroxide removal procedures either by adding dissolved CAT to the liquid or letting the liquid continuously passing through the biocatalytic yarns with catalase immobilized. To have a fair comparison between using dissolved catalase and immobilized catalase for room temperature bleach clean-up, the time used for peroxide removal with two forms of CAT was kept the same. When dissolved CAT was used to treat the post bleach liquid, TU-CAT product was added to 1 L post bleach liquid with a concentration of 0.05 g/L and stirred at room temperature for 50 minutes. In the meantime, another 1 L post bleach liquid was forced to pass through a yarn buddle made with five 35 cm long Chi-CAT (NaAc) yarn (**Figure 3.21**, b) using a transfer pipette.

After the peroxide removal using enzymes, the residual peroxide was tested using EMD Millipore™ MQuant™ Peroxide Test Strips with a detection range of 0.5 to 25 mg/L H_2O_2. Both liquid had final peroxide concentration close to 0 mg/L after 50 minutes, meaning immobilized CAT has the same capability of completely removing the peroxide from the post bleach liquid

compared to the dissolved CAT in the 50 minutes test period. To test the reusability of dissolved or immobilized CAT treated post bleach liquids in bleaching process, the above liquids were used to prepare the second 100 mM H_2O_2 (pH 9.5) bleach bath (**Figure 3.22**). O_2 bubble formation was observed right after adding fresh concentrated peroxide in the liquid treated with dissolved CAT and the peroxide decomposition continued during the adjustment of pH (the procedure was kept less than 5 minutes) of the liquid. Unbleached fabrics were then added to the second bleach bath prepared with recycled liquid to start the bleach procedure at 60 °C as described above.

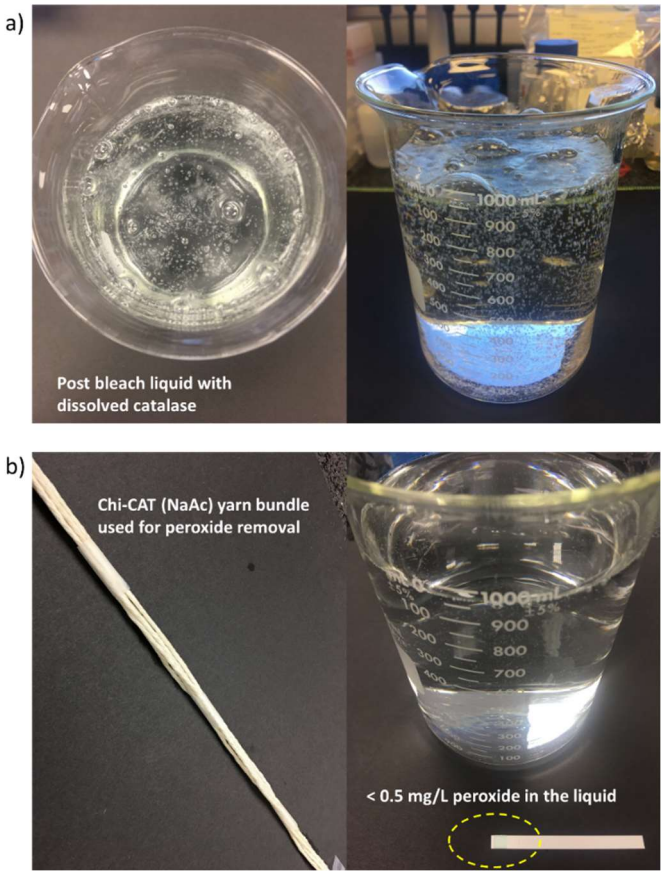

Figure 3.21 Bleach clean-up treatment of post-bleach solutions with a) dissolved catalase and b) immobilized catalase.

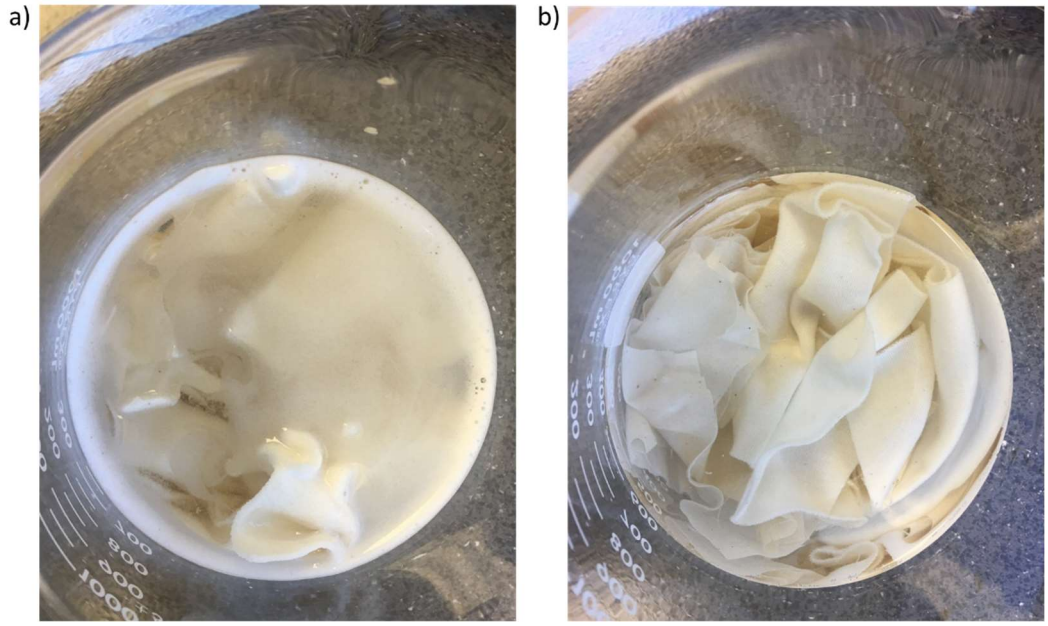

Figure 3.22 Second bleach bath (100 mM H_2O_2, pH 9.5) prepared using post-bleach liquid treated by a) dissolved catalase and b) immobilized catalase, with unbleached cotton fabrics inside. Continuous O_2 formation was observed in the secondary bleach bath prepared by liquid treated with dissolved catalase.

According to the measured CIE-Whiteness Index of the samples (**Table 3.6**), without additional enzyme inactivation steps (e.g. applying high temperature), the residual dissolved CAT impairs the reusability of the water from the bleach cleaned-up liquid in the second bleaching procedure. The residual CAT decomposing the freshly added peroxide in the second bleach bath (**Figure 3.22, a**), reducing the whiteness by about 42 units for woven cotton fabrics and 46 units for knitted cotton fabrics (**Table 3.6**). The second bleach bath made of recycled liquid treated with dissolved CAT almost has no bleaching effect on U-knit. On the contrary, when immobilized CAT was used to remove the peroxide from the post bleach liquid before reusing the liquid for fresh bleach bath, the whiteness difference between samples prepared by the first bleach bath and second bleach bath are within 2 units and 5 units of woven cotton fabrics and knitted cotton fabrics, respectively. In addition, the yarn is retrievable from liquid

environment, the biocatalytic yarn with CAT immobilized can be reused for continuous peroxide removal. Therefore, using reusable immobilized CAT can not only benefit the water reusability in the overall procedure without additional steps, it also reduces the requirement of adding enzymes to each post bleach solution.

Table 3.6 Whiteness of the cotton fabrics after bleach.

CIE-Whiteness Index	Unbleached samples	First bleach bath	Second* bleach bath from dissolved catalase treatment	Second* bleach bath from immobilized catalase treatment
Woven cotton	9.2 (±1.0)	57.1 (±1.8)	14.9 (±1.9)	54.7 (±0.9)
Knitted cotton	24.4 (±0.5)	70.1 (±1.1)	24.3 (±0.8)	65.1 (±0.6)

*Second bleach bath refers to the fresh bleach solution (pH 9.5) prepared using post bleach liquids treated with catalase.

3.7.3 Cotton dying procedure with catalase treated post-bleach liquid

To test the hypothesis 2, the remaining CAT treated post bleach solutions were used to prepare CI Reactive Red 120 solution. The cotton samples were dyed with 0.05 g/L Reactive Red 120 (47 mM Na_2CO_3, 85 mM Na_2SO_4, pH 10.5) prepared from dI water, untreated post bleach liquid, and post bleach liquid treated by either immobilized CAT or dissolved CAT, with a 1:40 liquor ratio at 80 °C for 6 hours (**Table 3.7**). pH of all the dye solutions were adjusted to 10.5, at alkaline condition, the hydroxyl groups in cotton react with the chlorine in the dye structure (**Figure 3.20**). When lab bleached fabrics were used in the dying experiments, the bleached fabrics were rinsed with dI water 5-6 times until the liquid had no detectible peroxide tested by the peroxide test strip. The dye solution prepared with untreated post-bleach liquid was used as negative control to show the impact of residual peroxide from the bleaching procedure on the dyeing process, while the dye solution prepared with dI water was used as a positive control for color difference calculation. The color measurement of dyed cotton fabrics was

described in the section *3.6.1*. The reflectance (R, %) at the maximum absorption wavelength (540 nm) was obtained to calculate the color strength (K/S) value using Equation 1:

Equation 1:

$$K/S = [\frac{(1-R)^2}{2R}]$$

In addition to the color strength of the dyed fabrics, the color different (ΔE) between samples was used to study the water reusability in the dying process. The ΔE value was calculated using L, a, b values obtained from color measurement and Equation 2.

Equation 2:

$$\Delta E_{ab} = \sqrt{(L_2 - L_1)^2 + (a_2 - a_1)^2 + (b_2 - b_1)^2}$$

Table 3.7 Sample codes and descriptions in the cotton dying experiments.

Fabric substrate	Sample code	Dye solution
400	Woven-dI	0.5 g/L dye prepared from dI water
	Woven- post bleach	0.5 g/L dye prepared from post bleach liquid
Lab bleached 400U	U-woven-dI	0.5 g/L dye prepared from dI water
	U-woven-post bleach	0.5 g/L dye prepared from post bleach liquid
	U-woven-post bleach-Icat	0.5 g/L dye prepared from post bleach liquid treated with immobilized catalase ([H_2O_2]< 0.5 mg/L)
	U-woven-post bleach-Dcat	0.5 g/L dye prepared from post bleach liquid treated with immobilized catalase ([H_2O_2]< 0.5 mg/L)
460	Knit-dI	0.5 g/L dye prepared from dI water
	Knit- post bleach	0.5 g/L dye prepared from post bleach liquid
Lab bleached 460U	U-knit-dI	0.5 g/L dye prepared from dI water
	U-knit-post bleach	0.5 g/L dye prepared from post bleach liquid
	U-knit-post bleach-Icat	0.5 g/L dye prepared from post bleach liquid treated with immobilized catalase ([H_2O_2]< 0.5 mg/L)
	U-knit-post bleach-Dcat	0.5 g/L dye prepared from post bleach liquid treated with immobilized catalase ([H_2O_2]< 0.5 mg/L)

Table 3.8 Color strength (K/S value) of samples prepared from different dye solution.

Sample code	K/S value
Woven-dI	0.63
Woven-post bleach	0.48
U-woven-dI	0.59
U-woven-post bleach	0.48
U-woven-post bleach-Icat	0.66
U-woven-post bleach-Dcat	0.64
Knit-dI	0.68
Knit-post bleach	0.54
U-knit-dI	0.69
U-knit-post bleach	0.55
U-knit-post bleach-Icat	0.71
U-knit-post bleach-Dcat	0.64

As expected, when using untreated post bleach liquid to prepare dye solution (**Table 3.8**) the color strength of dyed fabrics was about 19-24% lower compared to using the dye solution prepared with dI water, regardless the sample textile structure (Woven-post bleach/Knit-post bleach; U-woven-post bleach/ U-Knit-post bleach) and the bleach procedure applied previously (Woven-post bleach/ U-woven-post bleach; Knit-post bleach/U-Knit-post bleach). Lower temperature (60 °C) lab bleach condition has less impact on knit cotton fabrics according to the K/S values of U-knit-dI (0.69) and Knit-dI (0.68). The K/S value of dyed lab bleached woven fabric is slightly lower (0.59) than that of commercial bleached woven fabric (Woven-dI, 0.63), with less than 6% difference. Post bleach liquid treated either with dissolved CAT (U-woven-post bleach-Dcat and U-knit-post bleach-Dcat) or immobilized CAT (U-woven-post bleach-Icat and U-knit-post bleach-Icat) can be used in cotton dying process without negative influences on the color strength.

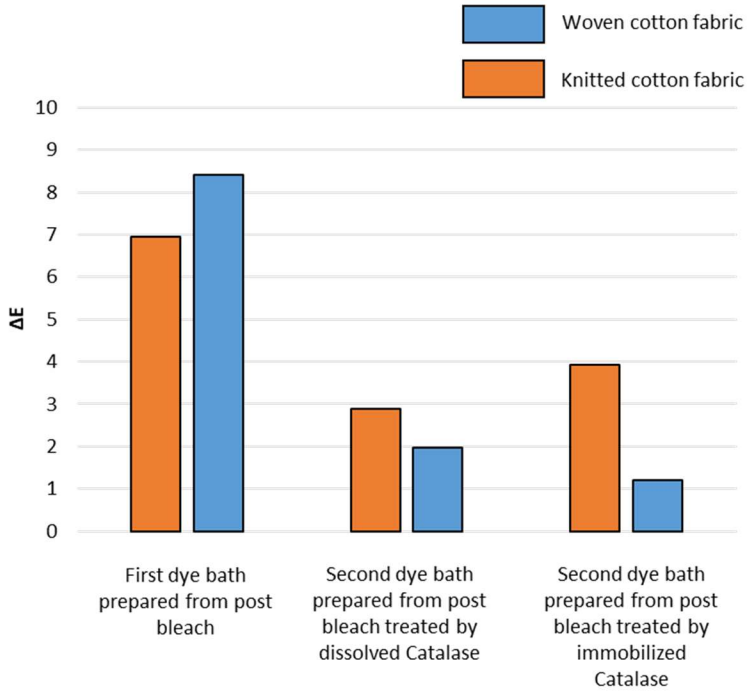

Figure 3.23 Color difference obtained by dyeing cotton fabrics with Reactive Red 120 prepared using post bleach solution, and post bleach solutions with catalase treatment. The color difference (ΔE) is relative to lab bleached positive control (U-woven-dI or U-knit-dI).

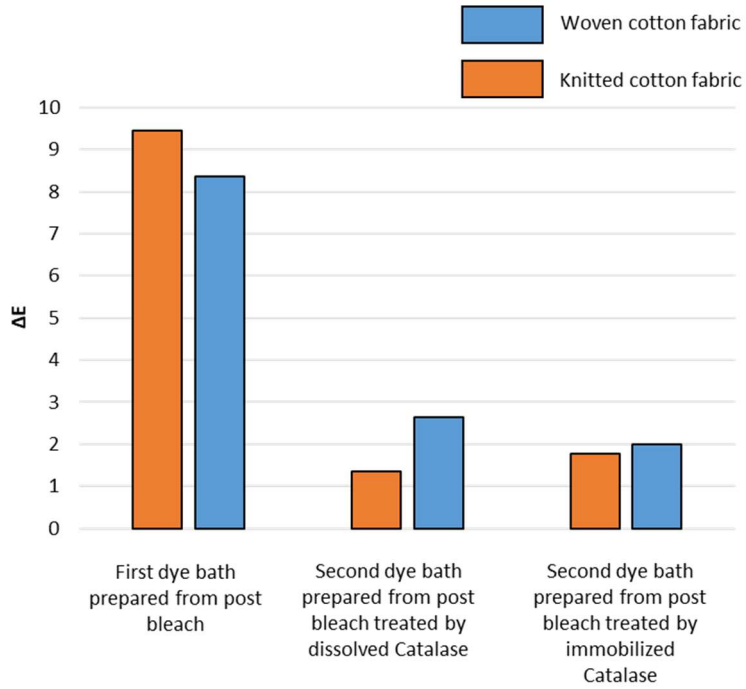

Figure 3.24 Color difference compared to commercial bleached fabrics obtained by dyeing cotton fabrics with Reactive Red 120 prepared using post bleach solution, and post bleach solutions with catalase treatment. The color difference (ΔE) is relative to lab bleached positive control (Woven-dI/Knit-dI).

The results of ΔE values showed similar results. **Figure 3.23** shows ΔE values of dyed lab bleached samples compared to positive control made with lab bleached fabrics (U-woven-dI or U-knit-dI), while **Figure 3.24** demonstrates ΔE values of dyed lab bleached samples compared to positive control made with lab bleached fabrics (Woven-dI or Knit-dI). Consistent with the K/S value data, post bleach solution treated with either dissolved CAT or immobilized CAT can prevent dye damage when recycling the post bleach water for fabric dying process. This means the immobilized CAT has the potential of being an economic and sustainable substitution of dissolved CAT in cotton finishing.

In a summary, we confirmed that the residual peroxide in post bleach liquid can be completely removed when allowing the liquid to pass through yarns containing immobilized CAT. The biocatalytic yarns can be reused in continuous peroxide removal procedures without the replenishment of dissolved enzymes. In addition, without the existence of large amounts of dissolved CAT in the liquid, the liquid treated with immobilized catalase can be reused to prepare not only the dye bath without interfering with the dyeing outcomes, but also the new bleach solution without an additional enzyme inactivation step. The results are consistent among woven and knitted cotton fabrics, which have different textile structures.

3.8 Summary

A novel enzyme immobilization approach was demonstrated by applying a chitosan-entrapped ultrafast enzyme, catalase, to a biobased textile support. The textile immobilization support was utilized as a hydrophilic biocatalytic conduit to contain and guide a liquid carrying substrates to the active sites of entrapped enzymes and to help release reaction products. By combining the structural and liquid transport function of a textile material with the catalytic

function of enzymes, a new category of multifunctional biocatalytic textile materials was created, offering a solution to the challenges of mass transfer for entrapped enzymes, such as ultrafast enzymes that catalyze heterogeneous reactions involving solid (immobilized enzymes), liquid and gas phases. During material fabrication, chitosan entrapped catalase was adsorbed as a thin coating to a cellulosic yarn support with a hierarchical fibrous structure. Chitosan-enabled enzyme entrapment at mild conditions (pH 5) plus affinity between the two polysaccharides, chitosan and cellulose, produced a robust material that withstood washing and allowed biocatalyst reuse in the application. As an added benefit, the yarn biocatalysts exhibited good stability during dry ambient storage, with samples found to be more than 60% active even after two years in ambient dry storage. Neutron imaging provided mechanistic insights to the observed high catalytic efficiency when biocatalytic yarns were used as flexible flow-through reactors. In the presence of a chitosan coating, the transport of water was slower compared to a pristine cotton yarn, water was confined in the yarn substructure where enzymes are present, and the high textile surface interface in the presence of water was preserved, assisting in the release of gaseous reaction products. Liquid flow through the yarns was assisted by wicking and by the force of gravity. When configured as a flow-through reactor, it was possible to deliver liquids through biocatalytic yarns at different useful controlled flow rates. The flow-through configuration was capable of decomposing substrate at a two-times faster rate and in twenty-times smaller reaction zone volume compared to a stirred tank configuration. Therefore, overall biocatalytic function was improved by controlling the location of dissolved substrates in the yarns and by promoting easy release of reaction products. The results of this study could be used to improve the chemical transformations of hydrogen peroxide in applications such as bleach clean-up during textile manufacturing, cold pasteurization in food processing and oxygen

generation for aerobic bioremediation (Kaushal et al., 2018; Nielsen et al., 2009; Puranen et al., 2014).

Based on these findings with catalase and the 4-ply yarn, we expect that different textile structures together with different enzymes or combinations of enzymes can be used to achieve single or cascade-type chemical reactions and enable multicomponent and modular reactor designs. For example, the techniques can be utilized to immobilize carbonic anhydrase, another ultra-fast enzyme that reversibly catalyzes CO_2 hydration, for applications including medical or industrial CO_2 gas separations. In on-going work, the functional textile materials and immobilization procedures developed here are being employed to make robust, flexible and biodegradable gas-liquid contacting materials that promote CO_2 hydration and can be fitted into gas scrubbing columns, air filters and other devices to improve biocatalytic reaction efficiency at ambient, biological and industrial conditions. Future studies would benefit from further use of modern characterization techniques such as neutron scattering to more deeply investigate the interaction between the chitosan coating, entrapped enzymes, and cellulosic support, and thereby optimize the fabrication of biocatalytic textiles. In addition, textile wet processing techniques, such as padding, are being explored as alternatives to dip coating to improve fabrication efficiency and produce prototype materials for use in a range of small- and large-format applications.

In addition, we showed application of this biocatalytic textile with CAT, which is related to the continuous peroxide removal and water recycling in cotton textile bleaching and dyeing processes. Unlike the treated liquid containing dissolved CAT, which cannot be used to prepare new bleach bath without additional enzyme inactivation, the immobilized CAT promotes the

reutilization of biocatalyst in practice and demonstrates an example of reducing the overall enzyme requirement by applying immobilized enzymes in the industrial process.

CHAPTER 4: DEUTERIUM LABELED CHITOSAN PREPARED FOR NEUTRON STUDIES OF ENTRAPPED ENZYME

Part of this chapter was published in:

Yuan, Y.; Li, H.; Leite, W.; Zhang, Q.; Bonnesen, P. V; Labbe, J. L.; Weiss, K. L.; Pingali, S. V.; Hong, K.; Urban, V. S.; Salmon, S.; O'Neill, H. Biosynthesis and Characterization of Deuterated Chitosan in Filamentous Fungus and Yeast. *Carbohydr. Polym.* **2021**, *257*. (Yuan, Li, et al., 2021)

4.1 Neutron Scattering Technique in Soft Matters

Small-angle X-ray scattering and visible light scattering are powerful techniques to investigate the properties of complex biological systems (Blanchet & Svergun, 2013; Dettenmaier et al., 1980; Stetefeld et al., 2016). These techniques help elucidate nanoscale structural features of the macromolecules or their complexes. Small angle neutron scattering (SANS) has an additional advantage for studying complex materials due to the sensitivity of neutrons to the light elements, in particular hydrogen and deuterium, which have very different neutron cross-sections (Burkoth et al., 2000; Heller et al., 2014; Lynn et al., 2006). It is possible to selectively highlight components of a complex system because of differences in the neutron scattering power of different biomolecular classes (e.g. proteins, nucleic acids, lipids) due to differences in their hydrogen content (Whitten & Trewhella, 2009). However, when the natural contrast match points of the biomolecules in a complex are similar (e.g. protein and polysaccharide), the scattering signals are averaged from the whole molecular assembly. To highlight structural features of a complex system, individual components can be deuterium labeled to allow the scattering signal of one component to be "matched out" at a particular D_2O concentration while the other component can be studied(Bali et al., 2013; DiCapua et al., 1989; Luo et al., 2009; Olah et al., 1994). For example, by deuterating chitosan, the structural features

and the conformations of other macromolecules (e.g. proteins) adsorbed on the surface of the chitosan or entrapped inside the chitosan matrix can be analyzed (Su et al., 2016).

4.2 Biodeuteration of Polysaccharides Including Chitosan

Non-exchangeable deuteration of polysaccharides is challenging because of the toxicity of deuterium to living organisms (Enright, 1971; M.-F. Lu et al., 2013; Newo et al., 2004). In previous studies, another abundant polysaccharide, cellulose, was successfully deuterated by cultivating bacteria in D_2O media with deuterated carbon sources, and the deuterated cellulose has been utilized in various neutron scattering experiments (Bali et al., 2013; J. He et al., 2014; O'Neill et al., 2015). However, only limited work has been done on chitosan deuteration (Russell et al., 2015). Yeast (*Pichia pastoris*) has been used routinely to produce deuterated recombinant proteins for NMR and neutron scattering studies (Y. Fan et al., 2015; Morgan et al., 2000), and one study has reported using it to produce perdeuterated chitosan (Russell et al., 2015). The authors concluded that the low yield (about 1 wt. % dry cell biomass) of free chitosan obtained from *P. pastoris* limits the potential of using this strain for biodeuteration of chitosan (Russell et al., 2015). Free chitosan refers to chitosan that occurs naturally in the *N*-deacetylated form without need for chemical deacetylation and that is not bound to or is easily separated from other biopolymers. Despite the low free chitosan yields, filamentous fungi have been studied as a potential source of non-animal derived chitosan (Nwe, Furuike, & Tamura, 2011). As described in a previous study, ^{13}C-labeled chitosan was obtained from the cultivation of *Abisidia coerulea* and *Gongronella butleri* in undefined media with ^{13}C-glucose feeding for the purpose of studying the enzymatic degradation of chitosan (Nwe, Furuike, Osaka, et al., 2011). However, deuteration of chitosan has not been performed in these microorganisms.

Here, we report on the approaches to obtain deuterated chitosan from *P. pastoris* and the filamentous fungus *Rhizopus oryzae*. *R. oryzae* has been widely used in industrial recombinant enzyme and other metabolite production, such as L-lactic acid, and it has been studied at bench scale for fungal chitosan production (Chatterjee et al., 2008; Sebastian et al., 2019; Tkacz & Lange, 2004). However, the impact of deuterated media on this strain and the chitosan yield were unknown. In our study, different cell culture methods were investigated to achieve successful fungal growth on deuterated media. Deuterated chitosan produced by the two strains was extracted by methods designed to obtain maximal recovery of theoretical free chitosan yields previously reported in the literature (Nwe, Furuike, & Tamura, 2011; Russell et al., 2015). The deuterated chitosans were characterized for both chemical structure and extent of deuteration. We obtained deuterated chitosan with the required level of solubility in dilute acids and film forming capability to be useful for enzyme immobilization and future neutron scattering experiments.

4.3 Biodeuteration of Chitosan from Yeast and Filamentous Fungus

4.3.1 Materials

P. pastoris was obtained from Invitrogen (Carlsbad, CA, USA) and *R. oryzae* Went et Prinsen Geerlings was obtained from American Type Culture Collection (ATCC® 9363™, VA, USA). Sodium hydroxide (NaOH), glacial acetic acid, sodium acetate and glucose were purchased from Fisher Scientific (Waltham, MA, USA). Ethylenediaminetetraacetic acid (EDTA) was purchased from Sigma-Aldrich (St. Louis, MO, USA). D-Glucose-1,2,3,4,5,6,6-d_7 (d_7-glucose) was purchased from Cambridge Isotope Laboratories (Andover, MA, USA). Yeast Mold Broth was purchased from BD (Difco™, NJ, USA). Yeast extract was purchased from Research Product International (Mt. Prospect, IL, USA) and peptone was purchased from Fisher

Scientific (Waltham, MA, USA). Heavy water (D_2O, 99.9% D) and acetic acid-d_4 (99.9 atom % D) were purchased from Sigma-Aldrich (St. Louis, MO, USA). Materials are used as received without further purification. Shrimp shell chitosan powder with an average molecular weight of 10^7 g/mol was obtained from Primex (Iceland), and further deacetylated using hot sodium hydroxide (Salmon & Hudson, 1995) to a degree of deacetylation (DD) of 89%, measured by titration.

4.3.2 Cultivation of P. pastoris for chitosan extraction

P. pastoris was cultivated on a Yeast-Peptone-Dextrose (YPD) agar plate and stored at 4 °C. YPD liquid medium was inoculated with a single colony and grown to OD 0.1 for yeast biomass production in Fernbach flasks and then incubated at 30 °C in a shaker (Model 4353, Thermo Scientific, USA) operated at 250 rpm. Minimal medium with glycerol as the carbon source (MGY) was also used to cultivate the strain to compare the yield and explore the potential of using a cheaper carbon source (deuterated glycerol) for deuteration with this strain.

4.3.3 Cultivation of R. oryzae for chitosan extraction

R. oryzae was maintained on Yeast-Mold (YM) agar plates at 4 °C. YPD agar and YPD liquid medium were used to cultivate *R. oryzae* for biomass production. To obtain clean cell mycelia from the agar plate, agar was covered by a sterile, EDTA-treated cellophane membrane (boiled for 5 minutes in EDTA 1 g L^{-1}, rinsed with water and autoclaved in water) and the cells were grown on the top of the membrane. To determine the nutrient composition for chitosan deuteration, *R. oryzae* was cultivated on Yeast-Mold (YM) agar, Potato-Dextrose agar (PDA) and Yeast-Peptone-Dextrose (YPD) agar plates for yield comparison. For solid state cultivation, a 1 cm x 1 cm cell mycelial mat from the stock plate was inoculated onto an agar plate containing 20 mL YPD medium. For liquid cultivation, 1 L YPD broth was prepared and

inoculated with three 1 cm x 1cm mycelial mats from the inoculum. Inoculated cultures were stored at 25 ± 1 °C and the mycelia were harvested before sporulation. The cell mycelia harvested from the liquid culture and solid agar plates were lyophilized (Freezone, Labconco, USA) for 3-4 days to determine the dry weight of biomass prior to chitosan extraction.

4.3.4 Chitosan extraction from P. pastoris and R. oryzae

Conventional alkali extraction (Synowiecki and Al-Khateeb, Nadia Ali Abdul Quawi, 1997) was modified in this study to reduce the amount of acid and base used during the extraction to maximize the chitosan yield. The freeze-dried *R. oryzae* mycelia were suspended in 2 N NaOH solution (1 g biomass: 100 mL solution) and autoclaved at 121 °C for 30 minutes. The alkali-insoluble pellets were vacuum filtered and washed with distilled water 6-7 times until the pH of the supernatant was between 9 and 10 and the absorbance at 280 nm was less than 0.03. Washed alkali-insoluble pellets were suspended in 10% acetic acid (1g biomass per 120 mL) for 24 hours, then filtered using a 0.45 µm pore size membrane, to obtain dissolved free chitosan in the filtrate. The transparent chitosan/acetic acid solution (filtrate) was titrated with an alkaline solution until free chitosan precipitated. The cloudy solution was centrifuged (Heraeus Megafuge 16R Centrifuge, Thermo Scientific, USA) at 4600 x g for 20 minutes at 20 ℃ and precipitates were collected. The precipitates were washed by repeated steps (6 in total) of resuspension in deionized water followed by centrifugation until the pH was approximately 7. The extracted chitosan was then lyophilized.

The extraction method for *P. pastoris* biomass was slightly changed to accommodate the different cell-wall composition between *P. pastoris* and *R. oryzae*. Instead of using filtration in the purification steps, centrifugation (Sorvall™ RC6+, Thermo Scientific, USA) at 22, 040 x g

for 40 to 60 minutes was used to separate the soluble free chitosan supernatant from insoluble cell wall components (cell, base-insoluble biomass or acid-insoluble biomass).

4.3.5 Cell growth and extracted chitosan

Appearances of extracted free chitosan from *P. pastoris* (a) and *R. oryzae* (c) are shown in **Figure 4.1**. Free chitosan, in the context of this study, refers to chitosan that can be dissolved in 10% (v/v) acetic acid with a polymer concentration of 50 mg/mL or greater, according to the extraction process developed in this study. The free chitosan from the yeast (*P. pastoris*) had a slightly brownish color while the fungal chitosan (*R. oryzae*) was nearly pure white.

Weight yields of free chitosan from the two microorganisms are listed in **Table 4.1**. The extractable free chitosan from *P. pastoris* was about 1.1-1.4 % of the dry cell weight, which is close to the value reported in a previous study (Russell et al., 2015). Growth in YPD or MGY media had limited impact on the free chitosan yield. However, because nutrient rich YPD medium resulted in a higher biomass yield, the total weight yield of free chitosan was higher using YPD than using MGY.

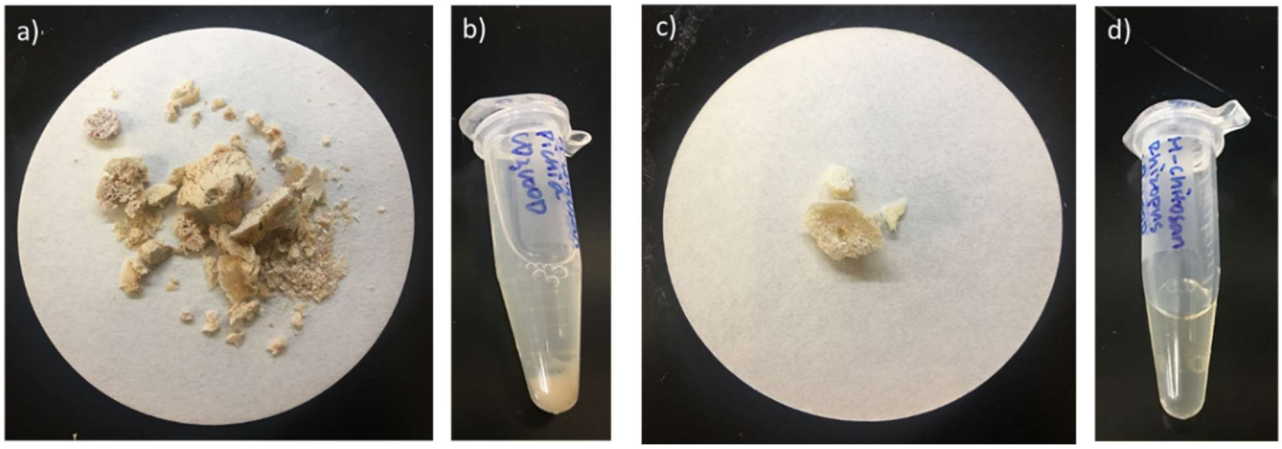

Figure 4.1. Appearance of a) purified protiated *P. pastoris* chitosan; b) 40 mg/mL protiated *P. pastoris* chitosan in D_2O containing 2% (v/v) acetic acid-d_4; c) purified protiated *R. oryzae* chitosan; d) 40 mg/mL protiated *R. oryzae* chitosan in D_2O containing 2% (v/v) acetic acid-d_4.

Table 4.1 Biomass and free chitosan weight yield from yeast *P. pastoris* and *R. oryzae*.

		Dry cell weight (g/L)	Free chitosan weight yield (wt.%)
P. pastoris	YPD (rich medium)	5.2 (± 0.6)	1.4 (± 0.1)
	MGY (minimal medium)	2.5 (± 0.4)	1.1 (± 0.1)
R. oryzae	Glucose YPD*	5.0 (± 2.0)	6.80 (± 0.20)
	Glucose YPD agar	17.5 (± 1.0)	6.60 (± 0.11)
	d_7-Glucose YPD agar	17.0 (± 1.5)	5.50 (± 0.33)
	YM agar	8.5 (± 3.0)	Not tested

*Cell growth in 30 days before sporulation.

The extractable free chitosan from *R. oryzae* was about 6.6-6.8% of the dry cell mycelia weight, which is comparable to the reported free chitosan yield previously reported for *R. oryzae* as well as from other fungi (Hang, 1990; Nwe, Furuike, & Tamura, 2011; Pochanavanich & Suntornsuk, 2002). Consistent with previous research, the fungal biomass harvested from solid state cultivation was about three times higher than that from submerged cultivation in liquid media before sporulation (**Table 4.1**) (Hang, 1990; Pochanavanich & Suntornsuk, 2002; S. C. Tan et al., 1996). However, the weight yield of extractable free chitosan was not influenced significantly by the utilization of solid or liquid cultivation conditions in this study. Notably, the nutrient composition in the fungal culture, especially the amount of carbon source, had a significant impact on biomass yield (**Figure 4.2**). The amount of biomass harvested from YPD plates was double that of YM plates. The major difference between the media types is the glucose content in the YPD medium (**Table 4.1**). Denser mycelial development was observed and higher final biomass yields were obtained on YPD agar plates (**Figure 4.2**) as compared to PDA plates in our experiments, although PDA was the typically reported media for cultivating

this filamentous fungi (Amorim et al., 2003; Hang, 1990; Yoshihara et al., 2003). In addition, we observed a delayed sporulation of *R. oryzae* on YPD plates compared to plates with other media. Therefore, solid YPD media was selected for *R. oryzae* chitosan production and deuteration.

Chitosan extracted from *P. pastoris* and *R. oryzae* grown at different culture conditions were dissolved in H_2O or D_2O containing 2% (v/v) acetic acid or acetic acid-d_4 for the film casting test, the protein entrapment test and characterization studies. The solubility of *P. pastoris* chitosan in dilute acetic acid was low, where the maximum observed concentration without precipitation was 10 mg/mL (**Figure 4.1**, b). This concentration (≤ 10 mg/mL) was not sufficient to produce a viscous solution and impaired its ability to form a uniform film. Chitosan solubility together with film formation are essential properties for the solution processing of this polymer.

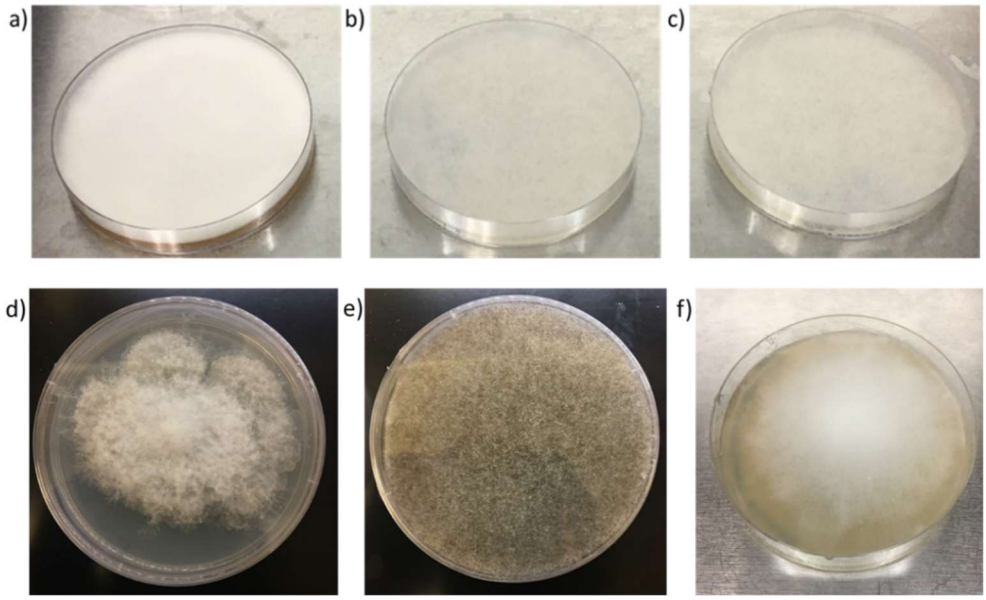

Figure 4.2 Photographs of *R. oryzae* growth after 2 days cultivation on a 9 cm-diameter Petri dish with agar: a) Yeast-Peptone-Dextrose (YPD) agar plate; b) Yeast-Mold (YM) agar plate; c) Potato-Dextrose agar plate and *R. oryzae* growth in deuterium media: d) 48 hours after inoculation on 50% D_2O YPD plate; e) Sporulation of *R. oryzae* after inoculation on 50% D_2O YPD plate for 3-4 days; f) 48 hours after inoculation on YPD plate with d_7-glucose.

4.3.6 Production of deuterated chitosan from Rhizopus oryzae

Either D_2O or deuterated carbon source (glucose) was used to deuterate chitosan from *R. oryzae*. In the preparation of liquid D_2O media for deuteration, YM powder or the ingredients of YPD media were dissolved in H_2O and D_2O mixed solvents (with D_2O percentages from 10% to 70%) at room temperature, followed by sterile filtration using a 0.2 μm pore size membrane. In the preparation of D_2O-YPD plates for deuteration, D_2O was sterile filtered using a 0.2 μm pore size membrane before mixing with autoclaved H_2O media containing an equal amount of agar. To prepare the d_7-glucose-YPD plates for deuteration, glucose was substituted with d_7-glucose in the YPD recipe while all other nutrients remained the same.

We first tested the *R. oryzae* growth in liquid and solid media in the presence of D_2O. Without the adaptation steps illustrated in **Figure 4.3**, *R. oryzae* growth was limited to 40% D_2O concentration in liquid media. Therefore, an adaptation process was required for growth in higher D_2O concentrations. Adapting *R. oryzae* to 70% D_2O liquid media took more than one month (**Figure 4.3**). Indeed, in submerged culture, *R. oryzae* like most of filamentous fungi grows in spherical pellets, consisting of compact heterogenous hyphal aggregates (Amanullah et al., 2001; Wösten et al., 2013). It is known that such pellet morphology may cause problems with internal transport of substrates and products developing local toxicity and growth issues depending on size and compactness of pellets (Dynesen & Nielsen, 2003). On the contrary, when cultivating *R. oryzae* on agar plates with D_2O concentrations from 20% to 70%, the adaptation was not a requirement. This is likely due to free mycelia growing on solid surface resulting with an optimal gas−liquid mass transfer which exhibit a different morphological behavior. Nonetheless, high D_2O concentrations often led to low cell density and early sporulation (M.-F. Lu et al., 2013) (**Figure 4.2**). Therefore, using D_2O as the sole deuterium source was not ideal for fungal chitosan deuteration regarding the long adaptation time and low biomass yield.

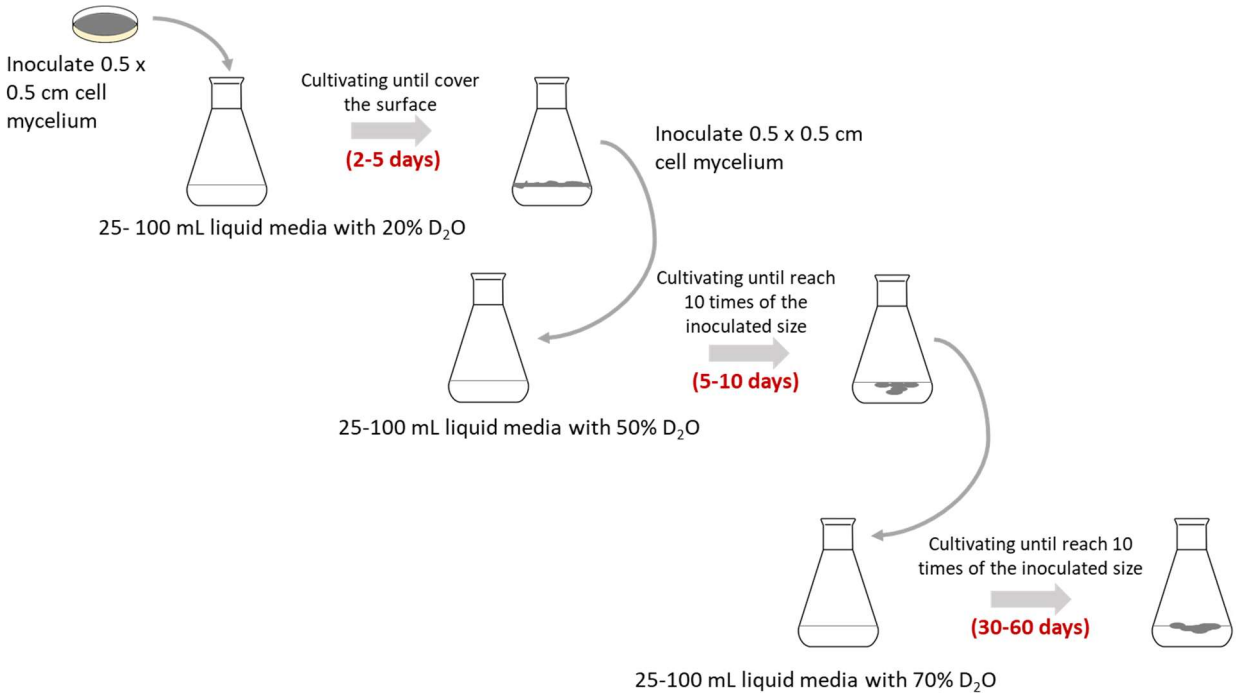

Figure 4.3 Schematic illustration of adapting filamentous fungus *R. oryzae* to liquid media containing 70% D_2O.

Because only partial deuteration of the chitosan is required for neutron scattering experiments, instead of using D_2O as the deuterium source, protiated glucose in the YPD media was substituted with deuterated d_7-glucose. Previous reports showed that exogenous glucose provided as a nutrient during growth is integrated into the chitin/chitosan structure during cell wall synthesis, providing support that feeding deuterated glucose would result in deuteration at non-exchangeable H positions in chitosan (Nwe, Furuike, & Tamura, 2011). With the same inoculation volume and cultivation time, *R. oryzae* cultivated on the d_7-glucose plates have higher cell density than that observed on plates containing D_2O, and has a similar morphology (**Figure 4.2**, f) to cells grown on protiated YPD plates (**Figure 4.2**, a). Surprisingly, the total biomass yield on d_7-glucose plates was similar to that from plates with protiated glucose (Table

1), although the d_7-glucose substitution in the culture slows down the cell growth. The extractable free chitosan from cell biomass harvested on d_7-glucose plates was about 83% of that from protiated glucose plates.

Chitosan deuteration was reported in a study using *P. pastoris* (Russell et al., 2015). This is an attractive source of deuterated biomolecules because, as a methylotrophic yeast, it can grow on deuterated methanol and D_2O and is therefore a cost effective approach for biopolymer deuteration (Morgan et al., 2000; Russell et al., 2015). However, the low solubility of *P. pastoris* derived chitosan (**Figure 4.1**, b) both interfered with our ability to characterize its chemistry by solution NMR and it was not suitable for processing into films or other solid matrices. The ability of chitosan to form a film is an important property for future applications for the development of functional composites so *P. pastoris* was not investigated further.

4.4 Gel Permeation Chromatography Characterizations

The molecular weight of the protiated and deuterated *R. oryzae* chitosan were obtained from Tosoh EcoSEC GPC System (HLC-8320) equipped with a Tosoh dual flow refractive index detector (RI). Two 6.0 mm ID × 15 cm, 3 μm particle size TSKgel® SuperH3000 columns preceded by the Tosoh guard column were used. The mobile phase was 0.5 M CH_3COOH/0.5 M CH_3COONa aqueous solution and the flow rate was 0.6 mL/min. The detector, pump oven, and column oven were maintained at 35 °C. Polyethylene Oxide (PEO) standards (Mw from 2.1 kg/mol to 1100 kg/mol) were used to calculate the relative molecular weights of *R. oryzae* chitosan samples.

The molecular weights of protiated chitosan (H-chitosan) and deuterated chitosan (D-chitosan) from *R. oryzae* are 150 kDa and 183 kDa, respectively. The difference between the two

molecular weights can be attributed to the incorporation of deuterium in the polymer, as well as the different interactions of H-chitosan and D-chitosan with solvents.

4.5 Fourier-transform Infrared Spectroscopy Characterizations

Freeze-dried chitosan powder was characterized using Attenuated Total Reflection-Fourier Transform Infrared Spectroscopy (ATR FTIR; FT/IR-6100, Jasco, USA) at room temperature from 550 to 4000 cm^{-1} with 16 scans. The resulting FTIR spectra were compared with a reference sample of shrimp shell chitosan and FTIR measurements were also used for screening the deuterated samples.

4.5.1 Chemistry of chitosan from three organisms

The ATR-FTIR spectra of dried *P. pastoris* chitosan (red solid line) and *R. oryzae* chitosan (blue long dashed line) are shown in **Figure 4.4**, along with chitosan extracted from shrimp shell (black short dash line) as a reference. The characteristic peaks of polysaccharide such as the hydroxyl bands and C-H bands, with wavenumbers of 2700 to 3500 cm^{-1}, were observed in the chitosan from all three organisms (Baxter, et al., 1992, Hang, 1990, Muzzarelli, et al., 1980). However, the peak splitting around 3400 cm^{-1}, which is a characteristic peak of chitosan, was more obvious in *R. oryzae* chitosan than in the other two specimens. Characteristic bands representing the primary amine functional group (1600-1550 cm^{-1}) were observed in all three chitosan samples. The relative extent of *N*-acetylation can be estimated from IR spectra by comparing the ratio of amide I band at 1655 cm^{-1} to that of C-H band at 3450 cm^{-1} (Baxter, et al., 1992, Kumirska, et al., 2010). This ratio in *P. pastoris* chitosan is much larger than that of chitosan from *R.oryzae* and shrimp, indicating that fewer free amine groups exist in the *P. pastoris* chitosan structure. Fungal chitosans also show peaks around 1640 cm^{-1}, which was not

observed in the shrimp chitosan spectra (**Figure 4.4**, a, inlet). According to studies by Muzzarelli et al., this can be attributed to the glucan structure (Muzzarelli, et al., 1980). Indeed, for almost all fungi the central core of the cell wall is a branched β -1,3/1,6 glucan that is linked to chitin via a β -1,4 linkage. The composition of the glucan can vary significantly in different fungal species, particularly in the content of mannan and glucan (Klis, et al., 1997, Latgé, 2007). The ratio of band at 1640 cm^{-1} to that of C-H band at 3450 cm^{-1} in *R. oryzae* chitosan spectra is lower than the ratio in *P. pastoris* chitosan spectra (**Figure 4.4**). The data indicates that there is a significant amount of β-glucan associated with *P. pastoris* chitosan and this, as well as the low degree of deacetylation, contributes to its low solubility in 2% acetic acid solution. These chemical features of the *P. pastoris* chitosan also explain a phenomenon observed during the chitosan extraction and purification process, where the pH required to precipitate *P. pastoris* chitosan was consistently lower than for *R.oryzae* chitosan by 1.5 to 2 units. This is because with the higher degree of deacetylation of *R. oryzae* chitosan required more base to titrate the higher number of protonated amino groups in the structure when precipitating chitosan from acidic solution.

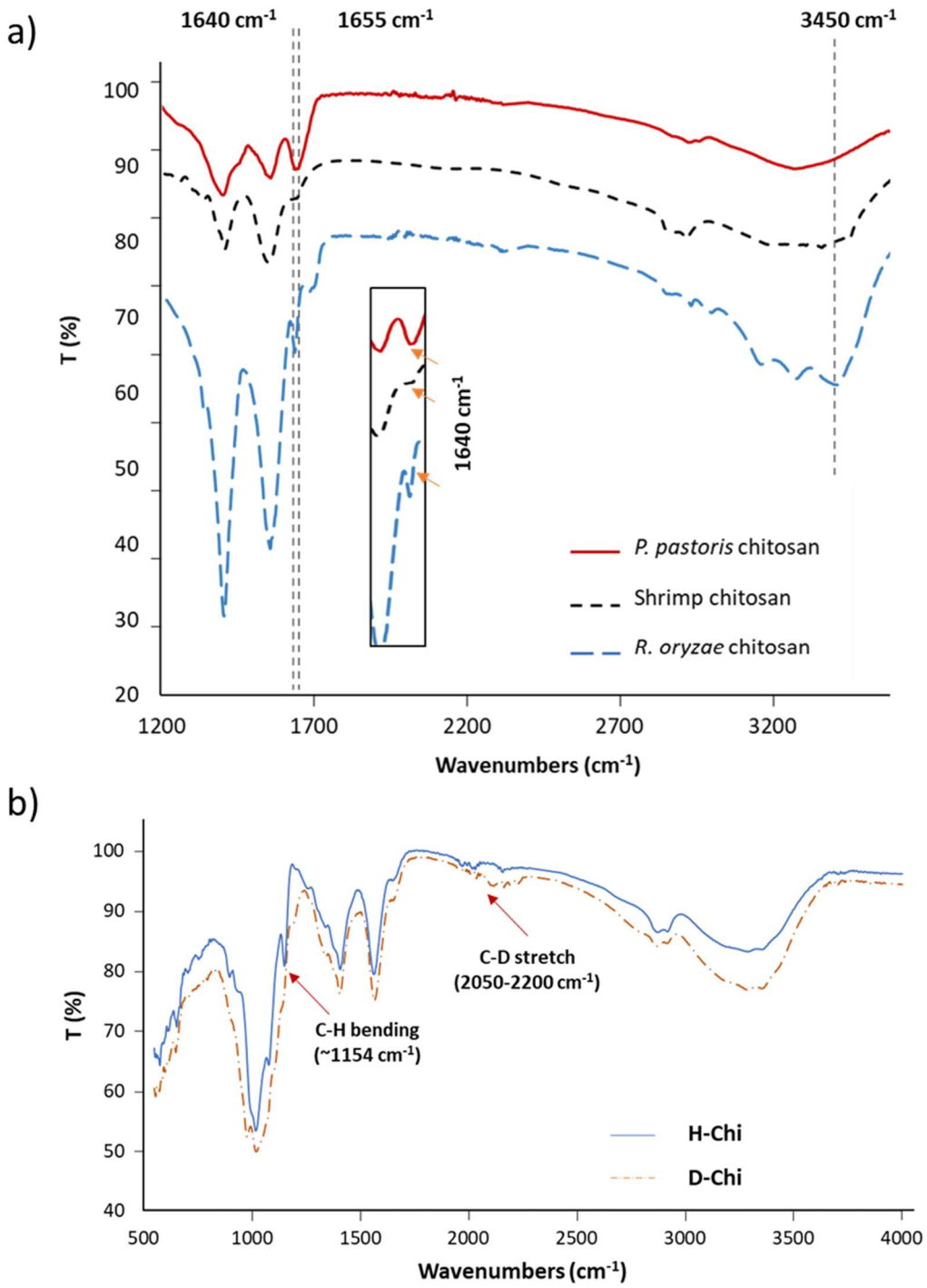

Figure 4.4 ATR-FTIR spectra of extracted chitosan samples: a) protiated chitosan extracted from *P. pastoris* (red solid line), shrimp (black short dashed line) and *R. oryzae* (blue long dashed line). The shrimp and *R. oryzae* spectra were offset by a factor of 0.9 and 0.8, respectively, from the protiated *P. pastoris* chitosan for clarity; b) chitosan isolated from *R. oryzae* cultivated on protiated glucose plates (H-Chi, blue solid line) and d_7-glucose plates (D-Chi, orange dash line).

4.5.2 Confirmation of deuteration with d_7-glucose feeding

The FTIR spectra of H-chitosan (blue solid line) and D-chitosan (orange dashed line) from *R. oryzae* are shown in **Figure 4.4**, b. The overall spectra of the two chitosans overlap well with each other and specific peak changes indicate that non-exchangeable deuteration on the chitosan backbone was achieved by d_7-glucose substitution in solid agar cultivation. Deuterated *R. oryzae* chitosan has a unique peak between 2050 to 2200 cm^{-1}, which is attributed to C-D stretching (Russell et al., 2015; Tyrode & Hedberg, 2012). In addition, the peak at 1154 cm^{-1}, corresponding to C-H bending in H-chitosan, was not observed in the D-chitosan spectrum indicating a decrease of C-H bonds in deuterated chitosan. To further measure deuteration levels of the chitosan obtained using our deuteration approach, we conducted ^{1}H and ^{13}C NMR studies on the *R. oryzae* H- and D-chitosan.

4.6 Nuclear Magnetic Resonance (NMR) analysis of extracted chitosan

NMR studies were performed on a Varian VNMRS 500 MHz spectrometer at 23 °C to identify the isolated biopolymer as well as to elucidate the deuterium incorporation at the non-exchangeable positions. ^{13}C NMR spectra were obtained using inverse-gated decoupling with a recycle delay of 25 seconds. D_2O solution containing 2% (v/v) acetic acid-d_4 was used to prepare protiated *P. pastoris* chitosan (10 mg/mL), protiated *R. oryzae* chitosan (40 mg/mL), and deuterated *R. oryzae* chitosan (30 mg/mL) for ^{1}H NMR and ^{13}C NMR measurements. The concentrations of each sample were different depending on solubility and signal sensitivity. A 40 mg/mL shrimp chitosan sample in 2% (v/v) acetic acid-d_4/D_2O solution was prepared and subjected to ^{1}H NMR characterization for comparison. The HOD peak was used as an internal chemical shift reference in this study.

Long acquisition (60 h) ^{13}C APT (attached proton test) measurements were conducted on the deuterated *R. oryzae* chitosan sample to determine its deuteration levels. The ^{13}C APT experiment helps distinguish the proton multiplicity of carbon atoms by showing negative signals for secondary (CH_2) and quaternary (C) carbon atoms, and positive signals for primary (CH_3) and tertiary (CH) carbon atoms. If a carbon atom is fully deuterated, it appears as quaternary.

^{1}H NMR spectra of free chitosan samples are shown in **Figure 4.5**. Because of the high gelation potential of D-chitosan in acetic acid-d_4 solution and the high viscosity of the solution, the concentration of D-chitosan for NMR characterization was limited to 30 mg/mL. From the ^{1}H NMR spectrum, the H3 to H6 atoms give characteristic signals between 3.6 and 3.9 ppm and H2 atom showed a single peak at 3.08 ppm (Yoshihara et al., 2003). Both H- and D-chitosan showed similar peaks at these positions but with much weaker intensities from D-chitosan. This indicates that the chitosan isolated from *R. oryzae* on d_7-glucose plates has been partially deuterated. Further calculation of the deuteration level from the ^{1}H NMR spectra suggests almost half of the hydrogen positions protons have been replaced by deuterium (**Figure 4.5** and **Table 4.2**). However, because bias may be introduced during the sample preparation process, e.g. moisture from air or calibration of sample concentration, the obtained deuteration levels may be different from their theoretical values. In addition, the H1 and NH peaks were not observed in the spectrum where they may overlap with HDO peak at 4.79 ppm. This overlap will also lead to an inaccurate deuteration level calculated from ^{1}H NMR results. Therefore, ^{13}C NMR studies were performed to quantify the deuteration level of the chitosan samples.

The ^{13}C NMR spectra of H- and D-chitosan in **Figure 4.6** reveal that substantial nonexchangeable deuteration of *R. oryzae* chitosan occurred. For the H-chitosan (**Figure 4.6**, a), six sharp signals at 95.64 (C1), 74.26 (C5), 72.83 (C3), 68.11 (C4), 57.92 (C6) and 53.82 (C2)

ppm can be attributed to the polysaccharide structure (Xiang et al., 2009). In the D-chitosan spectrum (**Figure 4.6**, b), these six signals were also observed, indicating that the chitosan was not perdeuterated. At the same time, deuteration also broadened the peaks. Extra peaks observed in the same region (from 50 to 100 ppm) can be assigned to the same carbon atoms but connected to deuterium (C(D)). An exception was C2, where no obvious additional carbon signal was observed close to the C2(H) peak, suggesting that the deuteration degree at C2 is low. This low deuteration was appeared as slightly down-field shifted carbon peaks in ^{13}C-NMR spectra. However, H2 position was found slightly deuterated in ^{1}H-NMR spectra (**Figure 4.5**) by the reducing of H2 peak area (**Table 4.2**). The peak at 97.4 ppm may come from C1, whose chemical shift is also influenced by the deuteration on adjacent carbon atoms. The peaks for C3, C4, C5 in the region between 65 and 75 ppm are very close and partially overlapped, hence no detailed assignment could be made based on this ^{13}C NMR spectrum.

In order to separate the signals from C3, C4, C5, a ^{13}C attached proton test (APT) NMR study (Jacobsen, 2007) was conducted on the D-chitosan sample. A long 60 h measurement was applied and the result is shown in **Figure 4.7** and **Figure 4.8**. Sufficient signal-to-noise was obtained for C3, C4, C5 for data analysis, but not for C1, C2 and C6. C3, C4 and C5 are all tertiary carbon atoms before deuteration, therefore their peaks can be integrated and separated from C(H) to C(D) in the APT experiment: C(D) gives negative signals while C(H) gives positive peaks, respectively. Based on this, the negative peaks at 73.72, 72.26, 70.81, 68.71, 67.59 ppm (blue in **Figure 4.8**,b) were assigned to C(D) and the positive peaks at 74.25, 72.62, 68.08 ppm (red in **Figure 4.8**, b) are from the C(H). The chemical shifts of the red peaks are consistent with those of the C3-C5 peaks in the ^{13}C NMR spectrum of the H-chitosan. Integration

of these carbon peaks gives the deuteration levels on C3, C4, and C5 between 63.4 - 83.6% (see **Table 4.3**, Equation 1).

Equation 1:

$$Deuteration\ level = [\frac{Area_{C(D)}}{Area_{C(D)}+Area_{C(H)}}],$$

where $Area_{C(D)}$ is the integral of the carbons connected to deuterium C(D), and $Area_{C(H)}$ is the integral of the carbons connected to proton C(H) obtained from the spectra.

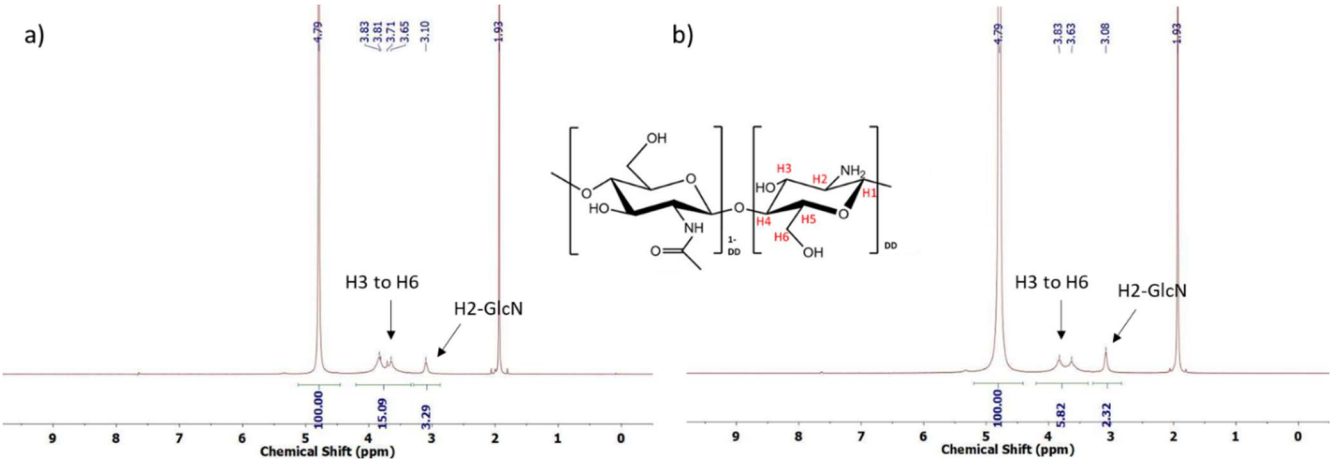

Figure 4.5 ^{1}H NMR spectra of *R. oryzae* chitosan in D_2O containing 2% (v/v) acetic acid-d_4, T = 23 °C. a) H-chitosan isolated from protiated glucose plates, 40 mg/mL; b) D-chitosan isolated from d_7-glucose plates, 30 mg/mL

Table 4.2 ^{1}H-NMR calculation for overall deuteration level.

	^{1}H Integral in protiated sample ($Area_H$)	^{1}H Integral in deuterated sample ($Area_D$)	Deuteration level*
Peak 1 (3.5-4 ppm)	15.09	5.82	48.6 %
Peak 2 (3 ppm)	3.29	2.32	6 %

*Calculated by 1-($Area_D$ /concentration of D sample)/ ($Area_H$ /concentration of H sample)

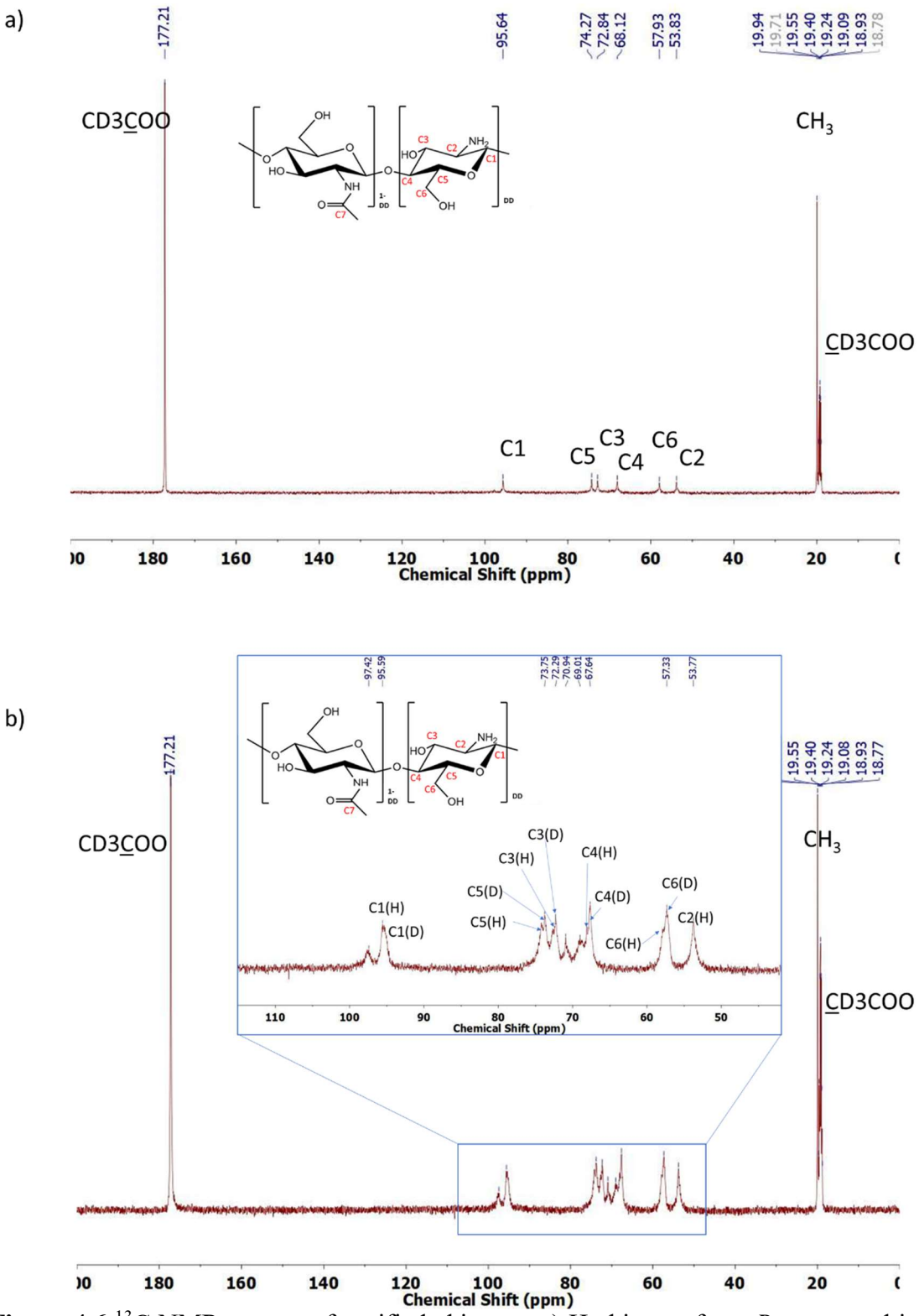

Figure 4.6 ^{13}C NMR spectra of purified chitosan: a) H-chitosan from *R.oryzae* cultivated on H-glucose YPD plates; b) D-chitosan from *R.oryzae* cultivated on d_7-glucose YPD plate.

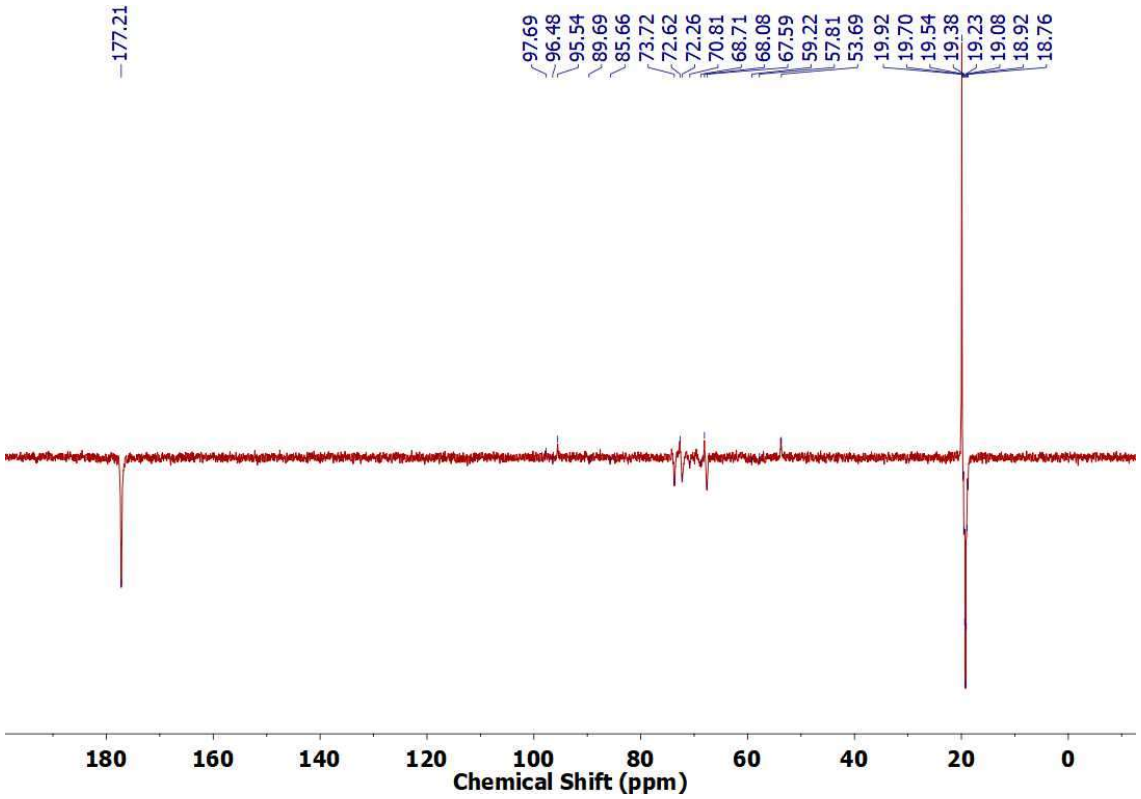

Figure 4.7 Full ^{13}C Attached Proton Test (APT) NMR spectrum of D-chitosan sample.

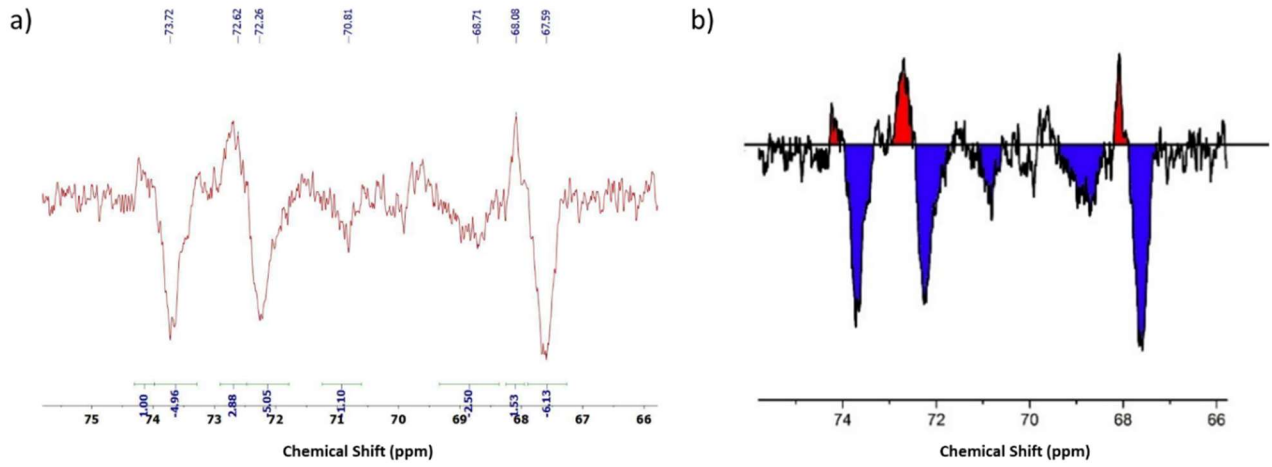

Figure 4.8 a) ^{13}C Attached Proton Test (APT) NMR spectra of D-chitosan samples; b) Deuteration levels are calculated based on peak integral. Red peaks with positive signals are from C(H) atoms and blue peaks with negative signals are from C(D) atoms.

Table 4.3 Calculation of deuteration levels on different carbon atoms in chitosan structure from APT study.

Carbon atom	Chemical shift (ppm)	$Integral_{CD}$[a]			$Integral_{CH}$			Deuteration level (averaged)[b]
C3	72-73	5.05	5.10	5.13	2.88	3.07	2.88	(63.4 ± 1.7)%
C4	67-69	6.13	6.46	6.25	1.53	1.57	1.65	(79.9 ± 3.5)%
C5	73-75	4.96	5.23	5.05	1.00	1.00	1.00	(83.6 ± 3.5)%

[a]three times measurements were conducted for each carbon signal integral, the integral of peak at 74.25 ppm was set as 1.00; [b]detailed calculation can be found in supporting information.

In fact, the real deuteration levels of C3-C5 atoms may be even higher, because the peaks at 70.81 and 68.71 ppm also show negative signals, indicating they are also C(D). These peaks may come from the different environment created by adjacent carbon atoms, either C(H) or C(D), for example, secondary isotope shift (Darwish et al., 2016). Other errors during the data interpretation may come from the baseline determination (**Table 4.4**). Overall, the NMR results show high deuteration levels (minimum~60-80%) of C3-C5 atoms and an extremely low deuteration level (~6%) on C2, which suggests that C2, the carbon atom connected to the amine group, might come from nutrients (e.g. amino acids) other than glucose. This gives insight that other deuterated nutrients, such as deuterated amino acids, may increase the deuterium incorporation at the C2 position in this strain. In addition, previous work proved that ^{13}C labeled glucosamine could be incorporated in chitosan by cultivating the fungus *Absidia coerulea* in medium containing 2-^{13}C-glucose, after which the polymer was hydrolyzed for mass spectrometry analysis (Nwe, Furuike, Osaka, et al., 2011). Therefore, by digesting chitosan through acidic or enzymatic hydrolysis, further analysis can be conducted to observe deuterium in glucosamine molecules in *R. oryzae* derived chitosan.

Table 4.4 ^{13}C-NMR calculation for deuteration level at C3, C4 and C5 carbon positions.

	Integral			Average integral	Standard deviation
	Test 1	Test 2	Test 3		
C3(D)	5.05	5.10	5.13	5.09	0.04
C4(D)	6.13	6.46	6.25	6.28	0.17
C5(D)	4.96	5.23	5.05	5.08	0.14
C3(H)	2.88	3.07	2.88	2.94	0.11
C4(H)	1.53	1.57	1.65	1.58	0.06
C5(H)	1.00	1.00	1.00	1.00	0
C3(H)+C3(D)	8.04				0.13
C4(H)+C4(D)	7.87				0.18
C5(H)+C5(D)	6.08				0.14
deuteration level					
C3	0.634				0.017
C4	0.799				0.035
C5	0.836				0.035

4.7 Small-angle Neutron Scattering

To prepare samples for small-angle neutron scattering (SANS) measurements, protiated and deuterated chitosans were transferred to previously tared centrifuge tubes. Sample weights were determined and 2% (v/v) acetic acid-d_4 solution in D_2O was added to each tube to prepare a final suspension of approximately 10 mg/ml. After mixing on a benchtop vortexer, the samples were incubated overnight at room temperature. On the following day, the tubes were vortexed, flash frozen in liquid nitrogen, and lyophilized overnight. After repeating the dissolution, incubation and lyophilization process, 2% (v/v) acetic acid-d_4 (v/v) in D_2O was again added to each sample to prepare final chitosan concentrations of 10 mg/ml. After mixing and incubating overnight, the chitosan solutions were then transferred to 1 mm pathlength quartz 'banjo' cells for SANS measurements.

SANS measurements were performed at the Bio-SANS instrument located at the High Flux Isotope Reactor in Oak Ridge National Laboratory (ORNL) (Heller et al., 2014). The main detector array was positioned at 15.5 m from the sample position, and the wing detector array was positioned 1.13 m from the sample position at an angle of 1.4° from direct beam. Using this configuration, the Q range spanning $0.003 < Q\ (Å^{-1}) < 0.8$ was obtained using 6 Å neutrons with a relative wavelength spread ($\Delta\lambda/\lambda$) of 15%. The scattering intensity profile, I(Q) versus Q, for each sample was obtained by azimuthally averaging the processed 2D images which were normalized to incident beam monitor counts, corrected for detector dark current, pixel sensitivity and scattering from backgrounds such as solvent and cuvette.

The SANS data were fit using the Modelling-II implementation in the IRENA package of Igor Pro software by Wavemetrics (Beaucage, 1995; Ilavsky & Jemian, 2009).The fitting approach was similar to analysis of cellulose described elsewhere (Shah et al., 2018).

Small-angle neutron scattering (SANS) analysis was carried out on the protiated and deuterated forms of the chitosan (**Figure 4.9**, a). The shapes of the curves are similar indicating overall polymer properties in solution were not affected by the substitution of deuterated glucose in the growth media or the incorporation of deuterium into the polymer. The continuously increasing intensity with decreasing wave-vector, *Q*, in the *Q*-range 0.003 to 0.09 $Å^{-1}$ suggests that the structure of chitosan is consistent with long elongated particles. The fitting parameters for the protiated and deuterated polymers are shown in **Table 4.5**. The organization of the individual chitosan chains within the fibers is represented by the power-law behavior and Guinier approximation in the high-*Q* range (0.09 - 0.5 $Å^{-1}$). The power-law exponents (*P*) that represent polymer chain conformation are similar and are consistent with a linear rod-like arrangement of the chitosan chains. The Guinier contribution for the high-*Q* range was fixed to

the value determined using the smallest radius (R_{min}) from the low-Q data. The low Q data (0.003 - 0.09 Å^{-1}) were fit to a radial distribution of cylinders. The smallest chitosan fiber radius (R_{min}) obtained from the fitting was ~34 Å for both forms of chitosan (**Figure 4.9**, b). However, the radial distribution of the fibers in solution is broad. A significant difference in the mean fiber radius, 297 ± 3 Å and 124 ± 5 Å was observed for the protiated and deuterated forms, respectively. Still, the maximum likelihood of fiber radius for the two chitosan forms is similar, 54 Å and 60 Å for the deuterated and protiated forms, respectively (**Figure 4.9**, b). This means that the radii of the individual fibers of protiated and deuterated have similar dimensions but there is a broader distribution of fiber radii in the protiated chitosan sample. The differences in the cross-sectional radius distribution of the two chitosan forms may reflect differences in the H-bonding interactions between the chitosan chains that assemble to form the fibers. A schematic representation of the shape and polydispersity of the chitosan fibrils is summarized in **Figure 4.9**, c. Overall, SANS data provide valuable insight into the organization of chitosan in solution and reveal the assembly pattern of the individual chitosan chains to form a fiber network with little impact of D-incorporation in the polymer structure.

Table 4.5 Structural model parameters of protiated and deuterated chitosan.

	High Q (0.09 - 0.5 Å^{-1})		**Low Q (0.003 - 0.09 Å^{-1})**		
	B (x10^{-6})	**P**	**R_{min} (Å)**	**R_{mean} (Å)**	**Length (Å)**
H-Chitosan	4.7	0.9 ± 0.2	35 ± 5	297 ± 5	>5000
D-Chitosan	0.1	1.1 ± 0.2	33 ± 5	124 ± 3	>5000

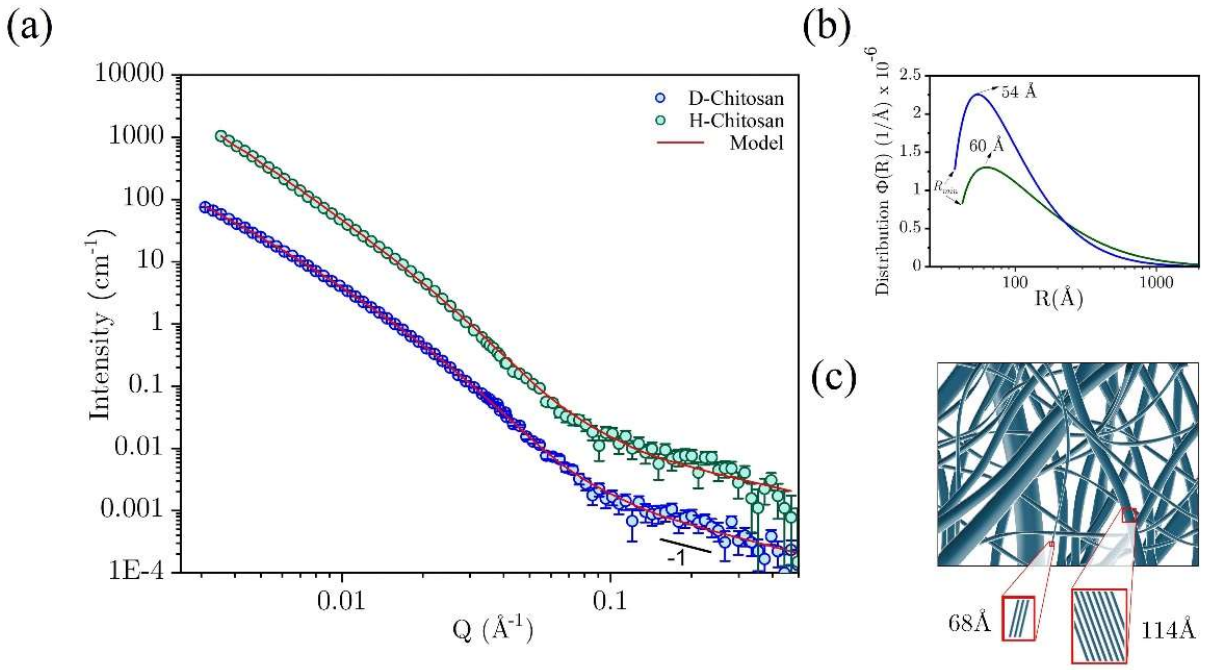

Figure 4.9 SANS analysis of protiated and deuterated chitosan: a) SANS profiles measured for protiated (green) and deuterated (blue) in 100% D_2O solvent. The fit lines obtained with two structural levels is shown in red. The high-Q data were fit with a power law exponent (*P*) and scale factor (*B*). The low-Q data were fit using a cylinder form factor with a log normal distribution of radius, fixed length, and minor and mean radius (R_{min} and R_{mean}); b) Volume polydispersity distribution of chitosan fibers; c) Schematic representation of chitosan fibers in solution, respectively. The minimum radii of fibers (R_{min} ~ 34 Å; D_{min} ~ 68 Å) and the mostly abundant radius (R_{mode} ~ 57 Å; D_{mode} ~ 114 Å) detected is represented in the figure by the fiber diameters (D_{min} and D_{mode}). Note: the number of chains within the two fibers depicted in the schematic was chosen for illustrative purposes and is not a measured quantity.

4.8 Catalase Entrapment in *R. oryzae* Chitosan Film

The compatibility of *R. oryzae* chitosan for enzyme entrapment was tested using catalase from bovine liver (2,000-5,000 units/mg protein, Millipore Sigma, St. Louis, USA) to demonstrate its utility for improving enzyme longevity in various applications. An *R. oryzae* chitosan film from acetic acid was re-dissolved in 100 mM sodium acetate solution (pH 5) and formed a 4 wt. % fungal chitosan solution. Lyophilized catalase powder was added to the fungal chitosan solution with a chitosan-to-enzyme weight ratio of 5:1. The solution was poured onto a

polytetrafluoroethylene (PTFE) tray and air-dried under a ventilated hood, forming a transparent film. To determine catalase activity after entrapment by *R. oryzae* chitosan, the biocatalytic film was submerged into 10 mL of 340 mg/L H_2O_2. The peroxide concentration in the solution was measured by EMD MILLIPORE™ MQUANT™ Peroxide Test Strips (Fisher Scientific, Hampton, New Hampshire, USA) with a detection range of 0.5 to 25 mg/L H_2O_2.

Use chitosan for enzyme entrapment is an example, where enzyme molecules trapped inside the chitosan matrix are stabilized to improve their longevity and reusability. The solubility of *R. oryzae* chitosan in 2% (v/v) acetic acid (pH 2.6) and 100 mM sodium acetate solution (pH 5) is comparable to conventional chitosan extracted from shrimp shell (about 4-5 wt %), which allows the further processing of this fungal chitosan for protein entrapment. In this study, enzyme entrapment was demonstrated by immobilizing catalase inside *R. oryzae* chitosan from a sodium acetate solution (pH 5) to form an almost colorless flexible uniform transparent film (**Figure 4.10**). When the *R. oryzae* catalase-containing chitosan film was immersed in a hydrogen peroxide solution, the entrapped catalase retained its hydrogen peroxide decomposition activity as evidenced by the formation of oxygen bubbles only at the surface of the film, indicating that catalase was securely entrapped inside the chitosan film (**Figure 4.10**, a). Also, the entrapped catalase retained its activity in the chitosan film after storing the film at ambient conditions for six months (**Figure 4.10**, b). The *R. oryzae* chitosan-catalase film lowered the peroxide concentration from 340 to 0 mg/L after 20 minutes (**Figure 4.10**, c). This demonstrates that fungal chitosan is a suitable biopolymeric matrix for enzyme entrapment, where the enzyme substrates/products can freely diffuse to/from the catalytic sites. Therefore, *R. oryzae* was selected for production of deuterated chitosan to study the properties of proteins either entrapped inside the chitosan matrix or adsorbed onto its surface using neutron scattering (Luo et al., 2009).

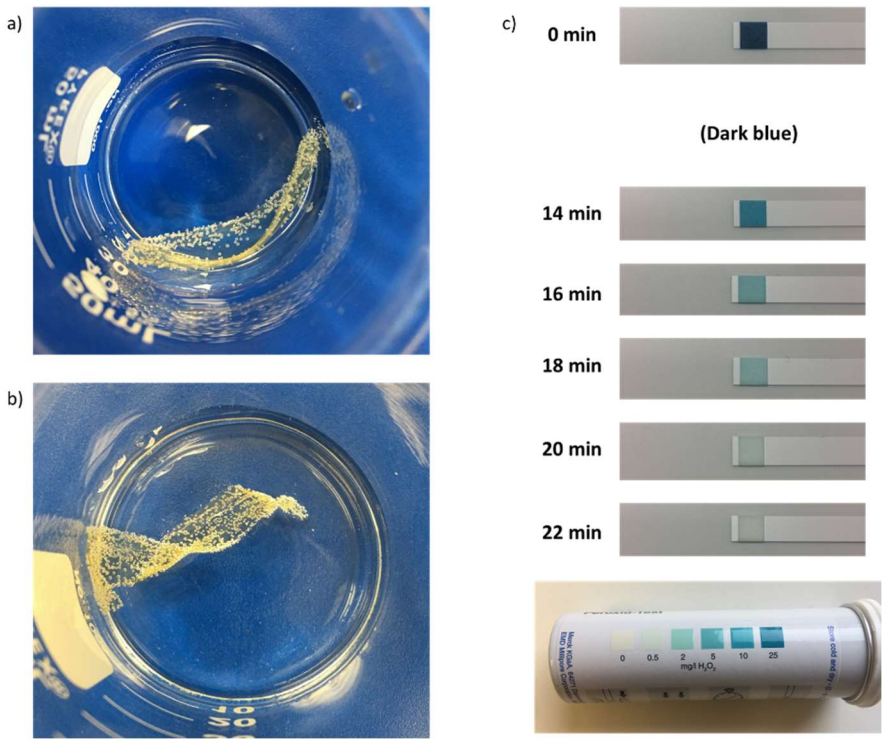

Figure 4.10 Catalytic activity of entrapped catalase in *R. oryzae* chitosan. The *R. oryzae* chitosan-catalase film was immersed in 340 mg/L H_2O_2. Oxygen bubbles from peroxide decomposition are observed only inside and on the surface of the a) fresh made film and b) film after 6-month storage at ambient conditions. c) Peroxide decomposition assay of entrapped chitosan after 6-month storage (25 mg/L H_2O_2 is the darkest blue color on the test strip scale; bottom image).

4.7 Summary

Our overall aim was to investigate fungal chitosan as a substitute for crustacean chitosan for materials applications such as enzyme entrapment and immobilization for bioconversion applications. Developing a fungal source of chitosan may be advantageous for future development of 'designer' chitosan for specific applications. The goal of the present study was to produce a deuterium-labeled chitosan for advanced characterization of chitosan-based biomaterials using neutron scattering techniques. We evaluated the feasibility of using two microorganisms for chitosan deuteration by analyzing and comparing chitosan extracted from *R. oryzae* and the yeast, *P. pastoris*, which has been the only microorganism used in prior chitosan deuteration work (Russell, et al., 2015).

This is the first report of chitosan deuteration from the filamentous fungus *R. oryzae*, as well as analysis of deuteration levels in its structure. To achieve this, the cultivation and extraction methods of *R. oryzae* were modified to achieve a yield of about 6-7% dry cell mass of free chitosan. The chitosan extracted from *R. oryzae* showed a superior solubility in dilute acid and it was possible to cast transparent thin films from a solution and entrap enzymes in the matrix. The observed solubility and processability of *R. oryzae* chitosan was attributed to the lower β-glucan content and higher degree of deacetylation in the structure compared to *P. pastoris* chitosan. These properties are beneficial to fabricate composite materials in different forms such as particles, fibers, and films. The physical behavior of non-deuterated fungal chitosan prepared by fungal culture methods mimicked that of shrimp shell chitosan and represents a new approach to producing a high-quality, non-animal-derived version of the versatile chitosan biopolymer without the need for conventional chemical deacetylation.

Partially deuterated *R. oryzae* chitosan was successfully prepared by substituting glucose with deuterium labeled d_7-glucose in the solid cultivation and the yield was similar to the yield obtained from protiated nutrients, offering a convenient method for the production of deuterium-enriched chitosan. Interestingly, NMR studies show that high deuteration levels were achieved for C3, C4 and C5, however, almost no protium was replaced by deuterium on C2. In addition, SANS showed that there were no significant structural changes in deuterated chitosan compared to its protiated counterpart. Based on these findings, we conclude that the deuterium labeled *R. oryzae* chitosan produced in this study is a suitable model for characterization of bio-composites using neutron scattering techniques. Future work will include the optimization of deuterium incorporation in chitosan by utilizing other deuterium sources in the cultivation media, such as

supplementing the growth medium with deuterated amino acids to increase the deuterium incorporation into chitosan.

CHAPTER 5: IMMOBILIZING CARBONIC ANHYDRASE FOR CARBON DIOXIDE SCRUBBING

Parts of this Chapter contributed to a DOE-BETO sponsored project in collaboration with NREL and University of Kentucky

5.1 CO_2 Scrubbing Challenge and Solution with Enzymes

In a report of the Department of Energy (DOE) and according to the 1992 U.N. Framework Convention on Climate Change, the preindustrial level of CO_2 level raised from 280 ppm a century ago to 380 ppm, and consensus was formed that the number must remain lower than 450 ppm to avoid catastrophic impact on global climate (Metz et al., 2007). Unfortunately, the predications of the prior decades are coming to reality as our Earth continues to warm. In addition, a report in 2010 pointed out that among all actions adopted in carbon capture and storage (CCS), the high-energy consumption and high cost of post combustion CO_2 treatment presents the biggest challenge. (Alivisatos & Buchanan, 2010) Therefore, finding an efficient industrial scale CO_2 separation technique is an important research area, in order to control the emission CO_2 to atmosphere from power plants and other CO_2 emission sources, in order to meet the COP21 commitments to limit warming to less than 2 °C (Bui et al., 2018).

Solvent based CO_2 absorption has been applied and evaluated for post combustion CO_2 capture, in which the most commonly used chemical solvents are amines, mainly monoethanolamine (MEA) (B. Rao & S. Rubin, 2002; Luis, 2016). However, it was not seen as the best strategy due to the high cost of the chemical and high energy input in the desorption process (Luis, 2016). To find a more sustainable CO_2 capture approach, soluble CA has been dissolved in liquid CO_2 absorbents for CO_2/N_2 separation, and enzyme performance and their compatibility with the absorbents were evaluated. (G. Hu et al., 2017; Leimbrink et al., 2018;

Salmon & House, 2015; S.-I. Tan et al., 2018) Initially discovered in biological systems for enhancing CO_2 hydration or dehydration (CO_2+ H_2O ↔ HCO_3^- +H^+), carbonic anhydrase (CA) is considered to be one of the fastest enzymes. Human carbonic anhydrase II (hCA II) is a globular dimer, which contains 259 amino acids and a divalent zinc ion at its active site (**Figure 5.1**). The approximate dimensions of hCA II is 5 × 4 × 4 nm^3 (C. T. Supuran, 2016).

It has a rate of 10^6 $second^{-1}$ in converting insoluble CO_2 gas molecules to water-soluble bicarbonate ions (Krishnamurthy et al., 2008), approaching the diffusion limitation of enzymes. As one of the most critical enzyme in cell metabolism, CA has been studied as a model enzyme for human disease and drug discovery (Krishnamurthy et al., 2008). In addition to the potential low energy CO_2 scrubbing application, CA has been used as model enzymes to study enzyme immobilization mechanisms (Lundqvist et al., 2004; Simsek-Ege et al., 2002).

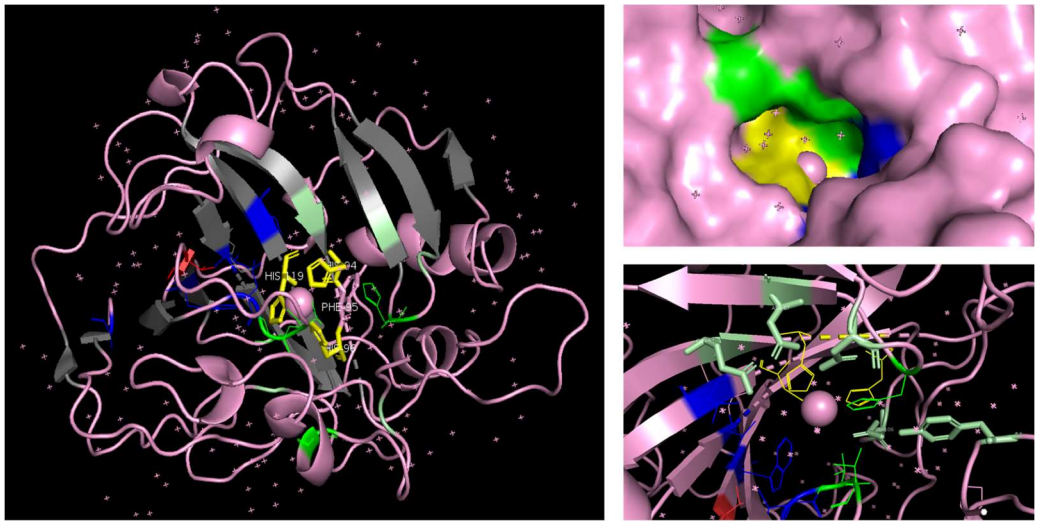

Figure 5.1 Structure and active site of human carbonic anhydrase II (PDB:1CA2) drawn in PyMOL software (Schrödinger, NY)

5.2 Carbonic Anhydrase (CA) Immobilization

To enhance enzyme longevity and improve feasibility of using CA for industrial scale CO_2 scrubbing, efforts have been made to immobilize CA to solid supports. A recent article (Yoshimoto et al., 2018) reviewed works in CA immobilization, where the attachment immobilization is the dominant method, and enhanced recyclability and enzyme stability after immobilization was reported (Hou, Ji, et al., 2015; Nemestóthy et al., 2018; Sahoo et al., 2015; Xu et al., 2019). It was also found that the Robeson upper bound in membrane based CO_2/N_2 separation (concentration of CO_2 vs. selectivity of CO_2) can be overcome with the presence of CA (Abdelrahim et al., 2017). In a study (Xu et al., 2019), amine-functionalized polyvinylidene fluoride (PVDF) hollow fiber membrane was used to chemically attach bovine CA. The hydrophobicity of the immobilization support was described as facilitating CO_2 adsorption, as well as promoting the efficient separation of generated bicarbonate ions from the gas stream (Xu et al., 2019). However, recent modeling work found that the hydrophobic surface hinders the activity of the immobilized CA (G. Chen et al., 2018). Therefore, there is no conclusive results yet in designing CA immobilized CO_2 scrubbing materials.

Although the enzyme entrapment method has been considered as a simple immobilization method, it still, upon the recent review of CA immobilization, lacks attention in both investigations and applications (Yoshimoto & Walde, 2018). Nevertheless, certain studies have shown good potential for polymer entrapped CA. Thermal stable CA entrapped in a silicone-based coating wacoated on a stainless steel support for a field test of CO_2 scrubbing, during which 90% CO_2 efficiency was observed over 45 days of gas scrubbing process (Akermin, 2013; Bucholz et al., 2015) (**Figure 5.2**). In other studies, fragile alginate beads with CA were placed inside porous ceramics, to protect the soft alginate beads that catalyzed CO_2 hydration in a vertical reactor (Y.

Zhu et al., 2016). Importantly, according to the literature, most isozymes used in CA immobilization studies were bovine CA and human CA. Although studies reported enhanced thermal or pH stability of these mammalian CAs after immobilization, the high cost of these vulnerable CAs also suggest the need to develop thermal (or pH) stable CA isozymes with less expensive protein productions (Migliardini et al., 2014; C. Supuran & Capasso, 2017). In our study, a proprietary microbial CA provided by Novozymes A/S (Bagsvaerd, Denmark) as a brown liquid concentrate (NCA) was used for assay development, enzyme-solvent compatibility tests, CA immobilization on textiles and the development of CA immobilized textile packing material for lab-scale CO_2 scrubbing tests.

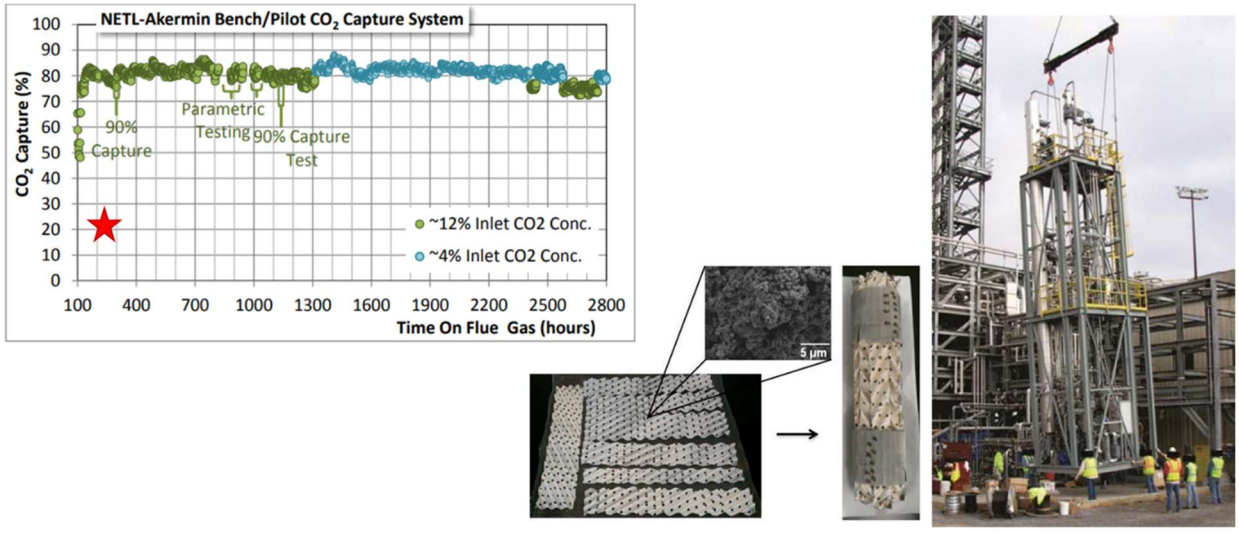

Figure 5.2 CO_2 capture data for bench unit at National Carbon Capture Center with coal flue gas and CA-containing porous silica coating (Bucholz et al., 2015) on a Salver M500X structured packing (Akermin, 2013).

Indeed, CA immobilization is an emerging research field with strong motivations, and CA immobilized materials are promising candidates as catalysts to enable low energy CO_2 scrubbing from post-combustion gases. However, most existing CA immobilization supports are inorganic

particles and synthetic polymeric membranes, which might cause environmental issues after their end uses. Therefore, more sustainable support materials comprising CA need to be developed for industrial CO_2 scrubbing.

5.3 Evaluation of Catalytic Activity of Carbonic Anhydrase

Two types of assay have been used to measure the catalytic activity of α-CAs. One is the p-nitrophenyl acetate (p-NPA) assay, which indicates the esterase activity of CA (Verpoorte et al., 1967), while another one measures the CA activity in catalyzing CO_2 hydration. The p-NPA assay is easier to set up and has a slower rate, whereas the later assay is more relevant to actual applications in CO_2 scrubbing. While the esterase activity is a more convenient method, care must be taken to correlate esterase with hydrase activity before relying on this method to characterize CA for CO_2 scrubbing, because for some CAs, such as a β-class CA from *Methanobacterium thermoautotrophicum* (Smith & Ferry, 1999), there is no direct correlation.

To evaluate the hydrase activity of CA, the accelerated CO_2 conversion to solvated bicarbonate in presence of CA can be measured by the pH change and to compare with that in absorbents without enzymes (Y.-T. Zhang et al., 2009; Y. Zhu et al., 2016). The rapid pH change can also be monitored by absorbance measurement with a spectrophotometer by using colorimetric pH indicator (Salmon et al., 2016). However, when immobilized CA is used in the assay, the rate of CO_2 hydration could be interfered by the mass transfer barrier induced by the physical supports, because, the rate of CO_2 hydration for immobilized CA is a combination of the retained CA activity, the diffusivity of the substrates (CO_2) to the catalytic site, and the diffusivity of the products (HCO_3^- and H^+) to the medium. Therefore, bench-scale (Leimbrink et al., 2018; Qi et al., 2018) and field test (Akermin, 2013) apparatuses have been built to evaluate the overall CO_2 scrubbing performance of CA immobilized materials, in which temperature, pH, ionic strength as

well as operation time can be manipulated to investigate the enzyme performance in the whole CO_2 scrubbing system (Bucholz et al., 2015; Hajba & Guttman, 2016; Jochems et al., 2011; Y.-T. Zhang et al., 2010; Y. Zhu et al., 2016). Alternatively, Vinoba et al. introduced a method of using the precipitation of $CaCO_3$ to estimate the concentration of bicarbonate ion generated in a short time period, and thus the hydrase activity of CA. (Vinoba et al., 2011) In this research, we used hydrase activity of CA to study the dissolved CA activity for temperature profile with the presence of N,N-dimethylglycine (DMG), a potential CO_2 gas scrubbing solvent, and an esterase assay was adopted to 24-well plates to measure the activity of biocatalytic textiles containing immobilized CA.

5.3.1 Colorimetric assay for CAs in 96-well plates

A modified Wilbur-Anderson assay with 12.5 mM Tris (pH 8.3) and 0.05 g/L Bromothymol blue was carried out to measure the activity of NCA and its compatibility with DMG solvents at different temperatures. Tris buffer has a pKa around 8.06 and can effectively delay the onset of color change of the Bromothymol Blue indicator (pKa~7.1) to varying extents depending on its concentration (**Table 5.1**). The procedure of the assay is illustrated in **Figure 5.3**. To eliminate the interference of solvent in the assay when testing the enzyme compatibility with DMG, all incubated samples were diluted 200x in 12.5 mM Tris (pH 8.3) prior to dosing in the assay (**Figure 5.3**). In addition to minimizing the solvent effect, extensive dilutions (Dilution factor, DF~ 4000 -8000) of enzyme product are necessary to obtain stable assay results within the detectable windows for data analysis. Half-strength CO_2 water was prepared by bubbling CO_2 to 40 mL dI water for at least 30 minutes and then diluted 2x with dI water with gentle mixing before using it in the assay.

Enzyme activity is calculated by the following equations:

Equation 1:

Raw Unit Activity $= (1/t_{CA} - 1/t_{Control})*1000$

where the t_{CA} is the time needed for a sample containing enzymes to reach optical density (OD) lower than 0.2 after dosing half-strength CO_2 water to the well and $t_{Control}$ is that of the corresponding control in the well next to the sample well (**Figure 5.4**). The t_{CA} and $t_{Control}$ in raw data are illustrated in **Figure 5.5**.

Then, Raw Unit Activity is normalized for the amount of enzyme present in the sample to give the Enzyme Unit Activity according to Equation 2,

Equation 2:

Enzyme Unit Activity (Units/µL) = Raw Unit Activity * DF/20 µL

where DF is the total enzyme dilution factor and 20 µL is the volume of diluted enzyme sample used in the assay.

When the initial enzyme sample concentration (mg/µL) is known, the Enzyme Unit Activity can be converted to U/mg according to Equation 3,

Equation 3:

Enzyme Unit Activity (Units/mg) = Enzyme Unit Activity (Units/µL)/Concentration (mg/µL).

When the purity of the enzyme sample is known, Enzyme Unit Activity can be converted to **Specific Activity** by accounting for the % purity in the calculations. However, due to the confidentiality of the NCA sample, only Enzyme Unit Activity was reported in this dissertation.

In addition to the Tris and Bromothymol Blue (CA-TB) combination, Bicine and Cresol Red (CA-BR) is another possible buffer-indicator combination for the CA hydrase assay in 96 well plates (**Table 5.1**) (Salmon et al., 2016). Although most the assay development evaluation was carried out using CA-TB method, the CA-BR method was tested, which shows promise for

lower %CV, particularly because the Bicine control reactions show less variability than the Tris controls (**Figure 5.6**, a). To differentiate assays carried out with two different buffer-indicator combinations, the Enzyme Unit Activity is reported with either kCA-TB/µL or kCA-BR/µL, referring to the Tris and Bromothymol Blue assay and Bicine and Cresol Red assay, respectively.

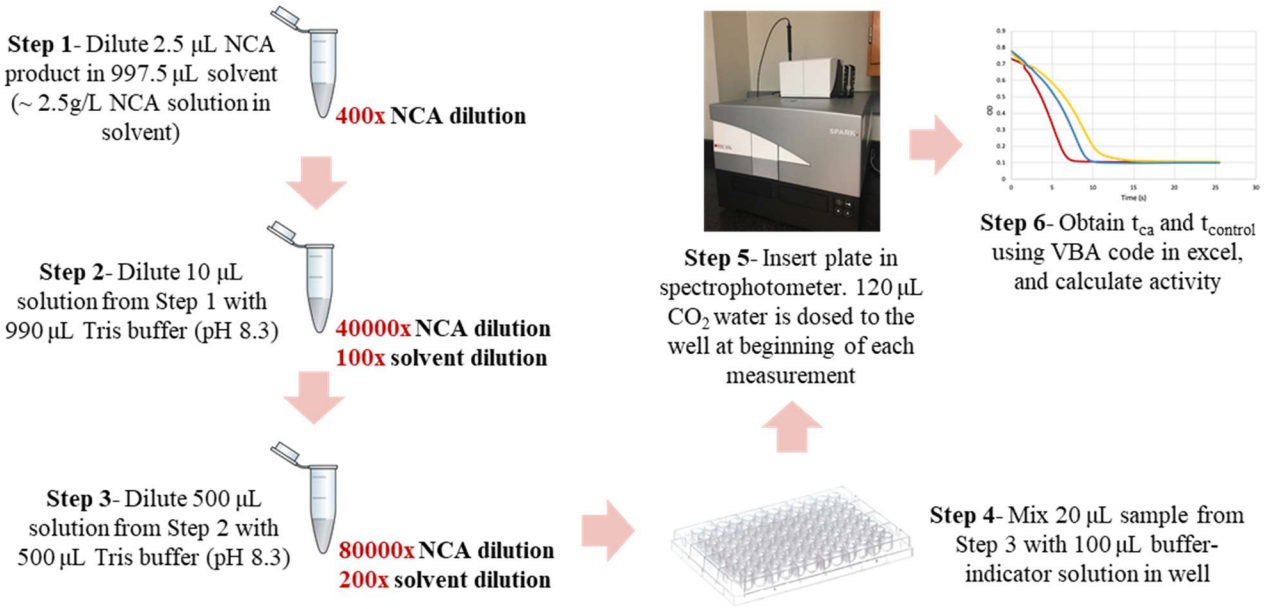

Figure 5.3 Schematic of Carbonic Anhydrase Colorimetric Assay steps.

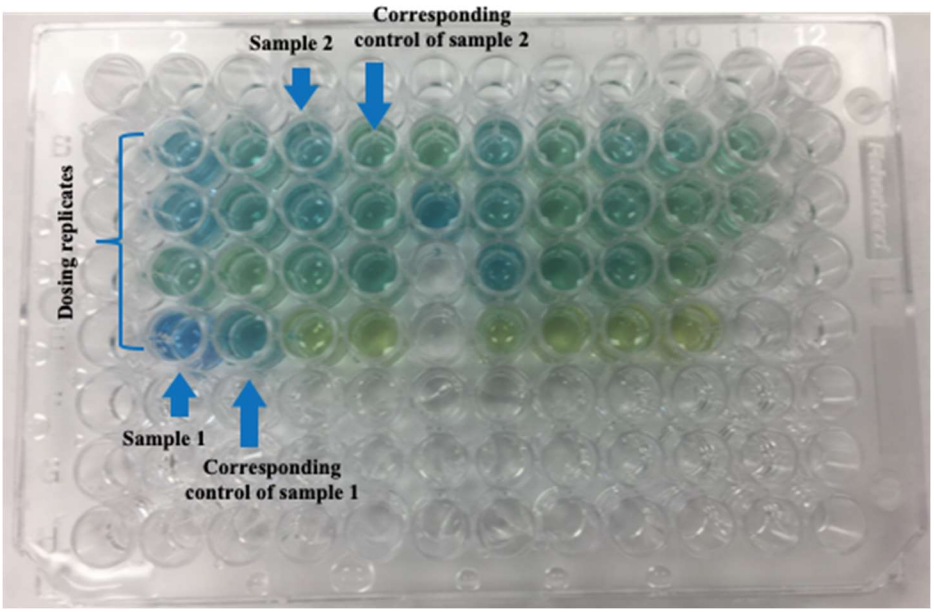

Figure 5.4 Enzyme sample and corresponding control (blank) adjacent to each other are used for activity calculation.

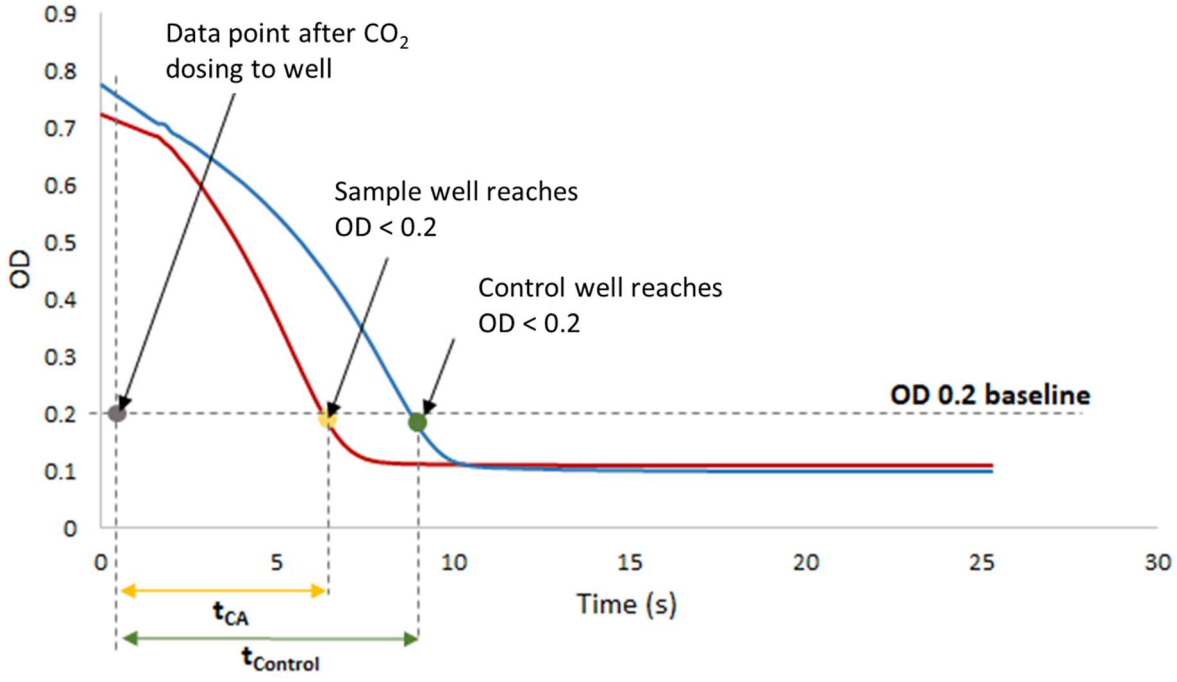

Figure 5.5 Illustration of the calculation of enzyme activity from raw data.

Table 5.1 Chemical structures of buffers and pH indicators used in the CA assay.

Assay	Buffer	pH indicator	Color change
Tris and Bromothymol Blue Method (TBB - Method)	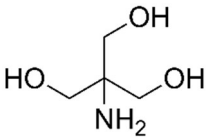	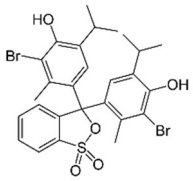	Color change from pH 7.6 (blue) to pH 6.0 (yellow) Absorbance monitored at 615 or 620 nm
Bicine and Cresol Red Method (BCR - Method)	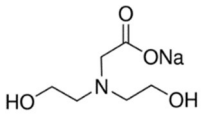	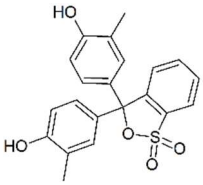	Color change from pH 8.8 (red) to pH 7.2 (yellow) Absorbance monitored at 574 nm

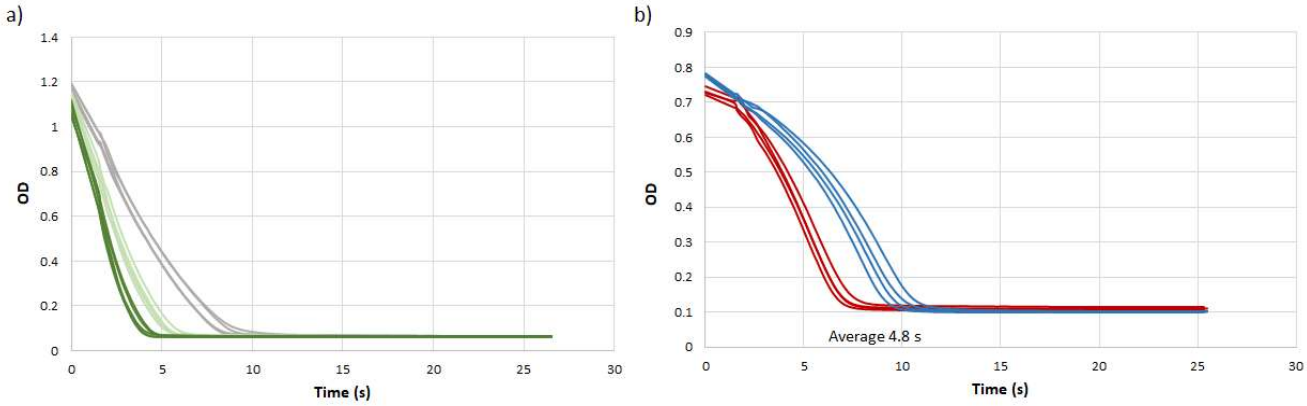

Figure 5.6 a) CA-BR assay results of 40000x (dark green), 80000x (light green) NCA dilution and control (grey). Plots of each sample include five dosing replicates. b) CA-TB assay results of 80000x (red) NCA dilution and control (blue). Plots of each sample include four dosing replicates.

5.3.2 NCA compatibility with DMG solvent at different temperature

As described above, to evaluate the solvent compatibility with DMG, fresh (lean) 30% wt. (about 2.9 M) DMG solution (pH 10.4) and 12.5 mM Tris buffer (pH 8.3) solution were

prepared and used to prepare 2.5 g/L solutions of NCA enzyme (corresponding to an initial enzyme concentrate dilution factor of about 400x in the solvent). Samples containing enzymes and solvents without enzymes were incubated at room temperature (~22°C), 60 or 80°C for 3 hours. A total of 8 replicate wells [2 (dosing)*2 (solutions prepared separately)*2 (plates with identical layout)] were used to calculate the room temperature samples and controls, including sample replicates (solutions prepared separately), technical replicates (dosing replicates) and plate to plate replicates (plates with identical layout). A total of 4 replicate wells [2(dosing)*2 (plates with identical lay out)] were used to calculate the samples and controls incubated at 60 or 80°C.

The CA-TB assay was conducted with freshly prepared lean 30 wt% DMG solvent containing enzyme, in order to test NCA-DMG compatibility at room temperature and after incubation at 80 °C for 3 hours (**Figure 5.7**). After high temperature (80°C) incubation in Tris buffer or DMG solvent, we observed aggregation of the enzymes (white solid in the clear solution). Also, exposure to high temperature extended the time needed for enzyme promoted CO_2 hydration in the assay, resulting in a decrease in enzyme activity for enzymes incubated at 80°C relative to the room temperature incubated samples (**Figure 5.7**). Enzyme incubated at 60°C in DMG also exhibited a decrease in activity (**Figure 5.7**). Notably, enzyme incubated in low (12.5 mM) concentration Tris at 60°C exhibited an increased activity. We believe this may be attributable to a "thermal annealing" effect, whereby enzyme in a "compatible" buffer gains sufficient thermal energy at 60°C to improve proper folding, which may have been disrupted at some point during enzyme production, recovery or subsequent handling. We believe this "annealing" effect does not occur in the 60°C incubated DMG sample due to the high (2.9 M)

concentration, and corresponding high viscosity, of the DMG solution, which could inhibit the molecular motion needed for enzyme to adjust its folding.

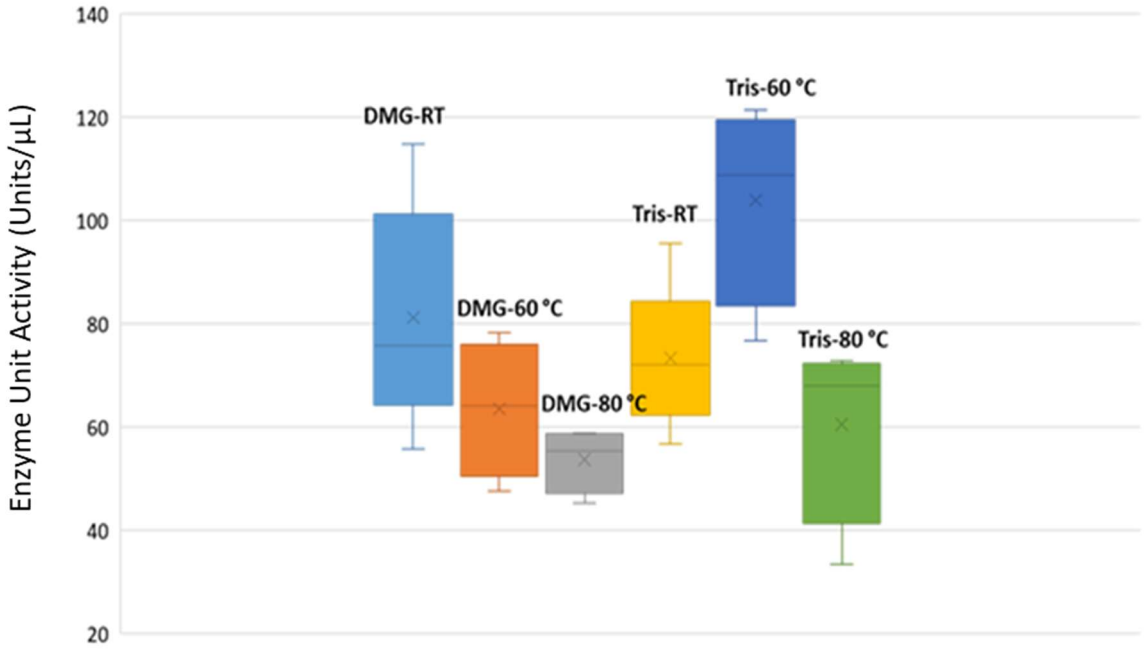

Figure 5.7 NCA Enzyme Activity (Units/µL) tested by CA-TB method after 3 hours incubation in solvents (2.9 M DMG or 12.5 mM Tris) at 60 or 80°C.

The CA-BR assay was used to repeat the enzyme-DMG compatibility test at either room temperature or 3 hours incubation at 80 °C. Surprisingly, when using the CA-BR method to measure residual NCA activity on one of the DMG-incubation days described above, the residual NCA activity (**Table 5.2**, ~20%) was much lower than found using the CA-TB. These apparently conflicting results remain unknown and should be explored further, and CA-TB was mainly used in this project for the consistency with other enzyme activity tests. The results of enzyme-solvent compatibility at different temperature measured by CA-BR method were consistent with that measured by CA-TB method, where the temperature has larger impact on NCA activity than the

presence of DMG solvent. NCA is compatible with 2.9 M DMG solvent with 81% residual activity while high temperature (80 °C) significantly reduced the enzyme activity without (~30% residual activity) or with (~22% residual activity) solvent.

We summarized the residual activity of NCA considering different factors in **Table 5.3** using different baselines for the residual activity calculations. According to the data, we can conclude that there were minor solvent effects and major temperature effects on NCA activity in DMG solvents. Therefore, the assay data prove that CA immobilization is necessary for using this biocatalyst in the industrial CO_2 scrubbing process. The immobilization can prevent CA from travelling to the high temperature (> 80 °C) gas stripper and thereby increase CA longevity in the gas scrubbing application.

Table 5.2 Incubated samples measured with CA-BR method. Results are averaged from four independently prepared sample replicates, incubated on different days, each sample replicate has five dosing replicates. (OD=0.2 cut-off)

Sample	Raw Unit Activity	Enzyme unit activity (kCA-BR/µL)	% CV	Residual Activity* (%)
Bicine- 80 °C	58 (±4)	232	13	30
Bicine-room temperature	196 (±13)	783	7	100
DMG-80 °C	44 (±5)	174	12	22
DMG-room temperature	158 (±5)	632	7	81

*The residual activity was calculated using enzyme activity incubation with bicine at room temperature as the 100% enzyme activity.

Table 5.3. Residual activities calculated for solvent effect or temperature* effect.

Factors	Samples used for calculations	Residual activity
Solvent effect	Enzyme in DMG after 80 °C incubation compare to that in Bicine after 80 °C incubation	75 ± 5 (%)
	Enzyme in DMG after room temperature incubation compare to that in Bicine after room temperature incubation	81 ± 5 (%)
Temperature effect	Enzyme in DMG after 80 °C incubation compared to Enzyme in DMG after room temperature incubation	28 ± 1 (%)
	Enzyme in Bicine after 80 °C incubation compared to Enzyme in Bicine after room temperature incubation	30 ± 1 (%)

*The residual activities regarding temperature effect (~29%) after incubation shown here were calculate with one sample lay-out in 96 well plates, and they are consistent with other CA-BR tests using different sample lay-out.

5.4 Biocatalytic Textiles with Carbonic Anhydrase for CO_2 Scrubbing

With our initial findings in applying biocatalytic coating made of diffusion limited enzymes and chitosan to cellulosic support, and the good enzyme longevity during the repeating catalytic reactions and storage, we incorporated the carbonic anhydrase (CA) into the substrates with the same compositions in order to fabricate sustainable, light weight packing material for CO_2/N_2 separation. As we described above, when diffusion limited enzymes are immobilized to

a membrane contactor, especially when enzymes are entrapped in a layer, the mass transfer efficiency could be impacted. Therefore, the hydrase assay can only be used to evaluate dissolved CA. To overcome this problem, an esterase assay was adapted to a 24 well plate format to measure the catalytic activity of CA immobilized textile material.

5.4.1 Adapted esterase assay for immobilized CAs

This assay measures the esterase activity of an active CA on a colorless ester substrate (4-Nitrophenyl Acetate (NPA), Mw: 181.1 g/mol) which releases a yellow-colored product (4-Nitrophenol (NP), λmax = 405nm, Mw 139.11 g/mol) that can be easily quantified using a spectrophotometer equipped with a microplate reader (Spark Microplate Reader, TECAN, USA). First, a standard curve was generated to convert the O.D. reading to product concentration with three dosing replicates at each 4-NP concentration. A standard curve is established relating the O.D. value of the standards to the amount of NP in each well. The standard curve was generated by plotting the average O.D. (3 dosing replicates) vs. NP amount per well **(Figure 5.8**). In the second step, the kinetics of NP release by measuring the absorbance in each well at 405 nm once every 30 seconds for 30 mins, totaling 60 cycles for each well (**Figure 5.9**). The kinetics of NP release were monitored for both the control (e.g. well A1 in **Figure 5.9**) and the sample (e.g. well A2 in **Figure 5.9**). When the O.D. values are plotted against time in minutes, the slope of the curve is the O.D. change per minute (**Figure 5.10**). Using the slope (O.D./min) of the NP standard curve, the NP release rate is obtained with a unit of nmol/minute. This slope can be further converted into µmol/min using standards in **Figure 5.8**.

The CA Esterase Activity Unit is defined as the amount of enzyme that catalyzes the release of 1 µmol of NP per minute from the substrate at 25 °C. (U=µmol/min) For immobilized CA fabricated from liquid product, esterase activity is calculated using Equation 4:

Equation 4:

CA Esterase Activity= rNP/V (U/ mL)

where, rNP is rate of pNP release due to CA (nmol/min) and V refers to the volume (in µL) of liquid enzyme product used in enzyme immobilization in each well, which can be calculated based on the immobilization formulation and weight of fabric samples in the well. To calculate the retained enzyme activity after immobilization, the measured activity of fabric containing CA was compared with esterase activity of dissolved NCA product (18.7 U/mL), which was determined in 24-well plate assay using 25 mM Tris buffer pH 7.2.

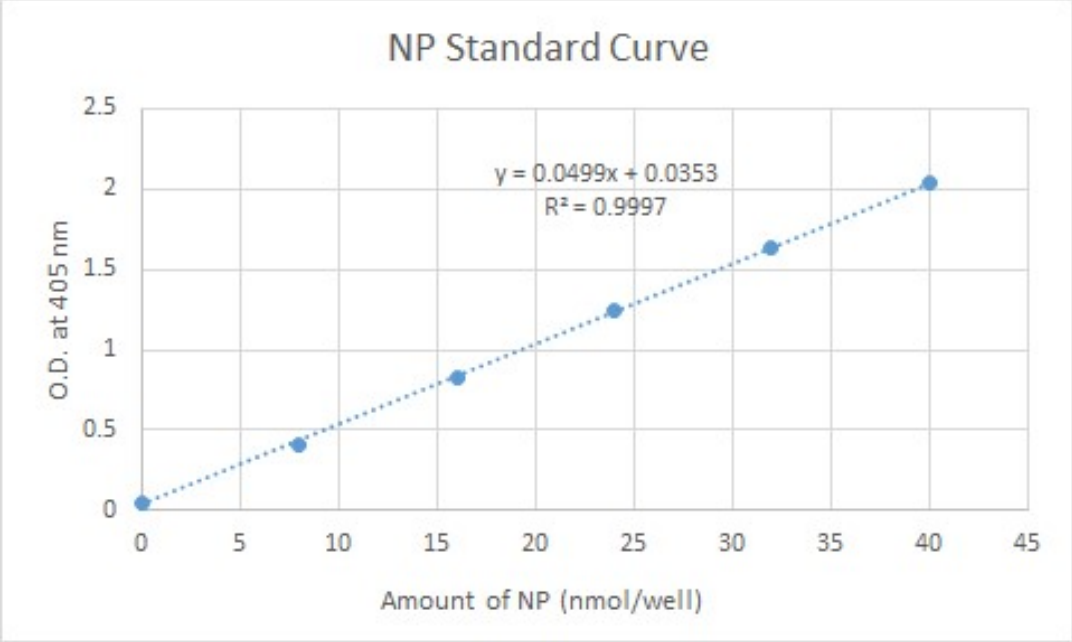

Figure 5.8 NP standard curve in 12.5 mM Tris buffer pH 8.3 at room temperature. Data was generated on a separate 24-well plate.

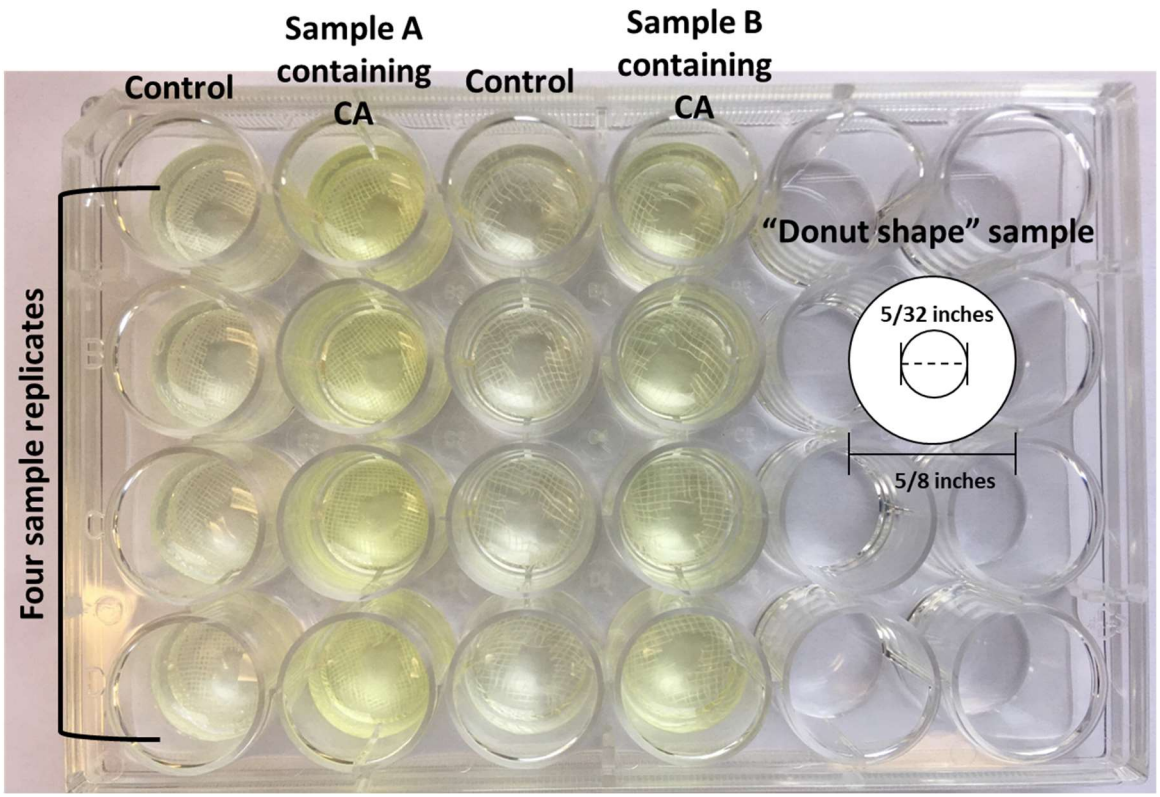

Figure 5.9 Example of sample layout in CA esterase assays adapted to 24-well plate for testing retained catalytic activity of textile containing immobilized CA.

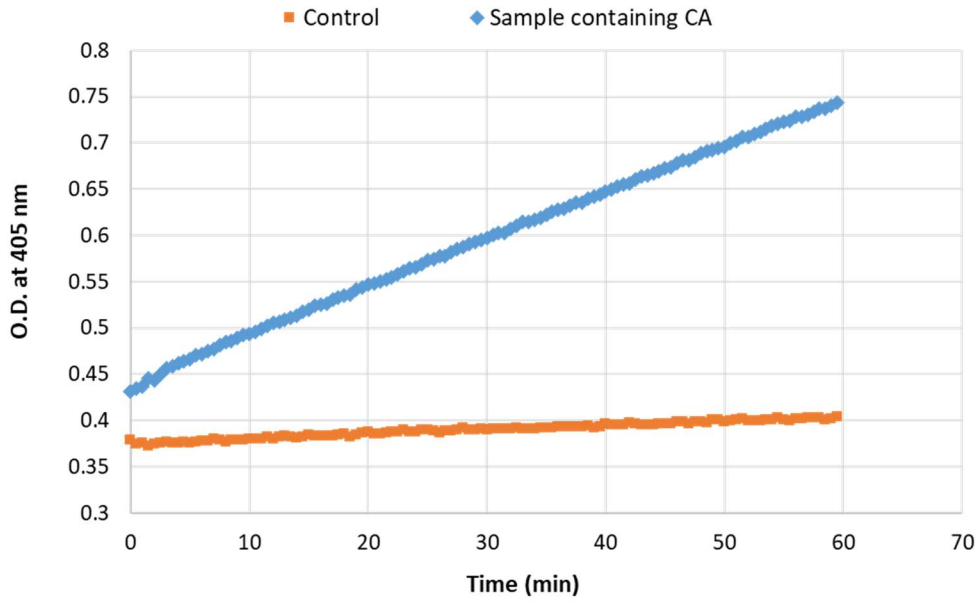

Figure 5.10 Kinetic pNP release curve of control fabric and fabric sample containing CA.

5.4.2 Immobilization of CAs onto cellulosic support material

NCA was immobilized onto cellulosic textiles using the generic entrapment method developed in Chapter 3 with CAT. Three different cotton textiles including cheese cloth and yarn were tested for CA immobilization. The retained catalytic activity after immobilization onto the cheese cloth substrate was evaluated by the pNPA assay described in section*5.3.1*. The biocatalytic yarn containing CA was assembled as a flexible gas scrubbing column packing material and was tested in the custom lab-scale CO_2 scrubber.

To prepare biocatalytic textiles with CA using cheese cloth, two coating methods were employed: dip coating and padding. The padding experiments were carried out with a 500mL wide horizontal padder (Mathis HVF, Mathis AG Inc, USA) as shown in **Figure 5.11**.

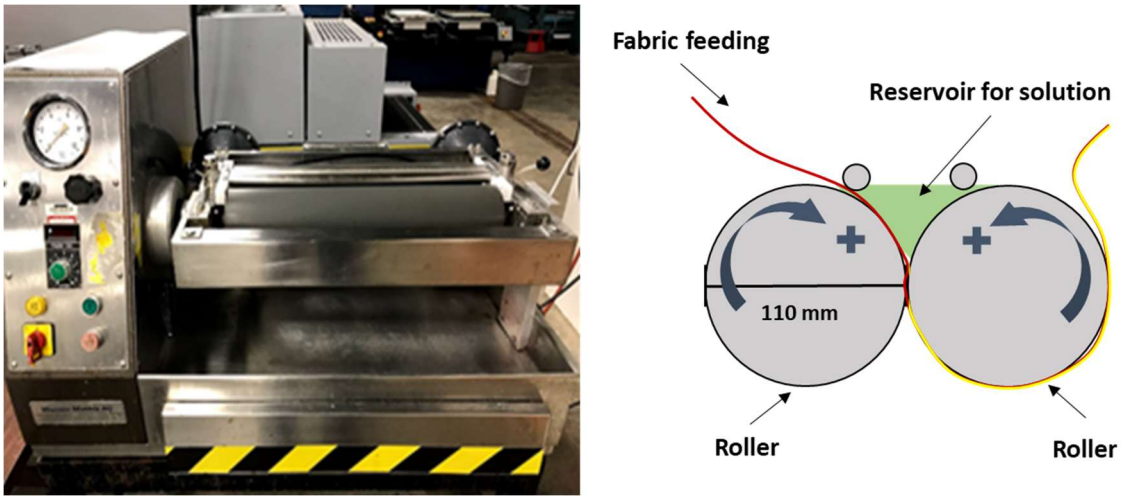

Figure 5.11 Lab scale padding machine (left) and schematics of its working mechanism (right).

Different formulations including varied enzyme to chitosan ratios and chitosan concentrations were investigated in the DOE-BETO sponsored project. Only parts of the sample preparation methods and evaluation of the retained activity after CA immobilization are

presented in this dissertation. For example, to prepare the CA entrapped biocatalytic textile with cheese cloth (cheese #50 and #90) through dip coating and padding. The 1 % wt. chitosan salt solution was prepared as described in the biocatalytic yarn fabrication section, Chapter 3, following by mixing NCA product to the chitosan salt solution to achieve 1:1 enzyme product to chitosan polymer weight ratio. Chitosan used in this section was ChitoClear® (44020-fg95LV, *Pandalus borealis,* 95% degree of deacetylation) purchased from Primex (Iceland) and used as received. The wet pickup was recorded after dip coating (when not dripping) and padding, in order to calculate the amount of enzyme product and polymer absorbed to the textile substrates.

The residual activity of immobilized NCA was measured using an esterase assay adapted to a 24-well plate, as described in section *5.3.1*. Cheese cloth based biocatalytic samples and controls were cut into donut shapes with an outside diameter of 5/8 inches and an inner diameter of 5/32 inches (**Figure 5.9**) using circular punch cutters. Four replicates of each sample (prepared from two separate batches) were used to collect the activity data. Residual activity of immobilized NCA and activity loss after 8 washes are listed in **Table 5.4**. The activity loss was calculated using Equation 5:

Equation 5:

Activity Loss = [(initial residual activity - residual activity after 8 washes)/initial residual activity] x 100%

NCA immobilized on cheese cloth #90 prepared by padding showed > 60% detectable activity compared to dissolved NCA (18.7 U/ml), and retained more than 50% residual activity after 8 washes with Tris buffer (pH 7.2). The results are consistent with samples prepared in other part of the DOE-BETO project which have different enzyme-to-chitosan ratio. Dip coating samples had lower (43.2% and 44.5% for cheese #50 and cheese #90, respectively) retained

activity after enzyme immobilization. . However, these samples showed lower subsequent activity loss (< 11%) in the longevity test with 8 washes.

According to the microscopic images (**Figure 5.12,** a and b), the samples prepared by padding method have similar morphology compared to control cotton cheese cloth, compared to that of dip coated samples. In the dip coated samples, chitosan chunks were observed between yarns in cheese cloth or on the edge of the yarns (**Figure 5.12,** c). Because the coating solution was nearly homogenous from according to the optical microscopic images (**Figure 5.13**), the chitosan chunks on dip coating samples indicates non-uniform chitosan coating on the surface when cheese #90 was used as the support material. This observation might explain why fabrics containing enzyme immobilized through dip coating method had lower retained activity after immobilization: the presence of chunk chitosan matrix in the sample increase the mass transfer barrier for immobilized NCA, especially when the assay was conducted in 24 well-plate with limited liquid volume and liquid flow. Also, because of the presence of these chunks, the biocatalyst could be harder to be dissolved or washed away (**Figure 5.14**) during the washing steps, exhibiting lower activity loss after repeated washing.

Table 5.4 Residual activity of immobilized NZCA and activity loss after 8 washes.

Sample	Residual activity* 1** (U/ml)	Residual activity 2*** (U/ml)	Residual activity 3**** (U/ml)	Activity loss after 8 washes (%)
#50 padding sample	31.8%	28.3%	26.8%	15.8%
#90 padding sample	63.8%	56.9%	55.1%	13.7%
#50 dip coating sample	43.2%	40.3%	39.0%	9.3%
#90 dip coating sample	44.5%	46.1%	39.6%	11.0%

*Relative to the dissolved NZCA activity (U/ml); **Refer to initial residual activity after immobilization *** Residual activity 2 was measured after 4 washes with Tris buffer; ****Residual activity 3 was measured after 8 washes with Tris buffer.

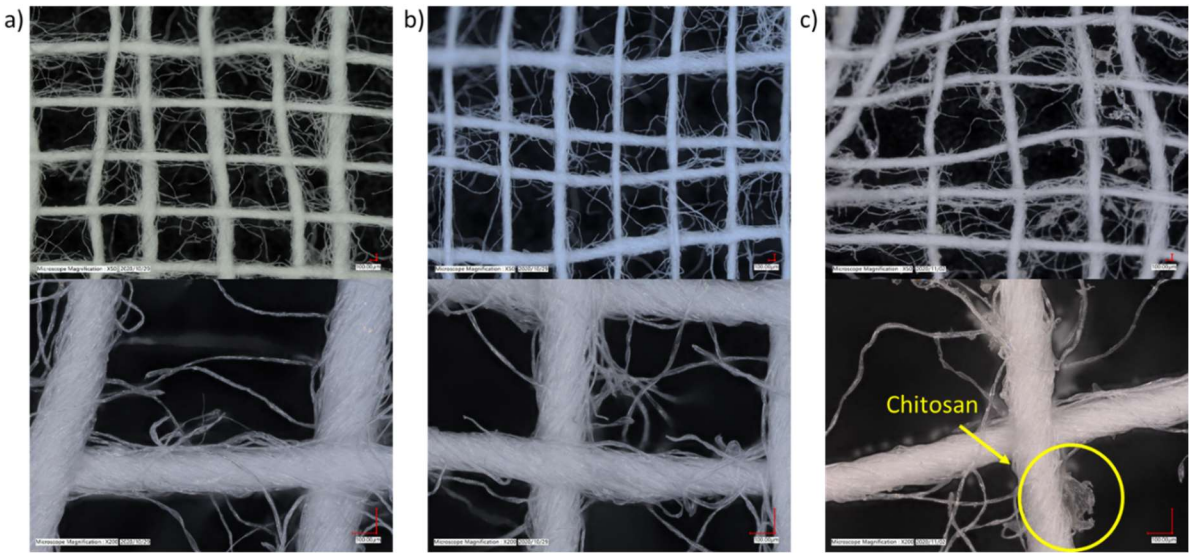

Figure 5.12 Microscopic images of a) control cheese #90 cloth; b) CA immobilized cheese #90 cloth by padding method with 1 % wt. chitosan solution and c) CA immobilized cheese #90 cloth by dip coating method with 1 % wt. chitosan solution.

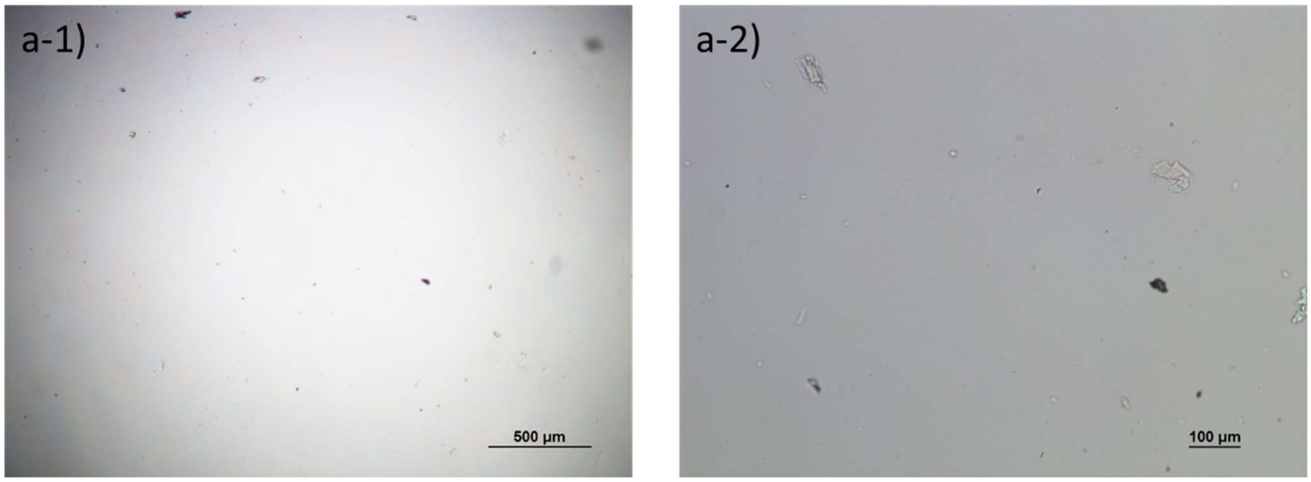

Figure 5.13 Optical microscopic images of chitosan salt-NCA solution used for padding and dip coating immobilizations.

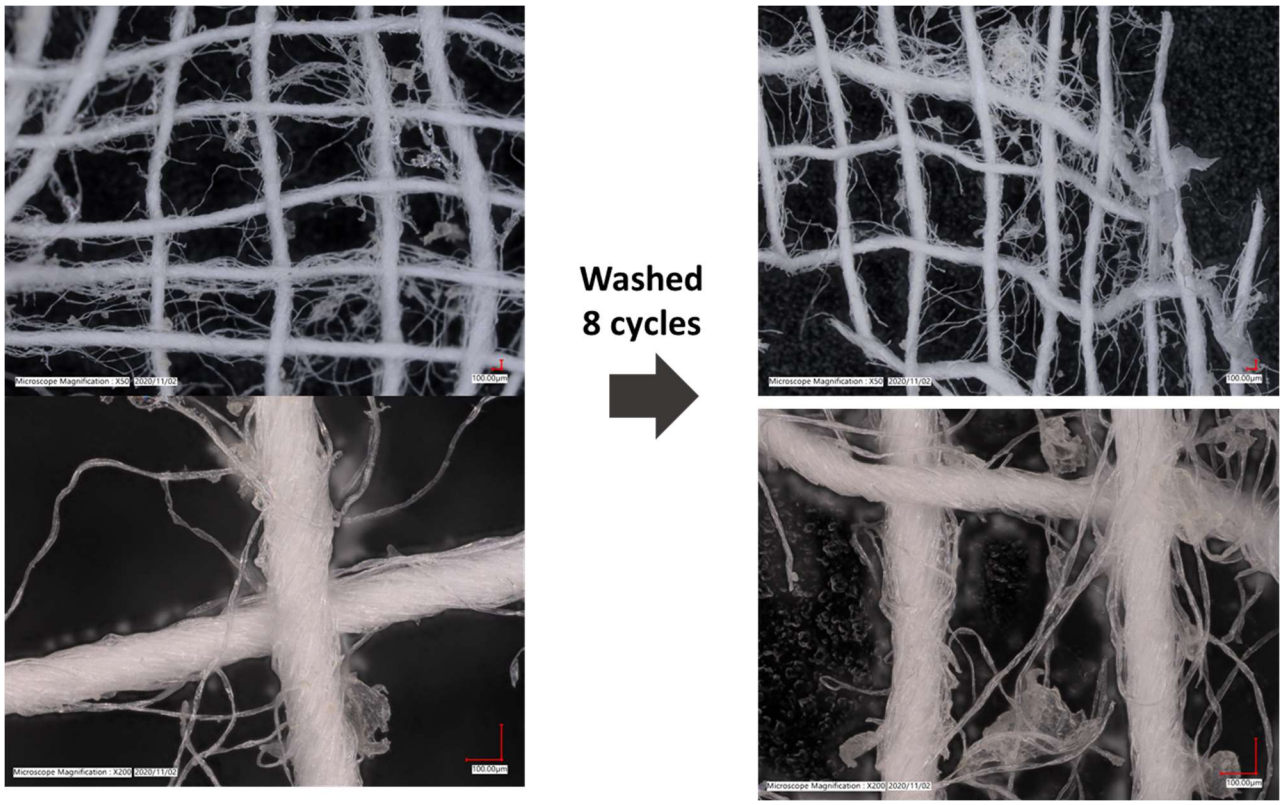

Figure 5.14 Optical microscopic images of chitosan-NCA dip coated cheese #90 sample before and after 8 washes with buffer.

5.4.3 Analysis the surface of CA immobilized textiles with mass spectrometry

To further analyze the surface of cheese cloth samples prepared with two different methods, Time-of-Flight Secondary Ion Mass Spectrometry (ToF-SIMS) characterization was carried out with cheese #90 sample sets. ToF-SIMS experiments were conducted using an ION-TOF TOF-SIMS V instrument with a bismuth analysis beam. Typical conditions were ~ 0.35 pA Bi3+ at 25 keV into a 100 x 100 μm^2 area and the sputter beam was Cs^+ at 20 nA at 10 keV (C. Zhou et al., 2020). An example of ion profiles is shown in **Figure 5.15**. Although many specific negative ions have been used to identify cellulose in literature, such as CH_2=$CHCOO^-$, CHO_2^- and $C_3H_3O_2^-$ (Mitchell et al., 2005; C. Zhou et al., 2020), because of the similarity in the chitosan and cellulose chemical structures, in this study, an ion fragment with a relatively high mass, $C_8H_{13}O_7^-$ (m/z= 221.0) (**Figure 5.16**), was identified as a negative ion fragment that could only originate cellulose because it lacks nitrogen in the structure. Smaller one to three carbon ion fragments could potentially originate from either cellulose or chitosan, which could cause ambiguity if these were selected as reference peaks. Therefore, $C_8H_{13}O_7^-$ peak was selected as the reference peak to normalize the peak intensities of other ion fragments in the spectrum. Results are shown in **Table 5.5**.

Based on the results in **Table 5.5**, HS^- (m/z=32.9) is attributed to the enzyme products at the sample surface. However, the precise origin of the sulfur is unknown. The NCA enzyme product may contain residual production impurities such as fermentation chemicals or recovery processing aids, therefore, it is not possible to prove that the HS^- ion was from the enzyme protein only. The normalized peak intensity of HS^- ion was very low in samples without NCA samples (control cheese #90 and chitosan coated cheese #90). Therefore, the HS^- ion can be used as an indicator of the presence of the NCA product on the sample surface. Although the assay

showed deceases of the residual activity of both dip coated and padded sample, the HS^- intensity remained the same (1.48 before washes and 1.49 after washes) after 8 washes in the padded sample and HS^- intensity in dip coated samples increased from 2.18 to 4.21 after 8 washes. This inconsistence in characterization and assay measurement could be attributed to the fact that the distribution of chitosan-enzyme coatings are not uniform in the coated sample (**Figure 5.12**, c), and the esterase assay evaluated the overall performance of a cut sample in the well while ToF-SIMS has much smaller field of view on the cut sample when generating the ion profiles.

$C_4H_6NO_2^-$ (m/z= 100.0) and $C_3H_4NO_2^-$ (m/z= 86.0) ions have been used in identifying chitosan coating in previous studies (D'almeida et al., 2017). However, in the present work, these two ion fragments were detected in all samples, although the cotton control (cheese #90) had relatively low intensity, especially for the $C_3H_4NO_2^-$ fragment. The $C_3H_3O_2^-$ (m/z=71) ion has been used as a marker for both cotton (C. Zhou et al., 2020) and chitosan (Rodrigues et al., 2012) in previous studies. As stated previously, the similarity in the structures of these two polysaccharides introduces difficulties in differentiating these two compounds from the sample surface using lower mass ion fragments. It is consistent that the intensities of $C_3H_3O_2^-$ ion dropped after NCA was immobilized to the materials, indicating the presence of enzyme (products) at the cheese cloth surface. Ion fragments CNO^- (m/z= 26.0) and CN^- (m/z= 40.9) have been attributed to protein fragmentation in literature (Wagner et al., 2002). However, according to the data (**Table 5.5**), the CN^- ion fragment peak was also very intense in chitosan coated sample (increased from 21.1 to 81.92 by applying chitosan coating to cotton) even without the presence of NCA product. It is also very interesting that the increases of the intensities of CN^-, CNO^-, $C_4H_6NO_2^-$, and $C_3H_4NO_2^-$ after 8 washes are consistent within each coating method. Intensities of these four ions increase about 2 folds in padded samples while

those of dip coated samples increased about 4-folds. When HS^- fragment was used as the indicator of the NCA product, the increase of HS^- intensity in dip coated sample after 8 washes was also twice as much in padded sample. Therefore, further investigation with ToF-SIMS (e.g multi spots characterization, using purified enzymes, characterize the ion profiles of control sample has chitosan only) might be valuable to draw further conclusions to link the changes in surface composition with the retained activity measured from assay.

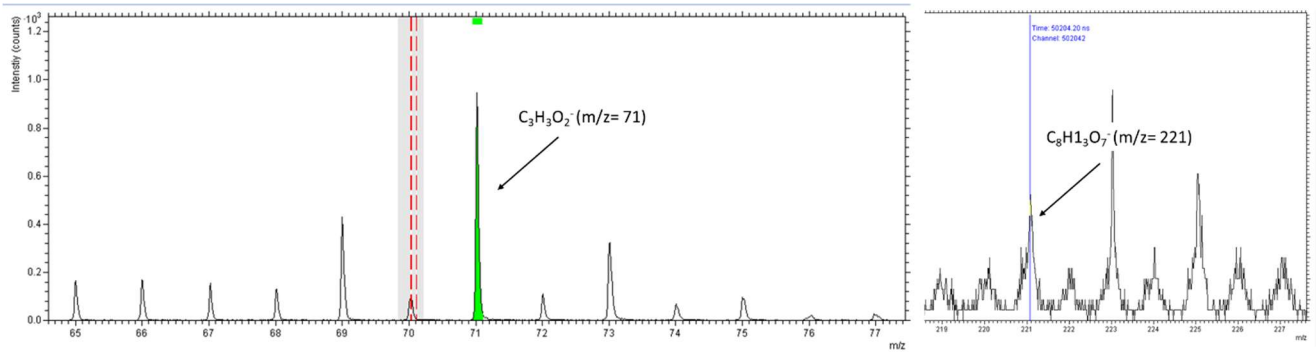

Figure 5.15 Example (chitosan coated cheese #90 sample) of ToF-SIMS spectrum used for analysis.

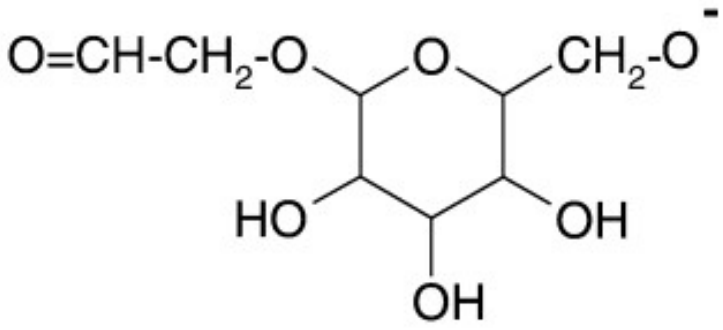

Figure 5.16 Structure of $C_8H_{13}O_7^-$ (m/z= 221^-) ion used in the ToF-SIMS analysis.

Table 5.5 Normalized ToF-SIMS peak intensity using $C_8H_{13}O_7^-$ as the reference peak.

	Protein/Chitosan			Chitosan		Chitosan/Cotton
	CN-	CNO-	HS-	$C_4H_6NO_2$-	$C_3H_4NO_2$-	$C_3H_3O_2$-
Cheese # 90	21.1	2.75	0.75	3.26	11.64	69.5
Chi coated cheese #90	81.29	3.36	0.52	7.2	14.75	62.47
P-Chi-NZCA	55.12	5.28	1.48	2.68	5.55	24.62
P-Chi-NZCA washed 8 times	136.16	10.29	1.49	6.29	10.03	48
D-Chi-NZCA	73.31	4.33	2.18	5.35	5.68	22.63
D-Chi-NZCA washed 8 times	329	15.22	4.21	21.44	23.09	66.47

According to the pNPA assay, depending on the substrate and preparation method, CA entrapped in a chitosan film matrix (with a 1:1 weight ratio of NCA product and chitosan polymer) and then applied to cellulosic textile can retain more than 50% of its dissolved enzyme activity, even after multiple washes (**Table 5.4**). The padding method can enhance the efficiency of raw material utilization as well as providing a more uniform coating, yielding consistent biocatalytic materials for the planned larger scale CO_2 scrubbing tests in the bench-scale gas scrubber at University of Kentucky. Also, the results show that the two coating methods can be applied to different loosely woven fabric structures with similar results in the esterase assay. In

general, the tighter weave of the cheese cloth #90 made it easier to handle, yet both fabrics could be useful for packing design.

5.4.4 Testing CO_2 scrubbing capability of NCA immobilized textile material

Biocatalytic yarns with NCA entrapped were used to prepare a gas scrubbing packing material. A 2.25 inches inner diameter × 12 inches tall glass column was installed on the custom lab scrubber and tested sequentially with two packings, one enzyme-immobilized (Chi-NCA packing) and one no-enzyme control (control Chi packing), each fabricated to fit the column using 4-ply cotton yarn and cheese cloth #90, and reinforced by a rigid mesh cotton-polyester-based backing material, 5 mesh latch hook canvas (No. 72-75676 Dimensions Crafts LLC) (**Figure 5.17**). The assembled cellulosic packing material was coated with either chitosan solution (1 % wt.) or 1 % wt. chitosan solution containing NCA (enzyme product to chitosan weight ratio = 1:1). The fabricated packing was allowed to soak in the relevant dip coating solution for 12 hours to allow sufficient time for the coating solution to penetrate the inner layers of the packing assembly. Coated samples were dried at ambient conditions for longer than 48 hours prior to testing. The total dry weight gains of packing materials (**Table 5.6**) were very small (< 3%), indicating that the samples were dried thoroughly before any testing in the scrubber, and indicating that relatively low amounts of chitosan and enzyme are incorporated into the packing material. The packing materials were pre-soaked in 10% wt. K_2CO_3/$KHCO_3$ (85/15 mixture pH ~10.5), the lean CO_2 scrubbing solvent, for 15 minutes before fitting snuggly into the glass column. The textile packing materials hold more than two times weight of the solvent compared to its own dry weight (**Table 5.6**). The test was carried out with mixed N_2/CO_2 gas flow rate of 4L/min, which contains 11% CO_2. The lean scrubbing solvent was pumped into

the column at the top of packing material and flowed down, at a flow rate of 150 mL/min, opposite to the upward flow of the gas stream.

According to the results, when NCA was immobilized to the column packing material, the absorbed CO_2 increased from 27% to 50% (**Figure 5.18**). It was observed that the CO_2 absorption was slightly decreased when Chi-NCA packing was used (200-650s window, **Figure 5.18**), this could be explained by the time needed for the equilibrium of bicarbonate generation in the contactor, because the packing was pre-soaked with lean solvent before fitting into the column. In addition, the textile packing without enzyme already had better gas scrubbing performance (~ 27.2 % CO_2 absorbed) compared to the glass Raschig ring packing (~ 3.6 % CO_2 absorbed) with the same height of packing material in the column **(Figure 5.18)**. In addition, the wet biocatalytic textile packing (290.4 g) weighs 25% less than Rischig ring packing (389 g). Findings of other experiments in the DOE-BETO project which include different packing designs, pointed out that the CO_2 absorption level almost doubled and gets close to the performance of a control packing with equivalent dose of dissolved NCA, if two NCA biocatalytic textiles packings are fitted in a taller gas scrubbing column.

Table 5.6 Weight of dip coated column packing materials.

	Control Chi packing	Chi-NCA packing
Dip coating experiments:		
Dry weight before coating (g)	87.7	88.5
Wet weight after coating (g)	248.4	297.1
Dry weight after coating (g)	90.3	89.4
CO_2 scrubbing test:		
Wet weight before scrubbing test (g)	311.2	290.4
Wet weight after scrubbing test (g)	279.9	264.0

*****Glass Raschig ring packing with the same height was about 389 g.

Even without material and process optimizations, the NCA immobilized biocatalytic textile fabricated using the coating combination developed in Chapter 3 showed significant improvement in CO_2 gas scrubbing. Depending on the parameters in the immobilization experiments, such as support material structure and properties, coating solution viscosity and packing design, this new category of biocatalytic material, "biocatalytic textile" (Salmon & Yuan, 2020), will have various properties that can be controlled to alter its catalytic performance, without requirement of redesigning the reactor ("drop in" option for existing infrastructure), and could also results in new, more efficient future gas-liquid contactor designs.

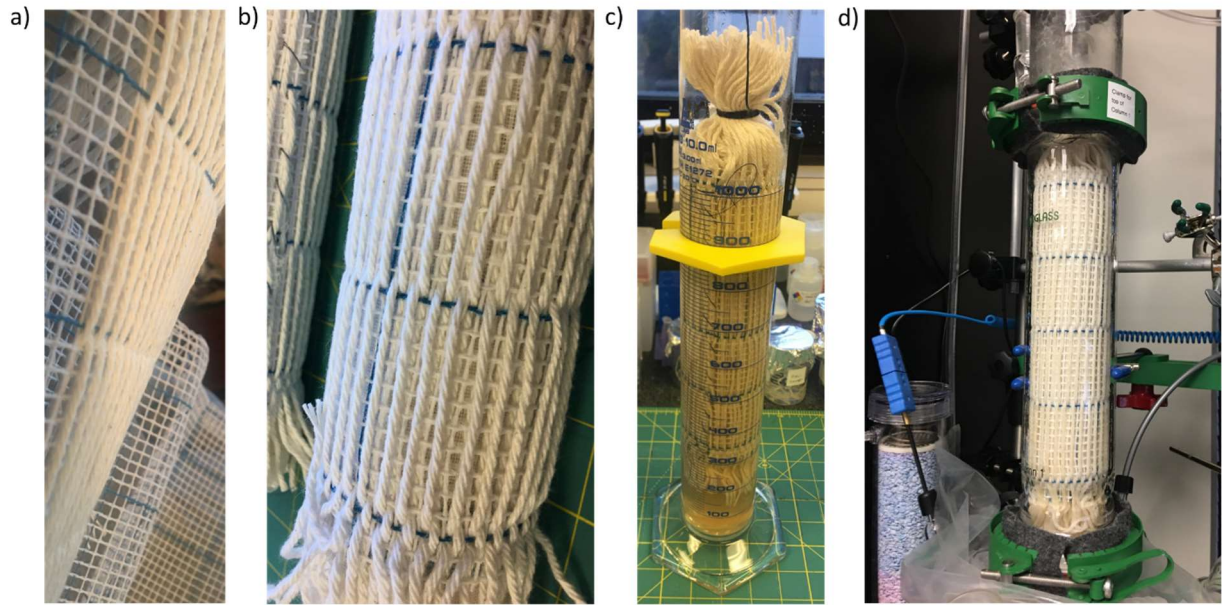

Figure 5.17 Biocatalytic textile (yarn) used for lab scale CO_2 scrubbing test: a) assembling the 4-ply yarn to a poly-cotton canvas support mesh; b) column packing material prepared by yarns, cheese cloth and canvas support mesh; c) dip coating packing material with chitosan solution as control or with chitosan-NCA solution; d) testing column packing material and its control in a lab-built CO_2 scrubbing column.

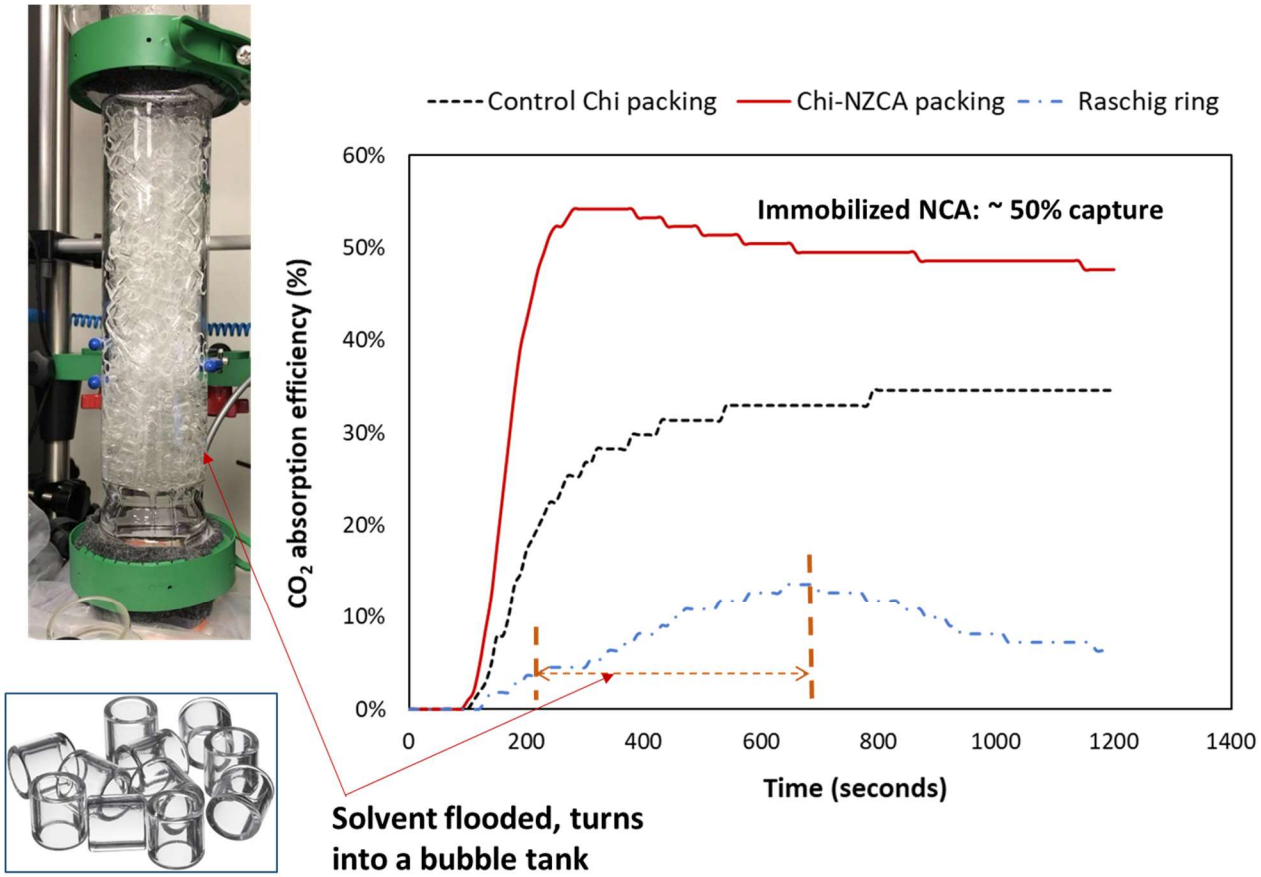

Figure 5.18 CO_2 absorption tests for large packing with total mixed gas flow rate of 4L/min and nominal 10% K_2CO_3/$KHCO_3$ (85/15 mixture pH ~10.5) solvent flow rate of 150 mL/min.

CHAPTER 6: CONCLUSIONS AND FUTURE WORK

In this dissertation research, prototype fiber-based heterogeneous catalytic materials were created by combing a naturally occurring polymer and diffusion limited biocatalysts (e.g. catalase, carbonic anhydrase) together with textile support material, with the ultimate goal of achieving low energy and low cost CO_2 gas scrubbing. The biobased catalytic system with > 70% retained CA activity as well as cyclability was developed through investigating various polymers, fiber structures and immobilization methods. The unique physical properties of fibrous materials allow us to use the biocatalytic matrix as a flexible reactor for efficient enzymatic reaction and gas-liquid separation.

As a prototype material, further mechanistic evaluations of the functional behavior of the materials needed to be developed for catalyzed CO_2 scrubbing to reveal critical features and identify opportunities for improvement. For instance, in the prototype system we developed using CAT, it is speculated that under novel mild material processing conditions, molecules stack due to the structural similarity of two polysaccharides and the favored interaction between charged chemical groups contribute to the longevity of entrapped enzymes. Therefore, one objective of future research is to develop methods to reveal the structural stability of entrapped enzymes and intermolecular interactions in the system. The structural stability of entrapped enzymes can be characterized *in situ* by small-angle neutron scattering (SANS) techniques with deuterium labeled polymers. To this end, a novel deuterium labelled chitosan was prepared and non-exchangeable deuteration was confirmed at certain carbon positions, as reported in this dissertation research. Therefore, with future optimization of deuteration, the labeled matrix material, D-chitosan, can be used to investigate the enzyme structural features at the molecular level. In addition to further optimize the labeled chitosan for neutron experiments, other

characterizations such as electron microscopy (EM) techniques can be explored to study the localization and aggregation of the enzymes in the material, as a complementary characterization tool to neutron scattering. The mechanistic analysis of the apparent activity of entrapped biocatalysts in the material during applications, as well as the in-depth research of a versatile heterogeneous catalytic material will inspire synthesis and modification of molecules for better material engineering in the future. Beyond the applications in novel integrated biocatalytic materials, isotope labeling of a versatile biopolymer emerging from the research will contribute to other fields where chitosan, the only cationic polymer in nature, is involved, including other functional materials (e.g. nanocomposites, sensors, drug/RNA delivery carriers).

In addition to the mechanistic analysis of molecule interactions at nano to submicron scales, the second objective of future research is to develop novel methods to analyze the integrated gas scrubbing system *in situ*, aimed at improving the overall material performance. Assay development studies in this dissertation research reveal that measured apparent activity of immobilized enzymes is a combination of enzyme structural stability and mass transfer efficiency in integrated catalytic matrices. For most entrapped enzymes, especially diffusion limited enzymes, the rate of molecular transfer hinders the overall catalytic performance. As described above, at NCSU, we are in the process of examining the impact that liquid flow behavior has on the efficiency of CO_2 scrubbing by our prototype CO_2 scrubbing materials using a custom lab-scale scrubber. Therefore, characterizing the liquid (aqueous solvents) behavior at the interface or inside these material is critical to advancing longer-term research objectives of enhancing material morphology through techniques such as etching and deposition, modifying surface chemistry for properties such as hydrophobicity and improving fabrication methods for material or process optimization.

Back to our ultimate goal of creating a low energy and low cost gas scrubbing system for industrial post-combustion CO_2 separation and better greenhouse gas management, continuing the fundamental research on the prototype biocatalytic textile system developed in this research will help us understand the contribution of molecule interactions, material chemistry and interfacial properties to the overall carbon capture performance, as well as maximizing the benefits of applying traditional textiles materials to advanced material innovation. Also, due to the versatility of methods developed in this dissertation research, and the intrinsic properties (e.g. liquid transport) of fibrous materials, advanced engineering work on cascade reactions, with both CAs and carboxylases entrapped can be a future work in material innovation for low energy carbon capture and utilization (CCU). Through this work, it is clear that multidisciplinary knowledge and skills from chemistry, biochemistry, material science and engineering and chemical engineering are essential for further development of fibrous polymeric materials that are capable of significantly improving immobilized enzyme catalytic efficiency.

REFERENCES

Abadulla, E., Tzanov, T., Costa, S., Robra, K.-H., Cavaco-Paulo, A., & Gübitz, G. M. (2000). Decolorization and detoxification of textile dyes with a laccase from Trametes hirsuta. *Applied and Environmental Microbiology*, *66*(8), 3357–3362.

Abdelrahim, M. Y. M., Martins, C. F., Neves, L. A., Capasso, C., Supuran, C. T., Coelhoso, I. M., Crespo, J. G., & Barboiu, M. (2017). Supported ionic liquid membranes immobilized with carbonic anhydrases for CO2 transport at high temperatures. *Journal of Membrane Science*, *528*, 225–230.

Abràmoff, M. D., Magalhães, P. J., & Ram, S. J. (2004). Image processing with imageJ. *Biophotonics International*, *11*(7), 36–41. https://doi.org/10.1201/9781420005615.ax4

Adeel, M., Bilal, M., Rasheed, T., Sharma, A., & Iqbal, H. M. N. (2018). Graphene and graphene oxide: Functionalization and nano-bio-catalytic system for enzyme immobilization and biotechnological perspective. *International Journal of Biological Macromolecules*.

Aebi, H. (1984). [13] Catalase in vitro. In *Methods in enzymology* (Vol. 105, pp. 121–126). Elsevier.

Ait Braham, S., Hussain, F., Morellon-Sterling, R., Kamal, S., Kornecki, J. F., Barbosa, O., Kati, D. E., & Fernandez-Lafuente, R. (2018). Cooperativity of Covalent Attachment and Ion Exchange on Alcalase Immobilization Using Glutaraldehyde Chemistry: Enzyme Stabilization and Improved Proteolytic Activity. *Biotechnology Progress*.

Akermin, I. (2013). *Advanced Low Energy Enzyme Catalyzed Solvent for CO 2 Capture Final Scientific / Technical Report For the Reporting Period : Beginning : Oct . 1 , 2010 Project Manager : Alex Zaks , Ph . D . Principal Investigator : John Reardon Report Issued : December 2*.

Akgöl, S., Kaçar, Y., Özkara, S., Yavuz, H., Denizli, A., & Arica, M. Y. (2001). Immobilization of catalase via adsorption onto l-histidine grafted functional pHEMA based membrane. *Journal of Molecular Catalysis B: Enzymatic*, *15*(4–6), 197–206.

Ali, F., Khan, S. B., Kamal, T., Alamry, K. A., Asiri, A. M., & Sobahi, T. R. A. (2017). Chitosan coated cotton cloth supported zero-valent nanoparticles: Simple but economically viable, efficient and easily retrievable catalysts. *Scientific Reports*, *7*(1), 16957.

Alivisatos, P., & Buchanan, M. (2010). Basic Research Needs for Carbon Capture: Beyond 2020. *Basic Research Needs for Carbon Capture: Beyond 2020*.

Altinkaynak, C., Tavlasoglu, S., & Ocsoy, I. (2016). A new generation approach in enzyme immobilization: Organic-inorganic hybrid nanoflowers with enhanced catalytic activity and stability. *Enzyme and Microbial Technology*, *93*, 105–112.

Amanullah, A., Leonildi, E., Nienow, A., & Thomas, C. (2001). Dynamics of mycelial aggregation in cultures of Aspergillus oryzae. *Bioprocess and Biosystems Engineering*, *24*(2), 101–107.

Amorim, R. V. S., Melo, E. S., Carneiro-da-Cunha, M. G., Ledingham, W. M., & Campos-Takaki, G. M. (2003). Chitosan from Syncephalastrum racemosum used as a film support for lipase immobilization. *Bioresource Technology*, *89*(1), 35–39.

An, H., Jin, B., & Dai, S. (2015). Fabricating polystyrene fiber-dehydrogenase assemble as a functional biocatalyst. *Enzyme and Microbial Technology*, *68*, 15–22.

Anjum, S., Arora, A., Alam, M. S., & Gupta, B. (2016). Development of antimicrobial and scar preventive chitosan hydrogel wound dressings. In *International journal of pharmaceutics* (Vol. 508, Issues 1–2, pp. 92–101). Elsevier.

Arazawa, D. T., Kimmel, J. D., Finn, M. C., & Federspiel, W. J. (2015). Acidic sweep gas with

carbonic anhydrase coated hollow fiber membranes synergistically accelerates CO2 removal from blood. *Acta Biomaterialia*, *25*, 143–149. https://doi.org/10.1016/j.actbio.2015.07.007

Arazawa, David T, Oh, H.-I., Ye, S.-H., Johnson Jr, C. A., Woolley, J. R., Wagner, W. R., & Federspiel, W. J. (2012). Immobilized carbonic anhydrase on hollow fiber membranes accelerates CO2 removal from blood. *Journal of Membrane Science*, *403*, 25–31.

Arola, S., Tammelin, T., Setälä, H., Tullila, A., & Linder, M. B. (2012). Immobilization–stabilization of proteins on nanofibrillated cellulose derivatives and their bioactive film formation. *Biomacromolecules*, *13*(3), 594–603.

Asakura, T., Kitaguchi, M., Demura, M., Sakai, H., & Komatsu, K. (1992). Immobilization of glucose oxidase on nonwoven fabrics with Bombyx mori silk fibroin gel. *Journal of Applied Polymer Science*, *46*(1), 49–53.

B. Rao, A., & S. Rubin, E. (2002). A Technical, Economic, and Environmental Assessment of Amine-Based CO2 Capture Technology for Power Plant Greenhouse Gas Control. *Environmental Science & Technology*, *36*(20), 4467–4475. https://doi.org/10.1021/es0158861

Babadi, A. A., Bagheri, S., & Hamid, S. B. A. (2016). Progress on implantable biofuel cell: Nano-carbon functionalization for enzyme immobilization enhancement. *Biosensors and Bioelectronics*, *79*, 850–860.

Badawy, M. E. I., & Rabea, E. I. (2011). A biopolymer chitosan and its derivatives as promising antimicrobial agents against plant pathogens and their applications in crop protection. *International Journal of Carbohydrate Chemistry*, *2011*.

Bagheri, M., Rodríguez, H., Swatloski, R. P., Spear, S. K., Daly, D. T., & Rogers, R. D. (2007).

Ionic liquid-based preparation of cellulose− dendrimer films as solid supports for enzyme immobilization. *Biomacromolecules*, *9*(1), 381–387.

Bali, G., Foston, M. B., O'Neill, H. M., Evans, B. R., He, J., & Ragauskas, A. J. (2013). The effect of deuteration on the structure of bacterial cellulose. *Carbohydrate Research*, *374*, 82–88.

Baliyan, A., Sital, S., Tiwari, U., Gupta, R., & Sharma, E. K. (2016). Long period fiber grating based sensor for the detection of triacylglycerides. *Biosensors and Bioelectronics*, *79*, 693–700.

Bankeeree, W., Prasongsuk, S., Imai, T., Lotrakul, P., & Punnapayak, H. (2016). A novel xylan-polyvinyl alcohol hydrogel bead with laccase entrapment for decolorization of reactive black 5. *BioResources*, *11*(3), 6984–7000.

Beaucage, G. (1995). Approximations leading to a unified exponential/power-law approach to small-angle scattering. *Journal of Applied Crystallography*, *28*(6), 717–728.

Bilal, M., Asgher, M., Cheng, H., Yan, Y., & Iqbal, H. M. N. (2019). Multi-point enzyme immobilization, surface chemistry, and novel platforms: a paradigm shift in biocatalyst design. *Critical Reviews in Biotechnology*, *39*(2), 202–219.

Bilal, M., Iqbal, H. M. N., Hu, H., Wang, W., & Zhang, X. (2017). Enhanced bio-catalytic performance and dye degradation potential of chitosan-encapsulated horseradish peroxidase in a packed bed reactor system. *Science of the Total Environment*, *575*, 1352–1360.

Biró, E., Németh, Á. S., Sisak, C., Feczkó, T., & Gyenis, J. (2008). Preparation of chitosan particles suitable for enzyme immobilization. *Journal of Biochemical and Biophysical Methods*, *70*(6), 1240–1246.

Blanchet, C. E., & Svergun, D. I. (2013). Small-angle X-ray scattering on biological

macromolecules and nanocomposites in solution. *Annual Review of Physical Chemistry*, *64*, 37–54.

Böhm, A., Trosien, S., Avrutina, O., Kolmar, H., & Biesalski, M. (2018). Covalent Attachment of Enzymes to Paper Fibers for Paper-Based Analytical Devices. *Frontiers in Chemistry*, *6*.

Bolibok, P., Wiśniewski, M., Roszek, K., & Terzyk, A. P. (2017). Controlling enzymatic activity by immobilization on graphene oxide. *Science of Nature*, *104*(3–4). https://doi.org/10.1007/s00114-017-1459-3

Buchholz, K., Kasche, V., & Bornscheuer, U. T. (2012). *Biocatalysts and enzyme technology*. John Wiley & Sons.

Bucholz, T. L., Hulvey, M. K., Reardon, J. P., Rambo, B. M., Pulvirenti, D. C., Weber, L. E., & Zaks, A. (2015). Development of an Organosilica Coating Containing Carbonic Anhydrase for Applications in CO2 Capture. In *Novel Materials for Carbon Dioxide Mitigation Technology* (pp. 117–147). Elsevier.

Bui, M., Adjiman, C. S., Bardow, A., Anthony, E. J., Boston, A., Brown, S., Fennell, P. S., Fuss, S., Galindo, A., Hackett, L. A., Hallett, J. P., Herzog, H. J., Jackson, G., Kemper, J., Krevor, S., Maitland, G. C., Matuszewski, M., Metcalfe, I. S., Petit, C., … Dowell, N. Mac. (2018). Carbon capture and storage (CCS): the way forward. | *Energy Environ. Sci*, *11*, 1062. https://doi.org/10.1039/c7ee02342a

Bulmuş, V., Ayhan, H., & Pişkin, E. (1997). Modified PMMA monosize microbeads for glucose oxidase immobilization. *The Chemical Engineering Journal and the Biochemical Engineering Journal*, *65*(1), 71–76.

Burkoth, T. S., Benzinger, T. L. S., Urban, V., Morgan, D. M., Gregory, D. M., Thiyagarajan, P., Botto, R. E., Meredith, S. C., & Lynn, D. G. (2000). Structure of the β-amyloid (10-35)

fibril. *Journal of the American Chemical Society*, *122*(33), 7883–7889.

Buschle-Diller, G., Yang, X. D., & Yamamoto, R. (2001). Enzymatic bleaching of cotton fabric with glucose oxidase. *Textile Research Journal*, *71*(5), 388–394.

Canbolat, M. F., Savas, H. B., & Gultekin, F. (2017). Enzymatic behavior of laccase following interaction with γ-CD and immobilization into PCL nanofibers. *Analytical Biochemistry*, *528*, 13–18.

Cao, L. (2005). Immobilised enzymes: science or art? *Current Opinion in Chemical Biology*, *9*(2), 217–226. https://doi.org/10.1016/j.cbpa.2005.02.014

Cao, L. (2006). *Carrier-bound immobilized enzymes: principles, application and design*. John Wiley & Sons.

Cao, L., van Langen, L., & Sheldon, R. A. (2003). Immobilised enzymes: carrier-bound or carrier-free? *Current Opinion in Biotechnology*, *14*(4), 387–394.

Cengiz, S., Çavaş, L., & Yurdakoç, K. (2012). Bentonite and sepiolite as supporting media: Immobilization of catalase. *Applied Clay Science*, *65*, 114–120.

Çetinus, Ş. A., & Öztop, H. N. (2000). Immobilization of catalase on chitosan film. *Enzyme and Microbial Technology*, *26*(7), 497–501.

Çetinus, Ş. A., & Öztop, H. N. (2003). Immobilization of catalase into chemically crosslinked chitosan beads. *Enzyme and Microbial Technology*, *32*(7), 889–894.

Chapman, J., Ismail, A. E., & Dinu, C. Z. (2018). catalysts Industrial Applications of Enzymes: Recent Advances, Techniques, and Outlooks. *Catalysts*, *8*(6), 238. https://doi.org/10.3390/catal8060238

Chatterjee, S., Chatterjee, S., Chatterjee, B. P., & Guha, A. K. (2008). Enhancement of growth and chitosan production by Rhizopus oryzae in whey medium by plant growth hormones.

International Journal of Biological Macromolecules, *42*(2), 120–126.

Chen, G. J., Kuo, C. H., Chen, C. I., Yu, C. C., Shieh, C. J., & Liu, Y. C. (2012). Effect of membranes with various hydrophobic/hydrophilic properties on lipase immobilized activity and stability. *Journal of Bioscience and Bioengineering*, *113*(2), 166–172. https://doi.org/10.1016/j.jbiosc.2011.09.023

Chen, G., Xu, W., Lu, D., Wu, J., & Liu, Z. (2018). Markov-state model for CO2 binding with carbonic anhydrase under confinement. *The Journal of Chemical Physics*, *148*(3), 35101.

Cheng, X., Ma, K., Li, R., Ren, X., & Huang, T. S. (2014). Antimicrobial coating of modified chitosan onto cotton fabrics. *Applied Surface Science*, *309*, 138–143.

Chiappisi, L., & Gradzielski, M. (2015). Co-assembly in chitosan–surfactant mixtures: thermodynamics, structures, interfacial properties and applications. In *Advances in Colloid and Interface Science* (Vol. 220, pp. 92–107). Elsevier.

Chiou, S.-H., & Wu, W.-T. (2004). Immobilization of Candida rugosa lipase on chitosan with activation of the hydroxyl groups. *Biomaterials*, *25*(2), 197–204.

Costa, J. B., Lima, M. J., Sampaio, M. J., Neves, M. C., Faria, J. L., Morales-Torres, S., Tavares, A. P. M., & Silva, C. G. (2019). Enhanced biocatalytic sustainability of laccase by immobilization on functionalized carbon nanotubes/polysulfone membranes. *Chemical Engineering Journal*, *355*, 974–985.

Costa, S A, Azevedo, H. S., & Reis, R. L. (2005). *Enzyme immobilization in biodegradable polymers for biomedical applications*.

Costa, Silgia A, Tzanov, T., Paar, A., Gudelj, M., Gübitz, G. M., & Cavaco-Paulo, A. (2001). Immobilization of catalases from Bacillus SF on alumina for the treatment of textile bleaching effluents. *Enzyme and Microbial Technology*, *28*(9–10), 815–819.

Criado-Gonzalez, M., Fernandez-Gutierrez, M., San Roman, J., Mijangos, C., & Hernández, R. (2019). Local and controlled release of tamoxifen from multi (layer-by-layer) alginate/chitosan complex systems. *Carbohydrate Polymers*, *206*, 428–434.

Crosley, M. S., & Yip, W. T. (2017). Silica sol–gel optical biosensors: ultrahigh enzyme loading capacity on thin films via kinetic doping. *The Journal of Physical Chemistry B*, *121*(9), 2121–2126.

Crow, L., Robertson, L., Bilheux, H., Fleenor, M., Iverson, E., Tong, X., Stoica, D., & Lee, W. T. (2011). The CG1 instrument development test station at the high flux isotope reactor. *Nuclear Instruments and Methods in Physics Research Section A: Accelerators, Spectrometers, Detectors and Associated Equipment*, *634*(1), S71–S74.

Cui, J., Feng, Y., & Jia, S. (2018). Silica encapsulated catalase@ metal-organic framework composite: A highly stable and recyclable biocatalyst. *Chemical Engineering Journal*, *351*, 506–514.

D'almeida, M., Attik, N., Amalric, J., Brunon, C., Ois Renaud, F., Abouelleil, H., Toury, B., & Grosgogeat, B. (2017). *Chitosan coating as an antibacterial surface for biomedical applications*. https://doi.org/10.1371/journal.pone.0189537

da Natividade Schöffer, J., Matte, C. R., Charqueiro, D. S., de Menezes, E. W., Costa, T. M. H., Benvenutti, E. V., Rodrigues, R. C., & Hertz, P. F. (2017). Directed immobilization of CGTase: The effect of the enzyme orientation on the enzyme activity and its use in packed-bed reactor for continuous production of cyclodextrins. *Process Biochemistry*, *58*, 120–127.

Dai, T., Miletić, N., Loos, K., Elbahri, M., & Abetz, V. (2011). Electrospinning of poly[acrylonitrile-co-(glycidyl methacrylate)] nanofibrous mats for the immobilization of candida antarctica lipase B. *Macromolecular Chemistry and Physics*, *212*(4), 319–327.

https://doi.org/10.1002/macp.201000536

Daneshfar, A., Matsuura, T., Emadzadeh, D., Pahlevani, Z., & Ismail, A. F. (2015). Urease-carrying electrospun polyacrylonitrile mat for urea hydrolysis. *Reactive and Functional Polymers*, *87*, 37–45.

Darwish, T. A., Yepuri, N. R., Holden, P. J., & James, M. (2016). Quantitative analysis of deuterium using the isotopic effect on quaternary 13C NMR chemical shifts. *Analytica Chimica Acta*, *927*, 89–98.

de Ruijter, C., Mendes, E., Boerstoel, H., & Picken, S. J. (2006). Orientational order and mechanical properties of poly(amide-block-aramid) alternating block copolymer films and fibers. *Polymer*, *47*(26), 8517–8526. https://doi.org/10.1016/j.polymer.2006.10.006

Debeche, T., Marmet, C., Kiwi-Minsker, L., Renken, A., & Juillerat, M.-A. (2005). Structured fiber supports for gas phase biocatalysis. *Enzyme and Microbial Technology*, *36*(7), 911–916.

Dedania, S. R., Patel, M. J., Patel, D. M., Akhani, R. C., & Patel, D. H. (2017). Immobilization on graphene oxide improves the thermal stability and bioconversion efficiency of D-psicose 3-epimerase for rare sugar production. *Enzyme and Microbial Technology*, *107*, 49–56.

Deringer, V. L., Englert, U., & Dronskowski, R. (2016). Nature, strength, and cooperativity of the hydrogen-bonding network in α-chitin. In *Biomacromolecules* (Vol. 17, Issue 3, pp. 996–1003). ACS Publications.

Dessouki, A. M., Issa, G. I., & Atia, K. S. (2001). Pullulanase immobilization on natural and synthetic polymers. *Journal of Chemical Technology & Biotechnology*, *76*(7), 700–706.

Dettenmaier, M., Fischer, E. W., & Stamm, M. (1980). Calculation of small-angle neutron scattering by macromolecules in the semicrystalline state. *Colloid and Polymer Science*,

258(3), 343–349.

DiCapua, E., Schnarr, M., & Timmins, P. A. (1989). The location of DNA in complexes of recA protein with double-stranded DNA. A neutron scattering study. In *Biochemistry* (Vol. 28, Issue 8, pp. 3287–3292). ACS Publications.

Dodane, V., & Vilivalam, V. D. (1998). Pharmaceutical applications of chitosan. *Pharmaceutical Science & Technology Today*, *1*(6), 246–253.

Doğaç, Y. İ., Deveci, İ., Mercimek, B., & Teke, M. (2017). A comparative study for lipase immobilization onto alginate based composite electrospun nanofibers with effective and enhanced stability. *International Journal of Biological Macromolecules*, *96*, 302–311.

Drevon, G. F., Urbanke, C., & Russell, A. J. (2003). Enzyme-containing Michael-adduct-based coatings. *Biomacromolecules*, *4*(3), 675–682.

Dynesen, J., & Nielsen, J. (2003). Surface hydrophobicity of Aspergillus nidulans conidiospores and its role in pellet formation. *Biotechnology Progress*, *19*(3), 1049–1052.

Ebaid, R., Wang, H., Sha, C., Abomohra, A. E. F., & Shao, W. (2019). Recent trends in hyperthermophilic enzymes production and future perspectives for biofuel industry: A critical review. In *Journal of Cleaner Production* (Vol. 238). Elsevier Ltd. https://doi.org/10.1016/j.jclepro.2019.117925

Edwards, J. V., Prevost, N. T., Condon, B., & French, A. (2011). Covalent attachment of lysozyme to cotton/cellulose materials: protein verses solid support activation. *Cellulose*, *18*(5), 1239–1249.

Elsabee, M. Z., Naguib, H. F., & Morsi, R. E. (2012). Chitosan based nanofibers, review. In *Materials Science and Engineering: C* (Vol. 32, Issue 7, pp. 1711–1726). Elsevier.

Enright, J. T. (1971). Heavy water slows biological timing processes. *Zeitschrift Für*

Vergleichende Physiologie, *72*(1), 1–16.

Fan, M., Dai, D., & Huang, B. (2012). Fourier transform infrared spectroscopy for natural fibres. In *Fourier transform-materials analysis*. Intechopen.

Fan, Y., Emami, S., Munro, R., Ladizhansky, V., & Brown, L. S. (2015). Isotope labeling of eukaryotic membrane proteins in yeast for solid-state NMR. In *Methods in enzymology* (Vol. 565, pp. 193–212). Elsevier.

Fazel, R., Torabi, S.-F., Naseri-Nosar, P., Ghasempur, S., Ranaei-Siadat, S.-O., & Khajeh, K. (2016). Electrospun polyvinyl alcohol/bovine serum albumin biocomposite membranes for horseradish peroxidase immobilization. *Enzyme and Microbial Technology*, *93*, 1–10.

Forciniti, D., Hall, C. K., & Kula, M. R. (1991). Protein partitioning at the isoelectric point: influence of polymer molecular weight and concentration and protein size. *Biotechnology and Bioengineering*, *38*(9), 986–994.

Fu, J., Li, D., Li, G., Huang, F., & Wei, Q. (2015). Carboxymethyl cellulose assisted immobilization of silver nanoparticles onto cellulose nanofibers for the detection of catechol. *Journal of Electroanalytical Chemistry*, *738*, 92–99.

Gatto, M., Ochi, D., Yoshida, C. M. P., & da Silva, C. F. (2019). Study of chitosan with different degrees of acetylation as cardboard paper coating. *Carbohydrate Polymers*, *210*, 56–63. https://doi.org/10.1016/j.carbpol.2019.01.053

Gill, I., & Ballesteros, A. (2000a). Bioencapsulation within synthetic polymers (Part 1): sol–gel encapsulated biologicals. *Trends in Biotechnology*, *18*(7), 282–296.

Gill, I., & Ballesteros, A. (2000b). Bioencapsulation within synthetic polymers (Part 2): non-sol–gel protein–polymer biocomposites. *Trends in Biotechnology*, *18*(11), 469–479.

Giovagnoli, S., Blasi, P., Ricci, M., & Rossi, C. (2004). Biodegradable microspheres as carriers

for native superoxide dismutase and catalase delivery. *AAPS PharmSciTech*, *5*(4), 1–9.

Gong, A., Zhu, C.-T., Xu, Y., Wang, F.-Q., Wu, F.-A., & Wang, J. (2017). Moving and unsinkable graphene sheets immobilized enzyme for microfluidic biocatalysis. *Scientific Reports*, *7*(1), 4309.

González, J. M., & Fisher, S. Z. (2014). Carbonic anhydrases in industrial applications. In *Carbonic Anhydrase: Mechanism, Regulation, Links to Disease, and Industrial Applications* (pp. 405–426). Springer.

Grigoras, A. G. (2017). Catalase immobilization—A review. *Biochemical Engineering Journal*, *117*, 1–20.

Grubecki, I. (2017). External mass transfer model for hydrogen peroxide decomposition by terminox ultra catalase in a packed-bed reactor. *Chemical and Process Engineering - Inzynieria Chemiczna i Procesowa*, *38*(2), 307–319. https://doi.org/10.1515/cpe-2017-0024

Gupta, R., & Chaudhury, N. K. (2007). Entrapment of biomolecules in sol-gel matrix for applications in biosensors: Problems and future prospects. In *Biosensors and Bioelectronics* (Vol. 22, Issue 11, pp. 2387–2399). Elsevier. https://doi.org/10.1016/j.bios.2006.12.025

Hajba, L., & Guttman, A. (2016). Continuous-flow biochemical reactors: Biocatalysis, bioconversion, and bioanalytical applications utilizing immobilized microfluidic enzyme reactors. *Journal of Flow Chemistry*, *6*(1), 8–12.

Haji, A. (2017). Improved natural dyeing of cotton by plasma treatment and chitosan coating; optimization by response surface methodology. *Cellulose Chemistry and Technology*, *51*(9–10), 975–982.

Hamedi, H., Moradi, S., Hudson, S. M., & Tonelli, A. E. (2018). Chitosan based hydrogels and their applications for drug delivery in wound dressings: A review. In *Carbohydrate*

Polymers (Vol. 199, pp. 445–460). Elsevier.

Han, D., Filocamo, S., Kirby, R., & Steckl, A. J. (2011). Deactivating chemical agents using enzyme-coated nanofibers formed by electrospinning. *ACS Applied Materials and Interfaces*, *3*(12), 4633–4639. https://doi.org/10.1021/am201064b

Hang, Y. D. (1990). Chitosan production fromRhizopus oryzae mycelia. *Biotechnology Letters*, *12*(12), 911–912.

He, J., Pingali, S. V., Chundawat, S. P. S., Pack, A., Jones, A. D., Langan, P., Davison, B. H., Urban, V., Evans, B., & O'Neill, H. (2014). Controlled incorporation of deuterium into bacterial cellulose. *Cellulose*, *21*(2), 927–936.

He, S., Song, D., Chen, M., & Cheng, H. (2017). Immobilization of Lipases on Magnetic Collagen Fibers and Its Applications for Short-Chain Ester Synthesis. *Catalysts*, *7*(6), 178.

Heck, D. E., Shakarjian, M., Kim, H. D., Laskin, J. D., & Vetrano, A. M. (2010). Mechanisms of oxidant generation by catalase. *Annals of the New York Academy of Sciences*, *1203*, 120.

Heller, W. T., Urban, V. S., Lynn, G. W., Weiss, K. L., O'Neill, H. M., Pingali, S. V., Qian, S., Littrell, K. C., Melnichenko, Y. B., & Buchanan, M. V. (2014). The Bio-SANS instrument at the high flux isotope reactor of Oak Ridge National Laboratory. *Journal of Applied Crystallography*, *47*(4), 1238–1246.

Hermanová, S., Zarevúcká, M., Bouša, D., Pumera, M., & Sofer, Z. (2015). Graphene oxide immobilized enzymes show high thermal and solvent stability. *Nanoscale*, *7*(13), 5852–5858.

Hou, J., Dong, G., Xiao, B., Malassigne, C., & Chen, V. (2015). Preparation of titania based biocatalytic nanoparticles and membranes for CO 2 conversion. *Journal of Materials Chemistry A*, *3*(7), 3332–3342.

Hou, J., Ji, C., Dong, G., Xiao, B., Ye, Y., & Chen, V. (2015). Biocatalytic Janus membranes for CO 2 removal utilizing carbonic anhydrase. *Journal of Materials Chemistry A*, *3*(33), 17032–17041.

Hoven, V. P., Tangpasuthadol, V., Angkitpaiboon, Y., Vallapa, N., & Kiatkamjornwong, S. (2007). Surface-charged chitosan: Preparation and protein adsorption. *Carbohydrate Polymers*, *68*(1), 44–53.

Hsieh, Y.-L. (1995). Liquid Transport in Fabric Structures. *Textile Research Journal*, *65*(5), 299–307. https://journals.sagepub.com/doi/pdf/10.1177/004051759506500508

Hu, G., Smith, K. H., Nicholas, N. J., Yong, J., Kentish, S. E., & Stevens, G. W. (2017). Enzymatic carbon dioxide capture using a thermally stable carbonic anhydrase as a promoter in potassium carbonate solvents. *Chemical Engineering Journal*, *307*, 49–55.

Hu, Z., & Gänzle, M. G. (2019). Challenges and opportunities related to the use of chitosan as a food preservative. *Journal of Applied Microbiology*, *126*(5), 1318–1331. https://doi.org/10.1111/jam.14131

Huang, H., Hu, N., Zeng, Y., & Zhou, G. (2002). Electrochemistry and electrocatalysis with heme proteins in chitosan biopolymer films. *Analytical Biochemistry*, *308*(1), 141–151. https://doi.org/10.1016/S0003-2697(02)00242-7

Hwang, S., Lee, K.-T., Park, J.-W., Min, B.-R., Haam, S., Ahn, I.-S., & Jung, J.-K. (2004). Stability analysis of Bacillus stearothermophilus L1 lipase immobilized on surface-modified silica gels. *Biochemical Engineering Journal*, *17*(2), 85–90.

Ilavsky, J., & Jemian, P. R. (2009). Irena: tool suite for modeling and analysis of small-angle scattering. *Journal of Applied Crystallography*, *42*(2), 347–353.

Inphonlek, S., Sunintaboon, P., Leonard, M., & Durand, A. (2020).

Chitosan/carboxymethylcellulose-stabilized poly (lactide-co-glycolide) particles as bio-based drug delivery carriers. *Carbohydrate Polymers*, 116417.

Ispas, C., Sokolov, I., & Andreescu, S. (2009). Enzyme-functionalized mesoporous silica for bioanalytical applications. *Analytical and Bioanalytical Chemistry*, *393*(2), 543–554.

Iwase, T., Tajima, A., Sugimoto, S., Okuda, K., Hironaka, I., Kamata, Y., Takada, K., & Mizunoe, Y. (2013). A simple assay for measuring catalase activity: a visual approach. *Scientific Reports*, *3*, 3081.

Jacobsen, N. E. (2007). *NMR spectroscopy explained: simplified theory, applications and examples for organic chemistry and structural biology*. John Wiley & Sons.

Jesionowski, T., Zdarta, J., & Krajewska, B. (2014). Enzyme immobilization by adsorption: A review. *Adsorption*, *20*(5–6), 801–821.

Jia, H., Zhu, G., Vugrinovich, B., Kataphinan, W., Reneker, D. H., & Wang, P. (2002). Enzyme-carrying polymeric nanofibers prepared via electrospinning for use as unique biocatalysts. *Biotechnology Progress*, *18*(5), 1027–1032. https://doi.org/10.1021/bp020042m

Jochems, P., Satyawali, Y., Diels, L., & Dejonghe, W. (2011). Enzyme immobilization on/in polymeric membranes: Status, challenges and perspectives in biocatalytic membrane reactors (BMRs). *Green Chemistry*, *13*(7), 1609–1623. https://doi.org/10.1039/c1gc15178a

Jung, D., Paradiso, M., Wallacher, D., Brandt, A., & Hartmann, M. (2009). Formation of Cross-Linked Chloroperoxidase Aggregates in the Pores of Mesocellular Foams: Characterization by SANS and Catalytic Properties. *ChemSusChem: Chemistry & Sustainability Energy & Materials*, *2*(2), 161–164.

Kasaai, M. R. (2009). Various methods for determination of the degree of N-acetylation of chitin and chitosan: a review. In *Journal of Agricultural and Food Chemistry* (Vol. 57, Issue 5, pp.

1667–1676). ACS Publications.

Kaushal, J., Mehandia, S., Singh, G., Raina, A., & Arya, S. K. (2018). Catalase enzyme: Application in bioremediation and food industry. *Biocatalysis and Agricultural Biotechnology*, *16*, 192–199. https://doi.org/10.1016/j.bcab.2018.07.035

Khan, M. A., & Mujahid, M. (2019). A review on recent advances in chitosan based composite for hemostatic dressings. In *International journal of biological macromolecules* (Vol. 124, pp. 138–147). Elsevier.

Kienle, D. F., Falatach, R. M., Kaar, J. L., & Schwartz, D. K. (2018). Correlating structural and functional heterogeneity of immobilized enzymes. *ACS Nano*, *12*(8), 8091–8103. https://doi.org/10.1021/acsnano.8b02956

Kikhney, A. G., & Svergun, D. I. (2015). A practical guide to small angle X-ray scattering (SAXS) of flexible and intrinsically disordered proteins. *FEBS Letters*, *589*(19), 2570–2577.

Kim, J. H., Park, S., Kim, H., Kim, H. J., Yang, Y.-H., Kim, Y. H., Jung, S.-K., Kan, E., & Lee, S. H. (2017). Alginate/bacterial cellulose nanocomposite beads prepared using Gluconacetobacter xylinus and their application in lipase immobilization. *Carbohydrate Polymers*, *157*, 137–145.

Kim, J., Kosto, T. J., Manimala, J. C., Nauman, E. B., & Dordick, J. S. (2001). Preparation of enzyme-in-polymer composites with high activity and stability. *AIChE Journal*, *47*(1), 240–244.

Kimmel, J. D., Arazawa, D. T., Ye, S.-H., Shankarraman, V., Wagner, W. R., & Federspiel, W. J. (2013). Carbonic anhydrase immobilized on hollow fiber membranes using glutaraldehyde activated chitosan for artificial lung applications. *Journal of Materials*

Science: Materials in Medicine, *24*(11), 2611–2621.

Kirk, O., Borchert, T. V., & Fuglsang, C. C. (2002). Industrial enzyme applications. In *Current Opinion in Biotechnology* (Vol. 13, Issue 4, pp. 345–351). Elsevier Ltd. https://doi.org/10.1016/S0958-1669(02)00328-2

Klibanov, A. M. . (1983). Immobilized Enzymes and Cells as Practical Catalysts. *Science*, *219*(4585), 722–727.

Kobayashi, Y., Matsuo, R., Ohya, T., & Yokoi, N. (1987). Enzyme-Entrapping behaviors in alginate fibers and their papers. *Biotechnology and Bioengineering*, *30*(3), 451–457.

Koloti, L. E., Gule, N. P., Arotiba, O. A., & Malinga, S. P. (2016). Recent Applications of Laccase Modified Membranes in the Removal of Bisphenol A and Other Organic Pollutants. *International Conference on Pure and Applied Chemistry*, 285–312.

Kopacic, S., Walzl, A., Hirn, U., Zankel, A., Kniely, R., Leitner, E., & Bauer, W. (2018). Application of industrially produced chitosan in the surface treatment of fibre-based material: Effect of drying method and number of coating layers on mechanical and barrier properties. *Polymers*, *10*(11). https://doi.org/10.3390/polym10111232

Krajewska, B. (2004). Application of chitin-and chitosan-based materials for enzyme immobilizations: a review. *Enzyme and Microbial Technology*, *35*(2–3), 126–139.

Krishnamurthy, V. M., Kaufman, G. K., Urbach, A. R., Gitlin, I., Gudiksen, K. L., Weibel, D. B., & Whitesides, G. M. (2008). Carbonic anhydrase as a model for biophysical and physical-organic studies of proteins and protein− ligand binding. *Chemical Reviews*, *108*(3), 946–1051.

Kumar, B., & Das, A. (2014). Vertical wicking behavior of knitted fabrics. *Fibers and Polymers*, *15*(3), 625–631. https://doi.org/10.1007/s12221-014-0625-x

Kuznetsova, I., Turoverov, K., & Uversky, V. (2014). What macromolecular crowding can do to a protein. *International Journal of Molecular Sciences*, *15*(12), 23090–23140.

Lawrie, G., Keen, I., Drew, B., Chandler-Temple, A., Rintoul, L., Fredericks, P., & Grøndahl, L. (2007). Interactions between Alginate and Chitosan Biopolymers Characterized Using FTIR and XPS. *Biomacromolecules*, *8*(8), 2533–2541. https://doi.org/10.1021/bm070014y

Lee, C., Sandig, B., Buchmeiser, M. R., & Haumann, M. (2018). Supported ionic liquid phase (SILP) facilitated gas-phase enzyme catalysis–CALB catalyzed transesterification of vinyl propionate. *Catalysis Science & Technology*, *8*(9), 2460–2466.

Lee, S. H., Yeo, S. Y., Cools, P., & Morent, R. (2018). Plasma polymerization onto nonwoven polyethylene/polypropylene fibers for laccase immobilization as dye decolorization filter media. *Textile Research Journal*, 0040517518817102.

Leimbrink, M., Nikoleit, K. G., Spitzer, R., Salmon, S., Bucholz, T., Górak, A., & Skiborowski, M. (2018). Enzymatic reactive absorption of CO2 in MDEA by means of an innovative biocatalyst delivery system. *Chemical Engineering Journal*, *334*, 1195–1205.

Li, D., Wang, Q., Huang, F., & Wei, Q. (2019). Chapter 26 - Electrospun Nanofibers for Enzyme Immobilization. In B. Ding, X. Wang, & J. B. T.-E. N. and A. Yu (Eds.), *Micro and Nano Technologies* (pp. 765–781). William Andrew Publishing. https://doi.org/https://doi.org/10.1016/B978-0-323-51270-1.00026-1

Li, L., Yuan, B., Liu, S., Yu, S., Xie, C., Liu, F., Guo, X., Pei, L., & Zhang, B. (2012). Preparation of high strength chitosan fibers by using ionic liquid as spinning solution. *Journal of Materials Chemistry*, *22*(17), 8585. https://doi.org/10.1039/c2jm30555k

Li, S.-F., Chen, J.-P., & Wu, W.-T. (2007). Electrospun polyacrylonitrile nanofibrous membranes for lipase immobilization. *Journal of Molecular Catalysis B: Enzymatic*, *47*(3–

4), 117–124.

Libertino, S., Giannazzo, F., Aiello, V., Scandurra, A., Sinatra, F., Renis, M., & Fichera, M. (2008). XPS and AFM characterization of the enzyme glucose oxidase immobilized on SiO2 surfaces. *Langmuir*, *24*(5), 1965–1972. https://doi.org/10.1021/la7029664

Lindskog, S., & Coleman, J. E. (1973). The Catalytic Mechanism of Carbonic Anhydrase. *Proceedings of the National Academy of Sciences*, *70*(9), 2505–2508. https://doi.org/10.1073/PNAS.70.9.2505

Liu, F., Wang, L., Wang, H., Yuan, L., Li, J., Brash, J. L., & Chen, H. (2015). Modulating the activity of protein conjugated to gold nanoparticles by site-directed orientation and surface density of bound protein. *ACS Applied Materials & Interfaces*, *7*(6), 3717–3724.

Liu, J., Wang, Q., Fan, X. R., Sun, X. J., & Huang, P. H. (2013). Layer-by-layer self-assembly immobilization of catalases on wool fabrics. *Applied Biochemistry and Biotechnology*, *169*(7), 2212–2222.

Liu, X. D., Nishi, N., Tokura, S., & Sakairi, N. (2001). Chitosan coated cotton fiber: preparation and physical properties. *Carbohydrate Polymers*, *44*(3), 233–238.

Liu, X., Fang, Y., Yang, X., Li, Y., & Wang, C. (2018). Electrospun epoxy-based nanofibrous membrane containing biocompatible feather polypeptide for highly stable and active covalent immobilization of lipase. *Colloids and Surfaces B: Biointerfaces*, *166*, 277–285.

Liu, Yingshuai, & Yu, J. (2016). Oriented immobilization of proteins on solid supports for use in biosensors and biochips: a review. *Microchimica Acta*, *183*(1), 1–19.

Liu, Yue, & Chen, J. Y. (2016). Enzyme immobilization on cellulose matrixes. *Journal of Bioactive and Compatible Polymers*, *31*(6), 553–567.

Lončar, N., & Fraaije, M. W. (2015). Catalases as biocatalysts in technical applications: current

state and perspectives. *Applied Microbiology and Biotechnology*, *99*(8), 3351–3357. https://doi.org/10.1007/s00253-015-6512-6

Lu, M.-F., Zhang, Y.-J., & Zhang, H.-Y. (2013). Isotope effects on cell growth and sporulation, and spore heat resistance, survival and spontaneous mutation of Bacillus cereus by deuterium oxide culture. *African Journal of Microbiology Research*, *7*(8), 604–611.

Lu, S., Wang, X., Lu, Q., Hu, X., Uppal, N., Omenetto, F. G., & Kaplan, D. L. (2009). Stabilization of enzymes in silk films. *Biomacromolecules*, *10*(5), 1032–1042.

Luis, P. (2016). Use of monoethanolamine (MEA) for CO2 capture in a global scenario: Consequences and alternatives. In *Desalination* (Vol. 380, pp. 93–99). Elsevier. https://doi.org/10.1016/j.desal.2015.08.004

Lundqvist, M., Sethson, I., & Jonsson, B.-H. (2004). Protein Adsorption onto Silica Nanoparticles: Conformational Changes Depend on the Particles' Curvature and the Protein Stability. *Langmuir*, *20*(24), 10639–10647. https://doi.org/10.1021/la0484725

Luo, G., Zhang, Q., Castillo, A. R. Del, Urban, V., & O'Neill, H. (2009). Characterization of sol− gel-encapsulated proteins using small-angle neutron scattering. *ACS Applied Materials & Interfaces*, *1*(10), 2262–2268.

Lv, B., Yang, Z., Pan, F., Zhou, Z., & Jing, G. (2015). Immobilization of carbonic anhydrase on carboxyl-functionalized ferroferric oxide for CO2 capture. *International Journal of Biological Macromolecules*, *79*, 719–725.

Lynn, G. W., Heller, W., Urban, V., Wignall, G. D., Weiss, K., & Myles, D. A. A. (2006). Bio-SANS—a dedicated facility for neutron structural biology at Oak Ridge National Laboratory. *Physica B: Condensed Matter*, *385*, 880–882.

Madhu, A., & Chakraborty, J. N. (2017). Developments in application of enzymes for textile

processing. *Journal of Cleaner Production*, *145*, 114–133.

Maghami, G., & Roberts, G. (1988). Studies on the adsorption of anionic dyes on chitosan. *Die Makromolekulare Chemie*, *189*(10), 2239–2243. https://doi.org/10.1002/macp.1988.021891003

Magne, V., Amounas, M., Innocent, C., Dejean, E., & Seta, P. (2002). Enzyme textile for removal of urea with coupling process: enzymatic reaction and electrodialysis. *Desalination*, *144*(1–3), 163–166.

Masri, M. S., Randall, V. G., & Stanley, W. L. (1978). Method for insolubilizing enzymes on chitosan. In *Method for insolubilizing enzymes on chitosan*. U.S Patents.

Maurer, H. W. (2009). Chapter 18 - Starch in the Paper Industry. In J. BeMiller & R. B. T.-S. (Third E. Whistler (Eds.), *Food Science and Technology* (pp. 657–713). Academic Press. https://doi.org/https://doi.org/10.1016/B978-0-12-746275-2.00018-5

McDonald, A. G., & Tipton, K. F. (2014). Fifty-five years of enzyme classification: Advances and difficulties. *FEBS Journal*, *281*(2), 583–592. https://doi.org/10.1111/febs.12530

Mei, Y., Miller, L., Gao, W., & Gross, R. A. (2003). Imaging the distribution and secondary structure of immobilized enzymes using infrared microspectroscopy. *Biomacromolecules*, *4*(1), 70–74. https://doi.org/10.1021/bm025611t

Metz, B., Davidson, O. R., Bosch, P. R., Dave, R., & Meyer, L. A. (2007). *Contribution of working group III to the fourth assessment report of the intergovernmental panel on climate change, 2007*.

Migliardini, F., De Luca, V., Carginale, V., Rossi, M., Corbo, P., Supuran, C. T., & Capasso, C. (2014). Biomimetic CO2 capture using a highly thermostable bacterial α-carbonic anhydrase immobilized on a polyurethane foam. *Journal of Enzyme Inhibition and*

Medicinal Chemistry, *29*(1), 146–150.

Migneault, I., Dartiguenave, C., Bertrand, M. J., & Waldron, K. C. (2004). Glutaraldehyde: behavior in aqueous solution, reaction with proteins, and application to enzyme crosslinking. *BioTechniques*, *37*(5), 790–802.

Miguel, S. P., Moreira, A. F., & Correia, I. J. (2019). Chitosan based-asymmetric membranes for wound healing: A review. In *International journal of biological macromolecules* (Vol. 127, pp. 460–475). Elsevier.

Miłek, J., Wójcik, M., & Verschelde, W. (2014). Thermal stability for the effective use of commercial catalase. *Polish Journal of Chemical Technology*, *16*(4), 75–79. https://doi.org/10.2478/pjct-2014-0073

Minussi, R. C., Pastore, G. M., & Durán, N. (2002). Potential applications of laccase in the food industry. *Trends in Food Science and Technology*, *13*(6–7), 205–216. https://doi.org/10.1016/S0924-2244(02)00155-3

Mitchell, R., Carr, C. M., Parfitt, M., Vickerman, J. C., & Jones, C. (2005). Surface chemical analysis of raw cotton fibres and associated materials. *Cellulose*, *12*(6), 629–639. https://doi.org/10.1007/s10570-005-9000-9

Mohamad, N. R., Marzuki, N. H. C., Buang, N. A., Huyop, F., & Wahab, R. A. (2015). An overview of technologies for immobilization of enzymes and surface analysis techniques for immobilized enzymes. *Biotechnology & Biotechnological Equipment*, *29*(2), 205–220. https://doi.org/10.1080/13102818.2015.1008192

Mohamed, S. A., Aly, A. S., Mohamed, T. M., & Salah, H. A. (2008). Immobilization of horseradish peroxidase on nonwoven polyester fabric coated with chitosan. *Applied Biochemistry and Biotechnology*, *144*(2), 169–179.

Morgan, W. D., Kragt, A., & Feeney, J. (2000). Expression of deuterium-isotope-labelled protein in the yeast Pichia pastoris for NMR studies. *Journal of Biomolecular NMR*, *17*(4), 337–347.

Mozaffar ’, S., Ueda ’, M., Kitatsuji ’, K., Shimizu2, S., Osumi, M., & Tanaka’ ’, A. (1986). Properties of catalase purified from a methanol-grown yeast, Kloeckera sp. 2201. In *Eur J. Biochem* (Vol. 155).

Mujtaba, M., Morsi, R. E., Kerch, G., Elsabee, M. Z., Kaya, M., Labidi, J., & Khawar, K. M. (2019). Current advancements in chitosan-based film production for food technology; A review. In *International journal of biological macromolecules* (Vol. 121, pp. 889–904). Elsevier.

Myllytie, P., Salmi, J., & Laine, J. (2009). The Influence of pH on the Adsorption and Interaction of Chitosan with Cellulose. *BioResources*, *4*(5), 1647–1662. https://ojs.cnr.ncsu.edu/index.php/BioRes/article/view/BioRes_04_4_1663_Myllytie_SL_Infl_pH_Ads_Chitosan_Cellulose

Nangia, S., Warkar, S., & Katyal, D. (2018). A review on environmental applications of chitosan biopolymeric hydrogel based composites. In *Journal of Macromolecular Science, Part A* (Vol. 55, Issues 11–12, pp. 747–763). Taylor & Francis.

Nemestóthy, N., Bakonyi, P., Németh, Z., & Bélafi-Bakó, K. (2018). Evaluation of pectin-reinforced supported liquid membranes containing carbonic anhydrase: The role of ionic liquid on enzyme stability and CO2separation performance. *Journal of CO2 Utilization*, *24*(July 2017), 59–63. https://doi.org/10.1016/j.jcou.2017.12.001

Newo, A. N. S., Pshenichnikova, A. B., Skladnev, D. A., & Shvets, V. I. (2004). Deuterium oxide as a stress factor for the methylotrophic bacterium Methylophilus sp. B-7741.

Microbiology, *73*(2), 139–142.

Neylon, C. (2008). Small angle neutron and X-ray scattering in structural biology: recent examples from the literature. *European Biophysics Journal*, *37*(5), 531–541.

Nielsen, P. H., Kuilderd, H., Zhou, W., & Lu, X. (2009). 5 - Enzyme biotechnology for sustainable textiles. In R. S. B. T.-S. T. Blackburn (Ed.), *Woodhead Publishing Series in Textiles* (pp. 113–138). Woodhead Publishing. https://doi.org/https://doi.org/10.1533/9781845696948.1.113

Nwe, N., Furuike, T., Osaka, I., Fujimori, H., Kawasaki, H., Arakawa, R., Tokura, S., Stevens, W. F., Kurozumi, S., & Takamori, Y. (2011). Laboratory scale production of 13C labeled chitosan by fungi Absidia coerulea and Gongronella butleri grown in solid substrate and submerged fermentation. *Carbohydrate Polymers*, *84*(2), 743–750.

Nwe, N., Furuike, T., & Tamura, H. (2011). Production, properties and applications of fungal cell wall polysaccharides: chitosan and glucan. In *Chitosan for Biomaterials II* (pp. 187–207). Springer.

O'Neill, H., Shah, R., Evans, B. R., He, J., Pingali, S. V., Chundawat, S. P. S., Jones, A. D., Langan, P., Davison, B. H., & Urban, V. (2015). Production of Bacterial Cellulose with Controlled Deuterium–Hydrogen Substitution for Neutron Scattering Studies. In *Methods in enzymology* (Vol. 565, pp. 123–146). Elsevier.

Oktay, B., Demir, S., & Kayaman-Apohan, N. (2015). Immobilization of α-amylase onto poly (glycidyl methacrylate) grafted electrospun fibers by ATRP. *Materials Science and Engineering: C*, *50*, 386–393.

Olah, G. A., Rokop, S. E., Wang, C.-L. A., Blechner, S. L., & Trewhella, J. (1994). Troponin I encompasses an extended troponin C in the Ca2 -bound complex: a small-angle X-ray and

neutron scattering study. In *Biochemistry* (Vol. 33, Issue 27, pp. 8233–8239). ACS Publications.

Ortiz, J. A., Matsuhiro, B., Zapata, P. A., Corrales, T., & Catalina, F. (2018). Preparation and characterization of maleoylagarose/PNIPAAm graft copolymers and formation of polyelectrolyte complexes with chitosan. *Carbohydrate Polymers*, *182*, 81–91.

Pakdel, P. M., & Peighambardoust, S. J. (2018). Review on recent progress in chitosan-based hydrogels for wastewater treatment application. In *Carbohydrate Polymers* (Vol. 201, pp. 264–279). Elsevier.

Pandey, V. P., Rani, J., Jaiswal, N., Singh, S., Awasthi, M., Shasany, A. K., Tiwari, S., & Dwivedi, U. N. (2017). Chitosan immobilized novel peroxidase from Azadirachta indica: Characterization and application. *International Journal of Biological Macromolecules*, *104*, 1713–1720.

Parada, M, Derome, D., Rossi, R. M., & Carmeliet, J. (2017). A review on advanced imaging technologies for the quantification of wicking in textiles. *Textile Research Journal*, *87*(1), 110–132. https://doi.org/10.1177/0040517515622151

Parada, Marcelo, Vontobel, P., Rossi, R. M., Derome, D., & Carmeliet, J. (2017). Dynamic Wicking Process in Textiles. *Transport in Porous Media*, *119*(3), 611–632. https://doi.org/10.1007/s11242-017-0901-5

Park, S., Daeschel, M. A., & Zhao, Y. (2004). Functional properties of antimicrobial lysozyme-chitosan composite films. *Journal of Food Science*, *69*(8), M215–M221.

Patrulea, V., Ostafe, V., Borchard, G., & Jordan, O. (2015). Chitosan as a starting material for wound healing applications. In *European Journal of Pharmaceutics and Biopharmaceutics* (Vol. 97, pp. 417–426). Elsevier.

Pereira, A. R., de Souza, J. C. P., Iost, R. M., Sales, F. C. P. F., & Crespilho, F. N. (2016). Application of carbon fibers to flexible enzyme electrodes. *Journal of Electroanalytical Chemistry*, *780*, 396–406. https://doi.org/10.1016/j.jelechem.2016.01.004

Pestov, A., & Bratskaya, S. (2016). Chitosan and its derivatives as highly efficient polymer ligands. In *Molecules* (Vol. 21, Issue 3, p. 330). Multidisciplinary Digital Publishing Institute.

Pialis, P., & Saville, B. A. (1998). Production of L-DOPA from tyrosinase immobilized on nylon 6, 6: enzyme stability and scaleup. *Enzyme and Microbial Technology*, *22*(4), 261–268.

Pinkert, A., Marsh, K. N., Pang, S., & Staiger, M. P. (2009). Ionic liquids and their interaction with cellulose. *Chemical Reviews*, *109*(12), 6712–6728.

Pochanavanich, P., & Suntornsuk, W. (2002). Fungal chitosan production and its characterization. *Letters in Applied Microbiology*, *35*(1), 17–21.

Prabhu, C., Wanjari, S., Gawande, S., Das, S., Labhsetwar, N., Kotwal, S., Puri, A. K., Satyanarayana, T., & Rayalu, S. (2009). Immobilization of carbonic anhydrase enriched microorganism on biopolymer based materials. *Journal of Molecular Catalysis B: Enzymatic*, *60*(1–2), 13–21. https://doi.org/10.1016/j.molcatb.2009.02.022

Puranen, T., Alapuranen, M., & Vehmaanperä, J. (2014). Trichoderma Enzymes for Textile Industries. *Biotechnology and Biology of Trichoderma*, 351–362. https://doi.org/10.1016/B978-0-444-59576-8.00026-6

Qi, G., Liu, K., House, A., Salmon, S., Ambedkar, B., Frimpong, R. A., Remias, J. E., & Liu, K. (2018). Laboratory to bench-scale evaluation of an integrated CO2 capture system using a thermostable carbonic anhydrase promoted K2CO3 solvent with low temperature vacuum stripping. *Applied Energy*, *209*, 180–189.

Rani, M., Agarwal, A., & Negi, Y. S. (2010). Chitosan based hydrogel polymeric beads–As drug delivery system. In *BioResources* (Vol. 5, Issue 4, pp. 2765–2807).

Rathke, T. D., & Hudson, S. M. (1994). Review of chitin and chitosan as fiber and film formers. In *Journal of Macromolecular Science, Part C: Polymer Reviews* (Vol. 34, Issue 3, pp. 375–437). Taylor & Francis.

Rodrigues, S., Costa, A. M. R. Da, & Grenha, A. (2012). Chitosan/carrageenan nanoparticles: Effect of cross-linking with tripolyphosphate and charge ratios. *Carbohydrate Polymers*, *89*(1), 282–289. https://doi.org/10.1016/j.carbpol.2012.03.010

Ruan, C., Wang, W., & Gu, B. (2006). Detection of alkaline phosphatase using surface-enhanced raman spectroscopy. *Analytical Chemistry*, *78*(10), 3379–3384. https://doi.org/10.1021/ac0522106

Russell, R. A., Garvey, C. J., Darwish, T. A., Foster, L. J. R., & Holden, P. J. (2015). Biopolymer deuteration for neutron scattering and other isotope-sensitive techniques. In *Methods in enzymology* (Vol. 565, pp. 97–121). Elsevier.

Sadeghi-Kiakhani, M., & Safapour, S. (2015). Salt-free reactive dyeing of the cotton fabric modified with chitosan-poly(propylene imine) dendrimer hybrid. *Fibers and Polymers*, *16*(5), 1075–1081. https://doi.org/10.1007/s12221-015-1075-9

Sahoo, P. C., Sambudi, N. S., Park, S. Bin, Lee, J. H., & Han, J.-I. (2015). Immobilization of carbonic anhydrase on modified electrospun poly (lactic acid) membranes: quest for optimum biocatalytic performance. *Catalysis Letters*, *145*(2), 519–526.

Salmon, S., & House, A. (2015). Enzyme-catalyzed Solvents for CO2 separation. In *Novel Materials for Carbon Dioxide Mitigation Technology* (pp. 23–86). Elsevier.

Salmon, S., House, A., & Whitener, M. (2016). *Compositions and Methods For Analysis of CO2*

Absorption. https://patents.google.com/patent/US20160010142A1/en

Salmon, S., & Hudson, S. M. (1995). Shear-precipitated chitosan powders, fibrids, and fibrid papers: Observations on their formation and characterization. *Journal of Polymer Science Part B: Polymer Physics*, *33*(7), 1007–1014.

Salmon, S., & Yuan, Y. (2020). *Chitosan Materials with Entrapped Enzyme and Biocatalytic Textiles and Other Biocatalytic Materials Comprising Same* (Patent No. US20200276057A1).

Sampaio, L. M. P., Padrão, J., Faria, J., Silva, J. P., Silva, C. J., Dourado, F., & Zille, A. (2016). Laccase immobilization on bacterial nanocellulose membranes: Antimicrobial, kinetic and stability properties. *Carbohydrate Polymers*, *145*, 1–12.

Santodonato, L., Bilheux, H., Bailey, B., Bilheux, J., Nguyen, P., Tremsin, A., Selby, D., & Walker, L. (2015). The CG-1D neutron imaging beamline at the oak Ridge National Laboratory high flux isotope reactor. *Physics Procedia*, *69*, 104–108.

Schneider, C. A., Rasband, W. S., & Eliceiri, K. W. (2012). NIH Image to ImageJ: 25 years of image analysis. *Nature Methods*, *9*(7), 671–675.

Sebastian, J., Rouissi, T., Brar, S. K., Hegde, K., & Verma, M. (2019). Microwave-assisted extraction of chitosan from Rhizopus oryzae NRRL 1526 biomass. *Carbohydrate Polymers*, *219*, 431–440.

Shah, R., Huang, S., Pingali, S. V., Sawada, D., Pu, Y., Rodriguez Jr, M., Ragauskas, A. J., Kim, S. H., Evans, B. R., & Davison, B. H. (2018). Hemicellulose–Cellulose Composites Reveal Differences in Cellulose Organization after Dilute Acid Pretreatment. *Biomacromolecules*, *20*(2), 893–903.

Shamshina, J. L., Zavgorodnya, O., Berton, P., Chhotaray, P. K., Choudhary, H., & Rogers, R.

D. (2018). Ionic Liquid Platform for Spinning Composite Chitin–Poly (lactic acid) Fibers. *ACS Sustainable Chemistry & Engineering*, *6*(8), 10241–10251.

Sheldon, R A. (2007). Cross-linked enzyme aggregates (CLEA® s): stable and recyclable biocatalysts. *Cross-Linked Enzyme Aggregates (CLEA® s): Stable and Recyclable Biocatalysts*.

Sheldon, Roger A. (2007). Enzyme immobilization: The quest for optimum performance. *Advanced Synthesis and Catalysis*, *349*(8–9), 1289–1307. https://doi.org/10.1002/adsc.200700082

Sheldon, Roger A. (2007). Enzyme immobilization: the quest for optimum performance. *Advanced Synthesis & Catalysis*, *349*(8-9), 1289–1307.

Shikha, S., Thakur, K. G., & Bhattacharyya, M. S. (2017). Facile fabrication of lipase to amine functionalized gold nanoparticles to enhance stability and activity. *Rsc Advances*, *7*(68), 42845–42855.

Shoseyov, O., Shani, Z., & Levy, I. (2006). Carbohydrate binding modules: biochemical properties and novel applications. *Microbiology and Molecular Biology Reviews*, *70*(2), 283–295.

Shuai, W., Das, R. K., Naghdi, M., Brar, S. K., & Verma, M. (2017). A review on the important aspects of lipase immobilization on nanomaterials. *Biotechnology and Applied Biochemistry*, *64*(4), 496–508.

Silva, C., Silva, C. J., Zille, A., Guebitz, G. M., & Cavaco-Paulo, A. (2007). Laccase immobilization on enzymatically functionalized polyamide 6, 6 fibres. *Enzyme and Microbial Technology*, *41*(6–7), 867–875.

Simsek-Ege, F. A., Bond, G. M., & Stringer, J. (2002). Matrix molecular weight cut-off for

encapsulation of carbonic anhydrase in polyelectrolyte beads. *Journal of Biomaterials Science, Polymer Edition*, *13*(11), 1175–1187.

Singh, P. (2016). Effect of chitosans and chitooligosaccharides on the processing and storage quality of foods of animal and aquatic origin. In *Nutrition & Food Science*. Emerald Group Publishing Limited.

Smith, K. S., & Ferry, J. G. (1999). A Plant-Type (-Class) Carbonic Anhydrase in the Thermophilic Methanoarchaeon Methanobacterium thermoautotrophicum. *Journal of Bacteriology*, *181*(20), 6247–6253. http://jb.asm.org/

Soares, R. M. D., Siqueira, N. M., Prabhakaram, M. P., & Ramakrishna, S. (2018). Electrospinning and electrospray of bio-based and natural polymers for biomaterials development. *Materials Science and Engineering: C*.

Solas, M. T., Vicente, C., Xavier, L., & Legaz, M. E. (1994). Ionic adsorption of catalase on bioskin: kinetic and ultrastructural studies. *Journal of Biotechnology*, *33*(1), 63–70.

Song, J. E., Song, W. S., Yeo, S. Y., Kim, H. R., & Lee, S. H. (2017). Covalent immobilization of enzyme on aminated woven poly (lactic acid) via ammonia plasma: evaluation of the optimum immobilization conditions. *Textile Research Journal*, *87*(10), 1177–1191.

Sreerama, N., & Woody, R. W. (1993). A Self-Consistent Method for the Analysis of Protein Secondary Structure from Circular Dichroism. *Analytical Biochemistry*, *209*(1), 32–44. https://doi.org/10.1006/abio.1993.1079

Srivastava, N., Srivastava, M., Mishra, P. K., Gupta, V. K., Molina, G., Rodriguez-Couto, S., Manikanta, A., & Ramteke, P. W. (2018). Applications of fungal cellulases in biofuel production: Advances and limitations. In *Renewable and Sustainable Energy Reviews* (Vol. 82, pp. 2379–2386). Elsevier Ltd. https://doi.org/10.1016/j.rser.2017.08.074

Stalling, D., Westerhoff, M., & Hege, H.-C. (2005). Amira: A highly interactive system for visual data analysis. *The Visualization Handbook*, *38*, 749–767.

Stetefeld, J., McKenna, S. A., & Patel, T. R. (2016). Dynamic light scattering: a practical guide and applications in biomedical sciences. *Biophysical Reviews*, *8*(4), 409–427.

Su, J., Raghuwanshi, V. S., Raverty, W., Garvey, C. J., Holden, P. J., Gillon, M., Holt, S. A., Tabor, R., Batchelor, W., & Garnier, G. (2016). Smooth deuterated cellulose films for the visualisation of adsorbed bio-macromolecules. *Scientific Reports*, *6*(1), 1–11.

Sulaiman, S., Cieh, N. L., Mokhtar, M. N., Naim, M. N., & Kamal, S. M. M. (2017). Covalent immobilization of cyclodextrin glucanotransferase on kenaf cellulose nanofiber and its application in ultrafiltration membrane system. *Process Biochemistry*, *55*, 85–95.

Sulaiman, S., Mokhtar, M. N., Naim, M. N., Baharuddin, A. S., & Sulaiman, A. (2015). A review: potential usage of cellulose nanofibers (CNF) for enzyme immobilization via covalent interactions. *Applied Biochemistry and Biotechnology*, *175*(4), 1817–1842.

Supuran, C., & Capasso, C. (2017). An overview of the bacterial carbonic anhydrases. *Metabolites*, *7*(4), 56.

Supuran, C. T. (2016). Structure and function of carbonic anhydrases. *Biochemical Journal*, *473*(14), 2023–2032. https://doi.org/10.1042/BCJ20160115

Sutay Kocabas, D., Bakir, U., Phillips, S. E. V, McPherson, M. J., & Ogel, Z. B. (2008). Purification, characterization, and identification of a novel bifunctional catalase-phenol oxidase from Scytalidium thermophilum. *Applied Microbiology and Biotechnology*, *79*(3), 407–415. https://doi.org/10.1007/s00253-008-1437-y

Tan, S.-I., Han, Y.-L., Yu, Y.-J., Chiu, C.-Y., Chang, Y.-K., Ouyang, S., Fan, K.-C., Lo, K.-H., & Ng, I.-S. (2018). Efficient carbon dioxide sequestration by using recombinant carbonic

anhydrase. *Process Biochemistry*, *73*, 38–46.

Tan, S. C., Tan, T. K., Wong, S. M., & Khor, E. (1996). The chitosan yield of zygomycetes at their optimum harvesting time. *Carbohydrate Polymers*, *30*(4), 239–242.

Tang, C., Saquing, C. D., Morton, S. W., Glatz, B. N., Kelly, R. M., & Khan, S. A. (2014). Cross-linked polymer nanofibers for hyperthermophilic enzyme immobilization: Approaches to improve enzyme performance. *ACS Applied Materials and Interfaces*, *6*(15), 11899–11906. https://doi.org/10.1021/am5033633

Taqieddin, E., & Amiji, M. (2004). Enzyme immobilization in novel alginate–chitosan core-shell microcapsules. *Biomaterials*, *25*(10), 1937–1945.

Tavares, A. P. M., Silva, C. G., Dražić, G., Silva, A. M. T., Loureiro, J. M., & Faria, J. L. (2015). Laccase immobilization over multi-walled carbon nanotubes: kinetic, thermodynamic and stability studies. *Journal of Colloid and Interface Science*, *454*, 52–60.

Tkacz, J. S., & Lange, L. (2004). *Advances in fungal biotechnology for industry, agriculture, and medicine*. Springer Science & Business Media.

Tong, X., Trivedi, A., Jia, H., Zhang, M., & Wang, P. (2008). Enzymic thin film coatings for bioactive materials. *Biotechnology Progress*, *24*(3), 714–719.

Turner, M. B., Spear, S. K., Holbrey, J. D., Daly, D. T., & Rogers, R. D. (2005). Ionic liquid-reconstituted cellulose composites as solid support matrices for biocatalyst immobilization. *Biomacromolecules*, *6*(5), 2497–2502.

Tyrode, E., & Hedberg, J. (2012). A comparative study of the CD and CH stretching spectral regions of typical surfactants systems using VSFS: Orientation analysis of the terminal CH3 and CD3 groups. *The Journal of Physical Chemistry C*, *116*(1), 1080–1091.

Ulu, A., Ozcan, I., Koytepe, S., & Ates, B. (2018). Design of epoxy-functionalized

Fe3O4@MCM-41 core–shell nanoparticles for enzyme immobilization. *International Journal of Biological Macromolecules*, *115*, 1122–1130. https://doi.org/10.1016/j.ijbiomac.2018.04.157

Velasco-Lozano, S., López-Gallego, F., Mateos-Díaz, J. C., & Favela-Torres, E. (2016). Cross-linked enzyme aggregates (CLEA) in enzyme improvement–a review. *Biocatalysis*, *1*(1), 166–177.

Verpoorte, J. A., Mehta, S., & Edsall, J. T. (1967). Esterase activities of human carbonic anhydrases B and C. *Journal of Biological Chemistry*, *242*(18), 4221–4229.

Vinoba, M., Bhagiyalakshmi, M., Jeong, S. K., Nam, S. C., & Yoon, Y. (2012). Carbonic anhydrase immobilized on encapsulated magnetic nanoparticles for CO2 sequestration. *Chemistry (Weinheim an Der Bergstrasse, Germany)*, *18*(38), 12028–12034. https://doi.org/10.1002/chem.201201112

Vinoba, M., Lim, K. S., Lee, S. H., Jeong, S. K., & Alagar, M. (2011). Immobilization of human carbonic anhydrase on gold nanoparticles assembled onto amine/thiol-functionalized mesoporous SBA-15 for biomimetic sequestration of CO2. *Langmuir*, *27*(10), 6227–6234.

Virgen-Ortíz, J. J., dos Santos, J. C. S., Berenguer-Murcia, Á., Barbosa, O., Rodrigues, R. C., & Fernandez-Lafuente, R. (2017). Polyethylenimine: A very useful ionic polymer in the design of immobilized enzyme biocatalysts. *Journal of Materials Chemistry B*, *5*(36), 7461–7490.

Wagner, M. S., McArthur, S. L., Shen, M., Horbett, T. A., & Castner, D. G. (2002). Limits of detection for time of flight secondary ion mass spectrometry (ToF-SIMS) and X-ray photoelectron spectroscopy (XPS): Detection of low amounts of adsorbed protein. *Journal of Biomaterials Science, Polymer Edition*, *13*(4), 407–428.

https://doi.org/10.1163/156856202320253938

Wang, Q., Fan, X., Hu, Y., Yuan, J., Cui, L., & Wang, P. (2009). Antibacterial functionalization of wool fabric via immobilizing lysozymes. *Bioprocess and Biosystems Engineering*, *32*(5), 633–639.

Wang, Y., & Hsieh, Y. L. (2008). Immobilization of lipase enzyme in polyvinyl alcohol (PVA) nanofibrous membranes. *Journal of Membrane Science*, *309*(1–2), 73–81. https://doi.org/10.1016/j.memsci.2007.10.008

Wang, Yuanming, Liu, C., Zhang, Y., Zhang, B., & Liu, J. (2015). Facile fabrication of flowerlike natural nanotube/layered double hydroxide composites as effective carrier for lysozyme immobilization. *ACS Sustainable Chemistry & Engineering*, *3*(6), 1183–1189.

Wang, Yuhong, & Hsieh, Y. (2004). Enzyme immobilization to ultra-fine cellulose fibers via amphiphilic polyethylene glycol spacers. *Journal of Polymer Science Part A: Polymer Chemistry*, *42*(17), 4289–4299.

Wang, Z.-G., Wan, L.-S., Liu, Z.-M., Huang, X.-J., & Xu, Z.-K. (2009). Enzyme immobilization on electrospun polymer nanofibers: an overview. *Journal of Molecular Catalysis B: Enzymatic*, *56*(4), 189–195.

Wang, Z.-G., Wang, J.-Q., & Xu, Z.-K. (2006). Immobilization of lipase from Candida rugosa on electrospun polysulfone nanofibrous membranes by adsorption. *Journal of Molecular Catalysis B: Enzymatic*, *42*(1–2), 45–51.

Wehrschütz-Sigl, E., Hasmann, A., & Guebitz, G. M. (2010). Smart textiles and biomaterials containing enzymes or enzyme substrates. In *Advances in Textile Biotechnology* (pp. 56–74). Elsevier.

Weiser, D., Sóti, P. L., Bánóczi, G., Bódai, V., Kiss, B., Gellért, Á., Nagy, Z. K., Koczka, B.,

Szilágyi, A., Marosi, G., & Poppe, L. (2016). Bioimprinted lipases in PVA nanofibers as efficient immobilized biocatalysts. *Tetrahedron*, *72*(46), 7335–7342. https://doi.org/10.1016/j.tet.2016.06.027

Whitten, A. E., & Trewhella, J. (2009). Small-angle scattering and neutron contrast variation for studying bio-molecular complexes. In *Micro and nano technologies in bioanalysis* (pp. 307–323). Springer.

Wijesena, R. N., Tissera, N. D., & de Silva, K. M. N. (2015). Coloration of cotton fibers using nano chitosan. *Carbohydrate Polymers*, *134*, 182–189.

Winartasaputra, H., Kuan, S. S., & Guilbault, G. G. (1982). Amperometric enzymic determination of triglycerides in serum. *Analytical Chemistry*, *54*(12), 1987–1990.

Wösten, H. A. B., van Veluw, G. J., de Bekker, C., & Krijgsheld, P. (2013). Heterogeneity in the mycelium: implications for the use of fungi as cell factories. *Biotechnology Letters*, *35*(8), 1155–1164.

Xiang, Y., Si, J., Zhang, Q., Liu, Y., & Guo, H. (2009). Homogeneous graft copolymerization and characterization of novel artificial glycoprotein: Chitosan-poly (L-tryptophan) copolymers with secondary structural side chains. *Journal of Polymer Science Part A: Polymer Chemistry*, *47*(3), 925–934.

Xing, K., Zhu, X., Peng, X., & Qin, S. (2015). Chitosan antimicrobial and eliciting properties for pest control in agriculture: a review. In *Agronomy for Sustainable Development* (Vol. 35, Issue 2, pp. 569–588). Springer.

Xu, Y., Lin, Y., Chew, N. G. P., Malde, C., & Wang, R. (2019). Biocatalytic PVDF composite hollow fiber membranes for CO2 removal in gas-liquid membrane contactor. *Journal of Membrane Science*, *572*, 532–544.

Yadav, R. R., Mudliar, S. N., Shekh, A. Y., Fulke, A. B., Devi, S. S., Krishnamurthi, K., Juwarkar, A., & Chakrabarti, T. (2012). Immobilization of carbonic anhydrase in alginate and its influence on transformation of CO2 to calcite. *Process Biochemistry*, *47*(4), 585–590.

Yang, H., Xu, Z., Fan, M., Gupta, R., Slimane, R. B., Bland, A. E., & Wright, I. (2008). Progress in carbon dioxide separation and capture: A review. *Journal of Environmental Sciences*, *20*(1), 14–27.

Yang, J., Kwon, G.-J., Hwang, K., & Kim, D.-Y. (2018). Cellulose–Chitosan Antibacterial Composite Films Prepared from LiBr Solution. *Polymers*, *10*(10), 1058.

Yang, Y., Asiri, A. M., Du, D., & Lin, Y. (2014). Acetylcholinesterase biosensor based on a gold nanoparticle–polypyrrole–reduced graphene oxide nanocomposite modified electrode for the amperometric detection of organophosphorus pesticides. *Analyst*, *139*(12), 3055–3060.

Yong, J. K. J., Cui, J., Cho, K. L., Stevens, G. W., Caruso, F., & Kentish, S. E. (2015). Surface engineering of polypropylene membranes with carbonic anhydrase-loaded mesoporous silica nanoparticles for improved carbon dioxide hydration. *Langmuir*, *31*(22), 6211–6219.

Yong, J. K. J., Stevens, G. W., Caruso, F., & Kentish, S. E. (2016). In situ layer-by-layer assembled carbonic anhydrase-coated hollow fiber membrane contactor for rapid CO2 absorption. *Journal of Membrane Science*, *514*, 556–565.

Yoshihara, K., Shinohara, Y., Hirotsu, T., & Izumori, K. (2003). Chitosan productivity enhancement in Rhizopus oryzae YPF-61A by D-psicose. *Journal of Bioscience and Bioengineering*, *95*(3), 293–297.

Yoshimoto, M., Schweizer, T., Rathlef, M., Pleij, T., & Walde, P. (2018). Immobilization of carbonic anhydrase in glass micropipettes and glass fiber filters for flow-through reactor

applications. *ACS Omega*, *3*(8), 10391–10405.

Yoshimoto, M., & Walde, P. (2018). Immobilized carbonic anhydrase: preparation, characteristics and biotechnological applications. *World Journal of Microbiology and Biotechnology*, *34*(10), 151.

Yuan, Y., Li, H., Leite, W., Zhang, Q., Bonnesen, P. V., Labbé, J. L., Weiss, K. L., Pingali, S. V., Hong, K., Urban, V. S., Salmon, S., & O'Neill, H. (2021). Biosynthesis and characterization of deuterated chitosan in filamentous fungus and yeast. *Carbohydrate Polymers*, *257*, 117637. https://doi.org/10.1016/j.carbpol.2021.117637

Yuan, Y., Zhang, Y., Bilheux, H., & Salmon, S. (2021). Biocatalytic Yarn for Peroxide Decomposition with Controlled Liquid Transport. *Advanced Materials Interfaces*, *In Press*, 2002104. https://doi.org/10.1002/admi.202002104

Zdarta, J., Meyer, A., Jesionowski, T., & Pinelo, M. (2018). A general overview of support materials for enzyme immobilization: Characteristics, properties, practical utility. *Catalysts*, *8*(2), 92.

Zhang, S., Wang, H., Liu, J., & Bao, C. (2020). Measuring the specific surface area of monolayer graphene oxide in water. *Materials Letters*, *261*, 127098. https://doi.org/10.1016/j.matlet.2019.127098

Zhang, Y.-T., Zhang, L., Chen, H.-L., & Zhang, H.-M. (2010). Selective separation of low concentration CO2 using hydrogel immobilized CA enzyme based hollow fiber membrane reactors. *Chemical Engineering Science*, *65*(10), 3199–3207.

Zhang, Y.-T., Zhi, T.-T., Zhang, L., Huang, H., & Chen, H.-L. (2009). Immobilization of carbonic anhydrase by embedding and covalent coupling into nanocomposite hydrogel containing hydrotalcite. *Polymer*, *50*(24), 5693–5700.

Zhang, Yan, Wu, C., Guo, S., & Zhang, J. (2013). Interactions of graphene and graphene oxide with proteins and peptides. *Nanotechnology Reviews*, *2*(1), 27–45.

Zhang, Yu, Yue, Q., Zagho, M. M., Zhang, J., Elzatahry, A. A., Jiang, Y., & Deng, Y. (2019). Core-Shell Magnetic Mesoporous Silica Microspheres with Large Mesopores for Enzyme Immobilization in Biocatalysis. *ACS Applied Materials and Interfaces*, *11*(10), 10356–10363. https://doi.org/10.1021/acsami.8b18721

Zhao, Z.-P., Wang, Z., & Wang, S.-C. (2003). Formation, charged characteristic and BSA adsorption behavior of carboxymethyl chitosan/PES composite MF membrane. *Journal of Membrane Science*, *217*(1–2), 151–158.

Zhou, C.-E., & Kan, C. (2014). Plasma-assisted regenerable chitosan antimicrobial finishing for cotton. *Cellulose*, *21*(4), 2951–2962.

Zhou, C., Stevie, F., & Garcia, R. (2020). Analysis of permethrin treated fabric using ToF-SIMS. *Journal of Vacuum Science & Technology B*, *38*(3), 034006. https://doi.org/10.1116/1.5141467

Zhu, C., Richardson, R. M., Potter, K. D., Koutsomitopoulou, A. F., van Duijneveldt, J. S., Vincent, S. R., Wanasekara, N. D., Eichhorn, S. J., & Rahatekar, S. S. (2016). High Modulus Regenerated Cellulose Fibers Spun from a Low Molecular Weight Microcrystalline Cellulose Solution. *ACS Sustainable Chemistry & Engineering*, *4*(9), 4545–4553. https://doi.org/10.1021/acssuschemeng.6b00555

Zhu, J., & Sun, G. (2012). Lipase immobilization on glutaraldehyde-activated nanofibrous membranes for improved enzyme stabilities and activities. *Reactive and Functional Polymers*, *72*(11), 839–845.

Zhu, Y., Li, W., Sun, G., Tang, Q., & Bian, H. (2016). Enzymatic properties of immobilized

carbonic anhydrase and the biocatalyst for promoting CO2 capture in vertical reactor. *International Journal of Greenhouse Gas Control*, *49*, 290–296.

Zucca, P., Fernandez-Lafuente, R., & Sanjust, E. (2016). Agarose and its derivatives as supports for enzyme immobilization. *Molecules*, *21*(11), 1577.

APPENDICES

Appendix A

Preliminary tests of enzyme entrapment using electrospinning

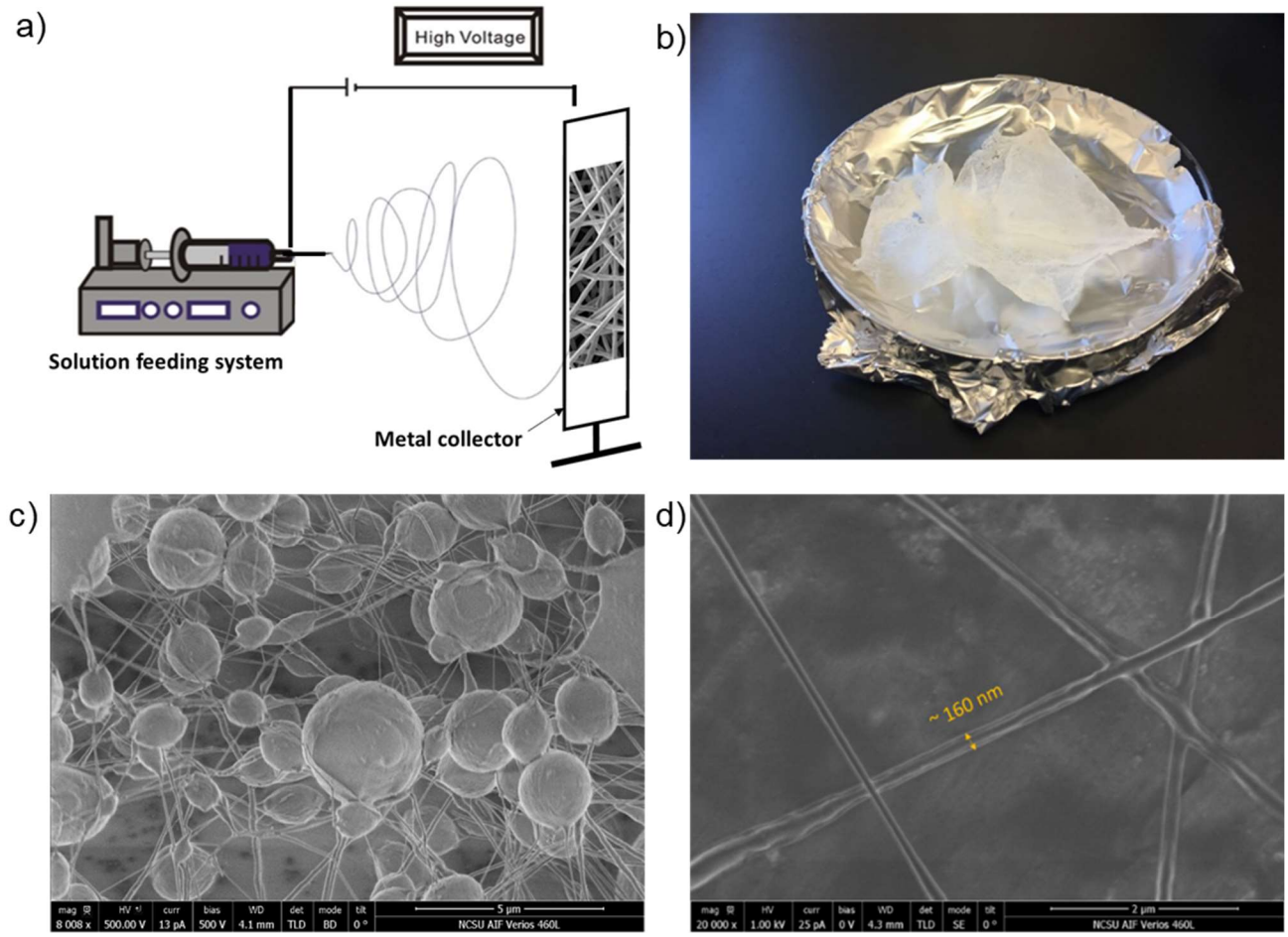

Figure A1. Enzyme entrapment using electrospun nanofibers: a) schematic drawing of the electrospinning setup used for enzyme entrapment; b) photograph of as-spun PEO membrane with bCA entrapped; c) beaded morphology of electrospun web with bCA entrapped; c) fibrous morphology of electrospun web with bCA entrapped**.**

Table A1. Compositions of PEO-CA membranes and critical electrospinning parameters of PEO-CA fiber formation.

Membrane	CA/PEO-CA weight ratio (w/w)	Voltage (kV)	Flow rate	PEO solution concentration (w/v)
E-PEO-bCA	7.9%	11-13 kV	1 ml/hour	6.7%
E-PEO-NCA	1% *	9-13 kV		

*The NCA samples was estimated based on measured solid content of the enzyme solution.

Electrospinning from which nano to submicron fibers are formed was used to investigate its potential in enzyme entrapment. As shown in **Figure A1.** a, the electrospinning apparatus consists of a solution feeding system, a high voltage supply, and a metal collector. During electrospinning, the polymer solution is extruded from the metal needle by electrostatic force, and the jet elongates in the electric field between the needle and the collector to form ultrathin fibers (nanometers to submicron meters). The solvent evaporates as the fiber is formed between the needle and collector. The spinability of formulated PEO-CA solutions depends on the capability of forming a stable "Taylor cone" at the needle tip. Critical electrospinning parameters such as viscosity, conductivity and surface tension of the electrospinning solutions and applied voltage contribute to the fiber formation as well as fiber morphology. Therefore, molecular weight of PEO, voltage and concentrations were adjusted to obtain fibrous matrices comprising CA.The electrospinning parameter such as polyethylene oxide (PEO) concentrations, voltage, and flow rate (**Table A1**) were studied to form membranes with CA entrapped, and the fiber morphologies were observed using a Scanning Electron Microscope (SEM) (FEI Verios 460L, ThermoFisher Scientific, MA, USA) to assess the quality of fiber production (**Figure A1**, c and d). When a low molecular weight PEO (~150,000 to 300,000 g/mol) was used, an unstable Taylor cone was observed and most morphologies obtained had beads-on-string structure (**Figure 3.2a**) even at high PEO concentration (~40%). Higher molecular weight PEO (>900,000 g/mol) can only form solutions with concentrations less than 5% (w/v). Due to low concentration, no Taylor cone observed in electrospinning with these solutions, and no fiber was formed. By adjusting the electrospinning parameters (including molecular weight of PEO, concentration, and voltage), major defects were eliminated, and relatively uniform fibers were obtained (**Figure 3.2b**) by using PEO with a molecular weight of 600,000 g/mol. Compositions

of E-PEO-CA electrospun membranes and critical electrospinning parameters are shown in Table A1. Because enzyme was present directly in the electrospinning solutions, these fibers comprise both PEO and CA enzyme, and the ability to produce such fibers was confirmed. In addition, CA activity was observed after re-dissolving these membranes with water, meaning the enzymes survived the electrostatic forces in the fiber formation process with certain polymer-solvent combinations. However, the yield of electrospun CA-entrapped membranes and the mechanical strength of membrane with nanofibers raise the limitations of using this technique to achieve one-step fabrication of packing materials for gas scrubbing with large quantity. Therefore, this technique was not further explored in this dissertation research.

Appendix B

Preliminary tests of enzyme entrapment using wet spinning with chitosan

Typically, chitosan is dissolved at low pH conditions (e.g. pH 2) to form a viscous spinning solution by protonation of chitosan amine groups. The chitosan solution is extruded through a spinneret directly into an alkaline (e.g. pH 14) coagulation bath which deprotonates the amine groups, causing chitosan to solidify. Continuous filaments can be produced this way by winding the coagulated fiber onto a take-up roller. Various ingredients have been incorporated into wet spun chitosan fibers by mixing the ingredients into the spinning solution before extrusion. However, some ingredients, such as many types of enzymes, will not tolerate the typically extreme swing in pH between chitosan dissolution and coagulation.

We developed a method to produce cast chitosan films or chitosan wet spun fibers using either solvent evaporation or a coagulation procedure, to entrap carbonic anhydrase (NCA and bCA) and catalase (bCAT and TU-CAT) enzymes under mild pH conditions. Enzyme was mixed with chitosan solution prior to wet spinning using mild chitosan dissolution condition (pH 5, as described in Chapter 3) to avoid enzyme denaturation. Coagulation conditions that solidified the fiber/film while maintaining enzyme activity were determined. (KOH, pH 14) was reported (El-Tahlawy and Hudson, 2006) as the optimal coagulation solvent for chitosan wet spun yarn formation. Although enzyme denaturation under extreme pH is time-dependent, we found CAT was irreversibly inactivated upon very short exposure (<10 s) of chitosan-CAT mixture in a Potassium hydroxide (KOH) bath, a typical coagulation bath for wet spun chitosan fiber, and no CAT activity was detected from the fiber produced. To solve the enzyme inactivation problem, we used bicarbonate and carbonate salt solutions as the coagulation bath. When ~30% (w/v) potassium carbonate (K_2CO_3, pH 12.5) was used, continuous catalytic chitosan fibers were obtained. Residual

CAT activity (oxygen bubble formation) was detected by immersing the fiber in H_2O_2 solution. These biocatalytic Chi-CAT wet spun fibers had an average diameter about 90 μm (**Figure B1,** a-2). Although the wet spinning for enzyme entrapment can be scaled up with existing techniques and setups, the thickness of wet spun fibers creates larger mass transfer barrier for the entrapped ultrafast enzymes. Therefore, this method was not further explored for the fabrication of reactive filters for peroxide decomposition and packing materials for gas scrubbing in this dissertation research.

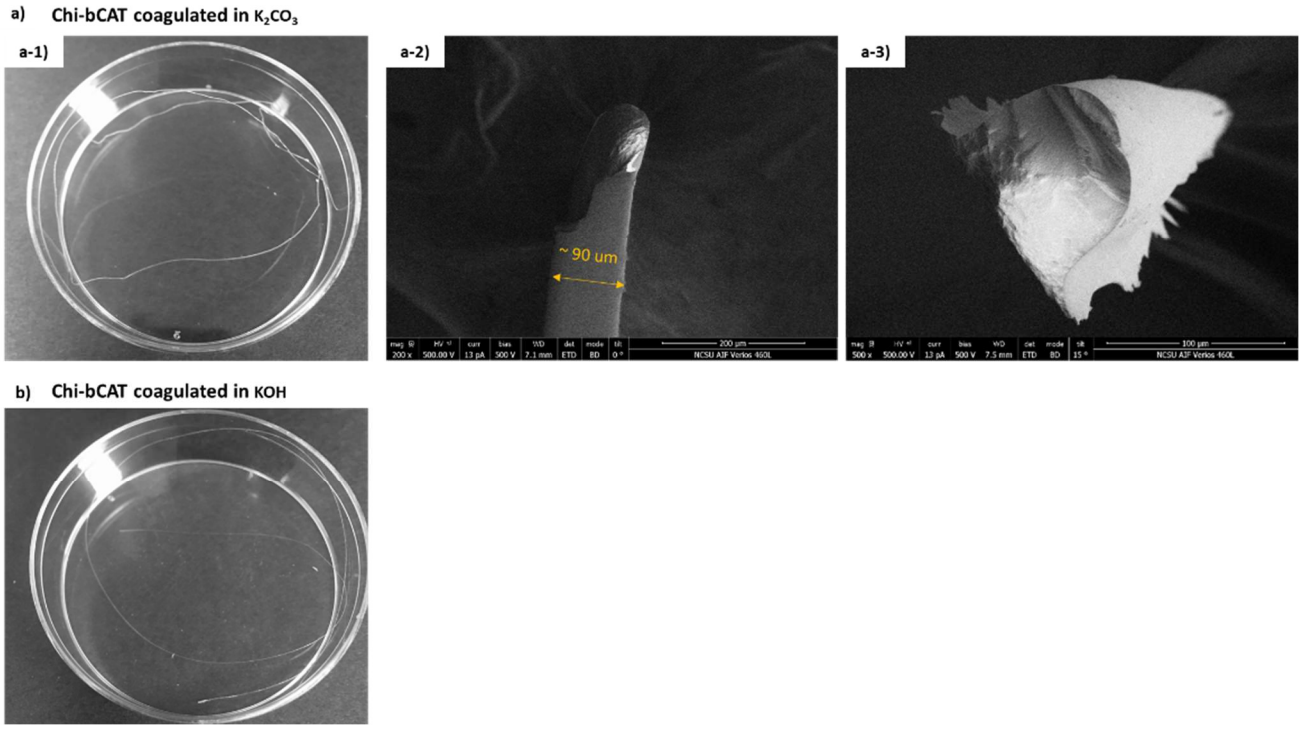

Figure B1. Photographic and SEM images of wet-spun chitosan fibers comprising bovine catalase (Chi-bCAT): a) fiber coagulated from 30% K_2CO_3 solution (pH 12.5) with retained enzyme activity (a-1) and shown in longitudinal view (a-2) and in cross-section view (a-3) to show the morphology; and, b) fiber coagulated from KOH solution with no retained enzyme activity.

Appendix C

Example of activity calculation in adapted esterase assay

For immobilized CA fabricated from liquid product, esterase activity is calculated using equation:

CA Esterase Activity= rNP/V (U/mL)

where, rNP is rate of pNP release due to CA (nmol/min) and V refers to the volume (in μL) of liquid enzyme product used in enzyme immobilization in each well. The V can be calculated based on the formulation and weight gain of fabrics after coating.

For example:

In the coating process, a gram (dry weight) of a piece of fabric weights b gram after coating (without liquid dripping from the fabric), the weight gain from the coating is (b-a) gram. If the enzyme weight percentage is n % wt. in the coating formulation, the enzyme weight on the whole coated fabric is calculated as:

$$Weight\ of\ enzyme\ producted\ coated\ on\ fabric\ = (b-a) * n\,\%$$

Assume the donut shape cut sample from the coated fabric used in esterase assay weight x g (usually the average of 4 donut shape fabrics was used in the calculation to reduce the error in the calculation), the weight of enzyme on each cut sample in the assay is calculated as:

$$Weight\ of\ enzyme\ product\ on\ cut\ sample\ in\ each\ well = \frac{(b-a) * n\,\%}{a} \times x$$

Because the density of enzyme product is known as ρ, the volume of enzyme product V can be calculated as:

$$Volume\ of\ enzyme\ product\ on\ cut\ sample\ in\ each\ well\ (V) = \frac{[\frac{(b-a) * n\,\%}{a} \times x}{\rho}]$$